School of Doctoral Studies in Biological Sciences

University of South Bohemia in České Budějovice, Faculty of Science

The role of p38-MAPKs in mouse preimplantation embryonic development: Regulating translation towards blastocyst maturation and lineage specification.

Ph.D. Thesis

Pablo Bora

Supervisor: *doc.* Alexander W. Bruce, Ph.D.

Department of Molecular Biology and Genetics
Faculty of Science, University of South Bohemia

České Budějovice, 2021

Bibliographic description:

This thesis should be cited as:

Bora, P. (2021): The role of p38-MAPKs in mouse preimplantation embryonic development: regulating translation towards blastocyst maturation and lineage specification. Ph.D. Thesis, in English – 190 pp., Faculty of Science, University of South Bohemia, České Budějovice, Czech Republic

Annotation: Preimplantation embryonic development in mammals is the period from fertilisation of the gametes to implantation of the blastocyst embryo in to the uterine walls, poised for post-implantation foetal development. This is a 5-day long process in mouse, and encompasses signalling and gene regulatory mechanisms, metabolic, cellular and organellar structural transformations, resulting in progressively reduced cellular potency and three distinct lineages. The outer and inner cells around the 16-32-cell stage are designated as the trophectoderm (TE) and the inner cell mass (ICM), respectively. 32-cell stage onwards, the ICM further differentiates to the pluripotent epiblast (EPI) and epithelial, multi-potent primitive endoderm (PrE). TE and PrE generates the extra-embryonic tissues, placenta and yolk sac, respectively, and EPI forms the embryo proper. Typical generation of extra-embryonic cells and tissues is indispensable for normal embryonic development. p38-MAPKs, a family of four stress-activated kinases, play crucial roles throughout early development, though mechanistic understanding is limited.

Studies within this thesis, building upon previous work, reports on the requirement of functional p38-MAPKs towards a translational landscape conducive for developmental cell fate specification and blastocyst maturation (E3.5 to E4.5). Phosphoproteomics, transcriptomics and experimental analysis revealed possible complications in ribosome biogenesis and an attenuated translational landscape upon inhibition of p38-MAPK activity, likely due to impaired function and localisation of downstream effectors. Some of the effectors identified, such as DDX21, MYBBP1A, and GNL3, are involved in rRNA transcription and processing, with null mutants demonstrating lethality prior to implantation. Similar to p38-MAPK inhibition, loss-of-function analysis of the effectors also resulted in fewer cells, particularly of GATA4 expressing PrE lineage. Experiments to identify the position of p38-MAPK in cell fate specifying signalling cascade revealed it as independent of the quintessential FGF4-FGFR-MEK/ERK pathway, but upstream of mTOR and potentially functional in the recently described FGFR2/PDGFRα-PI3K-mTOR pathway mediating PrE survival. p38-MAPK was also found to be functional in ameliorating amino acid deprivation induced oxidative stress during blastocyst maturation, by facilitating gene expression of anti-oxidant enzymes.

Declarations:

[In Czech]

Prohlašuji, že svoji disertační práci jsem vypracovala samostatně pouze s použitím pramenů a literatury uvedených v seznamu citované literatury.

Prohlašuji, že v souladu s § 47b zákona č. 111/1998 Sb. v platném znění souhlasím se zveřejněním své disertační práce, a to v úpravě vzniklé vypuštěním vyznačených částí archivovaných Přírodovědeckou fakultou elektronickou cestou ve veřejně přístupné části databáze STAG provozované Jihočeskou univerzitou v Českých Budějovicích na jejích internetových stránkách, a to se zachováním mého autorského práva k odevzdanému textu této kvalifikační práce. Souhlasím dále s tím, aby toutéž elektronickou cestou byly v souladu s uvedeným ustanovením zákona č. 111/1998 Sb. zveřejněny posudky školitele a oponentů práce i záznam o průběhu a výsledku obhajoby kvalifikační práce. Rovněž souhlasím s porovnáním textu mé kvalifikační práce s databází kvalifikačních prací Theses.cz provozovanou Národním registrem vysokoškolských kvalifikačních prací a systémem na odhalování plagiátů.

[In English]

I hereby declare that my Ph.D. thesis is my work alone and that I have used only those sources and literature detailed in the list of references.

Further, I declare that, in accordance with Article 47b of Act No. 111/1998 Coll. in the valid wording, I agree to the publication of my Ph.D. thesis [in unabbreviated form – in the form arising from the omission of marked parts archived at the Faculty of Science] in electronic form in a publically accessible part of the STAG database operated by the University of South Bohemia in České Budějovice on its webpage, with the preservation of my rights of authorship to the submitted text of this thesis. Further, I agree to the publication, via the same electronic portal, in accordance with the detailed regulations of Act 111/1998 Coll., of the reviews of the supervisor and opponents of the thesis as well as the record of proceedings and result of the defence of the thesis. I also agree to the comparison of the text of my thesis with the Theses.cz database operated by the National Registry of Theses and the Plagiarism Tracing System.

Place & Date: České Budějovice, 25th of May, 2021 **Pablo Bora**

Financial support:

Research contributing to this thesis was supported by grants awarded to A.W.B. from Czech Science Foundation/GAČR (18-02891S) and Ph.D. student award to P.B. by the Grant Agency of the University of South Bohemia (GAJU; 012/2019/P). Financial support information specific to the component manuscripts are detailed within the respective manuscripts.

Acknowledgements:

While I attempt to express gratitude towards the many who have made possible the realisation of this thesis, I am also aware that this acknowledgement is neither comprehensive nor adequate.

I begin by thanking my supervisor, Alexander W. Bruce, for giving me an opportunity to work in his laboratory, his support through the years, freedom to ask questions and experimentally pursue the evidence as I tried to answer some of those questions.

Though science is often a solitary endeavour, every bit of help, advice and discussion from and with fellow comrades-in-arms goes a long way. As such, I express gratitude to my colleagues in the home and neighbouring laboratories, past and present, for being there when need be. I would like to thank all those who helped me in the projects I worked on, particularly Zuzanna, Becky and Martina. Special thanks to Andrea in this regard, who has helped me considerably in realising some of the final goals of the project, all while enduring my explanations. Additionally, I also cherish their friendship. Finally, for her help during the most demanding experiments, in analysing the results, and for lending her time and senses to my tiresome tales of travails, trepidations, triumphs and temptations, I thank Lenka. I wonder if I would have completed my time here, had it not been for her friendship.

Many have given their time and effort towards actions that made my life here easier, both professionally and personally. Starting with Tomáš Doležal, who has often helped me out, be it in form of reference letters or in improving presentation skills. Working with administrative personnel is a part of academic life, and in the form of Petra Korcová and Marcela Jungwirthová, I have often found prompt aid. The wonderful Lucie Hrádková and Lucie Růžičková for their help in various aspects of procuring necessary materials. All the collaborators I have had the fortune to work with during these years. I thank them all. Not being a functional Czech-speaker, I often needed assistance in many facets of life in the Czech Republic (e.g. avoiding deportation), and for that and more, I would like to thank Pavla, Adam and Miriama, along with others unnamed or named above. Vitalising moments of joy brought by Veronika and Simon, too, will form cherished memories of my time here.

Sitting in another corner of the world, my parents and sister often humour my “embryo” and “stem cell” ramblings over the internet and still appear supportive of my (quixotic?) pursuit of science, and my late grandparents for sparking a scientific curiosity. To them, I express my gratitude.

Last, but not least, I would like to acknowledge the citizen taxpayers and the model organism. I hope the work here, in whatever miniscule way, is incremental and justifies the sacrifices made.

List of papers and manuscripts, and statements of contribution:

The thesis is composed of the following manuscripts:

Chapter I **Pablo Bora,** Lenka Gahurova, Tomáš Mašek, Andrea Hauserova, David Potěšil, Denisa Jansova, Andrej Susor, Zbyněk Zdráhal, Anna Ajduk, Martin Pospíšek and Alexander W. Bruce. p38-MAPK mediated rRNA processing and translation regulation enables PrE differentiation during mouse blastocyst maturation. **bioRxiv** 2020.11.30.403931; https://doi.org/10.1101/2020.11.30.403931

(accepted at **Communications Biology**, titled "p38-MAPK-mediated translation regulation during early blastocyst development is required for primitive endoderm differentiation in mice")

Contributions:

P.B. and A.W.B. conceived the project, designed experiments, analyzed results and wrote the manuscript. P.B. conducted experiments. P.B. and L.G. prepared samples for mass spectrometry and RNA sequencing. L.G. analyzed proteomic, phosphoproteomic and transcriptomic data and wrote associated portions within the manuscript. T.M. and M.P. designed and produced scarce-sample polysome profiling fractions. A.H. analyzed images for blastocoel cavity volume determination. D.P. and Z.Z. performed phosphoproteomic mass spectrometry, performed preliminary data analysis and wrote the associated methods. A.A. performed time-lapse imaging and analysis. D.J. and A.S. performed peripheral experiments. All authors reviewed the manuscript.

Chapter II **Pablo Bora,** Lenka Gahurova, Andrea Hauserova, Martina Stiborova, Rebecca Collier, David Potěšil, Zbyněk Zdráhal and Alexander W. Bruce. DDX21 is a p38-MAPK sensitive nucleolar protein necessary for mouse preimplantation embryo development and cell-fate specification. **bioRxiv** 2021.04.13.439318; https://doi.org/10.1101/2021.04.13.439318

(accepted at **Open Biology**)

Contributions:

P.B. and A.W.B. conceived the project, designed experiments, analysed results and wrote the manuscript. P.B. and L.G. prepared samples for mass spectrometry. P.B., A.H., M.S. and R.C. conducted experiments. A.H. also analysed some results. L.G. analysed proteomic and phosphoproteomic data. D.P. and Z.Z. performed phosphoproteomic mass spectrometry, did preliminary data analysis and wrote the associated methods. All authors reviewed the manuscript.

Chapter III **Pablo Bora,** Vasanth Thamodaran, Andrej Susor and Alexander W. Bruce. p38-mitogen activated kinases mediate a developmental regulatory response to amino

acid depletion and associated oxidative stress in mouse blastocyst embryos. **Front. Cell Dev. Biol.**, 08 November 2019; https://doi.org/10.3389/fcell.2019.00276

Contributions:

P.B., V.T., and A.W.B. conceived project and designed experiments. P.B. and V.T. conducted practical research. P.B. and A.Š. performed the western blotting experiments. P.B. and A.W.B. analysed data and wrote the manuscript. All authors reviewed the manuscript.

Table of Contents

Introduction:

1. Introduction to preimplantation development and cell fate specification.

Preimplantation development in eutherian mammals is the period from fertilization to implantation of the embryo in the uterine wall, where the remainder of the post-implantation *in utero* development takes place. The fertilised oocyte, termed the zygote, is the earliest embryo stage and is entirely dependent on maternal proteins and mRNA to go through the first cleavage division (in case of mice) or 2-3 cleavage divisions (in case of larger mammals)[1]. Mice serve as a widely studied and ideal model system to understand early embryonic development, and henceforth will be by default the organism being discussed throughout this thesis, unless stated otherwise. Around the first cleavage division (2-cell stage), the major wave of embryonic gene transcription/expression is observed, it is traditionally described as the major zygotic/embryonic-genome-activation (Z/EGA) and begins with a minor wave starting around the time of male pronuclei formation (10-hours-post-fertilization)[2–4]. This process is termed the maternal-to-zygotic transition (MZT). The minor ZGA is the beginning of the end of maternal cellular constituents, and by second cleavage division the majority of maternal mRNA is removed (although individual maternally provided proteins persist to varying degrees throughout preimplantation development). In fact, zygotic transcription is vital for an embryo to progress beyond the 2-cell stage[3,5]. Coordinated ZGA and decay of maternal transcripts, along with epigenetic reprogramming sets up the stage for embryonic totipotency. Absolute totipotency, i.e. the ability of a cell to give rise to a complete organism, is found only up to the first cleavage division i.e. 2-cell stage embryos[6,7].

As the totipotent 2-cell stage embryo undergoes subsequent rounds of cleavage division, the degree of "totipotency" is progressively lost. Individual blastomeres from 4-cell stage embryos can contribute to all embryonic and extra-embryonic lineages in a chimera, but cannot constitute an organism alone[6–8]. At the late 8-cell stage, cells are no longer loosely attached and spherical in appearance. The cells begin to compact and simultaneously establish cell-membrane bound polar apical domains, a vital organiser for establishment and segregation of the first preimplantation cellular lineages[9,10]. Cleavage divisions of polar 8-cell stage cells generate outer cells (with polar domains) and apolar inner cells by the 16-cell stage, also termed as the morula. The 16-32-cell transition is when the first two lineages are specified, with the inner cell mass (ICM) arising from apolar inner cells and the outer trophectoderm (TE) arising from the polar outer cells[9,10]. 32-cell stage onwards the embryo is also termed as blastocyst, marked by formation and expansion of a fluid-filled (blastocoel) cavity. Cellular cleavage divisions during blastocyst maturation results in further differentiation of ICM to the pluripotent epiblast (EPI) and the epithelial primitive endoderm (PrE) by around embryonic day (E) 4.5[9,10] (Figure 1 provides an overview of preimplantation development and lineage specification in mouse). Prior to going into the details of the lineage specification mechanisms it should be acknowledged that a number

of recent publications have demonstrated inherent, possibly stochastic, heterogeneities present as early as the 2-4-cell stage to have an influence on specification of all three preimplantation cellular lineages (recent comprehensive reviews[11,12]). For example, asymmetric presence and/or expression at 2-4-cell stage of long non-coding RNA *LincGET*[13] and binding partner histone methyltransferase CARM1[14,15], or duration of SOX2-DNA binding[16] will bias cells towards ICM, whereas asymmetrically inherited keratin filaments around 8-16-cell stage bias cells towards a TE fate[17]. Nevertheless, the basic cell biology, signalling and gene regulatory processes ultimately enabling these cell fate specification events are relatively well understood and will form the crux of this introduction.

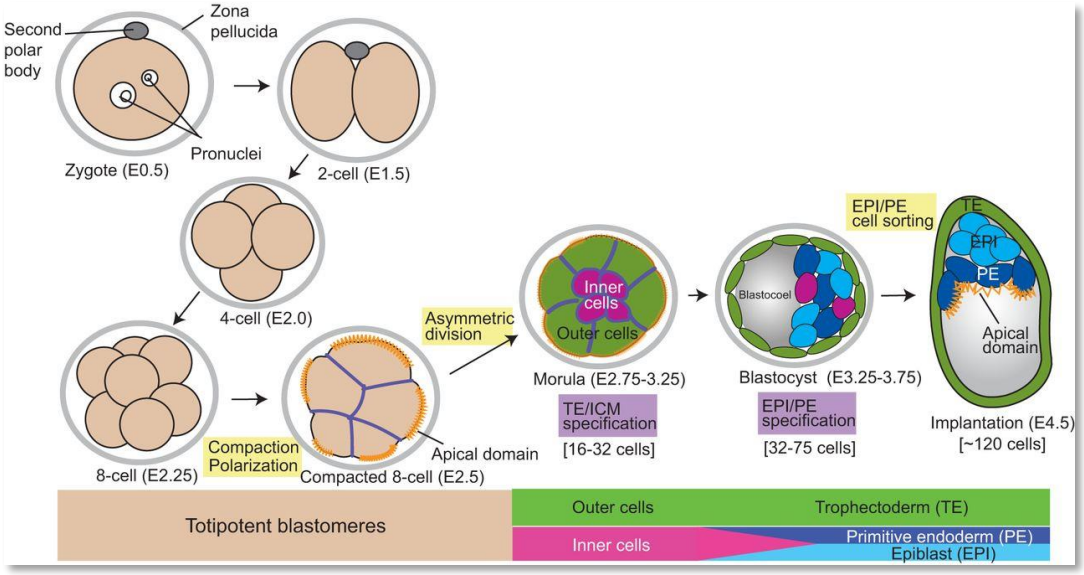

Figure 1: **Preimplantation mouse development.** The schematic represents major stages of preimplantation development in mice and demarcates the totipotent phases from the asymmetrically dividing and differentiating ones (from Chazaud and Yamanaka, 2016).

1.1. Specification of the trophectoderm and inner cell mass.

On the third day after fertilisation (E2.0-E2.5), the embryo contains eight loosely associated cells, and in the next few hours, the cells compact and attain a radially polarised form (Figure 2)[12]. The contact-free cell surface, marked by presence of cytoskeletal reorganising factors like Ezrin[18] (an actin-binding protein) and the PAR3/PAR6/aPKC complex[19], forms the polarised apical domain. The basal domain is composed of the cell surfaces in contact with neighbouring cells, and localises other set of factors like E-cadherin[20], PAR-1[19] and Na/K-ATPase[21], which is also present basolaterally in later trophectoderm, participating in blastocoel cavity formation and expansion[22]. These steps sets a stage for the first spatial segregation of cells during the 8-16-cell transition. The apical domain in the 8-cell stage embryo is reported to recruit one of the mitotic spindle poles, thus orienting and ensuring a degree of asymmetric inheritance of the apical domain between the resulting daughter cells after cytokinesis[23]. Hence, depending on the proportion of inherited apical domain, a daughter cell will be either inner (no apical domain

inherited), outer (typically ≥50% apical domain inherited) or in an intermediary state (>0% and <50% apical domain inherited). The intermediary state can be augmented by initiation of additional *de novo* polarisation or more frequently countered by active cell internalisation and the generation of an apolar inner cell [24,25]; typifying a period of plasticity wherein spatial reorganisation of the embryo cells occurs as development progresses[12,23].

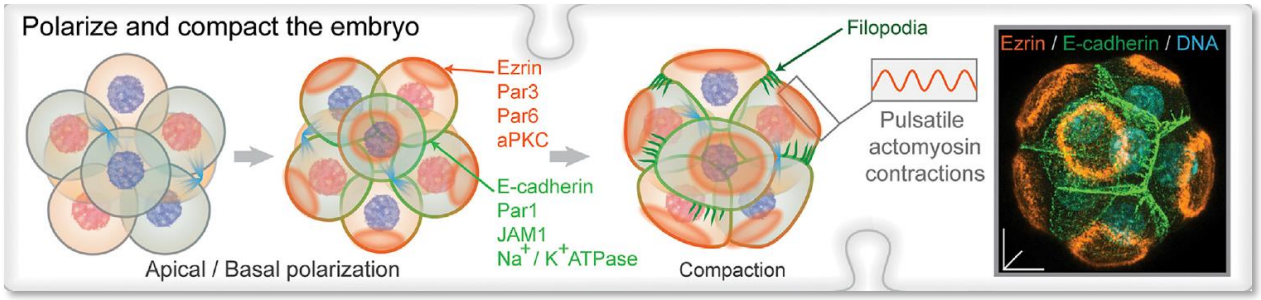

Figure 2: **Polarisation in 8-cell stage mouse embryos.** The schematic presents factors involved in polarisation and resultant morphological changes (from White et al., 2018).

Late 16-cell stage embryos (morula) harbour 2-3 internally localised cells, and based on differences in spatial organisation and polarity of the cells, the Hippo signalling pathway is either inactive (in outer cells) or active (inner cells), which further refines the inner and outer cell fates (described in following sections). An inactive Hippo pathway results in nuclear translocation of the transcription regulator YAP1 leading to the formation of an active transcriptional regulator complex with the DNA binding transcription factor (TF) TEAD4 and downstream transcription of TE specific TF genes *Gata2*, *Gata3* and *Cdx2*[26–28]. In the inner cells, under conditions of an active Hippo pathway causing YAP1 phosphorylation, YAP1 remains excluded from the nucleus, thus enabling expression of pluripotency genes. Continued expression of the respective lineage specific TFs establishes the TE and ICM as the embryo transitions towards the next round of cleavage divisions (i.e. the 32-cell stage).

1.2. Specification of the epiblast and primitive endoderm.

E3.5 is marked by formation of the fluid-filled blastocoel cavity, enabled by hydraulic fracture of cell-cell contacts during the 16-32-cell transition[29]. The fractures result in formation of microlumens that eventually coalesce to form the expanding blastocoel cavity, and are driven by the actions of aquaporins, tight-junction proteins and Na/K-ATPase in the TE cell membranes throughout the blastocyst maturation period (E3.5 to E4.5)[22,29–31]. Apart from an increase in overall volume, this period also encompasses the maturation of the ICM, thus specifying and deriving the EPI and PrE lineages. The mechanism of ICM lineage specification are primarily driven by heterogeneities in specific TF levels, resulting in differential expression of signalling ligands and ligand receptors (explained in detail in the following sections)[9].

At E3.5 (32-cell stage), the ICM cells initially express both NANOG and GATA6, lineage marker TFs for EPI and PrE, respectively. Individual cells specifying to either lineage are randomly scattered

throughout the ICM, in a manner termed the "salt & pepper" pattern[32]. As development progresses, these lineages continue to refine by down-regulating one of the two markers and by active lineage specific spatial reorganisation of the inner cells, primarily by movement of PrE fated cells towards the cavity. Thus, once sorted the PrE forms an epithelial layer in contact with the cavity, with the EPI residing deep within the ICM (encompassed by overlaying polar TE and the PrE itself). Recent reports have shown that such spatial patterning and indeed specification of the PrE lineage itself is, at least partially, dependent on typical blastocoel cavity expansion[33].

The gene regulatory network for PrE specification is a sequential expression of *Gata6*, *Sox17*, and *Gata4* and *Sox7* genes, with cells expressing GATA4 largely considered as committed PrE cells in the preimplantation embryo[34]. The pluripotent EPI, the future embryo proper, is marked by continued expression of NANOG and SOX2[35,36]. The following sections go into details pertaining to signalling cascades in relation to cell lineage specifications during preimplantation embryonic development.

2. Signalling in preimplantation development.

Though well-defined to be the signature of specific lineages, TFs are not universally observed to be the first point of segregation between differentiating cells of the preimplantation embryo[37]. Recent evidence points at factors such as duration of DNA binding and kinetics of key TFs to be lineage instructive, in as early as 4-cell stage blastomeres[16,38]. Some of the exciting evidence with regards to TF and chromatin dynamics vis-à-vis cellular heterogeneity in early developmental stages is rather recent, and it remains to be explored further. Nevertheless, evidence towards the mere act of transcription to be the initiating force towards differentiation has been limited. Consequently, researchers have considered the myriad, inter-connected signalling cascades at play during preimplantation development, to both understand the signalling network and to deduce their role in cell fate and differentiation (Figure 3 provides an overview of key lineage defining TFs and signalling elements at E3.5 and E4.5).

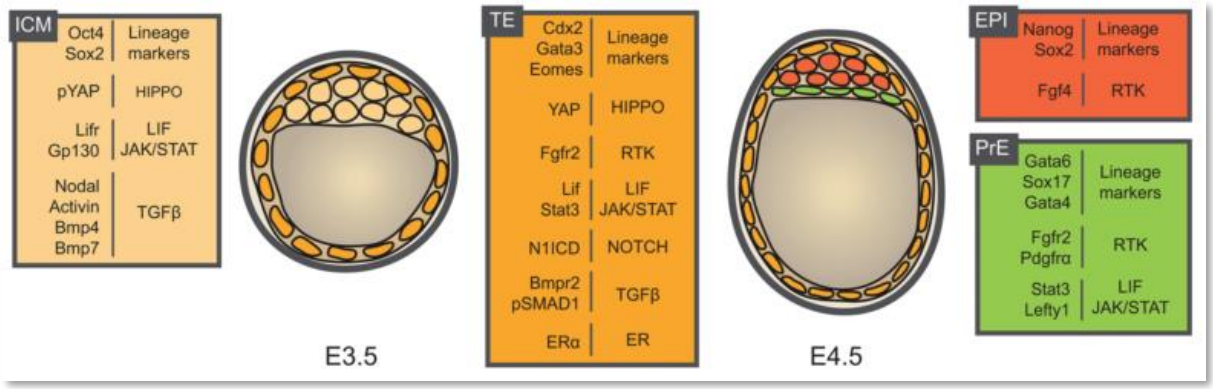

Figure 3: **Signalling elements and key TFs at E3.5 and 4.5.** This is an overview of key signalling pathway components and TFs which direct cell fate at E3.5 and E4.5 (from Menchero et al., 2016).

The following paragraphs will provide an overview of a few of the signalling pathways and components pertinent to the proposed project. Receptor tyrosine kinase (RTKs) family of cell surface receptor based signalling pathway, which includes p38 family of Mitogen-Activated Protein Kinases (MAPKs), will be described in more detail, not only with respect to preimplantation development in mice but also as a mechanism involved in development and biology in general.

Varied signalling pathways are functional during the period of preimplantation development. Among the central and best characterised in preimplantation development is the Hippo-signalling pathway. Expression of the *Cdx2* gene, the quintessential lineage marker and key TF of TE fate, is under the control of another TF, TEAD4.

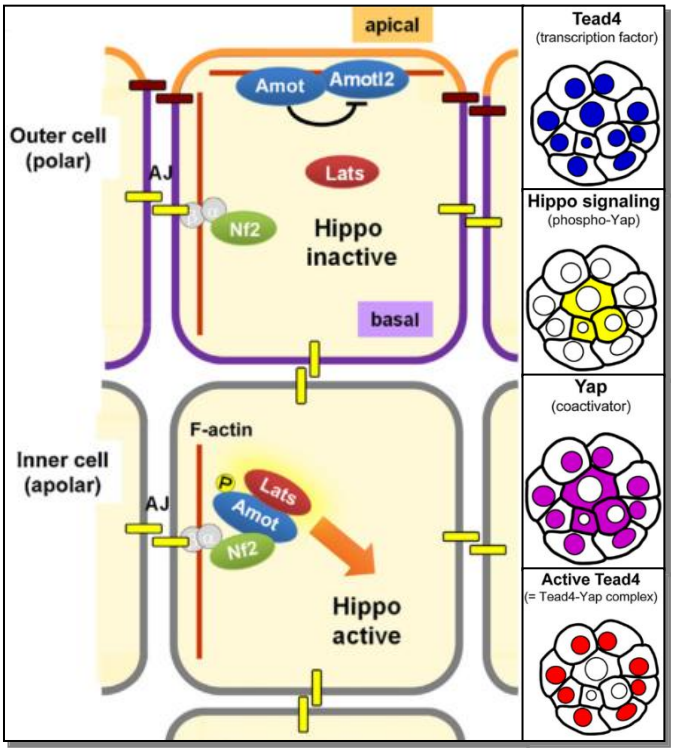

Figure 4: **Hippo signalling and first cell fate decision:** Panels on the right (top to bottom) demonstrates the overall process of Hippo signalling leading to TEAD4 activation in outer cells and subsequent TE fate. Panel on left details the differential Hippo state in inner and outer cells (from Sasaki, 2015).

Whereas TEAD4 protein is initially expressed in the nucleus of every blastomere from 4-cell stage onwards, LATS1/2 and AMOT dependent phosphorylation of the obligate TEAD4 co-transcriptional activator YAP1, limits the presence of YAP1 to the cytoplasm of apolar inner cells, from 16-cell stage onwards. However, in polarised outer cells, AMOT is sequestered at the apical domain thus not available for the activation of the downstream Hippo pathway. In turn, YAP1 remains unphosphorylated and can translocate into the nucleus and together with TEAD4 enables the expression of *Cdx2*, thus driving TE fate[26,37]. The accompanying figure (Figure 4) provides an overview of the signalling mechanisms and corresponding cellular fate during the formation of outer TE and inner ICM.

Another highly conserved signalling pathway, the Notch pathway, was thought to be of low significance in preimplantation stage of development because maternal/zygotic knockouts of vital signalling components did not hamper the process, at least till E9.5[37,39]. However, recently multiple labs have reported a convergence of Hippo and Notch signalling elements to be responsible for TEAD4 mediated expression of *Cdx2* in the TE and thus adding another dimension to the establishment of outer TE cells[39,40]. The canonical Notch pathway is activated following cell-cell interaction, wherein a ligand from one cell interacts with a transmembrane receptor on the receiving cell that in turn leads to a proteolytic cleavage of the receptor, thus liberating NICD (Notch intracellular domain) to translocate into the nucleus and subsequently bind the TF known as RBPJ (Recombination signal Binding Protein for immuno- globulin Kappa J region)[37]. The recent findings implicating Notch in preimplantation developmental stages demonstrate that NICD together with RBPJ and Hippo components TEAD4 and YAP, converge on to a *cis*-regulatory element located 5' to the *Cdx2* gene, termed the TE Enhancer (TEE), thus driving the expression of *Cdx2*[37,40]. Figure 5 presents a graphical summary of these findings, which is indeed non-functional in inner cells of ICM fate.

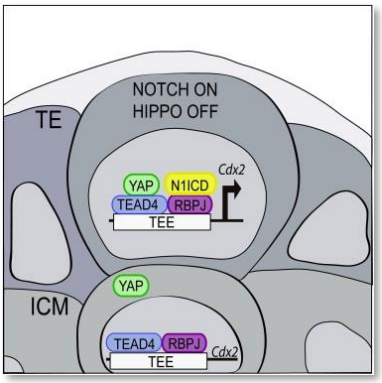

Figure 5: **Notch and Hippo signalling converge:** Elements of the two signalling pathways bind to *Cdx2* enhancer and drives its expression (from Rayon et al., 2014).

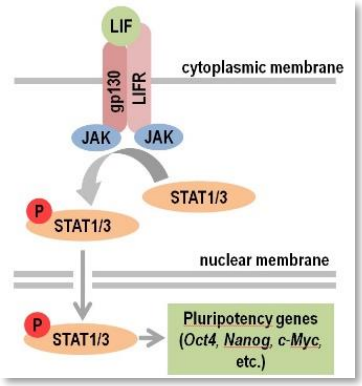

Figure 6: **Simplified LIF-JAK/STAT1/3 pathway** (from Arabadjiev et al., 2012).

One of the first components identified as vital for maintenance of pluripotency *in vitro* was leukaemia inhibitory factor (LIF). A member of the interleukin-6 family of cytokines, LIF binds to a heterodimeric cell-surface receptor composed of LIF-receptor (LIFR) and Glycoprotein 130 (GP130)[37]. As depicted in figure 6, members of the janus kinase (JAK) family of kinases are constitutively bound to the cytoplasmic domain of the heterodimeric receptor[37,41]. On being bound by LIF, the receptors induce auto-phosphorylation of JAK, which in turn phosphorylates STAT1/3 (pSTAT1/3) enabling its translocation from cytoplasm to nucleus and the subsequent activation of pluripotency related genes.

Subsequently, the localisation of these primary pathway components were elucidated in preimplantation embryos. LIF expression was found to be primarily restricted to the TE and LIFR and GP130 to the ICM. However, pSTAT3 was identified in the nuclei of all blastomeres from the 4-cell stage onwards, but by E4.5 its levels were elevated in the nuclei of PrE and TE cells[37]. However, unlike *in vitro*, LIF signalling has not been definitively proven to be important for *in vivo*

pluripotency or preimplantation development in general. A recent paper might have identified an important role for the JAK/STAT pathway in PrE formation during the developmental transit from E3.5 to E4.5[37,42]. Exposure to LIF was shown to have a positive impact on number of PrE cells and expression of pSTAT3 was also found to be higher in PrE as compared to EPI cells during the same blastocyst maturation period[42].

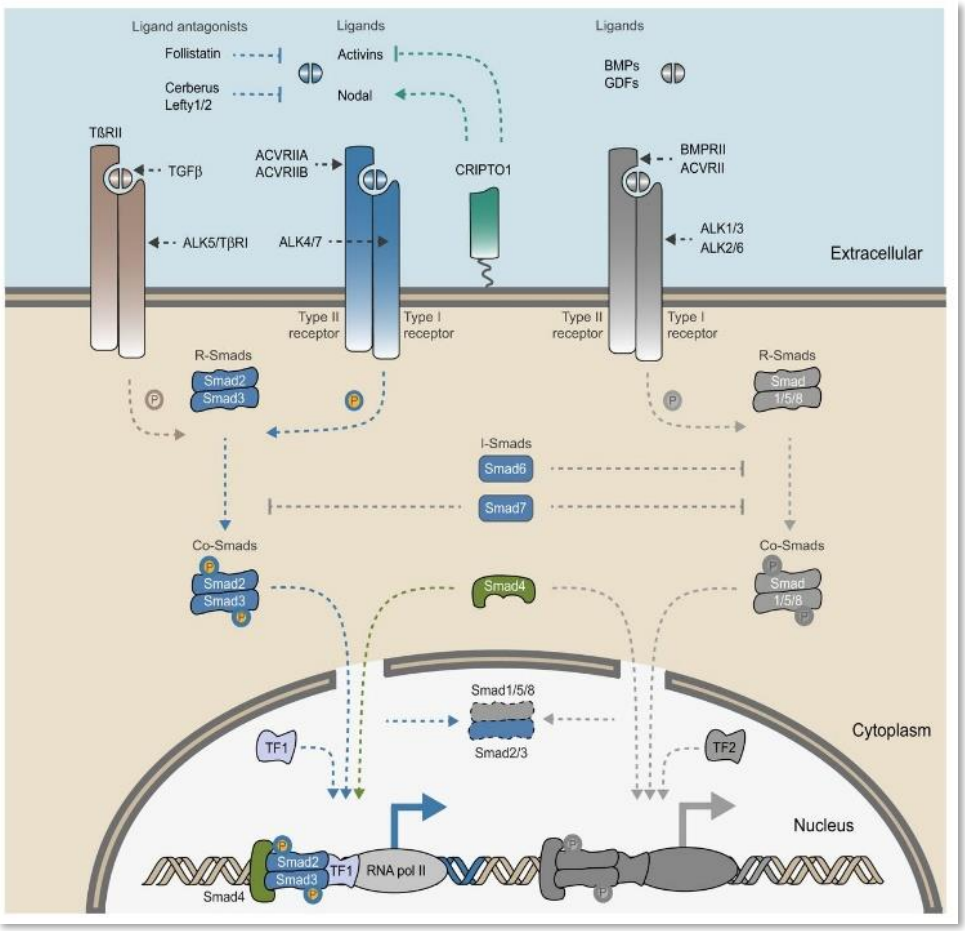

Figure 7: **Overview of TGFβ super-family of signalling molecules.** TGFβ isoforms, Activin, NODAL and BMPs bind to specific receptors and initiate phosphorylation based activation of downstream targets, leading to activation and nuclear translocation of SMAD proteins, that influence target gene expression via recruitment of co-factors and chromatin binding (from Pauklin & Vallier, 2015).

Another widely studied family of signalling factors, transforming growth factor beta (TGFβ), consisting of Activins, NODAL and bone morphogenetic proteins (BMPs), are known to be players within the arena of preimplantation development[37]. The general mechanism of action for TGFβ signalling involves processing of the ligand precursor by cleavage and dimerization to activate the ligand, which can be either Activins, NODAL or BMPs[43,44]. These then selectively bind to specific surface receptors; type II Activin receptors (ACTRII/IIB) for Activin and Nodal and heterotetrameric BMP receptors complexes composed of type I receptors (BMPR-1A, BMPR-1B, ActR-1A) and type II receptors (BMPR-2, ActR-2A, and ActR-2B) for BMPs[45–49]. Activin and NODAL

binding to ACTRII/IIB triggers recruitment and activation of type I Activin receptors (Activin receptor-like kinases, or ALKs), which for NODAL also requires the co-factor CRIPTO[43,46–49]. Once the receptors have been bound and activated, the family of heterodimeric SMAD downstream effectors are phosphorylated, activated and translocated to the nucleus. SMADs in turn influence a variety of DNA and chromatin binding factors, to enforce appropriate regulation of gene expression[37,43,45]. Figure 7 presents the general mechanism of action for these pathways[43].

Activin and NODAL have been observed to be differentially expressed within the late blastocyst embryo[37]. Whereas Activin expression changes from an ICM specific pattern at E3.5 to become exclusively present in the TE of hatched blastocysts[50,51], NODAL expression starts at E3.5 in ICM and continues to be observed within the lineages emerging from ICM, i.e. the EPI and PrE[52,53]. Similarly, BMP pathway factors also show differential expression within the blastocyst, for example, BMP7 and particularly BMP4 are specifically expressed in the inner cells between E3.5 and E6.5, with BMP7 being less abundant around implantation[36,54] and BMPR2 expression is TE specific[55]. Whereas SMAD1 can be found in all cells of the blastocyst, pSMAD1 is expressed at elevated levels in the inner cells at E4.5[56]. BMP signalling also appears to have a larger role in the late blastocyst, as siRNA mediated downregulation of *Bmp4* and *Bmp7* from E1.5 to E4.5 leads to a profound reduction in the number of extra-embryonic, TE and PrE, cells only[55].

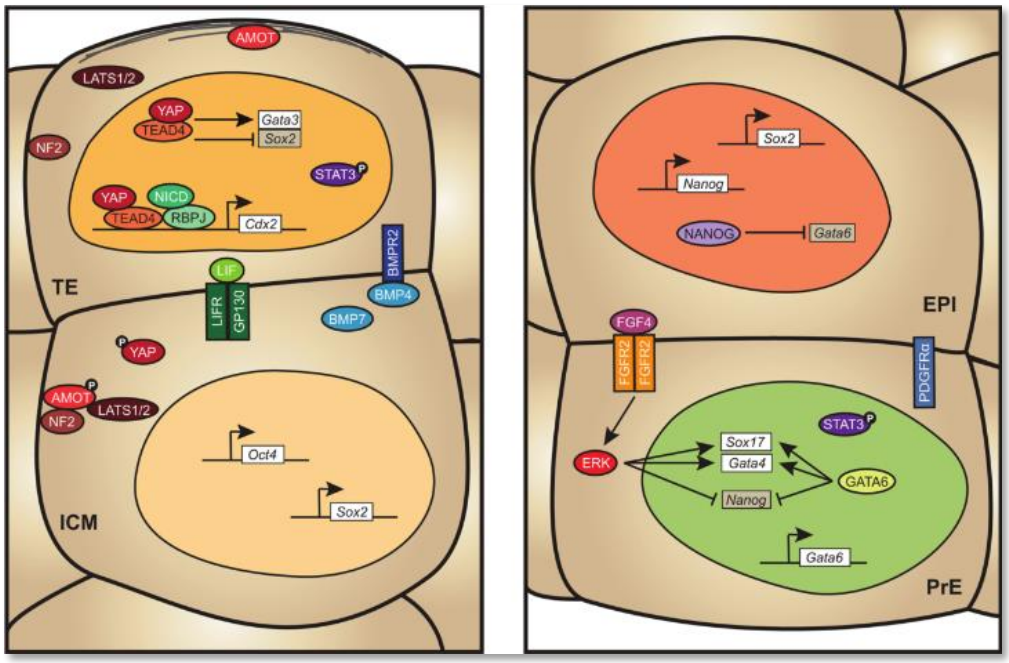

Figure 8: **Signalling pathways and preimplantation cell fates** (from Menchero et al., 2016).

Other major signalling pathways that have been investigated in early development include the Wnt/β-Catenin pathway, estrogen receptor based signalling, G-protein coupled receptors (GPCRs) and RHO/Rock based signalling. Similar to a few of the pathways described above, these too have been found to have some role in the preimplantation blastocyst, cell fate specification

and derivation, and during the process of implantation[37]. Figure 8 summarises some of the signalling pathways known to be active during both the first (TE versus ICM) and second (EPI versus PrE) cell-fate decisions. However, it should be noted that based on specific genetic knockout studies most have been observed to be dispensable for this period of development, although some lethality at a later developmental stage has been reported, i.e. post-implantation. The lack of any overt preimplantation phenotypes most likely reflects a high degree of functional redundancy between the various mechanisms/signalling pathways of cell fate specification/maintenance, that in combination with the potential for maternally inherited effects obscure the physiologically relevant roles of the investigated genes under conditions of unperturbed development. This can possibly help to explain the remarkably plastic and adaptive nature of development that is a hallmark of mammalian preimplantation stage embryos, *i.e.* the so-called 'regulative development'. Therefore, it is often difficult to identify one particular factor or pathway to be intrinsically vital in the stages of preimplantation development.

1.1. Receptor Tyrosine Kinases (RTKs).

Within the ambit of molecular signalling mechanisms and preimplantation development, RTK based signalling is of specific interest for this thesis as it also involves the p38 family of MAPKs. RTK based signalling mechanisms and other members of this family will be briefly introduced before delving into the roles of p38-MAPKs specifically.

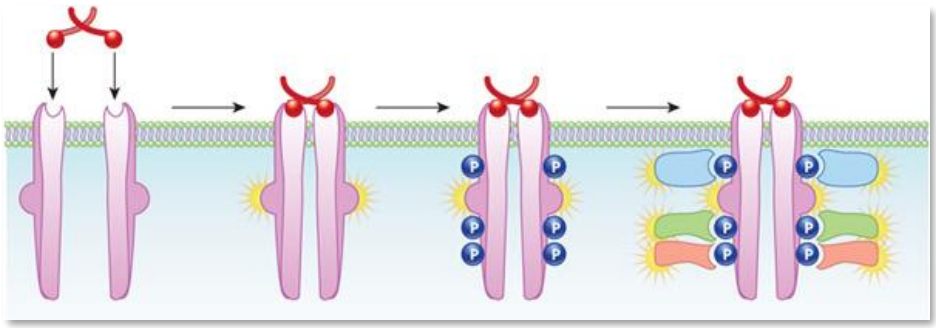

Figure 9: **Basic mechanism of initiation of signalling via Receptor Tyrosine Kinases** (from Scitable by Nature Education (link)).

The RTK group is the largest family of enzymatically active cell-surface receptors, which can bind a plethora of extracellular factors/ligands to activate functionally downstream cascades of intra-cellular kinase activity. Originally categorised into 19 families[57], the currently accepted 18 families of receptors include epidermal growth factor receptors (EGFR), insulin receptors (InsR), fibroblast growth factor receptor (FGFR), platelet-derived growth factor receptors (PDGFR) and vascular endothelial growth factor receptors (VEGFR) among others (recently reviewed[58]). The general mechanism of action involves binding of a ligand to the extra-cellular receptor-docking site of a transmembrane receptor. This causes an intrinsic conformational change to the receptor and subsequent auto- and cross-phosphorylation and receptor dimerization. This leads to the creation of a phosphorylation dependant intracellular docking platform wherein downstream effectors are bound and elicit intra-cellular signalling

cascades. Figure 9 provides a generalised description of this initiation of RTK based signalling cascade.

The MAPKs are a widely studied sub-group of effectors of RTK activations, with the three defined signalling cascades being the ERKs (extracellular-signal-regulated kinases), JNKs (c-Jun N-terminal kinases), and p38-MAPK/SAPKs (stress-activated protein kinases)[59]. Following the initiation phase of RTK activation, RAS, a membrane-anchored GDP-bound small G-protein, exchanges GDP for GTP and becomes activated. Thus, the pathway is also termed as RAS-MAPK signalling. What follows is a cascade of intra-cellular kinase activations. In general, the effector kinases are named based upon their position within the signalling cascade hierarchy. Therefore, immediately following active RAS are the MAP Kinase Kinase Kinases (MAP3K) followed by MAP2K and finally various MAPKs. These activated MAPKs thereafter phosphorylate and influence a vast array of cytoplasmic and nuclear proteins, which in turn can be related to transcriptional regulation, chromatin remodelling, RNA stability, cell cycle regulation, cell division, differentiation among other functional roles. Figure 10 describes the basic mechanisms that lie functionally downstream of those depicted in figure 9 (the initiation of RTK activation) and provides a general overview of the cascade.

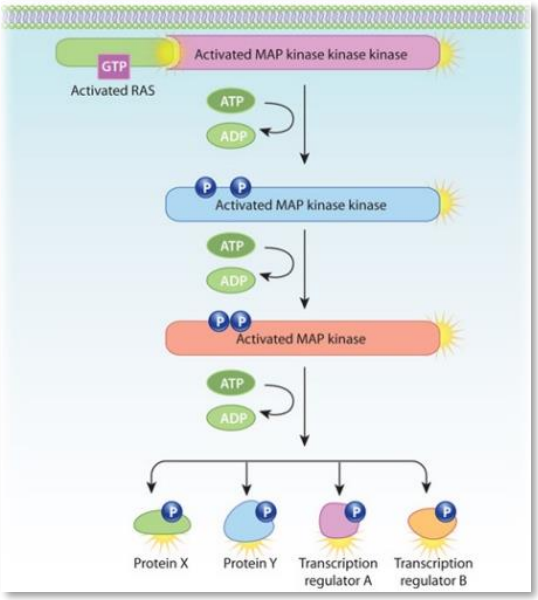

Figure 10: **General downstream kinase activity cascade following Ras activation** (from Scitable by Nature Education (link)).

The ERK pathways are activated by growth factors and cytokines, and can be further divided into two types. The classical growth-factor-activated pathways mediated by smaller ERK1 and ERK2 and the stress-activated pathway mediated by larger ERKs like ERK5[59,60]. The JNK and p38-MAPK/SAPK pathway are often activated by stress stimuli and are thus classically defined as the stress-response-kinases. Though, under physiological conditions, these signalling cascades often cross-over, and especially in case of JNK and p38-MAPK[60,61], are studied in combination. However, with regards to preimplantation mouse embryo development *in vitro*, there is evidence suggesting the two pathways might be distinct in function. The canonical immediate upstream activators and activating stimuli of the MAPKs are described in figure 11[59].

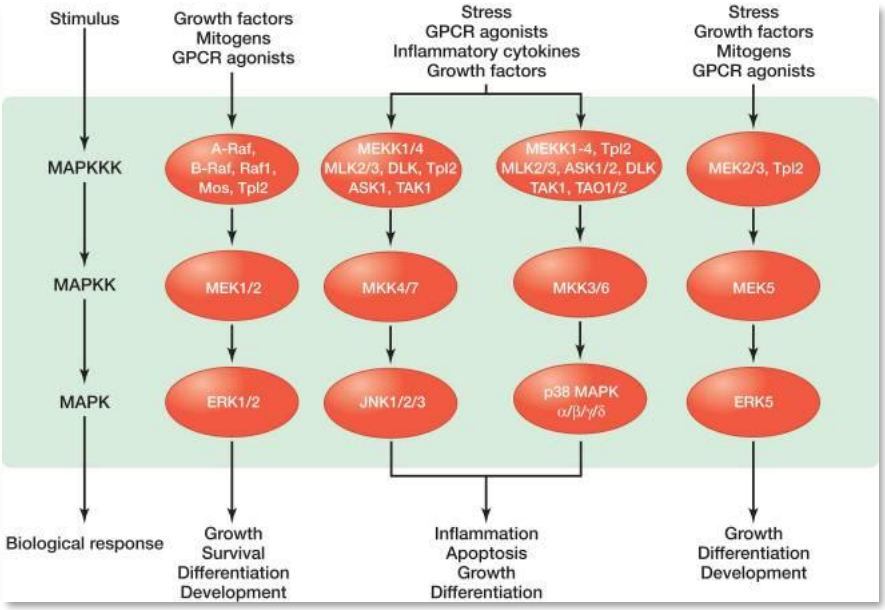

Figure 11: **Activation of MAPK family of signalling pathways** (from Morrison, 2012).

In *in vitro* mouse preimplantation embryos, all three of the MAPK pathways have been reported to play some role towards normal development. Starting with JNK pathway, one report suggests inhibition of the pathway starting from 8-cell stage onwards or even during blastocyst maturation period, results in deformed blastocysts at E4.5[62]. However, the embryo culture was carried out in M16 medium, which is reported to itself be sub-optimal for preimplantation embryo development and results in increased phosphorylation of JNKs in the embryos[63]. In fact, under optimal culture conditions, using potassium-simplex-optimized-medium (KSOM) with amino acids (AA), JNK inhibition from E1.5 to E4.5 is reported to result in improved blastocyst maturation and hatching[64]. Thus, JNK activity, or lack thereof, appears to be playing some role in *in vitro* embryo development; however, reports are few and ambiguous regarding the phenotype and mechanisms at play. Though p38-MAPKs will be discussed in some details later on, it should be noted that the aforementioned report on JNK inhibition being detrimental to embryo development, also reported on p38-MAPK inhibition to have similar phenotype[62]. p38-MAPKs are also more phosphorylated in the M16 medium, though in KSOM-AA conditions p38-MAPK phosphorylation levels in embryos appear similar to *ex vivo* embryos of equivalent stage[63]. Thus, based on reports from the laboratory (using KSOM-AA)[65–68] and others[69–72], it can be speculated that functioning of p38-MAPKs and JNKs in *in vitro* embryo development have no discernible overlap under optimal culture conditions.

The MEK1/2-ERK1/2 MAPK pathways are well studied in preimplantation embryonic development and are the most physiologically significant in proper maturation of the blastocyst and specification of the ICM to EPI and PrE lineages around E4.5. 24 hours of MEK1/2 inhibition (using PD98095) has been reported to result in fewer CDX2 expressing outer (TE) cells at the

morula stage and E3.5[73]. Autocrine FGF2-FGFR2 activation was also reported to influence TE integrity in the expanding blastocyst, with downregulation of either *Fgf2* or *Fgfr2* resulting in downregulation of genes necessary for a functional TE towards fluid-filling of the blastocoel cavity, like *Aqp3*, *Aqp9*, Na/K-ATPase[74].

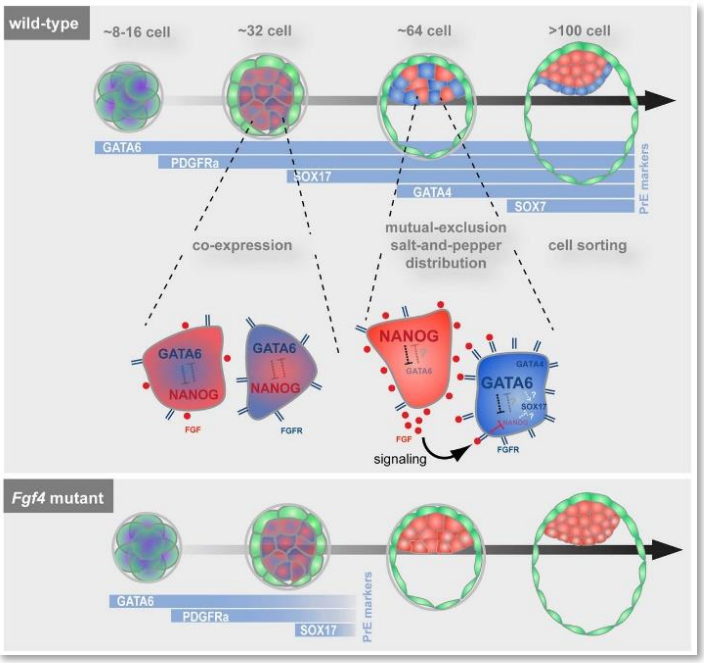

Figure 12: **Mechanism describing role of FGF4-FGFR in leading embryonic ICM cells from NANOG-GATA6 co-expression to mutually exclusive expression** (from Kang et al., 2013).

The activity of various RTK-MAPK components in the inner cells, enabling specification of EPI and PrE from the ICM, are quite well defined. Multiple reports have demonstrated the requirement for FGF4, FGFR2 and growth factor receptor-bound protein 2 (GRB2), an RTK-associated adaptor protein, to be important in PrE lineage specification[32,75–79]. Whereas the requirement of FGF4 and FGFR2 in preimplantation development was initially speculated based on genetic knockouts not being viable post-implantation[75,76], the role of GRB2 was defined as specifically required for formation of PrE, and the genetic knockout phenotype was similar to those of loss of *Fgf4* and *Fgfr2*[32]. Reports thereafter identified FGF4 as the ligand specifying, but not initiating, ICM cells to EPI and PrE[77,78], between E3.5 and E4.5; with the receptors being FGFR1[80,81] and FGFR2[36] and the intra-cellular MAPK pathway driving the specification being mediated by MEK1/2 and ERK1/2[77–79]. *Fgf4* is the first gene with reported bimodal expression within the ICM, starting at around E3.25[36,82], and is expressed in NANOG expressing (EPI fated) cells. Together with *Gata6* expression[83], FGF4-FGFR1/2-MEK1/2-ERK1/2 pathway acts to supress NANOG in ICM cells fated for PrE. Based on such observations, the model in figure 12 was proposed and depicts how ICM cells co-expressing both NANOG (EPI fate marker) and GATA6 (PrE fate) may slightly differ in their relative expression of FGF4 and FGFR2 (a RTK). In support of this model, an experimentally induced lack of FGF4 (*Fgf4*$^{-/-}$), though initially inconsequential to the NANOG and GATA6 co-expression stage, eventually gives rise to late-blastocyst embryos without a PrE layer of cells and a pan-ICM EPI fate[77].

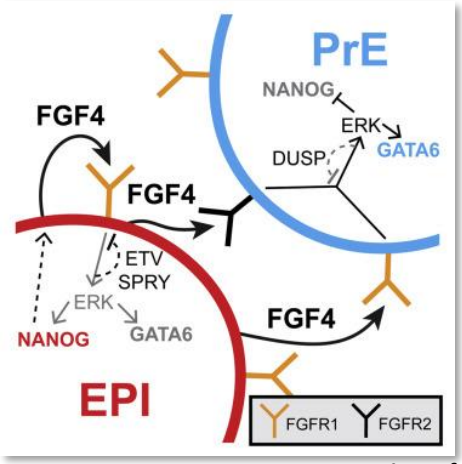

Figure 13: **Heterogeneous expression of FGFR1 & FGFR2 in ICM cells, with FGFR2 being expressed in PrE-biased cells.** Whereas FGFR1 enables biases between EPI and PrE cells, FGFR2 along with FGFR1 is required to finalise and maintain PrE fate (from Kang et al., 2017).

Presence of a heterogeneous expression pattern of the only two FGFR sub-types expressed at E3.5 (i.e. FGFR1 and FGFR2) and its mechanistic significance in EPI and PrE specification is a recent discovery[80,81]. FGFR1 is expressed in all ICM cells and FGFR2 is only expressed in ICM cells biased to ultimately form PrE[80]. Genetic evidence shows that it is FGFR1 (not FGFR2) that is the vital sub-type required for faithful derivation and segregation of ICM cells to both EPI and PrE lineages. Though exogenous FGF4 supplementation in wild-type embryos results in an exclusively PrE fated ICM; in *Fgf4*$^{-/-}$ blastocysts, exogenous FGF4 can either produce a NANOG exclusive ICM (of EPI progenitors) or a GATA6 and/or SOX17 exclusive one (of PrE progenitors)[77,79,80]. This heterogeneity in receptor molecules per ICM cell can result in differential responses to a homogeneous supply of exogenously provided FGF4. As depicted in the revised model of figure 13, it is currently proposed that FGF4 acting via the pan-ICM expressed FGFR1, differentially modulates lineage specific intra-cellular factors (ETV5, SPRY-family members in EPI precursors and DUSP-family members in PrE precursors). This ensures repression of NANOG and maintained expression of GATA6 in PrE precursors, and facilitates continued NANOG expression in EPI progenitors. Continued NANOG expression also ensures continued production of the FGF4 ligand, thus reinforcing separation of ICM cell fates[80,81]. In the case of specifying PrE cells, it is suggested the additional receipt of FGF4 signalling inputs via FGFR2, potentially simultaneously with a PDGFRα-PI3K-mTOR pathway acts to fine tune PrE differentiation and promote cell survival[80,81,84,85]. It is noteworthy that genes of two other members of the FGFR-family, *Fgfr3* and *Fgfr4*, are expressed at E4.5 (but not at E3.5) and in a PrE specific and *Fgf4*-dependent manner[82]. This suggest a PrE specific role of these receptors, though downstream of FGF4-FGFR1 mediated initial PrE specification events and possibly that of FGFR2 mediated PrE fate augmentation too.

Another member of the of RTK superfamily, PDGFRα, has been identified as a marker of PrE fate[33,84–87]. PDGFRα is shown to be expressed quite early on during the process of preimplantation development, but by late blastocyst stage, it is specifically located within the layer of PrE cells[86]. The role of PDGFRα in PrE fate was identified to be related to expression of GATA6 and possibly regulated by GATA6 at some level[87]. Using both embryos and blastocyst derived extraembryonic endoderm (XEN) cells, considered representative of *in vivo* PrE, PDGFRα was shown to induce a mitogenic effect enabling PrE lineage expansion and maintenance[87]; more recently speculated to be linked with FGF4 signalling via FGFR2[84,85], and potentially FGFR3 and FGFR4[82]. Figure 14 provides a graphical overview from the aforementioned research article and combines informed speculation and proven results from both *in vitro* and *in vivo* studies.

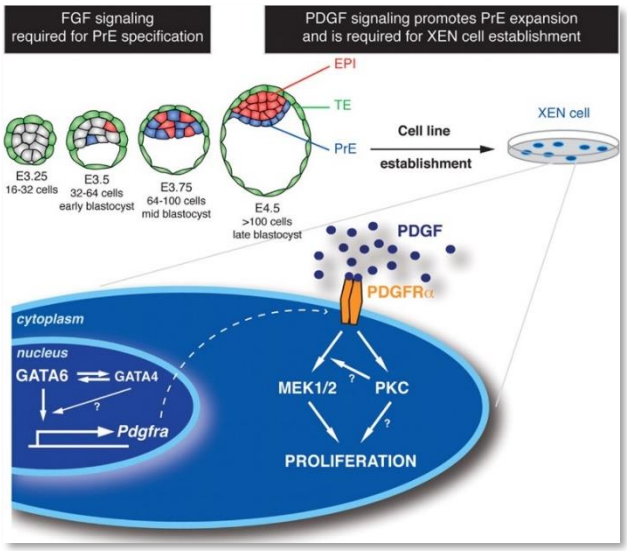

Figure 14: **Role of PDGFRα and PDGF in maintenance of PrE fate under the regulation of GATA6** (from Artus et al., 2010).

1.1.1. The p38 Family of Mitogen-Activated Protein Kinases.

The p38-MAPK pathway is classically defined as a stress-induced signalling pathway but is also associated with a wide range of cellular functions related to cell cycle, cell survival, differentiation, senescence, development, tumorigenesis and immune response among others[88,89]. The members of this kinase family are identified as a group of approximately 38kDa proteins, and thus are named p38. p38α was the first kinase of this family to be isolated and characterised in the early 1990s and was found to be rapidly phosphorylated on tyrosine residues in response to LPS (lipopolysaccharide) stimulation[61,88,89].

2.1.1.1. Physical characteristics of p38-MAPKs.

Currently, the p38-MAPK family is known to consist of four members; p38-α (Mapk14), -β (Mapk11), -γ (Mapk12), and -δ (Mapk13). Whereas the genes for p38-α (Mapk14) and -δ (Mapk13) are on chromosome 17 (17 A3.3) in mouse, p38-β (Mapk11), -γ (Mapk12) are located on chromosome 15 (15 E3). The encoded proteins range in size from 360 to 367 amino acids in length and consists of a conserved, ~300 amino acid kinase activity domain. At around their mid-point, these kinases contain a TxY motif of threonine and tyrosine residues termed the activation loop, that are targets of phosphorylation by upstream kinases necessary for p38-MAPK activation. Figure 15 provides both a cartoon and crystal structure depiction of p38-α (Mapk14), with both the kinase activity domain and TxY motif highlighted[90].

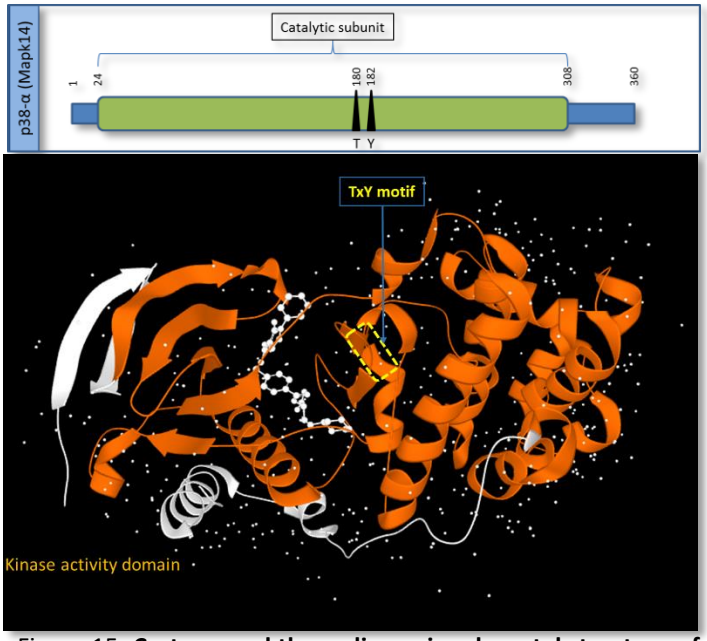

Figure 15: **Cartoon and three-dimensional crystal structure of mouse p38-α (MAPK14).** The conserved kinase activity domain and TxY motifs are highlighted in both formats Kinase activity domain is in red in crystal structure and green in cartoon depiction. Crystal structure of MAPK14 is together with an inhibitor (VPC00628; in white) and is from PDB-Europe (link).

2.1.1.2. Molecular pathways enabling p38-MAPK activation.

As with all other RTK-mediated MAPK pathways, p38-MAPK activation requires a cascade of upstream kinase activity, however, unlike MEKs, p38-MAPK activation does not have many well-described associations with RTK receptor-ligand interaction. Instead, p38-MAPK activating cascade has been observed to be switched on by extracellular stimuli such as UV light, heat, osmotic shock, oxidative stress, inflammatory cytokines (TNF-α and IL-1), growth factors (CSF-1), and GPCR activating ligands (for instance thrombin, endothelin or glutamate)[61,89]. In the canonical pathway, this eventually leads to activation of three dual-specificity MKKs/MAP2Ks (MAPK kinases); MKK6 and MKK3, being uniquely p38-MAPK specific, and MKK4. Whereas MKK6 can phosphorylate all four p38-MAPKs, MKK3 activates p38α, p38γ and p38δ, but not p38β. Additionally, p38α can also be phosphorylated by MKK4, which happens to be an activator of the JNK (Jun N-terminal kinase) pathway, as a result, functional overlap between the two MAPK pathways are frequently observed[88]. The kinases being activated not only depends on the initiating stimulus but have also been found to be cell-type or tissue specific[89]. Figure 16 briefly depicts both the canonical and alternative paths, described in the following paragraph, related to p38-MAPK activation.

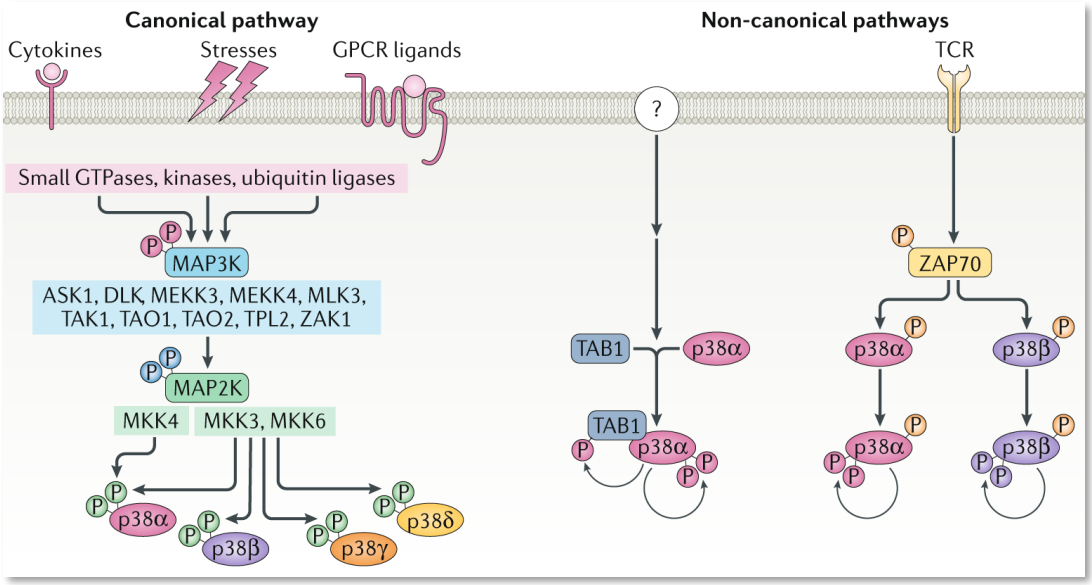

Figure 16: **Canonical and non-canonical modes of p38-MAPK activation.** The canonical pathway involves activation via upstream kinases i.e. MKK3/6. The non-canonical pathways, mostly, lead to auto-phosphorylation of p38α only, one via phosphorylation on Tyr323 by ZAP70 and the other is via direct interaction between p38α and TAB1 (from Canovas and Nebreda, 2021).

Though MKK3/6 knockout studies in mice have shown them to be important in p38-MAPK activation, alternate or non-canonical pathways of p38-MAPK activation have also been reported, which have been described to be MKK independent[61,88,89]. One of the well-defined alternate pathway, specifically observed in T-cells, involves phosphorylation of p38α and p38β on Tyr323 by the tyrosine kinases ZAP70[61,91,92], which enables p38α to auto-phosphorylate

preferentially Thr180 of the TxY activation loop[92]. However, p38α-knockin mice with Tyr323 replaced by phenylalanine were reported to be viable and fertile[93], suggesting that this non-canonical pathway does not play an exclusive, non-redundant role during pre- and post-implantation development. Another reported non-canonical pathway is involving auto-phosphorylation of p38α at the activation loop after interaction with TAB1 (transforming growth factor-β-activated protein kinase 1 (TAK1)-binding protein)[61,94]. However, TAB1 can also activate p38α canonically by binding with TAK1 (a MAP3K), thus further investigation is necessary to clearly define this non-canonical pathway and to identify if it has any role in development.

FGF-FGFR family of ligand-receptor (RTK) signalling have also been implicated in regulating p38-MAPKs, and warrant further consideration concerning preimplantation embryo development and cell fate specification. Gain-of-function mutations in *Fgfr2* gene (*Fgfr2*$^{+/Y394C}$ and *Fgfr2*$^{+/P253R}$ in modelled mice) are associated with congenital human disorders resulting in, among others, cranial and skin abnormalities such as Beare-Stevenson cutis gyrata syndrome (BSS) and Apert syndrome in humans. These mutations have been reported to enable phosphoactivation of p38-MAPKs and consequently, inhibition of p38-MAPKs has been reported to be ameliorative[95,96]. In blastocysts, FGF2-FGFR2 binding is also reported to activate the PKC-p38-MAPK pathway in TE cells and is necessary for blastocyst expansion[74]. Gain-of-function mutations in *Fgfr3* has been associated with bladder cancer, and a particular mutation (Y375C) has been reported to phosphoactivate p38-MAPKs too. This activation results in an up-regulated expression of the TF and proto-oncogene *Myc*, which in turn up-regulates *Fgfr3* gene transcription. Thus, p38-MAPK plays a crucial role in this positive feedback regulation[97].

2.1.1.3. Downstream effects of p38-MAPK activation.

The first substrate of p38α to be identified was MAPK-activated protein kinase 2 (MAPKAPK2 or MK2)[89]. Along with the closely related MK3, MK2 has been reported to activate various cytosolic and nuclear effectors, which can be grouped as having a mostly post-transcriptional regulatory role. MK2 and MK3 have been reported to activate various substrates, such as small heat shock protein 27 (HSP27), lymphocyte-specific protein 1 (LSP1), cAMP response element-binding protein (CREB) and transcription factor ATF1 among many others[89]. Interestingly, MK2 and MK3 have been found to phosphorylate ARE (AU-rich element)-binding proteins TTP (tristetraprolin), a RNA destabilising factor, and HuR, a RNA stabilising factor, and also regulates eEF2K (eukaryotic elongation factor 2 kinase), a factor important for elongation of nascent polypeptide chains during translation[88,89,98]. Thus, p38-MAPKs appear to be significant in the overall process of RNA stability and post-transcriptional regulation of gene expression, which is a poorly explored field,

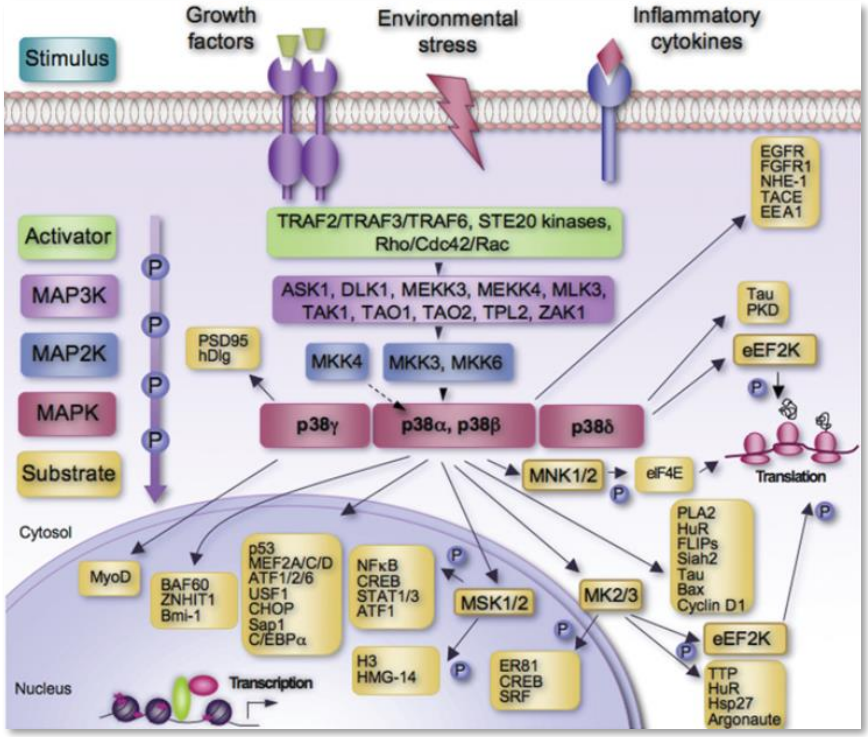

Figure 17: **p38-MAPK pathway; emphasising downstream effectors** (from Cuadrado and Nebreda, 2010).

particularly in the context of preimplantation developmental cell-fate. Continuing with the theme of post-transcriptional regulation, MK2 has also been reported to phosphorylate AGO2 (Argonaute 2) protein on Ser387, which localises AGO2 to stress-induced, cytoplasmic processing bodies (PB) *in vitro*. p38-MAPK inhibition or a serine to alanine mutation at that position was found to reduce PB localisation of AGO2[88,99]. AGO2 is a vital component of mammalian RNA interference (RNAi) and PB localisation of AGO2 is a stress-response mechanism, thus the aforementioned p38-MAPK regulation is speculated to be a stress-induced RNAi mechanism[88,99]. MSK (mitogen- and stress-activated kinase) 1 and MSK2, representing another group of p38-MAPK regulated factors, are more in-tune for immediate-early response to external stimulus[88]. MSK1 and MSK2 are known to directly interact with and activate a variety of transcription factors, and also phosphorylat other nucleosomal proteins, including histone H3 and HMG-14 (high-mobility group 14), in-turn associated with chromatin remodelling and gene-regulation[88]. MNK1 and MNK2 are two further kinase effectors of p38-MAPKs and can phosphorylate eukaryotic initiation factor-4e (eIF-4E)[88]. However, double knockout studies have produced viable and fertile offspring[100], and thus not of great significance during preimplantation embryonic development. p38-MAPK (MAPK14) has also been shown to phosphorylate FGFR1 at Ser777, resulting in FGF1 translocation into cells *in vitro*[101]. Figure 17 depicts the overall complexity and breadth of the known p38-MAPK signalling pathway. All of the details in this schematic are not covered in this review as it is not only vast but out of the scope of this thesis. However, some of the cited reviews

by Professor Angel R. Nebreda and colleagues are comprehensive, up-to-date and present more insights[61,88,102].

Physiologically, signalling via p38-MAPK pathway is known to play important roles in multitude of development and disease related events. Pro-inflammatory cytokines, like IL-1β, TNF-α and IL-6 plus other enzymes related to pathological inflammation such as COX2 and iNOS have been reported to be regulated by p38-MAPK. This in turn has led to findings that p38-MAPK dysfunction is related to rheumatoid arthritis, inflammatory bowel disorder, Alzheimer's disease, atherosclerosis among other pathologies. At the same time p38-MAPKs have also been shown to have regulatory roles in division and differentiation of immune system cells[89]. Developmentally, knockout studies have associated p38α (MAPK14) with cardiomyocyte proliferation, placental angiogenesis and foetal survival[103,104]. Whereas p38α knockout mice generally do not survive beyond mid-gestation, viable and fertile mice have been generated with p38β, p38γ and p38δ and double p38γ/p38δ knockouts[104–107]. The role of p38α appears to be one which is indispensable, at least during the post-implantation period of development (although it remains possible that the accumulated defects acquired during earlier developmental stages might be a factor in the later presentation of lethality; for example during the later stages of preimplantation blastocyst formation). That apart, cross-talk between p38-MAPKs and another major MAPK pathway, cJun N-terminal kinase (JNK), has been well-documented and associated with

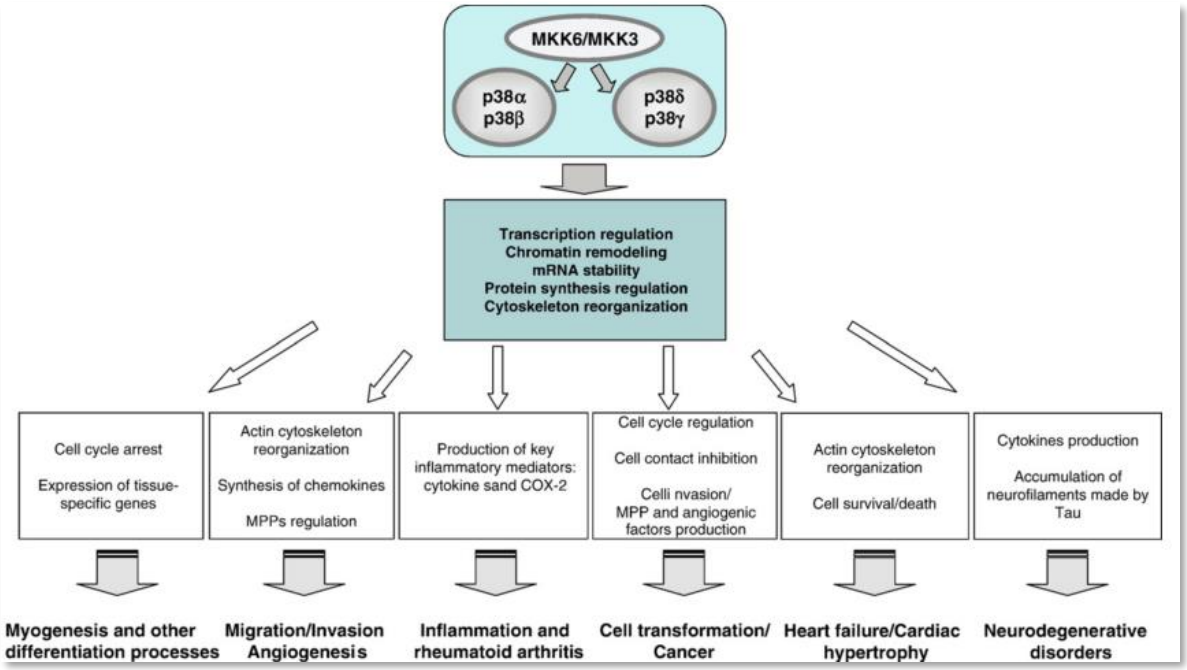

Figure 18: **Role of p38 MAPK in pathological and physiological conditions** (from Cuenda and Rousseau, 2007).

tumorigenesis, thus p38-MAPKs are often targets of pharmaceutical intervention[102]. Figure 18 is a general overview of all the potential diseases and developmental processes that have been reported to be connected with p38-MAPKs.

2.1.1.4. p38-MAPKs in development & differentiation.

Since their isolation and characterization in the early 1990's, p38-MAPKs have been reported to be involved in a variety of pathological conditions and associated with inflammation and tumorigenesis, however, reports of their role in development and differentiation have been limited. Evidence exists of p38-MAPKs being important in placental angiogenesis[89,104], and together with the JNK pathway have also been reported to be induced in primary term trophoblast upon exogenous supply of placenta growth factor (PGF), an angiogenic factor[108]. In the PC12 cell line model, a neural crest origin rat cell line, the process of differentiating into neuron-like cells upon induction by Nerve growth factor (NGF) has been reported to be mediated by the activation of p38-MAPK pathway, which in turn leads to neurite outgrowth, a mark of successful neuron-like differentiation of PC12 cells[109]. p38-MAPKs have been reported to be important in other *in vitro* models of differentiation, for example adipocyte differentiation of 3T3-L1 cells and erythropoietin-induced erythroid cell lineage differentiation[89].

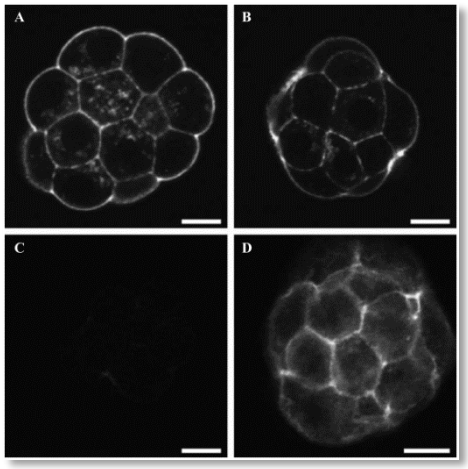

Figure 19: **Loss of filamentous actin upon p38α/β inhibition.** Rhodamine–phalloidin fluorescence to display typical actin network in 8- to 16-cell stage; A: the control group. B: group treated with 20μM SB202474 (inactive analogue). C: embryos cultured for 24 h with 20μM SB220025 displaying loss of F-actin. D: Upon removal from SB220025 treatment, embryos resumed development and restored F-actin network. Scale bar = 15μm (from Natale et al., 2004).

In preimplantation development, the role of p38 MAPKs was first reported in 2004, when p38-MAPKs along with other members of the pathway, such as, p38-MAPK-regulated or -activated kinase (PRAK; MK5), MAPK-activated protein kinase 2 (MK2), and heat shock protein 25 (HSP25) expression was reported to be affected upon exposure to small chemical inhibitors of p38-MAPKs (*i.e.* SB220025 and SB203580). 24 or 48 hour inhibition starting from E1.5 (2-cell stage) resulted in the slowing of cellular division and arrest of embryos at the 8-16-cell stages[69]. Secondly, blockade of p38-MAPKs for 24 hours led to complete loss of filamentous actin (F-actin) in 8-16-cell stages, as identified by rhodamine–phalloidin fluorescence (figure 19). This was however restored once the blockade was removed, and development resumed. Thus, p38-MAPKs were identified to be of importance in promoting development beyond the 8-16-cell stages, and to have a role in the regulation of the F-actin network during that period.

Later, it was reported that p38-MAPK and JNK pathway inhibition, but not MEK1/2 inhibition (reportedly blocking ERK1/2 and ERK5 pathways), from 8-cell stage onwards, resulted in developmental defects around the period of cavitation[62], though with the caveat of having used M16 medium, reportedly sub-optimal for *in vitro* preimplantation embryonic development[63,64]. Microarray

analysis of about 39,000 transcripts from blastocyst embryos (experimentally treated from 8-cell stage onwards) revealed a few genes with differential response to either p38-MAPK/JNK or MEK1/2 pathway inhibitions. Among the transcripts analysed further using RNAi mediated loss-of-function techniques and reported to be dependent on p38-MAPK/JNK inhibition were *Dkk1* (*Dickkopf-1*), with a possible role in inhibition of Wnt/β-catenin signalling, and *Cdx1* (*Caudal type homeobox 1*), both of which are known to be important in cell-fate and development at much later stages e.g. limb development[62]. With regards to Wnt/β-catenin signalling and its cross-talk with p38-MAPK pathway, it has been reported in mouse embryonic carcinoma F9 cells that WNT3A induced PrE-like differentiation requires Dishevelled (DVL) mediated activation of p38-MAPK, that in turn supresses GSK3β activity and ensures the activity of the canonical Wnt pathway (dependent on nuclear accumulation of β-catenin and subsequent transcriptional complexes)[110]. Accordingly, PrE differentiation of such F9 cells by WNT3A is blocked by concomitant p38-MAPK pharmacological inhibition[110]. This cross talk is depicted in figure 20 and gives an insight into how different signalling pathways can contribute towards a common phenotype.

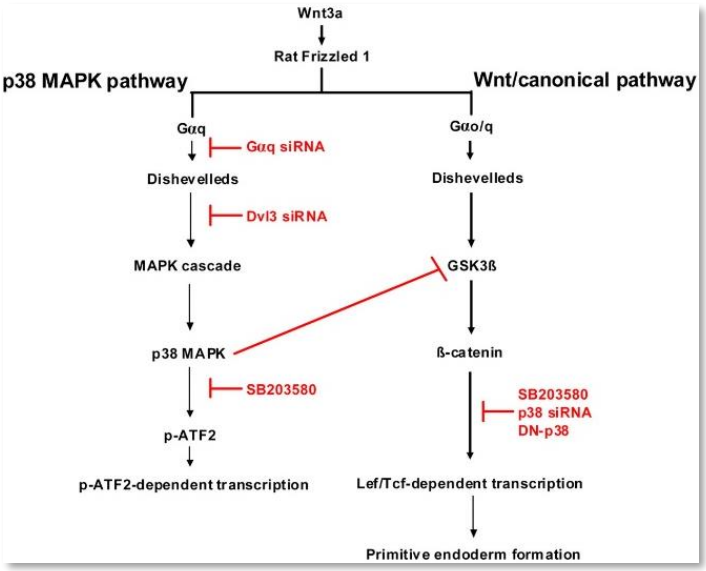

Figure 20: **Cross talk between canonical Wnt pathway and p38 MAPK pathway** (from Bikkavilli et al., 2008).

Continuing with the role of p38-MAPKs in the process of blastocyst formation, after reporting on the regulation of F-actin network formation during the 8- and 16-cell stage transition, Watson and colleagues further demonstrated a role of p38-MAPKs at the later stages of development (*i.e.* during blastocyst cavitation and hatching)[70]. They reported that early blastocyst embryos (89 hours post-hCG injection; ~E3.25) treated for 12 (~E3.75) or 24 hours (~E4.25) with p38-MAPK inhibitor, failed to either cavitate or hatch. This was shown to be a result of compromised tight junction (TJ) permeability in the TE, brought about by misregulated expression and localisation of factors important in the process of fluid filling of the blastocyst cavity, including TJ Protein1 (TJP1), Na/K-ATPase and aquaporins (AQP)[70]. Moreover, they reported that blastocysts treated for 24 hours also showed slightly increased rate of apoptosis as compared to 12 hour treatment or untreated control embryos, although they did not analyse any lineage specific effect within the blastocyst. As discussed previously, FGF2/FGFR2 mediated p38-MAPK activation has also been shown to be functional in the TE and drives blastocyst cavitation and formation (i.e. ensuring the derivation of a functional and epithelialized blastocyst)[74]. Thus, interplay between

the mechanisms driving cavitation (associated with TE specification/formation) and ICM differentiation are possible.

Work from the laboratory has demonstrated that p38-MAPK plays a role in the normal differentiation of ICM to PrE and EPI cells. Pharmacological blockade of p38-MAPKs, especially in the period of E3.5 to E3.75, results in fewer GATA4 expressing PrE cells at the late blastocyst stage (E4.5)[65].

As has been shown from multiple reports, p38-MAPK inhibition has an overall deleterious effect in and around the 16-cell to blastocyst stage of preimplantation embryo, and potentially through multiple modes of action. It was reported that p38-MAPK inhibition for 48 hours from 2-cell stage onwards, led to a decrease in both the protein and transcript levels of glucose transporters *Glut1* and *Glut4*; in addition to down-regulation in the expression of various lineage defining genes like *Nanog* and *Oct4* (EPI) and *Gata6* (PrE). This phenotype was also shown to be accompanied by apoptosis and cell death in the blastocyst, as summarised in the model (Figure 21[72]).

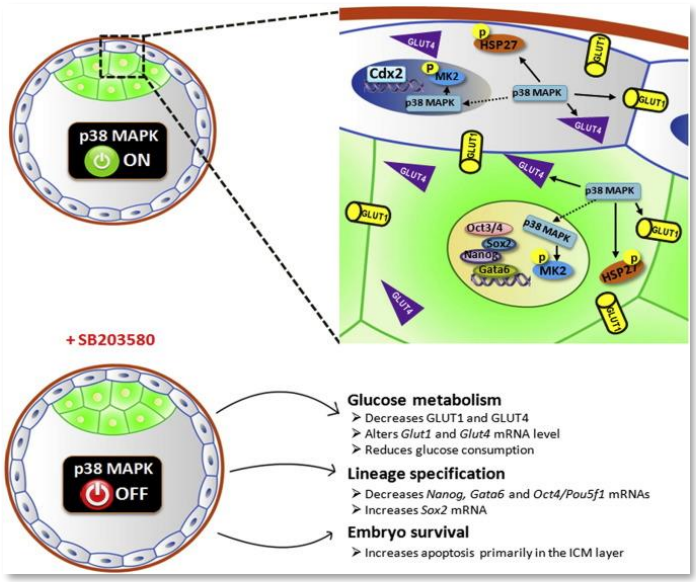

Figure 21: **Model for p38 inhibition induced regulation of GLUT1 and GLUT4 and subsequent alteration in glucose uptake.** Along with changes in the components of glucose uptake mechanism, changes were also observed in transcript levels of other important lineage defining genes and in cell death and apoptosis in blastocyst stage embryo (from Sozen et al., 2015).

In the study of preimplantation development and PrE cell fate, unlike the widely used EPI origin embryonic stem cell lines, *in vitro* models of the PrE lineage are not widespread. Thus, it is pertinent to acknowledge that there are more than one *in vitro* model of PrE lineage cells and these are being increasingly utilised, along with preimplantation embryo, to understand mechanisms behind ICM differentiation. PrE together with its derivatives are termed as extra-embryonic endoderm (ExEn) as these cells contribute to the extra-embryonic lineages that include the visceral endoderm (VE) and the parietal endoderm (PE). Three cell lines are known to be ExEn-like and comprise, PYS2 cells (derived from embryonal carcinomas (EC) and characterized as PE-like), END2 cells (also derived from ECs of another mouse strain and described as VE-like) and blastocyst derived XEN cells (described as being PrE-like)[111]. Though of different origins, these cell lines display overlapping marker gene expression and morphological phenotypes. Moreover, a detailed molecular analysis of these cell lines has revealed that the

TAK1 mediated pathway is prevalent in all three, *i.e.* harbouring the potential for a canonical pathway of p38-MAPK activation[61,111]. This also holds true in *in vitro* mouse preimplantation embryos, with chemical inhibition of TAK1 from E2.5 to E4.5 resulting in PrE deficient blastocysts[55,65]. Thus, these models provide a possible tool to analyse lineage segregation in the mouse blastocyst ICM, albeit in an *in vitro* condition. Figure 22 illustrates examples of these cell lines.

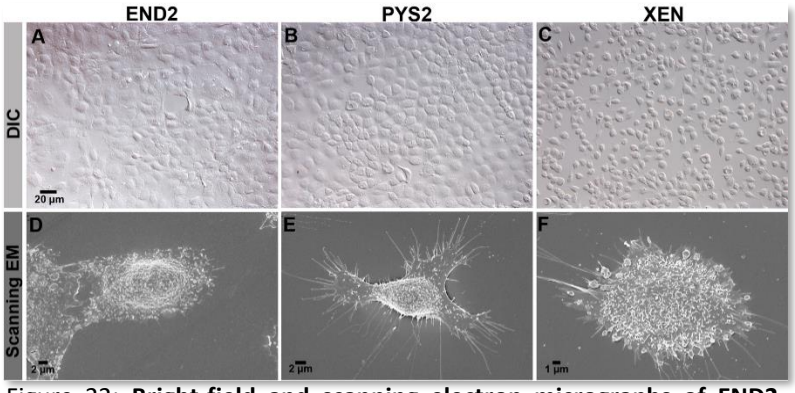

Figure 22: **Bright-field and scanning electron micrographs of END2, PYS2 and XEN cell lines** (from Brown et al., 2010).

Objectives of the thesis:

Previous work from the laboratory and others have identified functional p38-MAPKs to be a necessary component for normal preimplantation embryonic development in mice, with particular emphasis during morula to blastocyst transition and during blastocyst maturation. Though the effect of p38-MAPK inhibition on preimplantation embryo morphology and cell lineage specification have been described, mechanistic understanding remains limited. The overarching goal of the thesis is to better understand the role of p38-MAPKs during preimplantation development, specifically during blastocyst maturation, identify possible effectors and better define its position in the signalling cascades regulating developmental cell lineage specification.

Following are the primary aims:

- Refine temporal window of required p38-MAPK function during blastocyst maturation, with particular emphasis on PrE specification.
- Identify and experimentally validate potential targets of p38-MAPK phosphorylation activity necessary for normal preimplantation development and lineage specification.
    - Identification of candidates using phosphoproteomic mass spectrometry.
    - Experimental validation of candidates by microinjection of gene-specific siRNA at E1.5 and immunofluorescence confocal microscopy at E4.5 (assaying inner cell lineages), and image analysis.
- Identify system-wide effects of p38-MAPK activity and define its role towards regulating blastocyst maturation and associated lineage specification.
    - Proteomic mass spectrometry identified differences in proteome upon p38-MAPK inhibition during blastocyst maturation.
    - Multi time point transcriptomics to define differential gene expression dynamics facilitated by p38-MAPKs during blastocyst maturation.
- Further understanding of the mechanism of p38-MAPK activity towards typical blastocyst maturation and survival under conditions of amino acid deprivation.

Chapter I:

p38-MAPK-mediated translation regulation during early blastocyst development is required for primitive endoderm differentiation in mice.

Pablo Bora, Lenka Gahurova, Tomáš Mašek, Andrea Hauserova, David Potěšil, Denisa Jansova, Andrej Susor, Zbyněk Zdráhal, Anna Ajduk, Martin Pospíšek and Alexander W. Bruce.

(accepted at **Communications Biology**)

Pre-print title: p38-MAPK mediated rRNA processing and translation regulation enables PrE differentiation during mouse blastocyst maturation.

bioRxiv 2020.11.30.403931

p38-MAPK-mediated translation regulation during early blastocyst development is required for primitive endoderm differentiation in mice

Pablo Bora[1,*], Lenka Gahurova[1,2], Tomáš Mašek[3], Andrea Hauserova[1], David Potěšil[4], Denisa Jansova[2], Andrej Susor[2], Zbyněk Zdráhal[4], Anna Ajduk[5], Martin Pospíšek[3], Alexander W. Bruce[1,*]

[1]Laboratory of Early Mammalian Developmental Biology (LEMDB), Department of Molecular Biology & Genetics, Faculty of Science, University of South Bohemia, Branišovská 31, 37005 České Budějovice, Czech Republic.

[2]Laboratory of Biochemistry and Molecular Biology of Germ Cells, Institute of Animal Physiology and Genetics, CAS, Rumburská 89, 27721 Liběchov, Czech Republic.

[3]Laboratory of RNA Biochemistry, Department of Genetics and Microbiology, Faculty of Science, Charles University, Viničná 5, 12844 Prague 2, Czech Republic.

[4]Central European Institute of Technology, Masaryk University, 62500 Brno, Czech Republic.

[5]Department of Embryology, Institute of Developmental Biology and Biomedical Sciences, Faculty of Biology, University of Warsaw, Miecznikowa 1, 02-096, Warsaw, Poland.

***Corresponding authors**

E-mail: borapa00@prf.jcu.cz

E-mail: awbruce@prf.jcu.cz

Abstract

Successful specification of the two mouse blastocyst inner cell mass (ICM) lineages (the primitive endoderm (PrE) and epiblast) is a prerequisite for continued development and requires active fibroblast growth factor 4 (FGF4) signaling. Previously, we identified a role for p38 mitogen-activated protein kinases (p38-MAPKs) during PrE differentiation, but the underlying mechanisms have remained unresolved. Here, we report an early blastocyst window of p38-MAPK activity that is required to regulate ribosome-related gene expression, rRNA precursor processing, polysome formation and protein translation. We show that p38-MAPK inhibition-induced PrE phenotypes can be partially rescued by activating the translational regulator mTOR. However, similar PrE phenotypes associated with extracellular signal-regulated kinase (ERK) pathway inhibition targeting active FGF4 signaling are not affected by mTOR activation. These data indicate a specific role for p38-MAPKs in providing a permissive translational environment during mouse blastocyst PrE differentiation that is distinct from classically reported FGF4-based mechanisms.

Introduction

During the preimplantation stage of mouse embryonic development, three blastocyst lineages emerge from two cell fate decisions. The first decision involves spatial separation of an outer epithelium of extraembryonic and differentiating trophectoderm (TE) cells (precursors of the placenta) from a population of pluripotent inner cell mass (ICM) cells and is regulated by polarity-dependent differential Hippo pathway activation[1,2]. The second decision starts at approximately embryonic day (E) 3.25 and results in the specification and segregation of ICM cells between the pluripotent epiblast (EPI – contains the progenitor cells of the future fetus and resides deep in the ICM) and a second differentiating extraembryonic epithelium called the primitive endoderm (PrE – a polarized monolayer of superficial ICM contacting the fluid-filled cavity) by the late blastocyst (E4.5) stage[1]. Around the midpoint of blastocyst maturation (E4.0), the embryo no longer occupies a volume equivalent to that of the zygote and begins a process of nonlinear cavity expansion typified by pulsed expansions and contractions and eventual rupture of the encapsulating *zona pellucida* to permit uterine implantation (E4.5 onwards)[3].

Mouse blastocyst ICM lineage formation is under the regulation of the fibroblast growth factor (FGF)-extracellular signal-regulated kinase (ERK) signaling axis and initiates from an uncommitted population of early ICM cells coexpressing both the pluripotency-related transcription factor NANOG and the PrE-related transcription factor GATA6. Accordingly, FGF4 derived from specifying EPI progenitors acts upon precursor PrE cell populations, most significantly via FGF-receptor 1 (FGFR1), to drive precursor PrE cell differentiation[4,5]. The binding of FGF4 to FGFR1 (and to a lesser extent FGFR2) activates the ERK pathway to cause downregulation of NANOG protein expression and enables GATA6 to initiate transcription of other PrE lineage-specific genes (*e.g., Sox17* and *Gata4,* as reviewed previously[1,2]). Concomitantly, GATA6 protein expression is downregulated in EPI progenitors, resulting in a spatially randomized pattern of mutually exclusive NANOG and GATA6 expression within the ICM by the mid-blastocyst stage (E4.0)[4-10], termed the “salt & pepper” pattern of EPI and PrE progenitors[11]. This is then resolved by active cell movement, primarily mediated by migration of PrE-fated cells towards the cavity, and selective apoptosis to result in the defined ICM tissue layers of the late blastocyst (E4.5)[12,13]. Although homozygous *Fgf4* and combined *Fgfr1-Fgfr2* genetic knockouts can initiate coexpression of GATA6 and NANOG within nascent ICM nuclei, GATA6 expression is rapidly lost as the blastocyst matures (and all ICM cells solely express the EPI marker NANOG), underscoring the importance of the FGF-ERK signaling axis to PrE formation[4,5,7]. However, specified PrE survival is also dependent on platelet-derived growth factor (PDGF) signaling and activation of phosphoinositide 3-kinase (PI3K) and mechanistic target of rapamycin (mTOR)[14,15], possibly in association with activated FGFR2[16]. Recently, ICM lineage-specific specification and spatial refinement have also been reported to correlate with blastocyst cavity expansion[13], a process enabled by TE-mediated transport of water (via aquaporins), sodium ions (via sodium-potassium

(Na^+/K^+) ATPases), and chloride ions (via apical Cl^- channels) and by promotion of sodium-hydrogen ion exchange[17-21].

The members of the p38 family of mitogen-activated protein kinases (p38-MAPKs), comprising p38-α (MAPK14), p38-β (MAPK11), p38-γ (MAPK12/ERK6), and p38-δ (MAPK13/SAPK4), are widely studied stress-activated kinases implicated in inflammatory disease and development[22-24]. p38-MAPKs are known to be canonically activated by upstream mitogen-activated kinase kinases 3 and 6 (MAP2K3 and MAP2K6 – reviewed here[22]). However, members of the FGFR family of ligand-receptor kinases are also reported to activate p38-MAPKs (reviewed here[25]), and specific *Fgfr2* gain-of-function mutations (*Fgfr2*$^{+/Y394C}$ and *Fgfr2*$^{+/P253R}$) correlate with increased phosphorylation and activation of p38-MAPKs[26,27]. Indeed, Beare-Stevenson cutis gyrata syndrome, a genetic human condition caused by paralogous *FGFR2* mutations, results in increased phosphoactivation of the FGFR2 effector substrate FRS2[26], itself a known p38-MAPK (and ERK1/2) substrate (albeit in relation to FGF1-mediated signaling)[28,29]. p38-MAPKs are also reported to be phosphoactivated via FGFR3-mediated signaling cascades[30], and FGFR3 is robustly expressed in late blastocyst (E4.5) PrE but not EPI cells[31]. Hence, the full functional roles of p38-MAPK activity are not necessarily limited to the classically studied canonical pathways.

In the context of early mouse development, *Mapk14* genetic knockout causes aberrant placental phenotypes, impaired oxygen and nutrient transfer and embryonic lethality[32]. p38-MAPK pharmacological inhibition (p38-MAPKi) of *in vitro*-cultured 2-cell-stage embryos causes 8- to 16-cell-stage developmental arrest[33], and inhibition post 16-cell stage is reported to result in failed TE differentiation and function[34,35]. Previously, we demonstrated that p38-MAPKi beginning at E3.5 (to avoid inhibiting TE specification) robustly impairs ICM differentiation towards PrE and results in late blastocyst (E4.5) embryos with increased numbers of uncommitted ICM cells (coexpressing NANOG and GATA6) but has minimal effects on EPI cell generation (defined by sole expression of NANOG). Additionally, we have reported that p38-MAPK mitigates amino acid (AA) depletion-induced oxidative stress, which is detrimental to the formation of both ICM cell lineages. However, the underlying molecular processes by which p38-MAPK activity affects ICM, specifically PrE, lineage formation and the extent to which p38-MAPK is integrated within the existing framework of mechanistic knowledge remain largely unknown.

Using specific pharmacological-based interventions, we herein identified a minimum early mouse blastocyst window of p38-MAPK activity required for germane PrE differentiation. Employing (phospho-)proteomic and transcriptomic approaches to this window, we identified dysregulated protein translation as a major component of p38-MAPKi-induced PrE phenotypes. This dysregulation manifests as reductions in the expression of ribosome-related proteins, abnormal elevations in translation-related gene transcript levels, accumulation of unprocessed rRNA precursors and impairment of polysome formation and protein translation. We also report that these p38-MAPKi-mediated PrE phenotypes can be partially reversed by activating the archetypal

translational regulator mTOR but that a failed PrE differentiation phenotype associated with ERK pathway inhibition targeting active FGF signaling is not similarly reversed. Finally, we functionally assayed a list of candidate p38-MAPK effector proteins obtained via phosphoproteomic analyses of mouse blastocysts ±p38-MAPKi and identified MYBPP1A as a potential downstream p38-MAPK functional mediator of the PrE phenotypes described. Collectively, these data indicate a specific role for p38-MAPKs in providing a permissive translational environment that is compatible with PrE differentiation in the mouse blastocyst and is most likely distinct from classically reported FGF-based mechanisms of PrE derivation.

Results

Inhibition of p38-MAPK activity after E3.5 induces a PrE deficit and blastocyst cavity expansion defect

Previously, we identified p38-MAPK function between E3.5 and E3.75 as necessary for normal PrE differentiation by E4.5[36]. However, we wanted to further refine this required window and to assay the p38-MAPK-associated PrE phenotypes in more detail. We therefore exposed blastocysts to just three hours (E3.5 +4 to +7 hours (h)) of p38-MAPKi (20 μM SB220025[33,36,37] – dimethyl sulfoxide (DMSO) vehicle controls were also tested) and found that it was still sufficient to significantly impair PrE differentiation (Figure 1b), albeit not as robustly as when p38-MAPKi was provided throughout the blastocyst maturation period (E3.5 to E4.5 – Figure 1c). We previously also observed that such extended p38-MAPKi seemed to cause reduced blastocyst sizes and cavity volumes, particularly in the absence of supplemented AAs[37]. We therefore directly quantified cavity volumes in our fixed embryo samples after p38-MAPKi from E3.5-E4.5 (Figure 1d). We observed statistically significant smaller cavities after p38-MAPKi (3316 μm^2) than in controls (6255 μm^2), thus quantitatively confirming our previous observations[36,37]. Extending this analysis, we employed *in vitro* p38-MAPKi (E3.5-E4.5) blastocyst imaging to dynamically observe cavity formation (often used to report blastocyst viability in assisted reproductive technologies[38,39]). We found that p38-MAPKi blastocysts initially expanded and displayed pulse-like cavity volume oscillations akin to those of control blastocysts in the first three hours of culture (Figure 1e and Supplementary Videos 1-6). However, the rate of expansion in p38-MAPKi blastocysts markedly slowed in the succeeding seven hours (expansion from an average equatorial area of 6254 μm^2 to 7393 μm^2) compared to controls (expansion from 6491 μm^2 to 8769 μm^2 – Figure 1e (Hours 3 to 10)). The control blastocysts then continued expanding, albeit at a reduced rate (achieving an area of 9603 μm^2 after fifteen hours), but the p38-MAPKi blastocysts did not expand (7642 μm^2 – (Figure 1e (Hours 10 to 15)). From this point onwards (ending after 24 h and at E4.5), the control embryos continued the slower rate of expansion

(culminating in an average size of 10807 μm^2), and 90.6% hatched from the *zona pellucida*; in contrast, the p38-MAPKi embryos remained unexpanded (averaging 7047 μm^2 in size), and in 40.6% of cases, they failed to hatch and were often associated with cavity collapse (Figure 1e and e (Hours 15 to 22)).

We next assayed the mRNA levels of each p38-MAPK paralog (*i.e., Mapk11*, *Mapk12*, *Mapk13* and *Mapk14*, plus the ICM lineage markers *Nanog* and *Gata4*) during early blastocyst maturation in order to correlate the expression of these genes with the observed p38-MAPKi-sensitive period. The results revealed that *Mapk13* and *Mapk14* (encoding p38-δ and p38-α isoforms, respectively) were the only robustly expressed p38-MAPK transcripts in early blastocysts. Moreover, *Nanog* and *Gata4* mRNA levels increased when *Mapk14* transcript expression peaked between the assayed E3.5 +6 h and E3.5 +9 h time points (Figure 1f). This period partly overlaps with the minimum window of p38-MAPKi sensitivity regarding PrE differentiation (Figure 1b, c) and the transition from impaired to blocked cavity expansion (Figure 1e). These data implicate the *Mapk14* gene as the prime phenotype-mediating candidate. However, they do not rule out the other paralogs, especially *Mapk13*, given that *Mapk14*-null embryos are recovered in normal Mendelian ratios until E10.5[32], suggesting some level of functional redundancy and/or p38-MAPK maternal protein inheritance. Interestingly, *Mapk14* genetic knockout alone is embryonic lethal[32,40] (unlike knockout of the three other paralogs[41,42]).

Collectively, these introductory data confirm that p38-MAPK(s) plays a transient role during early blastocyst maturation, which subsequently ensures appropriate PrE differentiation and blastocyst cavity expansion. The most important period is between the third and tenth hours after E3.5 (but can be refined to a minimum 3-hour window).

p38-MAPK inhibition in developing blastocysts affects the translation machinery

To gain a molecular understanding of how p38-MAPK activity exerts its effect on PrE differentiation, we employed global analyses of (phospho-)proteomic changes induced by p38-MAPKi. Using a mass spectrometry (MS)-based approach, we assayed the total proteomes and phosphoproteomes of cultured mouse blastocysts exposed to seven hours of p38-MAPKi (spanning the confirmed minimum developmental sensitive window – E3.5 +2 to +9 h). We acknowledged that the output would comprise data from both TE and ICM lineages but reasoned that identification of differentially expressed (phospho-)proteins (between the p38-MAPKi and control conditions) might be able to provide important mechanistic insight and possibly (in the case of the phosphoproteome) identify direct p38-MAPK effector substrates. We detected 77 downregulated and 53 upregulated proteins associated with p38-MAPKi (Figure 2c and Supplementary Data 1). Subsequent ontological analysis revealed that the only significantly enriched terms were directly related to “translation” or “ribosome assembly” (hereafter

collectively referred to as “translation” – Figure 2b and Supplementary Data 1), which together comprised 28 of the differentially expressed proteins (Figure 2c). Of these, 23 were downregulated, and 5 were upregulated (Figure 2c). Hence, p38-MAPKi during early blastocyst maturation dysregulates a specific cohort of translation-associated proteins, mostly resulting in their reduced expression.

A similar investigation of acquired phosphoproteomic data revealed 156 significantly and differentially enriched phosphopeptides (exhibiting ≥1.5-fold differential abundance; 99 enhanced and 57 depleted). Collectively, these phosphopeptides represented 110 individual proteins and corresponded to 59 proteins with solely enhanced phosphorylation, 41 proteins with solely depleted phosphorylation and 10 proteins with both enhanced and depleted levels of phosphorylation at distinct sites (detailed in later sections). Of the 51 identified proteins for which at least one depleted phosphopeptide was detected (6 proteins contained two distinct depleted phosphopeptides), we identified 14 listed in the *PhosphoSitePlus* database[43] as confirmed or predicted p38-MAPK substrates (representing all four p38-MAPK isoforms in both human and mouse models – Supplementary Table 1). Twenty-four of the 57 depleted phosphopeptide sequences (42.1%) contained the consensus [S/T]P dipeptide phosphorylation motif typical of the proline-directed mitogen-activated kinase superfamily in general[44] (Supplementary Table 1), suggesting that they may be direct p38-MAPK substrates. An ontological analysis of all the phosphoproteomic screen-identified genes (comprising enhanced and/or depleted phosphopeptides) revealed enrichment of RNA regulation and stability terms (Figure 2d and Supplementary Data1) that were consistent with translation-related terms identified for the general proteome (Figure 2b). Collectively, these findings suggest that p38-MAPKi may impair general protein synthesis. We also noted terms related to cell cycle regulation, DNA replication and chromatin modification (Figure 2d and Supplementary Data 1), which was perhaps unsurprising given the known wide range of p38-MAPK effectors[23].

To complement the (phospho-)proteomic analyses and provide an extra layer of mechanistic insight, we conducted transcriptomic analyses of p38-MAPKi-treated blastocysts at three different early blastocyst time points (E3.5 +4 h, +7 h and +10 h of p38-MAPKi – Figure 3a). We detected 34 differentially expressed transcripts at the +4 h time-point, 1240 at the +7 h time-point and 480 at the +10 h time-point in the treated blastocysts compared to the control blastocysts; only 10 differentially expressed mRNAs overlapped all three inhibition regimes (Figure 3b and Supplementary Data 1). These data indicated the occurrence of large changes in the p38-MAPK-regulated transcriptome that are maximally centered around the E3.5 +7 h time-point (Figure 3b and Supplementary Data 1), specifically a cohort of differentially expressed transcripts comprising both upregulated and downregulated genes (Supplementary Data 1). Hierarchical clustering of this gene cohort across all assayed treatments and time points identified three clusters of coregulated genes (Figure 3c – a similar clustering of differentially

regulated genes at E3.5 +4 h and E3.5 +10 h is provided in Supplementary Fig. 1a and b and Supplementary Data 1). Cluster I represents transcripts that were downregulated after p38-MAPKi at the E3.5 +4 h time point, were maximally repressed at E3.5 +7 h but returned to levels equivalent to the control levels by E3.5 +10 h. The transcripts in cluster III demonstrated a similar but inverted trend. Namely, at E3.5 +4 h, p38-MAPKi initiated an increase in transcript expression that peaked by E3.5 +7 h, but the expression returned to control levels by E3.5 +10 h. Cluster II comprised similarly enhanced transcripts but was distinguished from cluster III in that its transcripts did not return to control levels by E3.5 +10 h (Supplementary Data 1 Fig. 3c (clusters II and III)). Thus, p38-MAPKi caused large-scale transcriptomic changes that peaked at the E3.5 +7 h time point and (with the exception of the enhanced gene transcripts of cluster II) largely returned to levels observed in control blastocysts by the E3.5 +10 h time point via compensation. Notwithstanding such compensation, it is important to recall that p38-MAPKi throughout this same period (or in the identified minimum window) is sufficient to ultimately impair PrE differentiation (Figure 1 and previous publications[36,37]), potentially due to impaired mRNA translation (see below). Interestingly, we did not observe statistically significant mRNA expression changes of the same differentially regulated genes among the three control conditions (+DMSO at E3.5+ 4 h, +7 h and +10 h), indicating these genes are not normally subject to dynamic regulation during this period. Remarkably, an ontological analysis of enriched terms associated with such p38-MAPKi-sensitive transcripts again identified translation-related terms as the most significantly enriched (Figure 3d and Supplementary Data 1), which was mostly reflected by upregulated expression (cluster III, Figure 3c). Of these 82 differentially expressed translation-related mRNAs (Supplementary Data 1 Fig. 3d, e), 79 were upregulated after p38-MAPKi (Supplementary Data 1 Fig. 3d, e). Interestingly, 13 of those 79 transcripts (mainly representing small ribosomal subunit proteins) were also identified as downregulated in the general proteome (Figure 3e and Supplementary Data 1). These data suggest that the accumulation of translation-related mRNAs caused by p38-MAPKi (peaking at E3.5 +7 h) may reflect impaired ribosomal assembly and/or functional protein translation. Moreover, they also indicate a potential positive feedback mechanism culminating in the observed transient increases in translation/ribosome-related gene transcript levels (Figure 3c and d). Other ontological terms enriched at E3.5 +7 h were connected to mitochondrial respiration (also upregulated – cluster III, Figure 3c) and splicing (associated with both upregulated and downregulated transcripts – clusters I and III, respectively, Figure 3c).

Overall, the combined results of the (phospho-)proteomic and transcriptomic analyses point to the regulation of translation as a primary function of p38-MAPK activity during early blastocyst maturation, which may help create a permissive state for germane PrE differentiation.

p38-MAPK inhibition reduces active translation during early blastocyst maturation

Informed by the (phospho-)proteomic and transcriptomic screens, we hypothesized that p38-MAPKi-induced PrE phenotypes are associated with disrupted protein translation during early blastocyst maturation. To test this hypothesis, we assayed the effect of p38-MAPKi on translation during a 10-hour period (starting from E3.5) utilizing an O-propargyl-puromycin (OPP) incorporation assay that permits direct fluorescent labeling and quantification of nascent translated polypeptides (Figure 4a). As expected, we observed nearly 50% less global protein synthesis under p38-MAPKi conditions than under control conditions (Figure 4b). We also verified the observed reduction in active translation (in the same time-period) using a polysome profiling approach, adopting our recently reported protocol of scarce-sample polysome (SSP) profiling[45]. This involved obtaining ten fractions representing individual ribosomal subunits, monosomes and polysomes from 10 blastocysts per control or p38-MAPKi condition in quadruplicate. The fractions were then processed for total RNA extraction and cDNA synthesis and analyzed by qRT-PCR to specifically assay 18S and 28S rRNA levels. We observed shifts in the distributions of both 18S and 28S rRNA abundance towards SSP fractions indicative of free rRNAs or associations with individual ribosomal subunits/monosomes (fractions 1-5) versus denser fractions indicative of polysomes (fractions 6-10) after p38-MAPKi (Figure 4c). We also expressed the results as calculated polysome-to-nonpolysome ratios (with increased ratios indicative of enhanced active translation – Figure 4d). Interestingly, the reduction in the polysome-to-nonpolysome ratio was greater for 28S rRNA than for 18S rRNA (Figure 4d). On the basis of these combined data, we conclude that active translation is reduced in intact early mouse blastocysts under p38-MAPKi conditions.

rRNA processing in early blastocysts is impaired by p38-MAPK inhibition

Due to the general dysregulation of translation-related gene expression in early blastocysts and the confirmed impairment of active protein translation caused by p38-MAPKi, we sought to identify other contributory mechanisms underlying the associated PrE differentiation phenotypes. Upon searching the list of potential p38-MAPK effectors identified in the phosphoproteomic screen, we identified MYBPP1A (from which 6 individual differentially expressed phosphopeptides had been detected under p38-MAPKi conditions; expanded below). MYBPP1A interacts with HTATSF1, a factor known to be involved in transcriptional and posttranscriptional regulation/processing of rRNA and mRNA and regulation of protein synthesis and a confirmed modulator of *in vivo* embryonic pluripotency (during the transition from pre- to postimplantation development)[46]. Thus, we assayed the effect of p38-MAPKi on 45S pre-rRNA processing during the early blastocyst developmental window (E3.5 +10 h – employing the same qRT-PCR primers used in the HTATSF1 report of Corsini *et al*.[46]). This revealed that p38-MAPK regulates rRNA processing (Figure 4e and f). Specifically, we observed enhanced levels of PCR amplicons indicative of impaired processing. For example, the levels of the internal transcribed

spacer 2 (ITS2) region, normally removed from processed 45S pre-rRNA, were increased nearly 3-fold by p38-MAPKi. Similarly, the levels of 5' external transcribed spacer (ETS) amplicons were increased, as were those of regions representative of the overlap between ITS2 and the mature 28S rRNA coding sequence, plus the overlapping region between the ETS and 18S rRNA; all of these changes indicated impaired 45S pre-rRNA processing. Upon assaying regions of the 45S pre-rRNA corresponding to mature (appropriately processed) rRNA transcripts, we also observed increases in 28S and 5.8S rRNA levels, presumably reflecting unprocessed 45S pre-rRNA intermediates. However, similar assays of the 18S rRNA transcript were not associated with increased abundance, suggesting that steady-state levels of processed 18S rRNA were not significantly affected. This was also reflected in the unchanged levels of ITS1 and distinguished p38-MAPKi-derived data from studies on *Htatsf1* genetic knockouts, in which ITS levels were increased (and ETS levels were reduced)[46]. Notwithstanding such differences, our data confirm a role for p38-MAPK in regulating 45S pre-RNA processing in early blastocysts that can feed forward to influence active protein translation.

Early blastocyst transcription is attenuated by p38-MAPK inhibition

In the context of peri-implantation embryonic development and *in vitro* pluripotency, recent reports have drawn important correlations between general translational status and permissive transcriptional landscapes. We investigated whether the observed p38-MAPKi-mediated defects in protein synthesis were also associated with reduced transcription (Figure 4g and h). Consistently, we observed reductions in the levels of histone H4-lysine 16 acetylation (H4K16ac, a posttranslational mark of actively transcribed chromatin[47]) in both inner and outer cells, as demarcated by the expression of CDX2 (an outer cell TE marker[48]), in p38-MAPKi-inhibited blastocysts (E3.5 +10 h). Similarly, immunofluorescence staining for actively elongating RNA polymerase II (using an antibody recognizing RNA polymerase II phosphorylated on serine-2 of the C-terminal domain – RNA pol II S2p[49]) showed marked decreases.

Hence, p38-MAPKi during early blastocyst maturation, known to negatively affect PrE differentiation (as described above[36,37]), is collectively associated with impaired translation, polysome formation, rRNA processing and a chromatin landscape suggesting reduced active transcription.

p38-MAPK and mTOR have partially overlapping roles in regulating blastocyst development

Although p38-MAPK activity is reported to regulate protein synthesis in some contexts[50], mTOR-mediated translation regulation is the most extensively studied pathway, particularly with regard to development[51]. Cancer biology studies have indicated a possible convergence of both

pathways that positively regulates eIF4E-sensitive cap-dependent mRNA translation[52,53]. Given the prominent role mTOR plays in translation regulation and a recent report describing blastocyst diapause caused by attenuated translation and transcription after mTOR inhibition[54], we investigated our observed p38-MAPKi phenotypes in conjunction with mTOR activity. First, we compared p38-MAPKi and mTOR inhibition phenotypes. Early blastocysts (E3.5) were cultured in the presence of DMSO (control), TORIN1 (an mTOR inhibitor[55]) and SB220025 (a p38-MAPK inhibitor) for 24 h and immunofluorescently stained for ICM cell lineage markers (NANOG for EPI and GATA4 & GATA6 for PrE – Figure 5a). mTOR inhibition, like p38-MAPKi, caused a statistically significant increase in the proportion of NANOG- and GATA6-coexpressing cells within the ICM (Figure 5b-d and p); NANOG and GATA6 coexpression is a hallmark of unspecified cells[11] and a potentially diapaused state. Likewise, the numbers of PrE cells (defined by sole GATA4 expression – Figure 5b-d, n and o) in both p38-MAPKi and mTOR inhibited blastocysts were also significantly reduced, confirming our previous p38-MAPKi observations[36,37] and the report of diapause in mTOR-inhibited blastocysts[54]. However, despite the similarities, mTOR-inhibited blastocysts had fewer EPI (and overall ICM) cells than p38-MAPKi and control embryos (defined by sole NANOG expression - Figure 5b-d, l and m), indicating that mTOR-inhibited blastocysts are diapaused at the early blastocyst stage and characterized by an unspecified ICM. Conversely, p38-MAPKi blastocysts did have specified EPI cells and exhibited impairment only in PrE formation (retaining a population of unspecified ICM cells), indicating that the p38-MAPKi phenotype and the associated translational defects are squarely centered on PrE differentiation. Therefore, p38-MAPKi does not merely phenocopy mTOR inhibition-induced diapause (as further supported by the inability of p38-MAPKi, unlike mTOR inhibition[54], to sustain long-term *in vitro* embryo survival after E4.5 – Supplementary Fig. 2). However, the data also do not exclude possible p38-MAPK and mTOR functional convergence in the limited context of PrE differentiation.

Therefore, we next tested whether the p38-MAPKi-mediated PrE phenotypes could be ameliorated by pharmacological activation of mTOR. We utilized the potent mTOR activator MHY1485[56], which, when provided in isolation to maturing blastocysts (E3.5-E4.5), did not affect development or derived ICM cell fate (Figure 5a, e and j-q). However, the number of GATA4-expressing PrE cells was statistically greater when MHY1485 was administered in combination with p38-MAPKi than when p38-MAPKi was administered alone (but was not at the levels seen in controls – Figure 5a, b, f and n). There was also a reduced contribution of the otherwise typical p38-MAPKi-induced population of unspecified ICM cells (Figure 5p), but there was no change in EPI cell numbers (also reflected by the calculated PrE-to-ICM ratios – Figure 5j-m). Intriguingly, mTOR activation under p38-MAPKi also resulted in coexpression of NANOG and GATA4 by a statistically significant population of ICM cells, which was seldom observed in all other conditions, including control conditions (Figure 5f and q). These data show that p38-MAPKi-mediated deficits in PrE differentiation associated with a unique population of unspecified PrE progenitors can be

partially overcome by activation of mTOR without an accompanying decrease in NANOG expression.

The FGF4-ERK signaling cascade is considered the archetypal ICM cell fate-determining mechanism of mouse blastocysts[57]. Therefore, we also assayed whether PrE differentiation phenotypes induced by inhibition of the ERK pathway (via targeting of MEK1/2, also known as MAP2K1/2, with PD0325901[58]) were sensitive to mTOR activation. While ERK pathway inhibition (E3.5-E4.5) resulted in the well-defined phenotype of largely pan-ICM expression of NANOG alone, PrE was not rescued by additional activation of mTOR; rather, PrE inhibition was augmented (Figure 5g, h and j-q). We conclude that the role of p38-MAPK in ICM cell fate specification via translation regulation is functionally and mechanistically distinct from that of the described FGFR-ERK pathway.

We have previously reported that p38-MAPK also acts to counter AA depletion-induced oxidative stress in mouse blastocysts, as revealed by an exacerbation of ICM cell fate phenotypes affecting both EPI and PrE when p38-MAPKi is combined with an absence of exogenous AA in the medium[37]. We hypothesized that activating mTOR may also alleviate such enhanced effects (E3.5-E4.5). However, unlike those cultured in the presence of supplemented AA, blastocysts cultured under such conditions did not demonstrate any induced inner cell GATA4 expression or increased inner cell numbers, nor were there any increases in the numbers of EPI cells expressing NANOG alone (Figure 5i and j-q). We conclude that the previously identified role of p38-MAPK in counteracting oxidative stress is distinct from that described here in relation to mTOR activity and translation.

MYBBP1a has a prominent role in preimplantation embryonic development

Having uncovered a role for p38-MAPK in regulating translation and PrE differentiation in early blastocysts, we sought to identify and functionally verify contributing p38-MAPK effectors. We anticipated that our list of p38-MAPKi-induced differentially expressed phosphoproteins would include strong candidates (Figure 2d and Supplementary Data 1). We filtered out detected phosphopeptides (and associated phosphoproteins) demonstrating <1.5-fold changes in phosphorylation and retained those exhibiting <1.3-fold changes in general protein abundance (Figure 6a and Supplementary Data 1). We further refined the list according to the published literature (identifying proteins/genes shown or hypothesized to regulate pluripotency, differentiation and protein translation) and selected six genes (highlighted in Figure 6a – associated with one or more differentially phosphorylated peptides/proteins) for functional assays in embryonic clonal loss-of-function experiments (*Dnmt1, Kdm2B, Ybx1, Mybbp1a, Rpl22l1* and *Nolc1*). All genes were robustly and equally expressed at the mRNA level in published screens of mouse blastocyst ICM and TE lineages, implying that their functional regulation is likely

to be post-transcriptional[59,60] (Supplementary Fig. 3). We employed candidate-specific siRNA constructs (or non-targeting controls) to knockdown gene expression in marked preimplantation embryo cell clones. The appropriate siRNA and a recombinant mRNA encoding a histone H2B-RFP fusion reporter were microinjected into one cell of 2-cell-stage (E1.5) embryos to create a fluorescently marked and traceable cell clone composing half the embryo. The embryos were cultured to the late blastocyst (E4.5) stage and immunofluorescently stained for ICM cell fate markers (NANOG for EPI and GATA4 for PrE). Two-cell-stage embryos microinjected in both blastomeres and cultured to the late blastocyst stage were subjected to qRT-PCR to assess specific candidate gene transcript knockdown (Figure 6b). We found that targeting *Mybbp1a* had the most substantial developmental impact among the six shortlisted genes, despite relatively modest (59%) transcript knockdown efficiency (Figure 6c); the effects of knockdown of the other candidate genes are summarized in the Supplementary Information (Supplementary Table 3). MYBBP1A is a predominantly nucleolar protein reported to negatively regulate RNA polymerase I-dependent rRNA gene transcription, cotranscriptional processing and ribosome biogenesis[61,62]; p53 tetramerization, cell senescence and apoptosis[63,64]; and *Hoxb2* gene transcription[65]. Additionally, homozygous *Mybbp1a*-null blastocysts resulting from crosses of heterozygous *Mybbp1a*-null mice cannot develop[66], implying an important but as-yet-undefined role(s) of *Mybbp1a* in preimplantation development. Clonal analysis of marked *Mybbp1a*-knockdown cells revealed a 19% contribution to the late blastocyst (E4.5)-stage ICM and a 40% contribution to the outer TE, compared to 50% and 51% contributions, respectively, in the control group (Figure 6d-f and Supplementary Fig. 4). However, such reduced contributions were also associated with an overall reduction in total clone size compared to that of equivalent microinjected clones of control siRNA-treated embryos (on average comprising 16.57 ±6.20 versus 39.33 ±4.71 cells, respectively) or noninjected sister clones (Figure 6f). Despite this reduction, *Mybbp1a*-knockdown cells that populated the ICM rarely, if at all, contributed to GATA4-expressing PrE (representing an average of only 0.11 ±0.42 cells per embryo or 4% of the total PrE population). Conversely, such clones readily contributed to NANOG-positive EPI (an average of 1.29 ±1.56 cells per embryo or 29% of the total EPI cell number). In contrast, in control siRNA-treated embryos, the contributions of both microinjected and non-microinjected clones between the ICM and outer TE and between the EPI and PrE lineages were always observed to be statistically equal (Figure 6d-f and Supplementary Fig. 4). Interestingly, clonal *Mybbp1a* knockdown mildly affected the non-microinjected clone, causing small and statistically nonsignificant reductions in total, outer and inner cell numbers. There were, however, reduced numbers of GATA4-positive cells (on average, 2.82 ±3.83 cells versus 5.2 ±2.77 cells in the equivalent clones of control siRNA embryos), although the numbers of EPI cells were not affected (3.93 ± 2.67 versus 4.22 ±2.77). This finding suggests that the overall reduced cell numbers of blastocysts with *Mybbp1a* clonal knockdown may also negatively affect PrE differentiation in the noninjected clones, *per se* (Figure 6d-f and Supplementary Fig. 4 and Supplementary Data 1).

We conclude that clonal knockdown of *Mybbp1a*, a known regulator of rRNA transcription and processing identified in this study as a candidate p38-MAPK substrate/effector during early blastocyst maturation (Figure 6a), biases ICM-resident clones against PrE differentiation. Hence, MYBBP1A, potentially subject to p38-MAPK activity, acts as an ICM cell fate regulator promoting PrE differentiation.

Discussion

p38-MAPKs are well-defined stress-activated kinases involved in inflammatory diseases, including cancers, that also play developmental roles in evolutionarily diverse species, including sea urchins, flies, frogs, zebrafish and mice[24]. Active p38-MAPK signaling was first defined to be necessary for blastocyst formation (*i.e.* progression past the morula stage)[33,34]. In addition, knockout of the *Mapk14* gene is embryonic lethal and associated with defective extraembryonic placental development and adsorption of homozygous null conceptuses at E12.5[32]. Our own previous studies (confirmed here) have demonstrated that p38-MAPK activity is also required for blastocyst PrE derivation[36,37], itself a precursor of the supportive extraembryonic parietal and visceral endodermal membranes[67]. In this study, we uncovered a multilayered role for p38-MAPK-mediated translational regulation, at least partially integrated with that of the mTOR pathway and including effectors such as MYBPP1A, that coincides within a limited early blastocyst developmental window required for PrE differentiation and blastocyst cavity expansion.

The fact that p38-MAPKi blastocysts (E3.5-E4.5) exhibit cavity expansion defects that are potentially related to maturation of TE tight junctions (see below) and have impaired PrE derivation (Figure 1)[36,37] is consistent with recent reports of positive correlations between cavity expansion and EPI and PrE cell fate specification and sorting[13]. For example, Ryan and colleagues found that both chemical modulation (using ouabain, an inhibitor of the ATP1 channel responsible for cavity fluid accumulation[68-70]) and mechanical modulation of blastocyst cavity size during early blastocyst maturation (E3.5-E4.0) reduces PrE marker protein expression (assayed at E4.0)[13]. Strikingly, the p38-MAPKi-associated PrE differentiation defects we have reported (here and previously[36,37]) closely resemble those of mechanically deflated blastocysts[13] (reduced GATA4 expression and normal EPI specification as indicated by either NANOG or SOX2 expression analysis). Indeed, late blastocyst p38-MAPKi PrE phenotypes involve a statically significant lack of GATA4-positive ICM cells compensated for by a population of unspecified progenitors coexpressing NANOG and GATA6[36,37]. We hypothesize that a similar population of unspecified PrE progenitors may also be found in mechanically deflated blastocysts[13]. Thus, it is possible that the impaired blastocyst PrE differentiation p38-MAPKi phenotypes are, at least in part, mediated by TE defects resulting in insufficient cavity expansion. In fact, p38-MAPKi has previously been reported to increase TE tight junction permeability and reduce *Aqp3* expression[34], which together with Na^+/K^+ pumps (such as ATP1) initiate and maintain blastocyst cavity expansion and luminal pressure[34,71] (reported to more than double between E4.0 and E4.5[71]). Interestingly, our

(phospho-)proteomic and transcriptomic data (derived from both TE and ICM lineages) indicate that p38-MAPKi induced downregulation of *Tjp1* and *Atp1a1* (respectively encoding tight junction protein 1 and one of the two subunits of ATP1 – deletion of which causes peri-implantation lethality and cavity collapse after *in vitro* culture[72]) at the protein and RNA levels (~50% and 40%, respectively – Supplementary Data Fig. 2b, 3b (+7 h) and Supplementary Table 3). Whether this reflects targeted regulation of such specific genes or is related to more general p38-MAPK mediated control of protein translation is not clear. Importantly, PrE differentiation can still occur in the absence of TE or a blastocyst cavity. For example, ICM immunosurgically isolated from E3.5-stage mouse blastocysts can support the formation of an outer layer of PrE within 24 h (mirroring PrE differentiation in intact blastocysts)[73], as can mouse embryonic stem (ES) cell-derived ICM organoids[74].

Within the blastocyst ICM, the role of FGF4-FGFR1/2-ERK1/2 signaling in appropriate lineage specification is well established[4,5,9,10]. ERK pathway inhibition (targeting MEK1/2) throughout the blastocyst maturation period completely blocks PrE differentiation; however, removal of MEK1/2 inhibition at any point prior to ~E4.25 is still permissive for PrE differentiation[9,10,36,75]. These data indicate a persistence of FGF4-based signaling from emerging EPI cells that, under unperturbed developmental conditions, drives the incremental specification and differentiation of PrE as blastocysts mature (ensuring a stable EPI:PrE ratio)[9]. The extent to which active FGF4 signaling may impact the PrE-supportive role of p38-MAPK in the mouse blastocyst ICM is questionable. Stimulation of p38-MAPK activity by various exogenous FGF ligands has been reported to occur in various cell models of proliferation and differentiation, although it has not been thoroughly characterized[76-80], and a role for FGF2 (acting via FGFR2) requiring p38-MAPK in mouse blastocyst TE formation has been described[81]. In the E3.75-stage mouse blastocyst ICM, *Fgfr1* is equally expressed in all cells irrespective of *Fgf4* expression, whereas *Fgfr2* is expressed at 4- to 6-fold higher levels in cells not expressing *Fgf4* (presumptive PrE progenitors)[82]. However, *Fgfr1* is the primary receptor directing PrE formation[4,5]. Interestingly, we observed reduced mRNA expression of *Fgfr1* and *Fgfr2* that was strongest at the E3.5 +7 h time-point, after p38-MAPKi, in our mRNA-Seq dataset (Supplementary Data Fig. 3b (+7 h)). However, *Fgf4* and double-*Fgfr1/2* gene knockouts have phenotypes that developmentally precede the newly identified p38-MAPKi sensitive window (relating to PrE differentiation). For example, they are associated with complete loss of GATA6 protein expression through the early blastocyst stages and result in all ICM cells solely expressing EPI markers (although GATA6 expression is normally initiated together with NANOG in all nascent ICM cells)[4,5,7]. This situation contrasts with p38-MAPKi phenotypes in which NANOG and GATA6 coexpression persists at the expense of PrE, but not EPI, differentiation[36,37]. Moreover, ERK phosphorylation, indicative of activated FGF4 signaling, begins at approximately E3.0-E3.25 and increases with time in a manner correlated with increasing GATA6 expression[82]. Additionally, we found that the reported pan-ICM conversion of cells to a PrE fate caused by exposure to exogenous FGF4[5,57,83,84] is not sensitive to concomitant p38-

MAPKi, unlike in the case of MEK1/2 inhibition (Supplementary Fig. 5 and 6 and Supplementary Data 1), although we acknowledge concerns about potentially supraphysiological FGF4 concentrations[85]. Collectively, these data indicate that the PrE-promoting role of p38-MAPK most likely does not function directly downstream of classically activated FGF4-FGFR1/2-ERK1/2 signaling or is at least not limited to this pathway. Non-MEK1/2-dependent activation of p38-MAPKs has been reported in multiple human *FGFR2* genetic mutation-induced pathophysiologies[26,27], suggesting the possible involvement of noncanonical FGFR2-mediated p38-MAPK activation mechanisms (as reviewed previously[25]). Considering the proposed PrE survival-specific role of FGFR2[16] in association with PDGFRa[14-16] and the p38-MAPKi-mediated PrE phenotypes we have described, it is tempting to speculate that such noncanonical signaling cascades may contribute (together with classical ERK pathway activation) to mouse blastocyst ICM cell fate derivation, albeit at slightly later developmental time points than the classical cascade. Another potential mechanism of emerging PrE-specific p38-MAPK activation may be via activated FGFR3. Although they are expressed at equally low levels in all early blastocyst (E3.5) ICM cells, *Fgfr3* transcripts are specifically enriched in an *Fgf4*-dependent manner in late blastocyst (E4.5) PrE[31]. Moreover, FGFR3 has been reported to activate p38-MAPK[30]. The PrE specificity of PDGFRa is well documented, and fluorescently tagged genetic knock-ins and knockouts are regularly used to identify PrE cells[13,15,16,86]. A recent report described PDGFRa-mediated signaling via PI3K and mTOR as enabling PrE survival[15]. Although inhibition of JAK or mTORC1 (one of two mTOR-containing complexes – see below) alone does not impact any preimplantation cell lineages, combined inhibition is particularly detrimental to PrE survival. Our observations that p38-MAPKi PrE phenotypes can be circumvented (at least partially) by mTOR activation implies that p38-MAPK acts functionally upstream of mTOR and downstream of potentially commonly activated receptor kinases, such as FGFR2, FGFR3, PDGFRa or others.

Notwithstanding the above discussion points regarding p38-MAPK activation, the central finding that p38-MAPK plays a fundamental role in regulating protein translation during early blastocyst maturation is consistent with the creation of metabolically permissive states compatible with PrE specification and differentiation. The finding that p38-MAPKi PrE deficits can be partially reversed by concomitant mTOR activation (Figure 5f and j-q) is important and emphasizes the importance of p38-MAPK-mediated regulation of translation. The mTOR signaling pathway (integrated by two mTOR-containing complexes, mTORC1 and mTORC2) is a global regulator of translation and maintains cellular energy homeostasis in response to extracellular stimuli such as growth factors and nutrient availability[51]. As part of mTORC1, mTOR specifically controls transcription and translation of ribosomal genes/proteins, synthesis and processing of rRNA, and biogenesis and availability of ribosomes to ultimately dictate general translation of all mRNA transcripts (mTORC2 is associated with cotranslational protein degradation and lipolysis)[51,87-90]. Our data indicate that there is considerable overlap between the described mTOR function and the role of p38-MAPK during early blastocyst maturation and eventual PrE formation. However, despite the

similarities and the partial reversal of the p38-MAPKi-induced PrE differentiation phenotype caused by simultaneous activation of mTOR, it is clear that p38-MAPKi does not merely phenocopy mTOR inhibition-induced diapause[54]. Rather, the p38-MAPKi-induced phenotype is specifically characterized by impaired PrE differentiation in the context of ongoing development (EPI specification is not impaired), which nevertheless has all the hallmarks of impaired translation. Notably, the restoration of GATA4-positive PrE cells in blastocysts subjected to both p38-MAPKi and mTOR activator treatment was frequently associated with coexpression of NANOG (Figure 5f and q), suggesting the occurrence of a pseudo-state that does not normally exist in which PrE differentiation was uncoupled from the ordinarily required need to downregulate NANOG. The PrE-specific effect of p38-MAPKi was further illustrated by the finding that the number of EPI cells (defined by sole expression of NANOG) was not altered regardless of cotreatment with the mTOR activator (Figure 5m). We also noted that the partial PrE differentiation "rescue" effects of mTOR activation on p38-MAPKi blastocysts were not associated with enhanced blastocyst cavity expansion (Supplementary Fig. 7), suggesting that these and the originally observed p38-MAPKi phenotypes are at least partly PrE progenitor cell autonomous.

The observed p38-MAPKi-induced upregulation of ribosomal protein transcripts (peaking at E3.5 +7 h – Figure 3; also associated with downregulation at the protein level – Figures 2c and 3e) suggested accumulation caused by confirmed overall impaired translation (Figure 4b-d) that most likely involved rRNA processing defects (Figure 4e and f). A previous study has described HTATSF1 as a regulator of rRNA/mRNA transcriptional and posttranscriptional processing, protein synthesis and the pre- to postimplantation transition from the embryonic naïve to primed pluripotent states[46]. HTATSF1-mediated repression of active translation during this transitory period is associated with increased intron retention in ribosomal protein-encoding mRNAs, which causes degradation of the mRNAs via the nonsense-mediated decay pathway[46]. Although we also observed reduced translation after p38-MAPKi (Figures 2c and 4b-d), we did not observe any similarly enhanced intron retention in our mRNA-Seq dataset (Supplementary Table 4). However, MYBPP1A, a confirmed HTATSF1 interaction partner[46], was identified in our phosphoproteomic screen for candidate p38-MAPK effectors (Figure 6a), clonal dysregulation of which was associated with PrE deficits (Figure 6d-f). Other cell culture studies have implicated MYBBP1A in the transcriptional repression of rRNA genes and in facilitation of pre-rRNA processing[61]. We propose that MYBBP1A (under the regulation of p38-MAPK) may act as a checkpoint agent enabling switching from homeostasis of cellular protein synthesis and the coordination of a functionally important translational response to externally provided differentiation cues (via regulation of mature rRNA levels available for functional ribosome biogenesis), as supported by reports in other models describing MYBBP1A-regulated rRNA expression and processing in the cellular stress response[63,64]. Interestingly, MYBBP1A is known to suppress mitochondrial respiration, and we identified mitochondrial respiration-related transcripts as the second most

statistically significant ontological class of gene transcripts with p38-MAPKi-mediated differential expression (Figure 3d – representing upregulated mRNA levels). Our phosphoproteomic screening data revealed multiple p38-MAPKi-sensitive phosphorylation sites within the MYBBP1A protein (Figure 6a and Supplementary Data 1); phosphorylation at serine 1280 (S1280) was decreased, but phosphorylation at S1303 and S1323, among other sites, was increased. Our results indicate that S1280 is a good candidate direct substrate for p38-MAPK, particularly as it contains the [S/T]P consensus phosphorylation motif for proline-directed mitogen-activated kinases in general[44] (Supplementary Table 1), but this remains to be experimentally validated. To our knowledge, the only verified MYBBP1A phosphorylation site is centered on S1303 and is a reported Aurora B kinase (AURKB) substrate[91]. The mechanistic details of how such phosphorylation events functionally impact MYBBP1A and to what extent they are involved in the described early blastocyst p38-MAPKi-induced translation and PrE phenotype remain to be examined.

In summary, we describe a role for p38-MAPK activity during a limited developmental window of early blastocyst maturation that is centered on the regulation of translation. This role ensures germane ICM cell fate specification, specifically facilitating PrE derivation by the late blastocyst (E4.5) stage. We propose that such positive translational regulation is at least partially integrated with the mTOR pathway and is necessary to prime subsequent differentiation of PrE progenitors (see model – Figure 7).

Methods

Mouse lines and embryo culture

All mouse-related experimental procedures (*i.e.,* collection of preimplantation-stage embryos for further study) complied with the Animal Research: Reporting of In Vivo Experiments (ARRIVE) guidelines and were carried out in accordance with EU directive 2010/63/EU (for animal experiments). The superovulation and strain mating regimens used to produce experimental embryos were as follows: F1 hybrid (C57Bl6 × CBA/W) females were intraperitoneally injected with 7.5 IU of PMSG (Folligon, MSD Animal Health, Boxmeer, Netherlands) and again with 7.5 IU of hCG (Sigma-Aldrich, St. Louis, Missouri, USA; Cat. No. CG10) after 48 h and then mated overnight with F1 males (successful mating was confirmed the next morning by the presence of vaginal plugs). E1.5 (2-cell)-stage embryos were isolated from female oviducts in M2 medium (prewarmed at 37°C for at least 2-3 h) and thereafter cultured in KSOM (Sigma-Aldrich, EmbryoMax KSOM Mouse Embryo Media; Cat. No. MR-020P-5F - prewarmed and equilibrated in 5% CO_2 and 37°C) either with or without AA supplementation. For KSOM+AA conditions, Gibco MEM Non-Essential Amino Acids Solution (100×) (Thermo Fisher Scientific, Paisley, Scotland; Cat. No. 11140035) and Gibco MEM Amino Acids Solution (50×) (Thermo Fisher Scientific; Cat. No.

11130036) were used at working concentrations of 0.5×. Embryos were cultured in microdrops prepared in 35 mm tissue culture dishes covered with light mineral oil (Irvine Scientific, Santa Ana, California, USA; Cat. No. 9305) in 5% CO_2 incubators maintained at 37°C until the appropriate stage. Pharmacological manipulations were carried out via addition of chemical agents dissolved in DMSO (Sigma-Aldrich; Cat. No. D4540) to KSOM±AAs (the concentration details, durations, *etc.* are given in Supplementary Table 5). Equivalent volumes of solvent control were used at final working concentrations of 0.2-0.5% by volume. The concentrations of the p38-MAPK inhibitor (SB220025 – 20 μM) and MEK1/2 inhibitor (PD0325901 – 1 μM) used were derived from empirical titrations that we performed previously[36] and/or from published literature[10,33]. All KSOM-based culture media with or without additional chemicals (AAs, pharmacological agents) were prewarmed and equilibrated in 5% CO_2 and 37°C for at least 3-4 h prior to embryo transfer.

Sample collection for mass spectrometric analysis of the differential (phospho-)proteome

Two-cell (E1.5)-stage embryos were cultured in normal KSOM+AA conditions until E3.5 +2 h. Thereafter, 300 embryos each were moved to control or p38-MAPKi conditions and cultured for another 7 h (E3.5 +9 h). The embryos were then washed with prewarmed Hank's balanced salt solution (HBSS, Sigma-Aldrich; Cat. No. H9269) and lysed in 1.5 ml centrifuge tubes containing approximately 15 µl of SDT lysis buffer (4% (w/v) SDS, 100 mM Tris-HCl pH 7.6, 0.1 M DTT) in a 95°C heat block for 12 minutes. The tubes were briefly centrifuged at 750 rpm, cooled to room temperature and stored at -80°C.

Sample preparation for liquid chromatography–mass spectrometry (LC-MS) analyses

Individual protein solutions were processed by the filter-aided sample preparation (FASP) method[92] with some modifications. The samples were mixed with 8 M UA buffer (8 M urea in 100 mM Tris-HCl, pH 8.5), loaded onto a Microcon device with a molecular weight cutoff (MWCO) of 30 kDa (Merck Millipore, Burlington, Massachusetts, USA) and centrifuged at 7000 × *g* for 30 minutes at 20°C. The retained proteins were washed (all centrifugation steps after sample loading were performed at 14000 × *g*) with 200 µl of UA buffer. The final protein concentrates retained in the Microcon device were mixed with 100 µl of UA buffer containing 50 mM iodoacetamide and incubated in the dark for 20 minutes. After the next centrifugation step, the samples were washed three times with 100 µl of UA buffer and three times with 100 µl of 50 mM $NaHCO_3$. Trypsin (1 µg, sequencing grade, Promega, Madison, Wisconsin, USA) was added onto the filter, and the mixture was incubated for 18 h at 37°C. The tryptic peptides were finally eluted by centrifugation followed by two additional elutions with 50 µl of 50 mM $NaHCO_3$. The peptides were then cleaned via liquid-liquid extraction (3 iterations) using water-saturated ethyl acetate[93].

One-tenth of the cleaned FASP eluate was removed for direct LC-MS measurements and evaporated completely in a SpeedVac concentrator (Thermo Fisher Scientific, Waltham, Massachusetts, USA). The peptides were further transferred into LC-MS vials using 50 µl of 2.5%

formic acid (FA) in 50% acetonitrile (ACN) and 100 µl of pure ACN with added polyethylene glycol (final concentration 0.001%) and concentrated in a SpeedVac concentrator.

Phosphopeptides were enriched from the remaining 9/10th of the cleaned FASP eluate after complete solvent evaporation (in a SpeedVac concentrator) using a High-Select TiO_2 Phosphopeptide Enrichment Kit (Thermo Fisher Scientific) according to the manufacturer's protocol. Phosphopeptide standards (0.1 pmol of MS PhosphoMix 1, 2, 3 Light; Sigma-Aldrich) was added to the suspended sample in binding/equilibration buffer. The flow-through fraction was dried and used for the second enrichment step using a High-Select Fe-NTA Phosphopeptide Enrichment Kit (Thermo Fisher Scientific) according to the manufacturer's protocol. The resulting phosphopeptides were extracted into LC-MS vials with 2.5% FA in 50% ACN and 100% ACN with added polyethylene glycol (final concentration 0.001%) and concentrated in a SpeedVac concentrator.

LC-MS analysis of peptides

LC-MS/MS analyses were performed for all peptide mixtures (3 peptide solutions for each sample: 1) not enriched, 2) enriched with phosphopeptides using a TiO_2 enrichment kit and 3) enriched with phosphopeptides using an Fe-NTA enrichment kit) using an RSLCnano system connected to an Orbitrap Fusion Lumos mass spectrometer (Thermo Fisher Scientific). Prior to LC separation, the tryptic digests were concentrated online and desalted using a trapping column (100 µm × 30 mm, column compartment temperature of 40°C) filled with 3.5 µm X-Bridge BEH 130 C18 sorbent (Waters). After washing the trapping column with 0.1% FA, the peptides were eluted (flow rate: 300 nl/min) from the trapping column onto an analytical column (Acclaim PepMap 100 C18, 3 µm particles, 75 µm × 500 mm, column compartment temperature of 40°C, Thermo Fisher Scientific) by using a 50- or 100-minute nonlinear gradient program (1-56% mobile phase B; mobile phase A: 0.1% FA in water; mobile phase B: 0.1% FA in 80% ACN) for analysis of phosphopeptide-enriched fractions or non-enriched peptide mixtures, respectively. The trapping column and the analytical column were equilibrated prior to sample injection into the sample loop. The analytical column outlet was directly connected to a Digital PicoView 550 (New Objective) ion source with the sheath gas option and SilicaTip emitter (New Objective; FS360-20-15-N-20-C12) utilization. An Active Background Ion Reduction Device (ABIRD, ESI Source Solutions, Woburn, Massachusetts, USA) was installed.

MS data were acquired in a data-dependent strategy with a cycle time of 3 seconds and with a survey scan (350-2000 m/z). The resolution of the survey scan was 60000 (200 m/z) with a target value of 4×10^5 ions and a maximum injection time of 50 ms. Higher-energy collisional dissociation (HCD) MS/MS (30% relative fragmentation energy, normal mass range) spectra were acquired with a target value of 5.0×10^4. The MS/MS spectra were recorded in Orbitrap at resolving power of 30000 or 15000 (200 m/z), and the maximum injection time for MS/MS was 500 or 22 ms for

analysis of phosphopeptide-enriched fractions or non-enriched peptide mixtures, respectively. Dynamic exclusion was enabled for 60 seconds after one MS/MS spectrum acquisition. The isolation window for MS/MS fragmentation was set to 1.6 m/z.

The raw mass spectrometric data files were analyzed using MaxQuant software (version 1.6.6.0) with the default settings unless otherwise noted. MS/MS ion searches were performed against the modified Common Repository of Adventitious Proteins (cRAP) database (based on http://www.thegpm.org/crap, 112 protein sequences) containing protein contaminants such as keratin and trypsin and the UniProtKB protein database for *Mus musculus* (ftp://ftp.uniprot.org/pub/databases/uniprot/current_release/knowledgebase/reference_proteomes/Eukaryota/UP000000589_10090.fasta.gz; downloaded 8.5.2019, version 2019/05, number of protein sequences: 22287). Oxidation of methionine and proline, deamidation (N, Q) and acetylation (protein N-terminus) were the optional modifications, and the trypsin/P enzyme with 2 allowed missed cleavages and a minimum peptide length of 6 AAs were set. Only peptides and proteins meeting a false discovery rate (FDR) threshold <0.01 and proteins with at least one unique or razor peptide were considered. Match-between-runs was set separately for all enriched and non-enriched peptide solution analyses. The same experimental name was used for differently enriched peptide solution analyses coming from the same sample.

The protein intensities reported in the proteinGroups.txt file and the evidence intensities reported in the evidence.txt file (output from the MaxQuant program) were further processed using the OmicsWorkflows software container environment (https://github.com/OmicsWorkflows), version 3.7.1a. The processing workflow is available upon request. Briefly, the workflow featured 1) protein level data processing, including a) removal of decoy hits and contaminant protein groups, b) log2 transformation of protein group intensities, c) LoessF normalization and d) differential expression using the LIMMA statistical test (qualitative changes were considered separately without statistical evaluation); 2) phospho-peptide level data processing, including a) removal of evidence associated with non-phosphorylated and contaminant proteins, b) grouping of the evidence for the identical combinations of peptide sequences and sets of modifications, c) LoessF normalization and d) differential expression analysis using the LIMMA statistical test (qualitative changes were considered separately without statistical evaluation). Differentially abundant phosphopeptide candidates (phosphopeptides exhibiting ≥1.5-fold differential abundance; note that the cutoff was applied to acknowledge the potential sensitivity threshold limitations when such scarce starting material is used) were selected based on the criteria mentioned within the Results section. The mass spectrometry proteomics data have been deposited to the ProteomeXchange Consortium via the PRIDE[94] partner repository with the dataset identifier PXD025711.

mRNA sequencing (mRNA-Seq) library preparation and sequencing

Two-cell (E1.5)-stage embryos were cultured in normal KSOM+AA conditions until E3.5. Thereafter, 30 embryos each were moved to control or p38-MAPKi conditions and cultured for another 4, 7 or 10 h. The embryos were then processed for total RNA isolation using the ARCTURUS PicoPure RNA Isolation Kit (Thermo Fisher Scientific; Cat. No. KIT0204) following the manufacturer's protocol. Oligo dT-based mRNA isolation was carried out using an NEBNext Poly(A) mRNA Magnetic Isolation Module (NEB, Ipswich, Massachusetts, USA; Cat. No. E7490), and libraries were prepared using an NEBNext Ultra II Directional RNA Library Prep Kit for Illumina (NEB; Cat. No. E7760), as directed by the manufacturer. The libraries were sequenced as 50 bp single-end reads on an Illumina HiSeq 4000 platform. The mRNA-Seq datasets are available in the Gene Expression Omnibus (GEO) database with accession number GSE162233.

Data processing and bioinformatics analysis

The sequenced reads were adapter- and quality-trimmed using Trim Galore! v0.4.1 and mapped to the mouse GRCm38 genome with HISAT2 v2.0.5. Differentially expressed genes between control and p38-MAPKi embryos at individual time points were identified by DESeq2 within SeqMonk v1.45.4 using GRCm38_v90 transcriptome annotation. Hierarchical clustering was performed in SeqMonk v1.45.4 with mean-centered expression values. Gene Ontology (GO) analysis was performed using GOrilla[95,96]. Due to the omission of spiked-in controls during mRNA-Seq library preparation, it was not possible to assay normalized global transcriptional output from these data.

Embryo manipulation via microinjection

Single (for immunofluorescence confocal microscopy) or double (for qRT-PCR) blastomere microinjections of 2-cell (E1.5)-stage embryos were performed using a FemtoJet or FemtoJet 4i (Eppendorf, Hamburg, Germany; Cat. No. 5252000013) microinjector, a mechanical micromanipulator (Leica, Wetzlar, Germany; Cat. No. ST0036714) and a CellTram Vario (Eppendorf; Cat. No. 5176000033) pneumatic handler under a negative capacitance-enabled current controlled by an Electro 705 Electrometer (WPI, Sarasota, Florida, USA; Cat. No. SYS-705) and on the stage of an Olympus IX71 inverted fluorescence microscope. The embryos were pneumatically handled and immobilized for microinjection using a borosilicate glass capillary holder (without filament – Harvard Apparatus, Holliston, Massachusetts, USA; Cat. No. 30-0017). Injection needles prepared from filamented borosilicate glass capillaries (Harvard Apparatus; Cat. No. 30-0038) using a Narishige PC-10 capillary glass needle puller (Narishige Scientific Instrument Lab., Tokyo, Japan) were connected to the microinjector. All siRNAs (Supplementary Table 6) were co-microinjected at 10 µM concentrations with 50 ng/µl *H2b-RFP* mRNA in prewarmed drops of M2 medium overlaid with mineral oil on the surfaces of concave microscope slides.

Immunofluorescence staining, confocal microscopy and image acquisition

To remove the *zona pellucida*, blastocysts were quickly washed and pipetted in prewarmed drops of acidic Tyrode's solution (Sigma-Aldrich; Cat. No. T1788) until the *zona pellucida* was visually undetectable and were then immediately washed in prewarmed drops of M2 medium. Thereafter, the embryos were fixed in the dark with 4% paraformaldehyde (Santa Cruz Biotechnology, Inc., Dallas, Texas, USA; Cat. No. sc-281692) for 20 minutes at room temperature. Permeabilization was performed by transferring the embryos to a 0.5% solution of Triton X-100 (Sigma-Aldrich; Cat. No. T8787) in phosphate-buffered saline (PBS) for 20 minutes at room temperature. All washes after the fixation, permeabilization and antibody staining procedures were performed in PBS with 0.05% TWEEN 20 (Sigma-Aldrich; Cat. No. P9416) (PBST) by transferring the embryos between two drops of PBST or wells (of 96-well microtiter plates) containing PBST for 20 minutes at room temperature. Blocking and antibody staining were performed in 3% bovine serum albumin (BSA; Sigma-Aldrich; Cat. No. A7906) in PBST. For blocking, embryos were incubated for 30 minutes at 4°C before both primary and secondary antibody staining. For primary antibody staining (in blocking buffer), embryos were incubated overnight (~16 h) at 4°C. Secondary antibody staining was carried out in the dark at room temperature for 70 minutes. The stained embryos were mounted with VECTASHIELD mounting medium containing DAPI (Vector Laboratories, Inc., Burlingame, California, USA; Cat. No. H-1200), placed under coverslips on glass-bottomed 35 mm culture plates and incubated at 4°C for 30 minutes in the dark prior to confocal imaging. Details of the primary and secondary antibody combinations used can be found in Supplementary Table 7. Confocal images were acquired using an FV10i confocal laser scanning microscope and FV10i-SW image acquisition software (Olympus, Tokyo, Japan). The images were analyzed using FV10-ASW 4.2 Viewer (Olympus) and Imaris X64 Microscopy Image Analysis Software (version 6.2.1; Bitplane AG - Oxford Instruments plc, Abingdon, United Kingdom). The cells were counted both manually and semi-automatically using Imaris X64.

Time-lapse imaging

Embryos at E3.5 were placed in 20 µl droplets of KSOM+AAs (+DMSO or +SB220025) in 16-well dishes (PrimoVision, Vitrolife, Gothenburg, Sweden) at a density of one embryo per well within a PrimoVision imaging system and cultured for 24 h (until E4.5) under standard culture conditions. The embryos were imaged every 10 minutes, the equatorial areas were recorded, and the data were analyzed (Figure 1e and as described previously[97]).

Scarce-sample polysome (SSP) profiling

Two-cell (E1.5)-stage embryos were cultured in KSOM+AAs and transferred to control or p38-MAPKi conditions for 10 h starting from E3.5 (E3.5 +10 h; as depicted in Figure 4a). Prior to harvesting, the embryos were transferred to cycloheximide (0.1 mg/ml)-containing medium for

10 minutes and then washed 3× in PBS (supplemented with 0.1 mg/ml cycloheximide) and 1× in transfer medium (0.1% PVA in PBS + 0.1 mg/ml cyclohexamide). The embryos were then transferred to 0.5 ml low DNA-binding tubes in a minimal volume of transfer medium, flash-frozen in liquid nitrogen and stored at -80°C. Cellular lysis and sucrose gradient centrifugation to procure ribosomal fractions followed by isolation of corresponding rRNA were performed as described previously[45]. The resultant fractions representing rRNA corresponding to nonpolysomes (fractions 1 to 5; from the upper (lighter) fractions) and polysomes (fractions 6 to 10; from the lower (heavier) fractions) were resuspended in 20 µl of nuclease-free water. cDNA was then prepared. Briefly, 4.0 µl of total RNA was mixed with 1.6 µl of 0.183 µg/µl random hexamers and 3.0 µl of nuclease-free water. The samples were incubated on a heat block at 70°C for 5 minutes, placed on ice for 5 minutes and then briefly microfuged. Then, 3.9 µl of nuclease-free water, 4.0 µl of 5× reaction buffer, 1.0 µl of RevertAid H Minus reverse transcriptase (Thermo Fisher Scientific; Cat. No. EP0451), 0.5 µl of RiboLock RNase inhibitor (Thermo Fisher Scientific; Cat. No. EO0381) and 2.0 µl of dNTP mix (Thermo Fisher Scientific; Cat. No. R0192) were added. The preparations were processed in a thermocycler with the following program: 25°C for 10 minutes, 37°C for 5 minutes, 42°C for 75 minutes and 70°C for 10 minutes. The synthesized cDNA was stored at -20°C, and 2.0 µl aliquots were used as templates for qRT-PCR (as described previously[45]).

O-propargyl-puromycin (OPP) quantification of de novo protein synthesis

Mouse embryos were cultured *in vitro* from E1.5 to E3.5 in KSOM+AAs and then further cultured under control or p38-MAPKi conditions for 10 h (E3.5 +10 h). OPP staining was then performed using a Click-iT Plus OPP Alexa Fluor 488 Protein Synthesis Assay Kit (Thermo Fisher Scientific; Cat. No. C10456) following the prescribed protocol with modifications for *in vitro* preimplantation embryo culture. In brief, equilibrated culture dishes (described above) containing drops of KSOM (without AA supplementation) and 40 µM solutions of OPP supplemented with either control DMSO or 20 µM SB220025 were prepared. Following a 60-minute pre-incubation period, control and p38-MAPKi blastocysts were transferred to their respective OPP-containing dishes and incubated for an additional 60 minutes. Thereafter, the embryos were fixed, permeabilized and washed as described above (immunofluorescence confocal microscopy). To enable fluorescent visualization of the incorporation of OPP into nascent polypeptides, Click-iT reactions were set up as described in the kit manual (with Click-iT reaction buffer, copper protectant, Alexa Fluor 488 picolyl azide and reaction buffer additive). The fixed embryos were incubated in the reaction mixture for 25 minutes at room temperature in the dark. Thereafter, the embryos were washed in a 1:1 mixture of kit-provided wash buffer and PBST, mounted in VECTASHIELD, imaged using standard confocal microscope settings (as described above) to detect the Alexa Fluor 488 fluorophore and quantified as described.

Cell number quantification, statistical analysis and graphical representation

The cells counted as part of the total embryo cell numbers (plus outer and inner cell populations) from confocal acquired micrographs (based on DAPI nuclear staining) were further subcategorized as EPI or PrE cells based on detectable and exclusive NANOG and GATA4 protein expression (confocal images in Figures 1b and c, 5 and 6 and graphs in Figure 1b and c, 5 and 6). Cells not located within blastocyst ICMs that also did not stain for GATA4 and/or NANOG were designated outer/TE cells. In relation to Figure 5p specifically, ICM cells that were positively stained for both GATA6 and NANOG at E4.5 were designated as uncommitted/unspecified in terms of cell fate, and the population of similarly GATA4- and NANOG-positive ICM cells (primarily resulting from coinhibition and coactivation of p38-MAPK and mTOR, respectively – Figure 5f) was also recorded. In Figure 4g and h, cells were designated "outer cells" based on detectable CDX2 (TE marker[48]) expression. The relative levels of H4K16ac-modified chromatin (Figure 4g) were quantified to determine global chromatin status, and RNA pol II S2p (Figure 4h) levels were quantified to determine active transcriptional elongation, as described below in the section on fluorescence intensity quantification and statistical analysis. Initial recording and data accumulation were carried out using Microsoft Excel, and further statistical analysis and graphical representations were performed with GraphPad Prism 8. Based on the normality and lognormality comparisons, appropriate statistical tests were used for the compared datasets (summarized in Supplementary Table 8). Unless otherwise stated within individual graphs with specific P values (if the differences were statistically nonsignificant), the following significance intervals were recognized: $P < 0.0001$ (****), 0.0001 to 0.001 (***), 0.001 to 0.01 (**) and 0.01 to 0.05 (*). All dot plots represent the total sample size, with the associated means and standard deviation bars provided.

Fluorescence intensity quantification and statistical analysis

The fluorescence intensity pertaining to OPP incorporation (Figure 4b) was quantified for the minimum complete confocal z-series of each embryo as a whole using Fiji (ImageJ)[98]. The confocal images from the channel pertaining to the 488 nm wavelength were analyzed as follows: Image>Stacks>Z Project. The projection type "Sum Slices" was used to obtain a Z-projected image for the entire embryo. The levels of H4K16ac (Figure 4g) and RNA pol II S2p (Figure 4h) were quantified as the fluorescence intensity per cell, and the cells were defined as inner or outer cells based on the absence or presence of CDX2 immunofluorescence, respectively. The measurements for all of the above were set with the command Analyze>Set Measurements, and the following options were chosen: Area, Mean gray value and Integrated density. Using the "Polygon selections" tool, an area encompassing the Z-projected embryo image (for OPP) or individual cell nuclei (for H4K16ac and RNA pol II S2p) was demarcated, and the aforementioned measurements were recorded. The selected area was then moved to encompass an area excluding the embryo or cell nucleus, and background measurements were recorded. This process was continued for all the embryos analyzed under both control and p38-MAPKi

conditions, and the results were transferred to a spreadsheet for further calculations. The corrected total cell fluorescence (CTCF), in arbitrary units, was measured for each embryo as follows: CTCF = integrated density – (area of selected cell × mean fluorescence of background readings)[99,100] (Supplementary Data 1 Fig. 4b, g, h). The calculated CTCFs are plotted in scatterplots, with the means and standard deviations marked. The CTCF differences were statistically tested using the Mann-Whitney test, and the results, unless otherwise stated within individual graphs with specific P values (if statistically nonsignificant), are marked according to the following significance intervals: P < 0.0001 (****), 0.0001 to 0.001 (***), 0.001 to 0.01 (**) and 0.01 to 0.05 (*).

Blastocyst size and volume calculations

The equatorial areas of blastocoel cavities (Figure 1d) were calculated by measuring the inner circumference of the centrally located widest Z-stack using Fiji (ImageJ)[97]. To compare the volumes of p38-MAPK-inhibited blastocoel cavities with those reported by Ryan *et al*.[13], we deduced the volumes from inner circumference measurements. The calculated areas and corresponding volume measurements are tabulated in Supplementary Data 1 Fig. 1d. The equatorial area and total volume measurements for whole blastocysts were obtained by similarly measuring the outer circumferences (as reported in Supplementary Fig. 7). The measurements were set with the command Analyze>Set Measurements, and the "Perimeter" option was selected. Using the "Polygon selections" tool, the inner circumference was traced and measured. The radius was deduced from the measured circumference, and that value was used to calculate an approximate equatorial section area (or volume) for all the embryos analyzed under both control and p38-MAPKi conditions. The calculated areas in μm^2 (or volumes in picoliters (pl)) are plotted in scatterplots, with the means and standard deviations marked. The differences were statistically analyzed using the Mann-Whitney test, and the results, unless otherwise stated within individual graphs with specific P values (if statistically nonsignificant), are marked according to the following significance intervals: P < 0.0001 (****), 0.0001 to 0.001 (***), 0.001 to 0.01 (**) and 0.01 to 0.05 (*).

Quantitative real-time PCR (qRT-PCR)

Embryos from each stated experimental condition were collected and immediately processed for RNA extraction and isolation using an ARCTURUS PicoPure RNA Isolation Kit (Thermo Fisher Scientific; Cat. No. KIT0204) following the manufacturer's protocol. The entire eluted volume of total RNA was immediately DNase treated with TURBO DNase (Thermo Fisher Scientific; Cat. No. AM2238) according to the manufacturer's protocol. The whole sample was then subjected to cDNA synthesis using SuperScript III Reverse Transcriptase (Thermo Fisher Scientific; Cat. No. 18080044) as directed by the manufacturer with oligo d(T)16 (for Figure 1f and 6c) (Thermo Fisher Scientific; Cat. No. N8080128) or random hexamers (for Figure 4c, d and f) (Thermo Fisher

Scientific; Cat. No. SO142), dNTP Mix (Thermo Fisher Scientific; Cat. No. R0192) and RNase Inhibitor (Thermo Fisher Scientific; Cat. No. N8080119). The synthesized cDNA was diluted as required with nuclease-free water, and 1 µl was used in 10 µl individual final SYBR Green-based qRT-PCR volumes (PCR Biosystems Ltd., London, United Kingdom; Cat. No. PB20.11). A Bio-Rad CFX96 Touch Real-Time PCR Detection System was used for data acquisition with the standard settings, and the initial analysis was performed with the accompanying Bio-Rad CFX Manager software. Triplicate measurements were obtained for each gene (the sequences of the individual oligonucleotide primers used at final concentrations of 300 nM are provided in Supplementary Table 9) from two biological replicates that were each technically replicated. The averaged transcript levels of the analyzed genes were determined after internal normalization against *Tbp* or *H2afz* mRNA levels. The raw data were acquired and initially analyzed with CFX Manager and then processed in Microsoft Excel (for biological and technical replicate averaging) and GraphPad Prism 8 (for graphical output). The statistical tests used are detailed in Supplementary Table 8. Unless otherwise stated within individual graphs with specific P values (if statistically nonsignificant), the following significance intervals were recognized: $P < 0.0001$ (****), 0.0001 to 0.001 (***), 0.001 to 0.01 (**) and 0.01 to 0.05 (*). The error bars denote the calculated standard deviations.

Statistics and reproducibility

All statistical tests conducted are detailed in Supplementary Table 8 and results thereof, if not mentioned within respective figures, are detailed in Supplementary Data 1 (corresponding to respective figures or supplementary figures). The data analyzed was typically from not less than 10 embryos per condition, and are detailed within respective figure legends. Details regarding biological and/or technical replicates are provided within respective methodological sections.

Data availability

The RNA sequencing datasets are available in the GEO database with accession number GSE162233. The mass spectrometry proteomics data have been deposited to the ProteomeXchange Consortium via the PRIDE partner repository with the dataset identifier PXD025711.

Code availability

No custom code was used. All software and code are available through the cited references.

References

1. Chazaud, C. & Yamanaka, Y. Lineage specification in the mouse preimplantation embryo. *Development* **143,** 1063-1074 (2016).

2. Płusa, B. & Piliszek, A. Common principles of early mammalian embryo self-organisation. *Development* **147,** dev183079 (2020).

3. Shahbazi, M. N. Mechanisms of human embryo development: from cell fate to tissue shape and back. *Development* **147,** dev190629 (2020).

4. Molotkov, A., Mazot, P., Brewer, J. R., Cinalli, R. M. & Soriano, P. Distinct requirements for FGFR1 and FGFR2 in primitive endoderm development and exit from pluripotency. *Dev. Cell* **41,** 511-526.e4 (2017).

5. Kang, M., Garg, V. & Hadjantonakis, A. K. Lineage establishment and progression within the inner cell mass of the mouse blastocyst requires FGFR1 and FGFR2. *Dev. Cell* **41,** 496-510.e5 (2017).

6. Artus, J., Piliszek, A. & Hadjantonakis, A. K. The primitive endoderm lineage of the mouse blastocyst: sequential transcription factor activation and regulation of differentiation by Sox17. *Dev. Biol.* **350,** 393-404 (2011).

7. Kang, M., Piliszek, A., Artus, J. & Hadjantonakis, A. K. FGF4 is required for lineage restriction and salt-and-pepper distribution of primitive endoderm factors but not their initial expression in the mouse. *Development* **140,** 267-279 (2013).

8. Schrode, N., Saiz, N., Di Talia, S. & Hadjantonakis, A. K. GATA6 levels modulate primitive endoderm cell fate choice and timing in the mouse blastocyst. *Dev. Cell* **29,** 454-467 (2014).

9. Saiz, N., Williams, K. M., Seshan, V. E. & Hadjantonakis, A. K. Asynchronous fate decisions by single cells collectively ensure consistent lineage composition in the mouse blastocyst. *Nat. Commun.* **7,** 13463 (2016).

10. Bessonnard, S. *et al.* ICM conversion to epiblast by FGF/ERK inhibition is limited in time and requires transcription and protein degradation. *Sci. Rep.* **7,** 12285 (2017).

11. Chazaud, C., Yamanaka, Y., Pawson, T. & Rossant, J. Early lineage segregation between epiblast and primitive endoderm in mouse blastocysts through the Grb2-MAPK pathway. *Dev. Cell* **10,** 615-624 (2006).

12. Plusa, B., Piliszek, A., Frankenberg, S., Artus, J. & Hadjantonakis, A. K. Distinct sequential cell behaviours direct primitive endoderm formation in the mouse blastocyst. *Development* **135,** 3081-3091 (2008).

13. Ryan, A. Q., Chan, C. J., Graner, F. & Hiiragi, T. Lumen expansion facilitates epiblast-primitive endoderm fate specification during mouse blastocyst formation. *Dev. Cell* **51,** 684-697.e4 (2019).

14. Artus, J., Kang, M., Cohen-Tannoudji, M. & Hadjantonakis, A. K. PDGF signaling is required for primitive endoderm cell survival in the inner cell mass of the mouse blastocyst. *Stem Cells* **31,** 1932-1941 (2013).

15. Bessonnard, S., Vandormael-Pournin, S., Coqueran, S., Cohen-Tannoudji, M. & Artus, J. PDGF signaling in primitive endoderm cell survival is mediated by PI3K-mTOR through p53-independent mechanism. *Stem Cells* **37,** 888-898 (2019).

16. Molotkov, A. & Soriano, P. Distinct mechanisms for PDGF and FGF signaling in primitive endoderm development. *Dev. Biol.* **442,** 155-161 (2018).

17. Manejwala, F. M., Cragoe, E. J., Jr. & Schultz, R. M. Blastocoel expansion in the preimplantation mouse embryo: role of extracellular sodium and chloride and possible apical routes of their entry. *Dev. Biol.* **133,** 210-220 (1989).

18. Zhao, Y., Doroshenko, P. A., Alper, S. L. & Baltz, J. M. Routes of Cl−transport across the trophectoderm of the mouse blastocyst. *Dev. Biol.* **189,** 148-160 (1997).

19. Kidder, G. M. & Watson, A. J. Roles of Na,K-ATPase in early development and trophectoderm differentiation. *Semin. Nephrol.* **25,** 352-355 (2005).

20. Leese, H. J. Metabolism of the preimplantation embryo: 40 years on. *Reproduction* **143,** 417-427 (2012).

21. Kumar, R. P. *et al.* Regulation of energy metabolism during early mammalian development: TEAD4 controls mitochondrial transcription. *Development* **145,** dev162644 (2018).

22. Cuadrado, A. & Nebreda, A. R. Mechanisms and functions of p38 MAPK signalling. *Biochem. J.* **429,** 403-417 (2010).

23. Cuenda, A. & Rousseau, S. p38 MAP-kinases pathway regulation, function and role in human diseases. *Biochim. Biophys. Acta* **1773,** 1358-1375 (2007).

24. Bradham, C. & McClay, D. R. p38 MAPK in development and cancer. *Cell Cycle* **5,** 824-828 (2006).

25. Brewer, J. R., Mazot, P. & Soriano, P. Genetic insights into the mechanisms of Fgf signaling. *Genes Dev.* **30,** 751-771 (2016).

26. Wang, Y. *et al.* p38 Inhibition ameliorates skin and skull abnormalities in Fgfr2 Beare-Stevenson mice. *J. Clin. Invest.* **122,** 2153-2164 (2012).

27. Wang, Y. *et al.* Activation of p38 MAPK pathway in the skull abnormalities of Apert syndrome Fgfr2(+P253R) mice. *BMC Dev. Biol.* **10,** 22 (2010).

28. Zakrzewska, M., Opalinski, L., Haugsten, E. M., Otlewski, J. & Wiedlocha, A. Crosstalk between p38 and Erk 1/2 in downregulation of FGF1-induced signaling. *Int. J. Mol. Sci.* **20,** 1826 (2019).

29. Sørensen, V. *et al.* Phosphorylation of fibroblast growth factor (FGF) receptor 1 at Ser777 by p38 mitogen-activated protein kinase regulates translocation of exogenous FGF1 to the cytosol and nucleus. *Mol. Cell. Biol.* **28,** 4129-4141 (2008).

30. Mahe, M. *et al.* An FGFR3/MYC positive feedback loop provides new opportunities for targeted therapies in bladder cancers. *EMBO Mol. Med.* **10,** e8163 (2018).

31. Ohnishi, Y. *et al.* Cell-to-cell expression variability followed by signal reinforcement progressively segregates early mouse lineages. *Nat. Cell Biol.* **16,** 27-37 (2014).

32. Adams, R. H. *et al.* Essential role of p38alpha MAP kinase in placental but not embryonic cardiovascular development. *Mol. Cell* **6,** 109-116 (2000).

33. Natale, D. R., Paliga, A. J., Beier, F., D'Souza, S. J. & Watson, A. J. p38 MAPK signaling during murine preimplantation development. *Dev. Biol.* **268,** 76-88 (2004).

34. Bell, C. E. & Watson, A. J. p38 MAPK regulates cavitation and tight junction function in the mouse blastocyst. *PLoS One* **8,** e59528 (2013).

35. Maekawa, M. *et al.* Requirement of the MAP kinase signaling pathways for mouse preimplantation development. *Development* **132,** 1773-1783 (2005).

36. Thamodaran, V. & Bruce, A. W. p38 (Mapk14/11) occupies a regulatory node governing entry into primitive endoderm differentiation during preimplantation mouse embryo development. *Open Biol.* **6,** 160190 (2016).

37. Bora, P., Thamodaran, V., Šušor, A. & Bruce, A. W. p38-mitogen activated kinases mediate a developmental regulatory response to amino acid depletion and associated oxidative stress in mouse blastocyst embryos. *Front. Cell Dev. Biol.* **7,** 276 (2019).

38. Sciorio, R., Thong, K. J. & Pickering, S. J. Spontaneous blastocyst collapse as an embryo marker of low pregnancy outcome: a Time-Lapse study. *JBRA Assist. Reprod.* **24,** 34-40 (2020).

39. Kovačič, B., Taborin, M. & Vlaisavljević, V. Artificial blastocoel collapse of human blastocysts before vitrification and its effect on re-expansion after warming - a prospective observational study using time-lapse microscopy. *Reprod. Biomed. Online* **36,** 121-129 (2018).

40. Mudgett, J. S. *et al.* Essential role for p38alpha mitogen-activated protein kinase in placental angiogenesis. *Proc. Natl. Acad. Sci. U. S. A.* **97,** 10454-10459 (2000).

41. Sabio, G. *et al.* p38gamma regulates the localisation of SAP97 in the cytoskeleton by modulating its interaction with GKAP. *EMBO J.* **24,** 1134-1145 (2005).

42. Beardmore, V. A. *et al.* Generation and characterization of p38beta (MAPK11) gene-targeted mice. *Mol. Cell. Biol.* **25,** 10454-10464 (2005).

43. Hornbeck, P. V. *et al.* PhosphoSitePlus, 2014: mutations, PTMs and recalibrations. *Nucleic Acids Res.* **43,** D512-D520 (2015).

44. Bardwell, L. Mechanisms of MAPK signalling specificity. *Biochem. Soc. Trans.* **34,** 837-841 (2006).

45. Masek, T. *et al.* Identifying the translatome of mouse NEBD-stage oocytes via SSP-profiling; a novel polysome fractionation method. *Int. J. Mol. Sci.* **21,** 1254 (2020).

46. Corsini, N. S. *et al.* Coordinated control of mRNA and rRNA processing controls embryonic stem cell pluripotency and differentiation. *Cell Stem Cell* **22,** 543-558.e12 (2018).

47. Taylor, G. C., Eskeland, R., Hekimoglu-Balkan, B., Pradeepa, M. M. & Bickmore, W. A. H4K16 acetylation marks active genes and enhancers of embryonic stem cells, but does not alter chromatin compaction. *Genome Res.* **23,** 2053-2065 (2013).

48. Strumpf, D. *et al.* Cdx2 is required for correct cell fate specification and differentiation of trophectoderm in the mouse blastocyst. *Development* **132,** 2093-2102 (2005).

49. Komarnitsky, P., Cho, E. J. & Buratowski, S. Different phosphorylated forms of RNA polymerase II and associated mRNA processing factors during transcription. *Genes Dev.* **14,** 2452-2460 (2000).

50. Yamagiwa, Y., Marienfeld, C., Tadlock, L. & Patel, T. Translational regulation by p38 mitogen-activated protein kinase signaling during human cholangiocarcinoma growth. *Hepatology* **38,** 158-166 (2003).

51. Fonseca, B. D. *et al.* The ever-evolving role of mTOR in translation. *Semin. Cell Dev. Biol.* **36,** 102-112 (2014).

52. Prabhu, S. A., Moussa, O., Miller, W. H., Jr. & Del Rincón, S. V. The MNK1/2-eIF4E axis as a potential therapeutic target in melanoma. *Int. J. Mol. Sci.* **21,** 4055 (2020).

53. Topisirovic, I. & Sonenberg, N. mRNA translation and energy metabolism in cancer: the role of the MAPK and mTORC1 pathways. *Cold Spring Harb. Symp. Quant. Biol.* **76,** 355-367 (2011).

54. Bulut-Karslioglu, A. *et al.* Inhibition of mTOR induces a paused pluripotent state. *Nature* **540,** 119-123 (2016).

55. Thoreen, C. C. *et al.* An ATP-competitive mammalian target of rapamycin inhibitor reveals rapamycin-resistant functions of mTORC1. *J. Biol. Chem.* **284,** 8023-8032 (2009).

56. Choi, Y. J. *et al.* Inhibitory effect of mTOR activator MHY1485 on autophagy: suppression of lysosomal fusion. *PLoS One* **7,** e43418 (2012).

57. Nichols, J., Silva, J., Roode, M. & Smith, A. Suppression of Erk signalling promotes ground state pluripotency in the mouse embryo. *Development* **136,** 3215-3222 (2009).

58. Ciuffreda, L. *et al.* Growth-inhibitory and antiangiogenic activity of the MEK inhibitor PD0325901 in malignant melanoma with or without BRAF mutations. *Neoplasia* **11,** 720-731 (2009).

59. Zhang, B. *et al.* Allelic reprogramming of the histone modification H3K4me3 in early mammalian development. *Nature* **537,** 553-557 (2016).

60. Wang, C. *et al.* Reprogramming of H3K9me3-dependent heterochromatin during mammalian embryo development. *Nat. Cell Biol.* **20,** 620-631 (2018).

61. Hochstatter, J. *et al.* Myb-binding protein 1a (Mybbp1a) regulates levels and processing of pre-ribosomal RNA. *J. Biol. Chem.* **287,** 24365-24377 (2012).

62. Tan, B. C. *et al.* Epigeneitc silencing of ribosomal RNA genes by Mybbp1a. *J. Biomed. Sci.* **19,** 57 (2012).

63. Kumazawa, T. *et al.* Gradual reduction in rRNA transcription triggers p53 acetylation and apoptosis via MYBBP1A. *Sci. Rep.* **5,** 10854 (2015).

64. Ono, W. *et al.* The nucleolar protein Myb-binding protein 1A (MYBBP1A) enhances p53 tetramerization and acetylation in response to nucleolar disruption. *J. Biol. Chem.* **289,** 4928-4940 (2014).

65. Díaz, V. M. *et al.* p160 Myb-binding protein interacts with Prep1 and inhibits its transcriptional activity. *Mol. Cell. Biol.* **27,** 7981-7990 (2007).

66. Mori, S. *et al.* Myb-binding protein 1A (MYBBP1A) is essential for early embryonic development, controls cell cycle and mitosis, and acts as a tumor suppressor. *PLoS One* **7,** e39723 (2012).

67. Bassalert, C., Valverde-Estrella, L. & Chazaud, C. Primitive endoderm differentiation: from specification to epithelialization. *Curr. Top. Dev. Biol.* **128,** 81-104 (2018).

68. Wiley, L. M. Cavitation in the mouse preimplantation embryo: Na/K-ATPase and the origin of nascent blastocoele fluid. *Dev. Biol.* **105,** 330-342 (1984).

69. Watson, A. J. The cell biology of blastocyst development. *Mol. Reprod. Dev.* **33,** 492-504 (1992).

70. Madan, P., Rose, K. & Watson, A. J. Na/K-ATPase beta1 subunit expression is required for blastocyst formation and normal assembly of trophectoderm tight junction-associated proteins. *J. Biol. Chem.* **282,** 12127-12134 (2007).

71. Chan, C. J. *et al.* Hydraulic control of mammalian embryo size and cell fate. *Nature* **571,** 112-116 (2019).

72. Barcroft, L. C., Moseley, A. E., Lingrel, J. B. & Watson, A. J. Deletion of the Na/K-ATPase α1-subunit gene (Atp1a1) does not prevent cavitation of the preimplantation mouse embryo. *Mech. Dev.* **121,** 417-426 (2004).

73. Wigger, M. *et al.* Plasticity of the inner cell mass in mouse blastocyst is restricted by the activity of FGF/MAPK pathway. *Sci. Rep.* **7,** 15136 (2017).

74. Mathew, B. *et al.* Mouse ICM organoids reveal three-dimensional cell fate clustering. *Biophys. J.* **116,** 127-141 (2019).

75. Yamanaka, Y., Lanner, F. & Rossant, J. FGF signal-dependent segregation of primitive endoderm and epiblast in the mouse blastocyst. *Development* **137,** 715-724 (2010).

76. Raucci, A., Laplantine, E., Mansukhani, A. & Basilico, C. Activation of the ERK1/2 and p38 mitogen-activated protein kinase pathways mediates fibroblast growth factor-induced growth arrest of chondrocytes. *J. Biol. Chem.* **279,** 1747-1756 (2004).

77. Williamson, A. J., Dibling, B. C., Boyne, J. R., Selby, P. & Burchill, S. A. Basic fibroblast growth factor-induced cell death is effected through sustained activation of p38MAPK and up-regulation of the death receptor p75NTR. *J. Biol. Chem.* **279,** 47912-47928 (2004).

78. Matsumoto, T., Turesson, I., Book, M., Gerwins, P. & Claesson-Welsh, L. p38 MAP kinase negatively regulates endothelial cell survival, proliferation, and differentiation in FGF-2-stimulated angiogenesis. *J. Cell Biol.* **156,** 149-160 (2002).

79. Maher, P. Phorbol esters inhibit fibroblast growth factor-2-stimulated fibroblast proliferation by a p38 MAP kinase dependent pathway. *Oncogene* **21,** 1978-1988 (2002).

80. Maher, P. p38 mitogen-activated protein kinase activation is required for fibroblast growth factor-2-stimulated cell proliferation but not differentiation. *J. Biol. Chem.* **274,** 17491-17498 (1999).

81. Yang, J. *et al.* Binding of FGF2 to FGFR2 in an autocrine mode in trophectoderm cells is indispensable for mouse blastocyst formation through PKC-p38 pathway. *Cell Cycle* **14,** 3318-3330 (2015).

82. Azami, T. *et al.* Regulation of the ERK signalling pathway in the developing mouse blastocyst. *Development* **146,** dev177139 (2019).

83. Frankenberg, S. *et al.* Primitive endoderm differentiates via a three-step mechanism involving Nanog and RTK signaling. *Dev. Cell* **21,** 1005-1013 (2011).

84. Krawchuk, D., Honma-Yamanaka, N., Anani, S. & Yamanaka, Y. FGF4 is a limiting factor controlling the proportions of primitive endoderm and epiblast in the ICM of the mouse blastocyst. *Dev. Biol.* **384,** 65-71 (2013).

85. Frum, T. & Ralston, A. Culture conditions antagonize lineage-promoting signaling in the mouse blastocyst. *Reproduction* **160,** V5-V7 (2020).

86. Artus, J., Panthier, J. J. & Hadjantonakis, A. K. A role for PDGF signaling in expansion of the extra-embryonic endoderm lineage of the mouse blastocyst. *Development* **137,** 3361-3372 (2010).

87. Piazzi, M., Bavelloni, A., Gallo, A., Faenza, I. & Blalock, W. L. Signal transduction in ribosome biogenesis: a recipe to avoid disaster. *Int. J. Mol. Sci.* **20,** 2718 (2019).

88. Iadevaia, V., Liu, R. & Proud, C. G. mTORC1 signaling controls multiple steps in ribosome biogenesis. *Semin. Cell Dev. Biol.* **36,** 113-120 (2014).

89. Mayer, C. & Grummt, I. Ribosome biogenesis and cell growth: mTOR coordinates transcription by all three classes of nuclear RNA polymerases. *Oncogene* **25,** 6384-6391 (2006).

90. Hussein, A. M. *et al.* Metabolic control over mTOR-dependent diapause-like state. *Dev. Cell* **52,** 236-250.e7 (2020).

91. Perrera, C. *et al.* Identification of Myb-binding protein 1A (MYBBP1A) as a novel substrate for Aurora B kinase. *J. Biol. Chem.* **285,** 11775-11785 (2010).

92. Wiśniewski, J. R., Ostasiewicz, P. & Mann, M. High recovery FASP applied to the proteomic analysis of microdissected formalin fixed paraffin embedded cancer tissues retrieves known colon cancer markers. *J. Proteome Res.* **10,** 3040-3049 (2011).

93. Yeung, Y.-G., Nieves, E., Angeletti, R. H. & Stanley, E. R. Removal of detergents from protein digests for mass spectrometry analysis. *Anal. Biochem.* **382,** 135-137 (2008).

94. Perez-Riverol, Y. *et al*. The PRIDE database and related tools and resources in 2019: improving support for quantification data. *Nucleic Acids Res.* **47**(D1):D442-D450 ((2019).

95. Eden, E., Lipson, D., Yogev, S. & Yakhini, Z. Discovering motifs in ranked lists of DNA sequences. *PLoS Comput. Biol.* **3,** e39 (2007).

96. Eden, E., Navon, R., Steinfeld, I., Lipson, D. & Yakhini, Z. GOrilla: a tool for discovery and visualization of enriched GO terms in ranked gene lists. *BMC Bioinformatics* **10,** 48 (2009).

97. Milewski, R., Szpila, M. & Ajduk, A. Dynamics of cytoplasm and cleavage divisions correlates with preimplantation embryo development. *Reproduction* **155,** 1-14 (2018).

98. Schindelin, J. *et al.* Fiji: an open-source platform for biological-image analysis. *Nat. Methods* **9,** 676-682 (2012).

99. McCloy, R. A. *et al.* Partial inhibition of Cdk1 in G 2 phase overrides the SAC and decouples mitotic events. *Cell Cycle* **13,** 1400-1412 (2014).

100. Potapova, T. A., Sivakumar, S., Flynn, J. N., Li, R. & Gorbsky, G. J. Mitotic progression becomes irreversible in prometaphase and collapses when Wee1 and Cdc25 are inhibited. *Mol. Biol. Cell* **22,** 1191-1206 (2011).

Acknowledgements

We acknowledge the Institute of Parasitology (Biology Centre of the Czech Academy of Sciences, in České Budějovice) for housing mice, Marta Gajewska (Institute of Oncology, Warsaw, Poland) and Anna Piliszek (Institute of Genetics and Animal Breeding, Polish Academy of Sciences, Jastrzębiec, Poland) for providing founder CBA/W mice, Alena Krejčí (Faculty of Science, University of South Bohemia, Czech Republic) for pooling resources and other members of our laboratory for providing valuable input and discussions. We further acknowledge Markéta Hančová (IAPG, Liběchov) for her help in carrying out experiments. We also acknowledge the core facility at Masaryk University, Brno, Czech Republic - Faculty of Informatics, supported by the MEYS CR (LM2018129 Czech-BioImaging), for assistance with image analysis. CIISB, Instruct-CZ Centre of Instruct-ERIC EU consortium, funded by the MEYS CR infrastructure project LM2018127, is gratefully acknowledged for financial support of measurements at the CEITEC Proteomics Core Facility. Computational resources were supplied by the project e-Infrastruktura CZ (e-INFRA LM2018140) provided within the program Projects of Large Research, Development and Innovations Infrastructures. We also thank our peer reviewers for their insightful and helpful comments during the revision process. This work was supported by a project grant from the Czech Science Foundation/GACR (18-02891S), a Marie Curie Individual Fellowship (MSC IF 708255) awarded to L.G. and a Ph.D. student award given to P.B. by the Grant Agency of the University of South Bohemia (GAJU; 012/2019/P).

Author contributions

P.B. and A.W.B. conceived the project, designed experiments, analyzed results and wrote the manuscript. P.B. conducted experiments. P.B. and L.G. prepared samples for mass spectrometry and RNA sequencing. L.G. analyzed proteomic, phosphoproteomic and transcriptomic data and wrote associated portions within the manuscript. T.M. and M.P. designed and produced scarce-sample polysome profiling fractions. A.H. analyzed images for blastocoel cavity volume determination. D.P. and Z.Z. performed phosphoproteomic mass spectrometry, performed preliminary data analysis and wrote the associated methods. A.A. performed time-lapse imaging and analysis. D.J. and A.S. performed peripheral experiments.

Competing interests

The authors declare no competing interests.

Figure legends

Figure 1. Temporal resolution and morphological effects of inhibiting p38-MAPK signaling in developing blastocysts.

a) Scheme illustrating the experimental protocol used to resolve the temporal nature of p38-MAPKi in the PrE deficit phenotype. The lineage markers NANOG and GATA4 denote EPI and PrE cells, respectively.

b) Quantification of the ratio of GATA4-positive PrE cells to total ICM cells in control (n=21) and p38-MAPKi (n=22) conditions from confocal images of E4.5 embryos transiently cultured with DMSO or SB220025 between E3.5 +4 h and E3.5 +7 h (right); the means and standard deviations are highlighted. Representative z-section blastocyst projections are shown on the left (scale bars = 20 µm).

c) Quantification of the ratio of GATA4-positive PrE cells to total ICM cells in control (DMSO) (n=42) and p38-MAPKi (SB220025) (n=38) conditions for treatment between E3.5 and E4.5 (recapitulation of previously published observations[36,37]); the means and standard deviations are highlighted.

d) Quantification of the equatorial cavity areas (μm^2) in fixed blastocysts cultured (E3.5-E4.5) in control (DMSO; n=20) and p38-MAPKi (SB220025; n=17) conditions. Representative confocal equatorial z-sections of each embryo group are shown, with the cavity circumference indicated (dashed yellow line) (upper panel scale bar = 20 µm)

e) Equatorial areas of control (DMSO; n=32) and p38-MAPKi (SB220025; n=32) blastocysts imaged in live culture from E3.5-E4.5 (Supplementary Table 1d). The sub-panels show segments of the recordings between 3 h and 10 h, 10 h and 15 h, and 15 h and 22 h. The bar graph denotes the percentages of hatching blastocysts observed at the end of the imaging period (E4.5).

f) qRT-PCR-derived expression levels (normalized to *Tbp*) of the ICM lineage markers *Nanog* and *Gata4* (upper) and the p38-MAPK paralogous genes *Mapk11-14* (lower) during early blastocyst maturation (at E3.5 +0 h, E3.5 +3 h, E3.5 +6 h, E3.5 +9 h and E3.5 +10 h).

Figure 2. Proteomic and phosphoproteomic analyses of the effects of p38-MAPKi in developing blastocysts.

a) Experimental design of sample collection for control (DMSO; n=3 (300 embryos per repeat)) and p38-MAPKi (SB220025; n=3 (300 embryos per repeat)) blastocysts after 7 h of chemical exposure (at E3.5 +9 h) prior to mass spectrometric analysis of the (phospho-)proteome (300 blastocysts per condition were tested in biological triplicates).

b) The most statistically significantly enriched GO terms for the differentially detected proteins between control and p38-MAPKi blastocysts.

c) Volcano plot of the detected differentially expressed proteins associated with p38-MAPKi. Proteins associated with the indicated enriched GO terms are highlighted in blue (translation), purple (ribosomal small subunit biogenesis) and green (ribosomal small subunit assembly) (note that there is overlap); the proteins associated with other terms are in red, while the proteins that were not statistically significantly changed are in gray.

d) Statistically significantly enriched GO terms for the differentially detected phosphopeptides between control and p38-MAPKi blastocysts.

Figure 3. Temporal transcriptomic analysis of the effects of p38-MAPKi during early blastocyst maturation.

a) Experimental design for transcriptome sample collection for the control (DMSO) and p38-MAPKi (SB220025) conditions from E3.5 to +4 h, +7 h or +10 h (biological duplicates of 30 blastocysts per condition were tested per time point).

b) Venn diagram showing the numbers of differentially expressed mRNAs (as determined by DESeq2 analysis) and their overlap between control and p38-MAPKi blastocysts at the three selected time points (*i.e.,* E3.5 +4 h, +7 h and +10 h).

c) Hierarchical clustering heatmap depicting the expression of mRNAs that were significantly changed by p38-MAPKi at the +7 h time point and the transcript levels of those same genes at the +4 and +10 h time points. The mRNAs formed three distinct expression clusters.

d) Top 15 terms identified in GO enrichment analysis for the p38-MAPK-regulated transcriptome at the +7 h time-point (excluding generalized terms).

e) Hierarchical clustering heatmap of genes originally identified as downregulated at the protein level and associated with translation-related GO terms after p38-MAPKi (Figure 2b and c) at the three assayed early blastocyst ±p38-MAPKi time points.

Figure 4. Effects of p38-MAPKi on active translation, rRNA processing and the transcriptional landscape in developing blastocysts.

a) Experimental design for analysis of the roles of p38-MAPK activity in developmental translation and transcription in maturing blastocysts (between E3.5 and E3.5 +10 h).

b) Representative confocal z-projection micrographs (upper) of E3.5 +10 h blastocysts in control (DMSO; n=12) and p38-MAPKi (SB220025; n=12) conditions depicting cell nuclear staining (DAPI) and *de novo* translation (after OPP incorporation); scale bar = 20 μm. The scatterplot

shows the corrected total cell fluorescence (CTCFs) of OPP incorporation between the two conditions (lower); the means and standard deviations are.

c) qRT-PCR analyses quantifying 18S and 28S rRNA levels in each of ten SSP profiling fractions representative of polysome-associated (F6-F10) and non-polysome-associated (F1-F5) rRNA transcripts obtained from both control and p38-MAPKi blastocysts (E3.5 +10 h). Box-and-whisker plots represents the proportion of the overall amount of rRNA transcript detected for a given fraction. The data were generated from four sets of 10 embryos each, per condition.

d) Ratios of polysome- to non-polysome-quantified rRNAs (as derived from the data in Figure 4c) for 18S and 28S separately (top panel) and combined (bottom panel). The data are presented in interleaved box-and-whisker plots, with the whiskers depicting the minimum and maximum values and the boxes including the medians and the 25^{th} and 75^{th} percentiles.

e) Schematic representation of 45S pre-rRNA highlighting the qRT-PCR amplicons assayed and quantified to analyze rRNA processing status ±p38-MAPKi (E3.5 +10 h).

f) Box and whisker plots (25^{th} to 75^{th} percentile in box and minimum and maximum by whiskers, with median marked by horizontal bar and showing all points; n=4) representing the mean qRT-PCR-quantified fold-changes of the different specific amplicons (normalized against *H2afz* cDNA) in p38-MAPKi versus control blastocysts (DMSO). "+" denotes the mean.

g) Representative single z-stack micrographs (upper) of E3.5 +10 h blastocysts under control (DMSO; n=13 embryos) and p38-MAPKi (SB220025; n=15 embryos) conditions. Individual channel micrographs for DAPI (blue pan-nuclear stain; shows the total number of cells), H4K16ac (grayscale; a posttranslational histone chromatin mark associated with transcriptional activity) and CDX2 (grayscale; marks outer TE cells) plus a merged H4K16ac (red) and CDX2 (green) image are shown (scale bar = 20 μm). Scatterplots (lower) quantifying the H4K16ac (CTCF) level per nucleus in control (DMSO) and p38-MAPKi (SB220025) blastocysts differentiated between inner (n=129 for DMSO and n=143 for SB220025) and outer (n=136 for DMSO and n=145 for SB220025) cell populations are also shown; the means and standard deviations are depicted.

h) Similar to (g) but describes the expression levels of the RNA pol II S2p protein. Quantification was performed for inner cells (n=187 for DMSO and n=135 for SB220025) and outer cells (n=209 for DMSO and n=123 for SB220025) from n=11 embryos in DMSO and n=14 embryos in SB220025 conditions, with the means and standard deviations shown.

Figure 5. Functional interplay between mTOR and p38-MAPK during blastocyst maturation and PrE differentiation.

a) Experimental schematic for analysis of the potential functional overlap of mTOR and p38-MAPK with regard to PrE differentiation (via assay of ICM lineage marker protein expression)

during blastocyst maturation. E3.5-stage blastocysts were cultured for 24 h in medium (±AAs) containing the indicated pharmacological supplements (vehicle control: DMSO; p38-MAPK inhibitor: SB220025; mTOR inhibitor: TORIN1; mTOR activator: MHY1485; MEK1/2 inhibitor: PD0325901) or combinations thereof.

b–i) Representative confocal z-series projections of blastocysts cultured under the conditions described in (**a**) and stained with DAPI (blue) and for NANOG, GATA4 and GATA6 protein expression (cyan, yellow and red in the provided merged image); scale bar = 20 μm. (**b**) DMSO (n=21), (**c**) p38-MAPKi, SB220025 (n=17), (**d**) mTOR inhibition, TORIN1 (n=15), (**e**) mTOR activation, MHY1485 (n=32), (**f**) p38-MAPKi and mTOR activation, SB220025 + MHY1485 (n=22), (**g**) MEK inhibition, PD0325901 (n=15), (**h**) MEK inhibition and mTOR activation, PD0325901 + MHY1485 (n=16) and (**i**) p38-MAPKi and mTOR activation, SB220025 + MHY1485 in KSOM not supplemented with AAs (n=24). In panel (**f**) and the expanded view, the white arrowheads highlight differentiated PrE cells expressing GATA4 (and GATA6) but not NANOG, whereas the yellow arrowheads show ICM cells coexpressing GATA4 and NANOG (which were comparatively enriched in this condition).

j)-**q**) Scatterplots showing the total, outer and inner blastocyst cell numbers (as indicated by DAPI staining) and the numbers of NANOG-, GATA4- and GATA6-expressing ICM cells under the culture conditions described in (**a**) (with the means and standard deviations highlighted). **j**) Total cells; **k**) outer cells; **l**) inner cells; **m**) NANOG-expressing inner cells; **n**) GATA4-expressing inner cells; **o**) the ratio of GATA4-positive, NANOG-negative PrE cells to total ICM cells; **p**) the ratio of NANOG- and GATA6-coexpressing cells to total ICM cells; and **q**) the ratio of NANOG- and GATA4-coexpressing cells to total ICM cells.

Figure 6. Analysis of the roles of MYBBP1A (a candidate target of p38-MAPK activity) in preimplantation embryonic development and ICM cell fate specification.

a) Phosphoproteome-to-proteome scatterplot for MS-detected peptides demonstrating <1.3-fold differences in abundance in the general proteome and >1.5-fold changes in phosphorylation levels. Candidates of interest (based on literature research; *e.g.*, MYBBP1A), are highlighted (and were assayed for PrE phenotypes in clonal siRNA microinjection-mediated loss-of-function assays – Figure 6c-f, Supplementary Figure 4, and Supplementary Table 3).

b) Experimental design for analysis of the efficiency of siRNA-mediated *Mybbp1a* gene mRNA knockdown in microinjected embryos cultured to the equivalent late blastocyst (E4.5) stage (qRT-PCR analysis) and for analysis of the contributions of marked *Mybbp1a* knockdown clones to late blastocyst cell lineages (Lineage quantification).

c) Comparison of qRT-PCR-derived relative *Mybbp1a* transcript levels (normalized to *H2afz* mRNA levels) between embryos injected with nontargeting control (NTC) siRNA and embryos injected with siRNA specific for *Mybbp1a* mRNA.

d) Confocal micrograph z-projections of representative late (E4.5)-stage blastocysts initially microinjected (in one blastomere at the 2-cell stage) with NTC siRNA (n=9) plus recombinant *H2b-RFP* fluorescent reporter mRNA (identifying the clonal progeny of the injected cell). Individual DAPI (blue pan-nuclear stain; indicates the total number of cells), NANOG (grayscale; EPI cells) and GATA4 (grayscale; PrE cells) channel micrographs, plus merged NANOG (cyan), GATA4 (green) and H2B-RFP (microinjected clone) images, are shown (scale bar = 20 μm). (d') Target diagrams describing the average percentage contributions of NTC siRNA-microinjected and non-microinjected clones to either outer and inner cell populations (black and yellow targets) or mutually exclusive NANOG- and GATA4-expressing ICM cell lineages (red and blue targets).

e) Similar to (**d**). (e') is similar to (d'), but the results were obtained after microinjection of *Mybbpa1*-specific siRNA (n=28).

f) Scatterplots describing the contributions of non-microinjected (blue) and microinjected (red) cell clones (plus the combined number – gray) of NTC/*Mybbp1a* siRNA-treated embryos to the total cell count, number of inner cells expressing NANOG only, and number of inner cells expressing GATA4 only. The means and standard deviations are highlighted.

Figure 7. Working model of the role of p38-MAPK in regulating protein translation to prime PrE differentiation during preimplantation-stage blastocyst maturation.

During the period of blastocyst maturation (E3.5 to E4.5), p38-MAPKs, potentially acting via MYBBP1A, enable pre-rRNA processing and regulates global translational and co-transcriptional events, which is necessary for normal development and PrE specification. p38-MAPKs appear to be acting upstream of mTOR, towards a pathway supporting PrE survival in the maturing blastocyst.

Supplementary materials legends

Supplementary Fig. 1

a) Genes significantly differentially expressed in E3.5 +4 hours.

b) Genes significantly differentially expressed in E3.5 +10 hours.

Supplementary Fig. 2: Embryo survival curve E3.5 onwards.

Supplementary Fig. 3: Gene expression profile in preimplantation embryo and associated cellular lineages.

Supplementary Fig. 4 (supplementary to Fig. 6d-f): Mybbp1a KD embryo cell lineage quantification (outer and inner cells and ratio of PrE to ICM).

Supplementary Fig. 5: Cellular lineage and cell numbers with addition of FGF4 (+Heparin) along with p38-MAPK inhibition.

Supplementary Fig. 6: Cellular lineage and cell numbers with addition of FGF4 (+Heparin) along with MEK inhibition (PD0325901).

Supplementary Fig. 7: Blastocyst size for embryos inhibited for 24 hours (E3.5 to E4.5).

Supplementary Table 1: Supplementary table with putative p38-MAPK conensus motifs and/or reported p38-MAPK interaction for phosphopeptides identified.

Supplementary Table 2: Additional phosphoproteome candidate knockdown.

Supplementary Table 3: Atp1a1 proteome readout.

Supplementary Table 4: Introns detected (as RPKM) for "translation" related genes; related to Fig. 3e.

Supplementary Table 5: Pharmacological agents used.

Supplementary Table 6: siRNA.

Supplementary Table 7: Antibodies.

Supplementary Table 8: Statistical tests.

Supplementary Table 9: Primers (oligo) used.

Supplementary Video 1: Control (DMSO) E3.5 to E4.5 (first set of 16 embryos).

Supplementary Video 2: Control (DMSO) E3.5 to E4.5 (second set of 16 embryos).

Supplementary Video 3: Control (DMSO) E3.5 to E4.5 (One representative embryo magnified).

Supplementary Video 4: p38-MAPKi (SB220025) E3.5 to E4.5 (first set of 16 embryos).

Supplementary Video 5: p38-MAPKi (SB220025) E3.5 to E4.5 (second set of 16 embryos).

Supplementary Video 6: p38-MAPKi (SB220025) E3.5 to E4.5 (One representative embryo magnified).

Fig. 1: Temporal resolution and morphological effects of inhibiting p38-MAPK signaling in developing blastocysts.

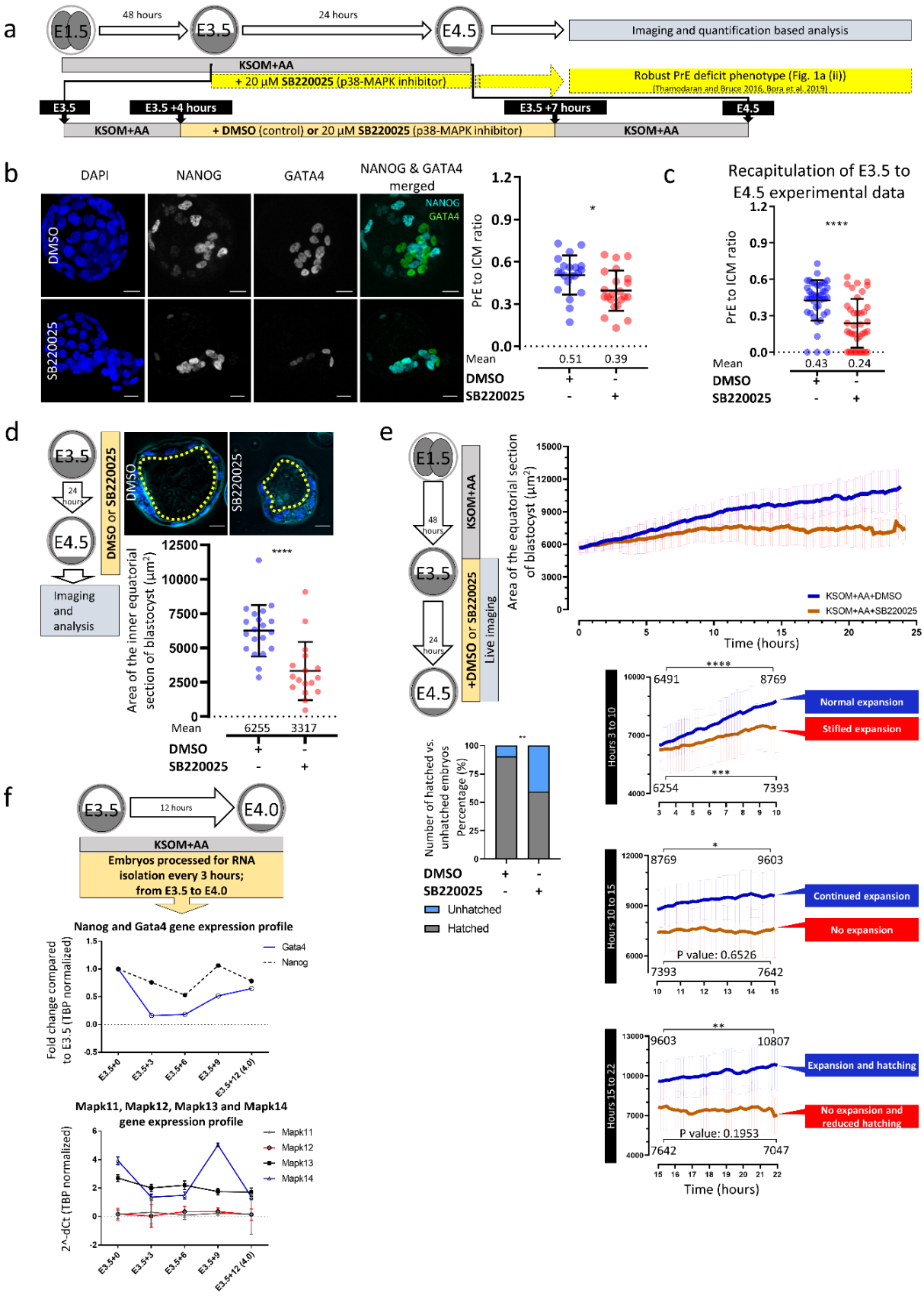

Fig. 2: Proteomic and phosphoproteomic analyses of the effects of p38-MAPKi in developing blastocysts.

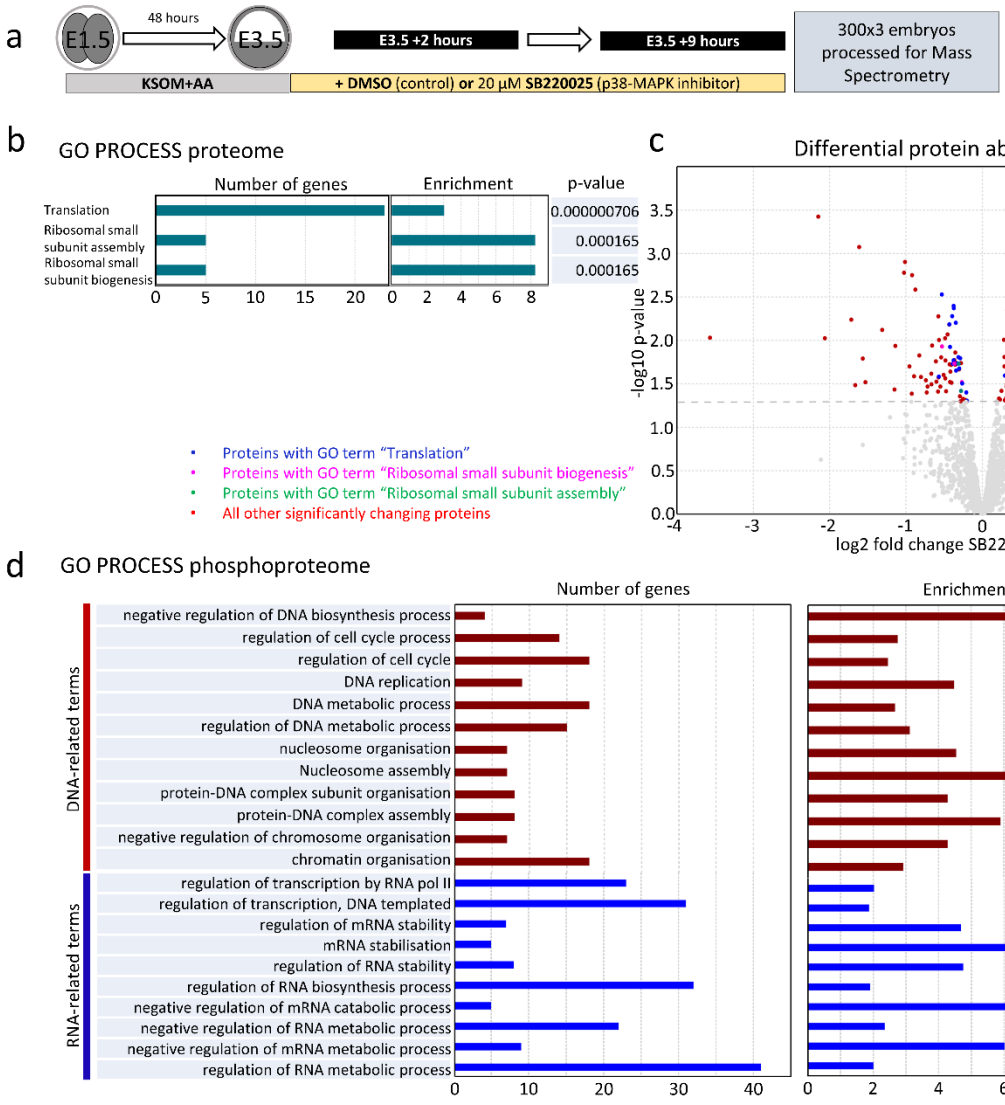

Fig. 3: Temporal transcriptomic analysis of the effects of p38-MAPKi during early blastocyst maturation.

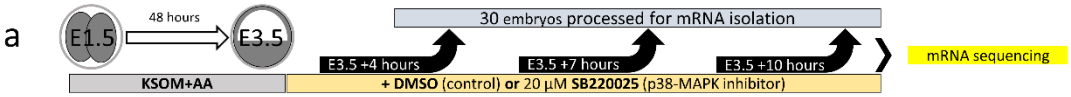

b Differentially expressed genes; DMSO vs SB220025 (DESeq2)

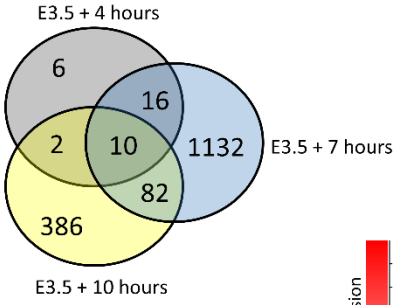

c Genes significantly differentially expressed in E3.5 +7 hours (numbered are clusters with 20+ genes)

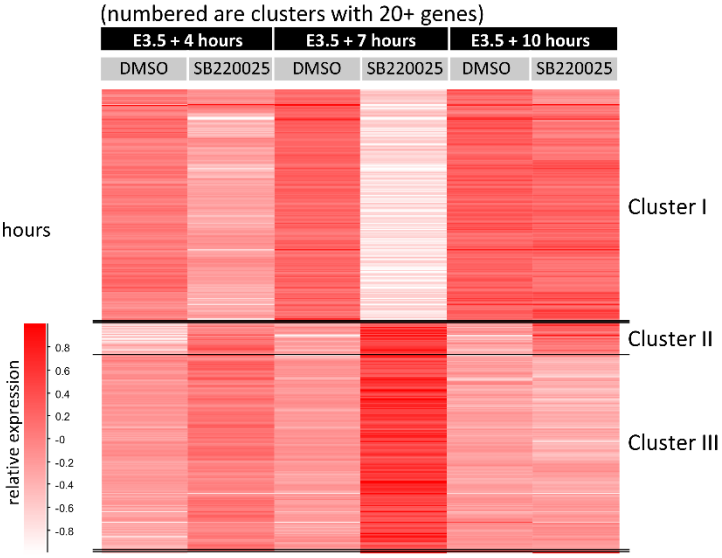

d GO analysis of top 15 terms from E3.5 +7 hours (excluding generalised terms e.g. cellular processes)

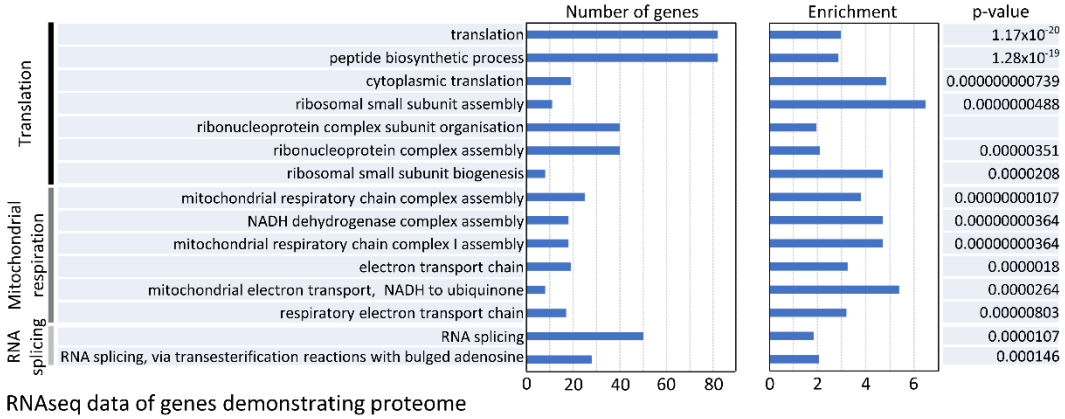

e RNAseq data of genes demonstrating proteome level downregulation

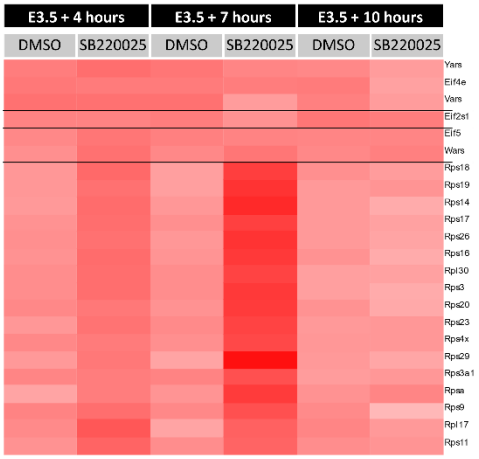

Fig. 4: Effects of p38-MAPKi on active translation, rRNA processing and the transcriptional landscape in developing blastocysts.

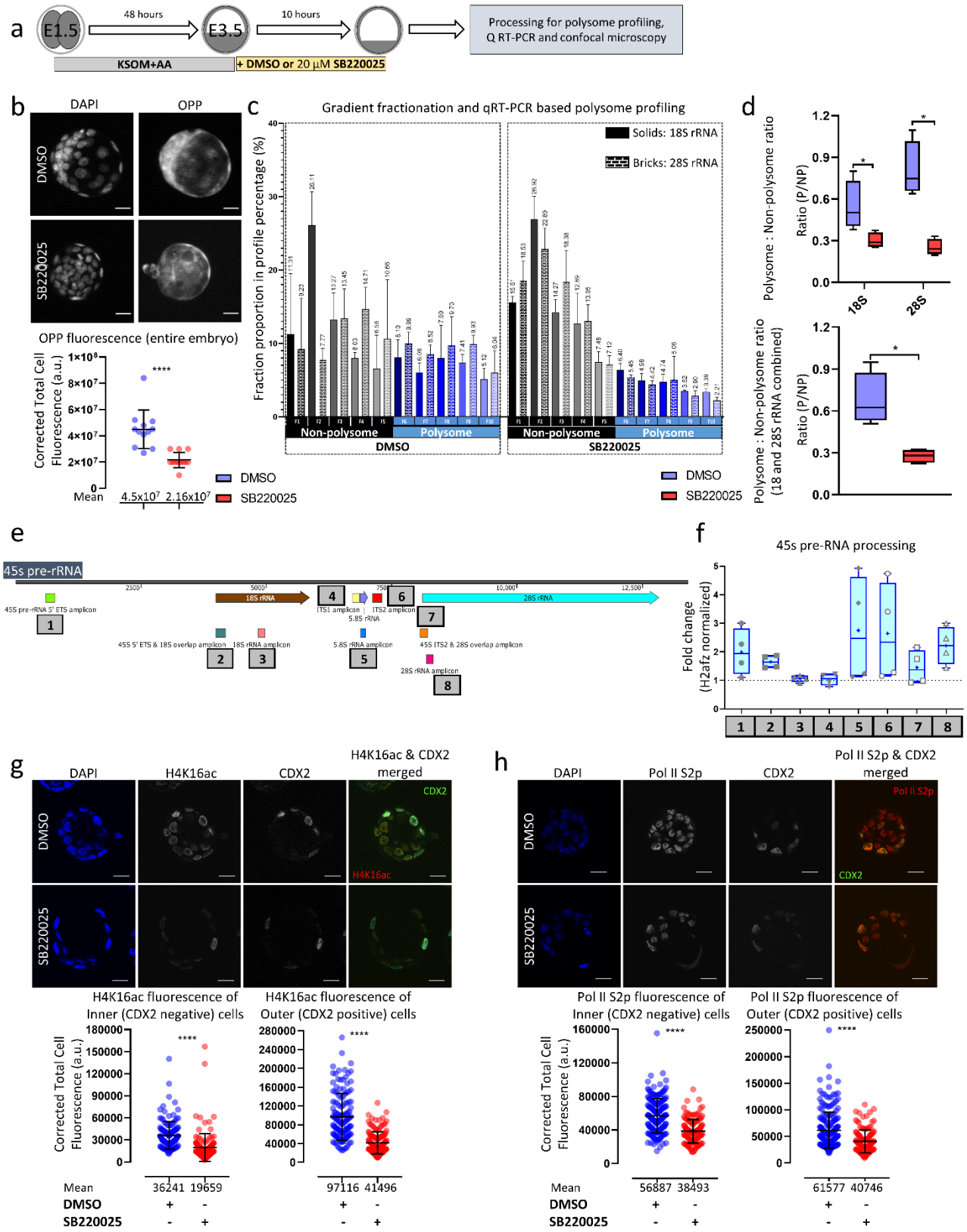

Fig. 5: Functional interplay between mTOR and p38-MAPK during blastocyst maturation and PrE differentiation.

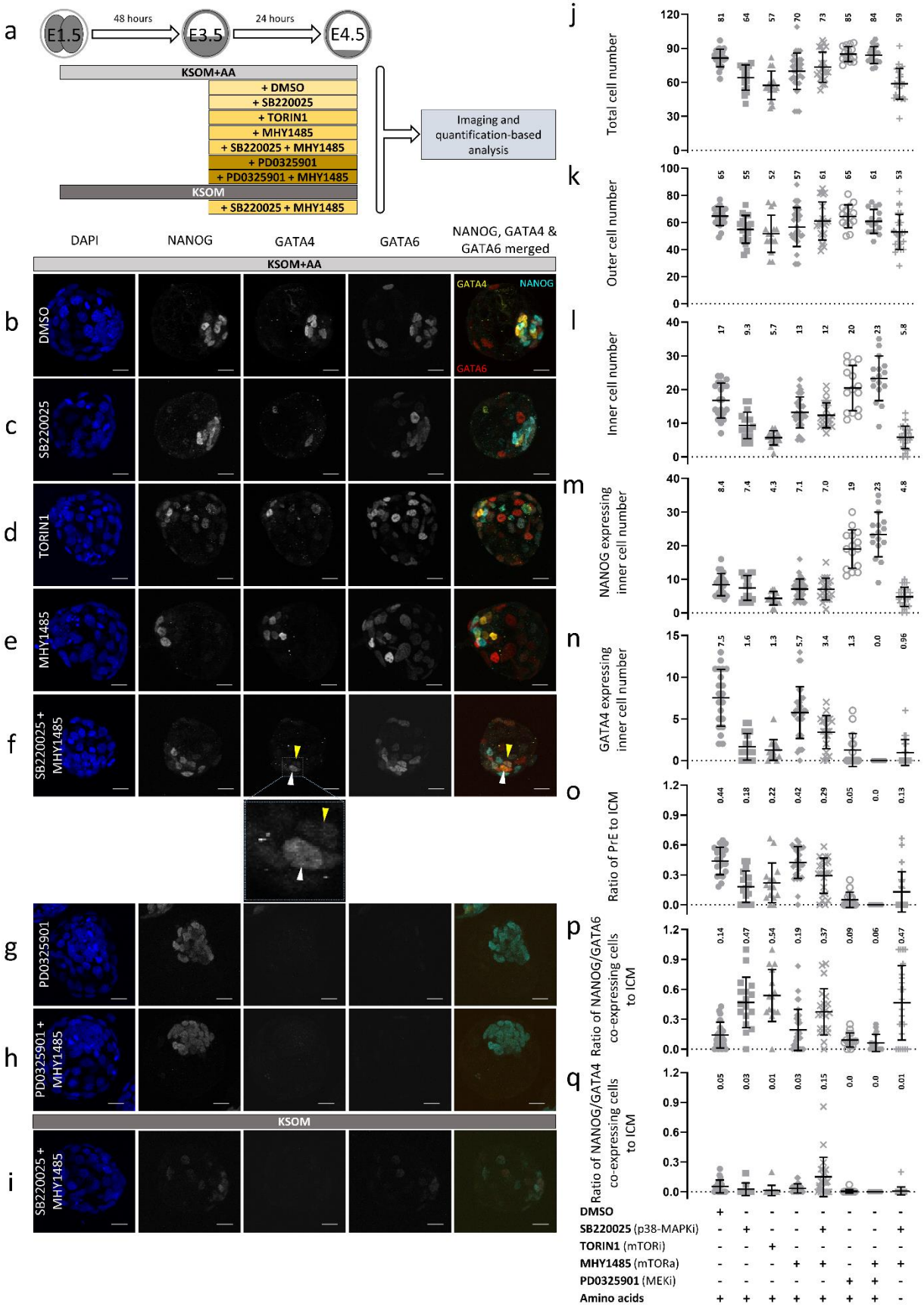

Fig. 6: Analysis of the roles of MYBBP1A (a candidate target of p38-MAPK activity) in preimplantation embryonic development and ICM cell fate specification.

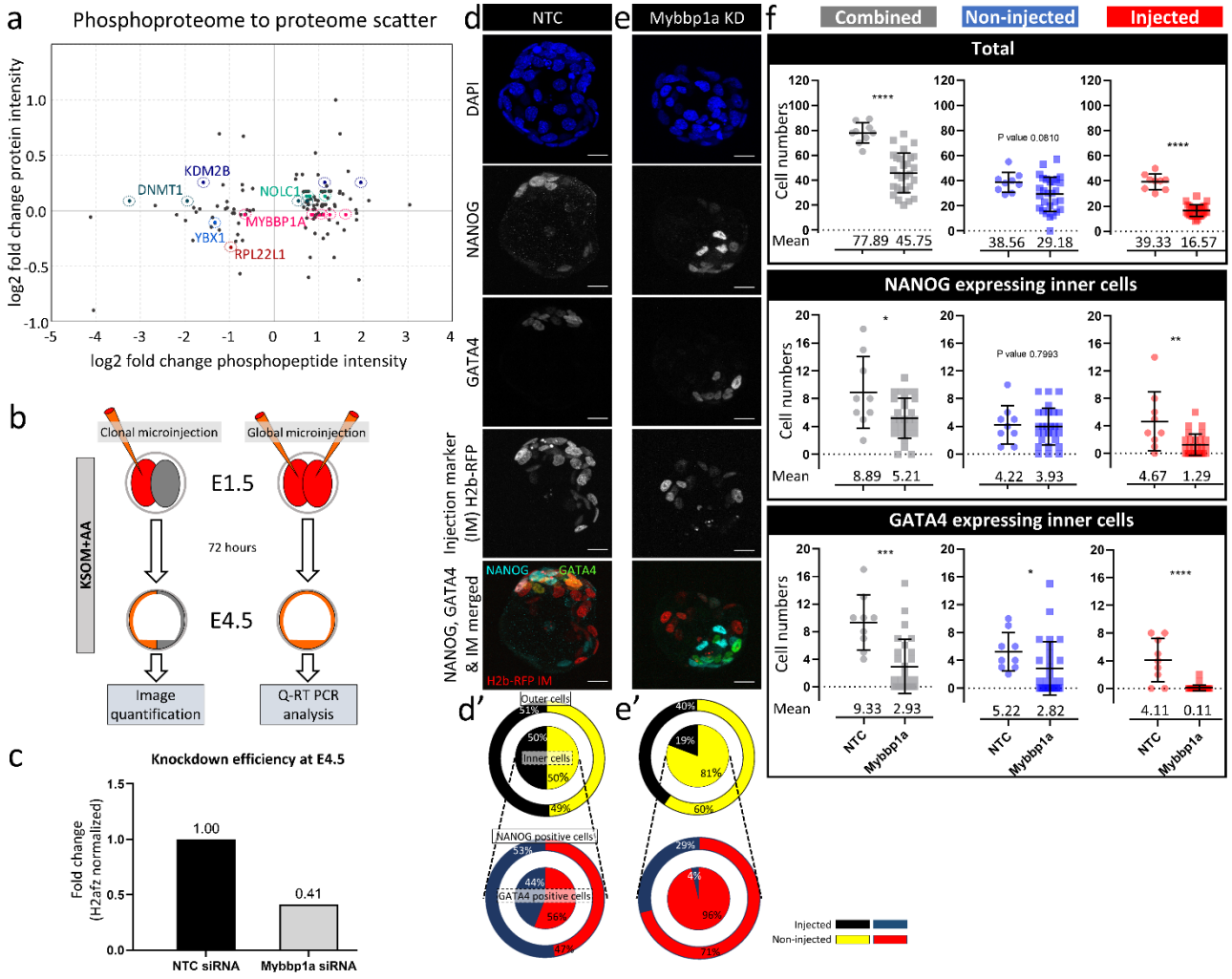

Fig. 7: Working model of the role of p38-MAPK in regulating protein translation to prime PrE differentiation during preimplantation-stage blastocyst maturation.

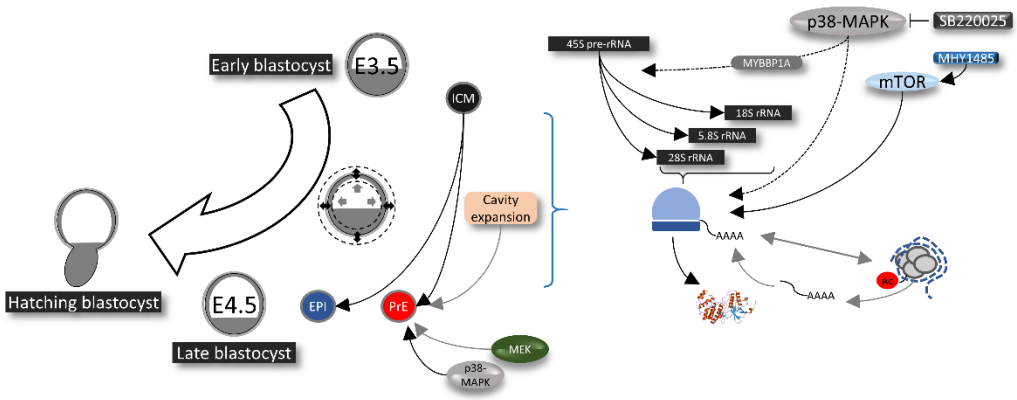

Supplementary Fig. 1

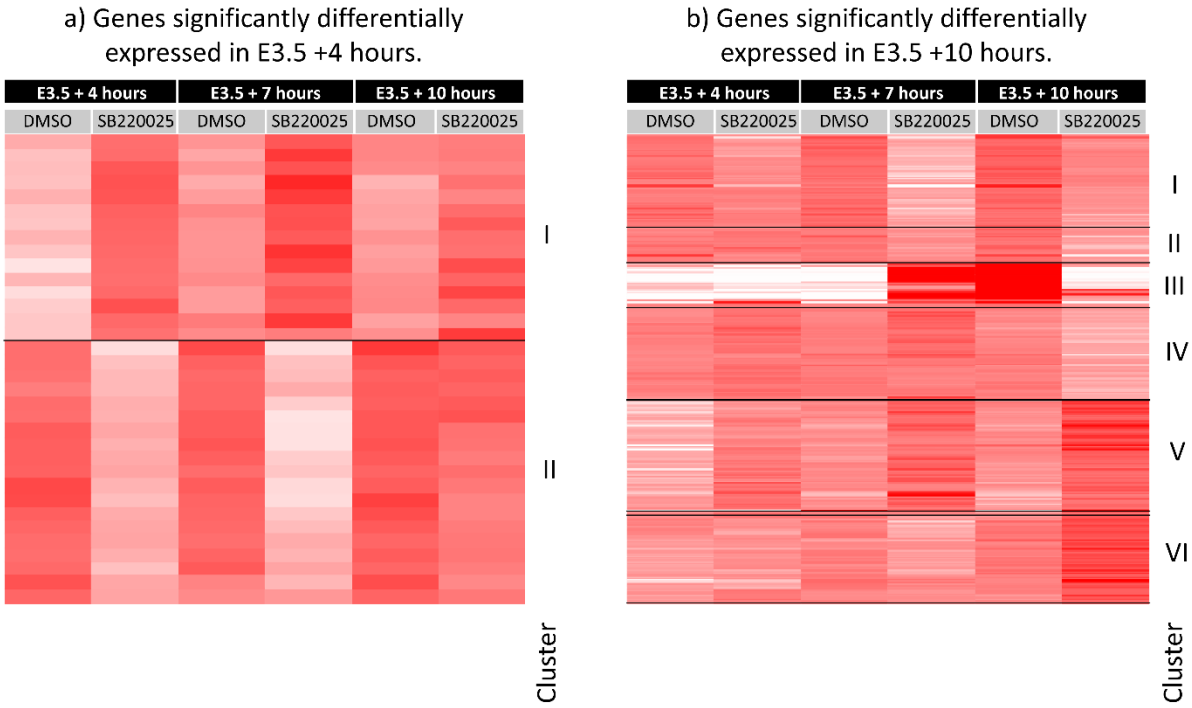

Hierarchical clustering heat-map depicting the expression of significantly changing gene mRNAs elicited by p38-MAPKi at the +4h (a) and +10h (b) time-points and the status of the transcript levels of those same genes at the two other time-points; forming two and six distinct expression clusters respectively (details in Supplementary Data 1).

Supplementary Fig. 2

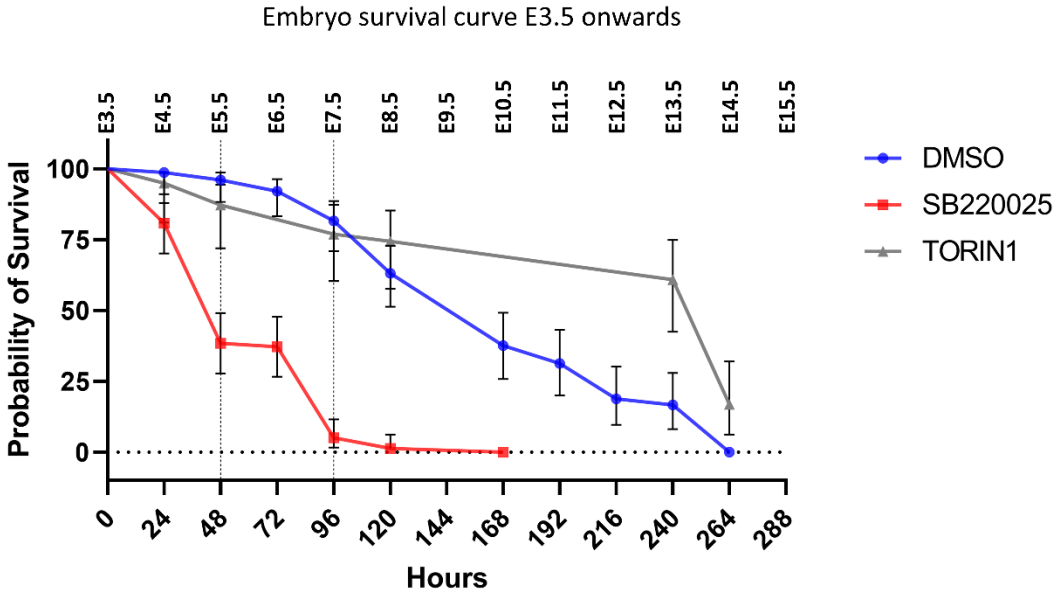

Brightfield images based analysis of survival of embryos cultured in control (DMSO; n=76), p38-MAPK inhibited (SB220025; n=78) and mTOR inhibited (TORIN1; n=39) conditions starting from E3.5.

Supplementary Fig. 3

Gene expression profile in preimplantation embryo and associated cellular lineages

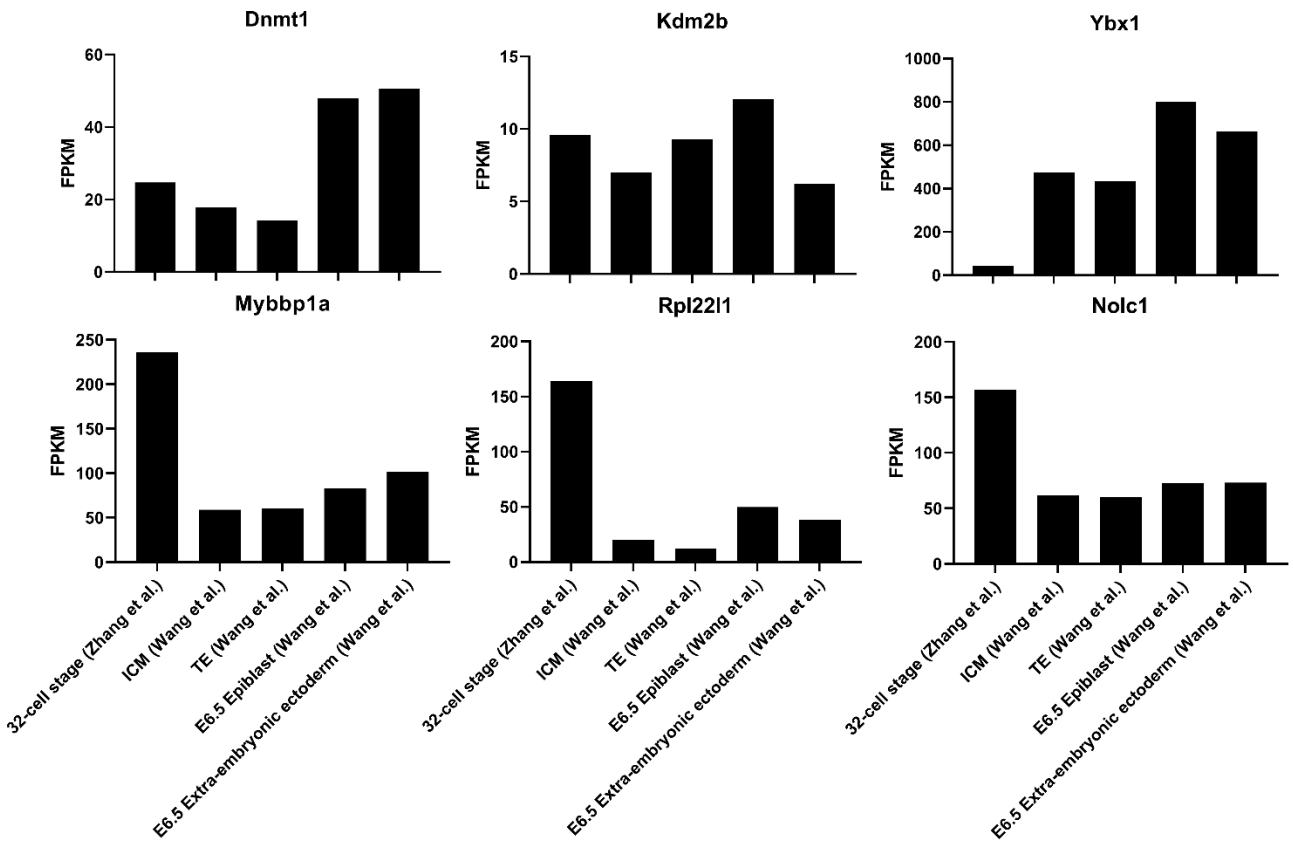

Gene expression profile of candidates identified via phosphoproteomic screen for siRNA mediated gene knockdown analysis in preimplantation embryos. Data collected from *Zhang, B., Zheng, H., Huang, B. et al. Allelic reprogramming of the histone modification H3K4me3 in early mammalian development. Nature 537, 553–557 (2016)* and *Wang, C., Liu, X., Gao, Y. et al. Reprogramming of H3K9me3-dependent heterochromatin during mammalian embryo development. Nat Cell Biol 20, 620–631 (2018)*.

Supplementary Fig. 4 (supplementary to Fig. 6d-f)

Mybbp1a KD embryo cell lineage quantification (outer and inner cells and ratio of PrE to ICM).

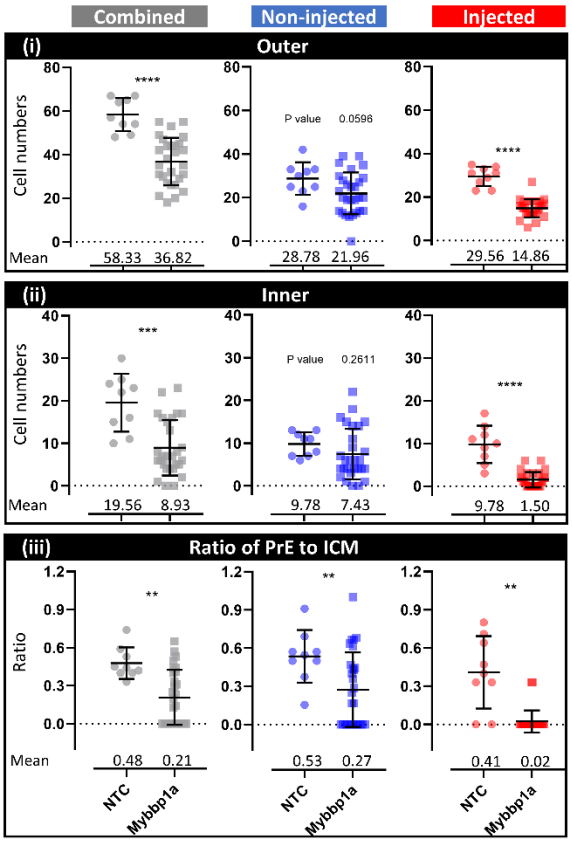

Quantification of the number of inner and outer cells and ratio of GATA4 expressing PrE to ICM upon clonal Mybbp1a knockdown. Data is supplementary to that in figure 6 (d-f).

Supplementary Fig. 5

Cellular lineage and cell numbers with addition of FGF4 (+Heparin) along with p38-MAPK inhibition.

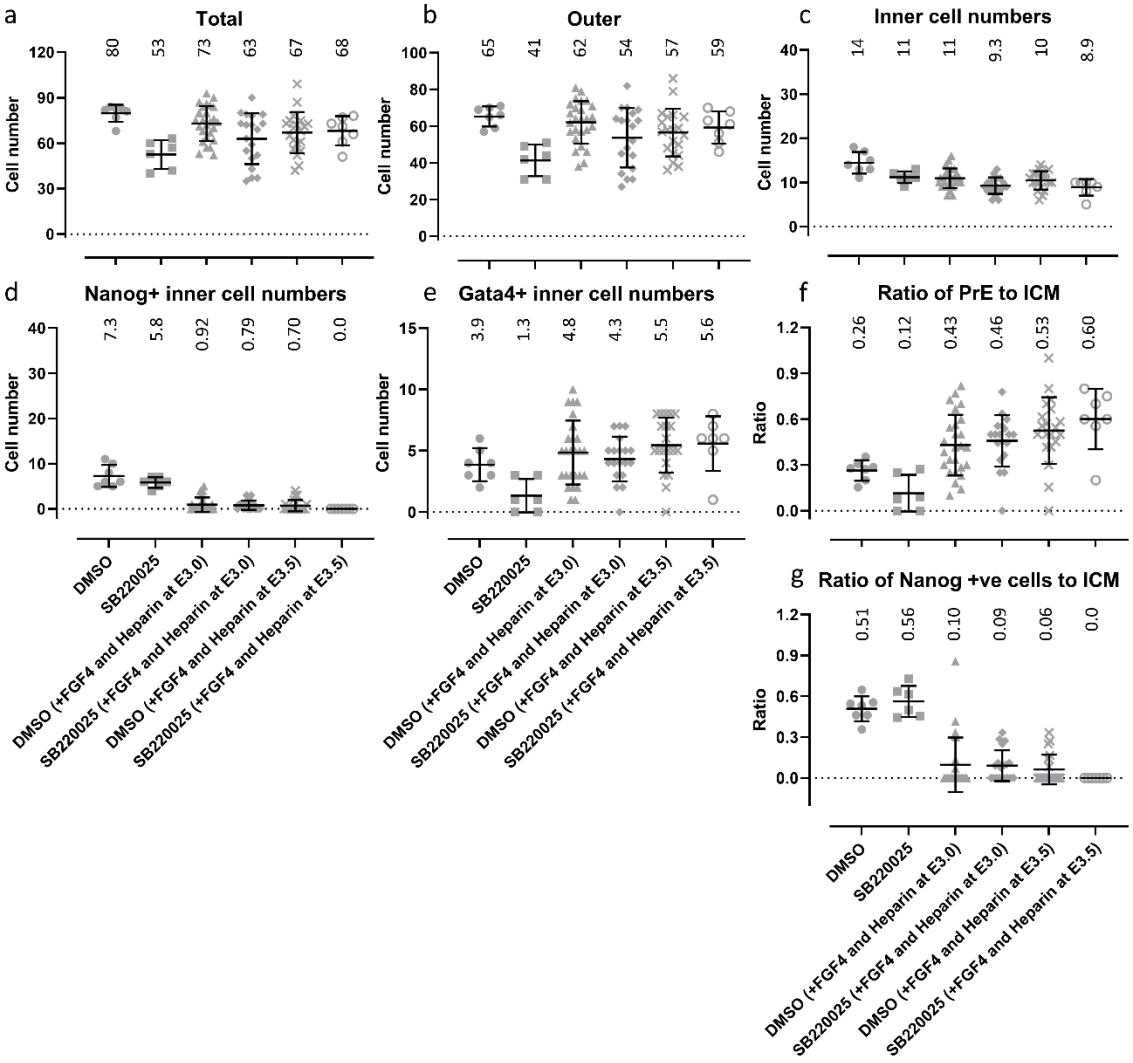

Cellular lineage and number quantification upon p38-MAPK inhibition coupled with FGF4 (+Heparin) supplementation. p38-MAPK inhibition (SB220025) and control (DMSO) treatments are beginning from E3.5, addition of FGF4 (+Heparin) was carried out at either E3.0 or E3.5. DMSO (n=7), SB220025 (n=6), DMSO + (FGF4 (+Heparin) from E3.0) (n=26), SB220025 + (FGF4 (+Heparin) from E3.0) (n=19), DMSO + (FGF4 (+Heparin) from E3.5) (n=20) and SB220025 + (FGF4 (+Heparin) from E3.5) (n=7). Tabulated cell numbers and statistical test results are in Supplementary Data1. Statistical tests used are detailed in Supplementary Table 8.

Supplementary Fig. 6

Cellular lineage and cell numbers with addition of FGF4 (+Heparin) along with MEK inhibition (PD0325901).

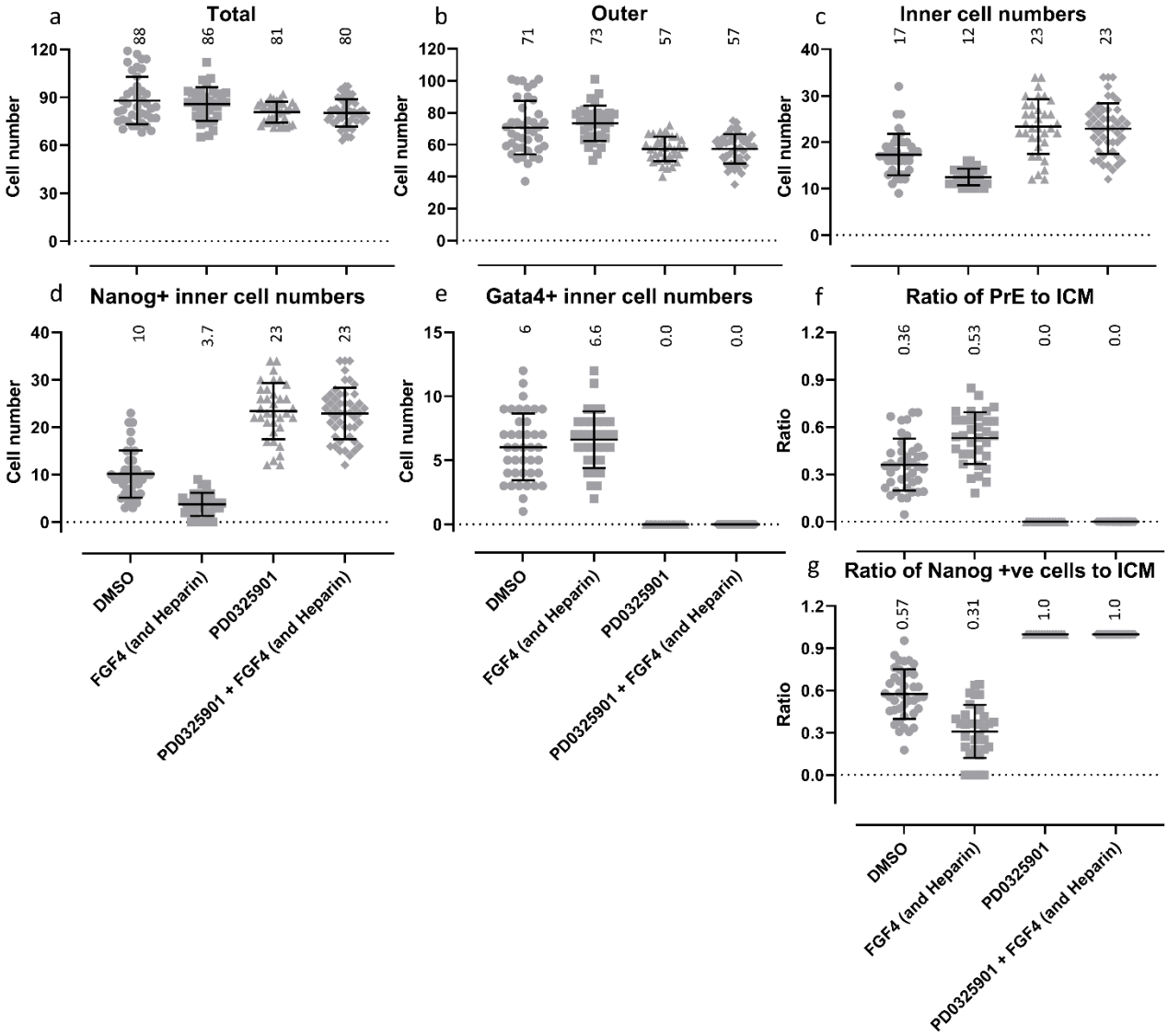

Cellular lineage and number quantification upon MEK inhibition coupled with FGF4 (+Heparin) supplementation. MEK inhibition (PD0325901) and control (DMSO) treatments are beginning from E3.5, addition of FGF4 (+Heparin) was carried out at E3.5. DMSO (n=40), FGF4 (+Heparin) (n=33), PD0325901 (n=35) and PD0325901 + FGF4 (+Heparin) (n=49). Tabulated cell numbers and statistical test results are in Supplementary Data1. Statistical tests used are detailed in Supplementary Table 8.

Supplementary Fig. 7

Blastocyst size for embryos inhibited for 24 hours (E3.5 to E4.5)

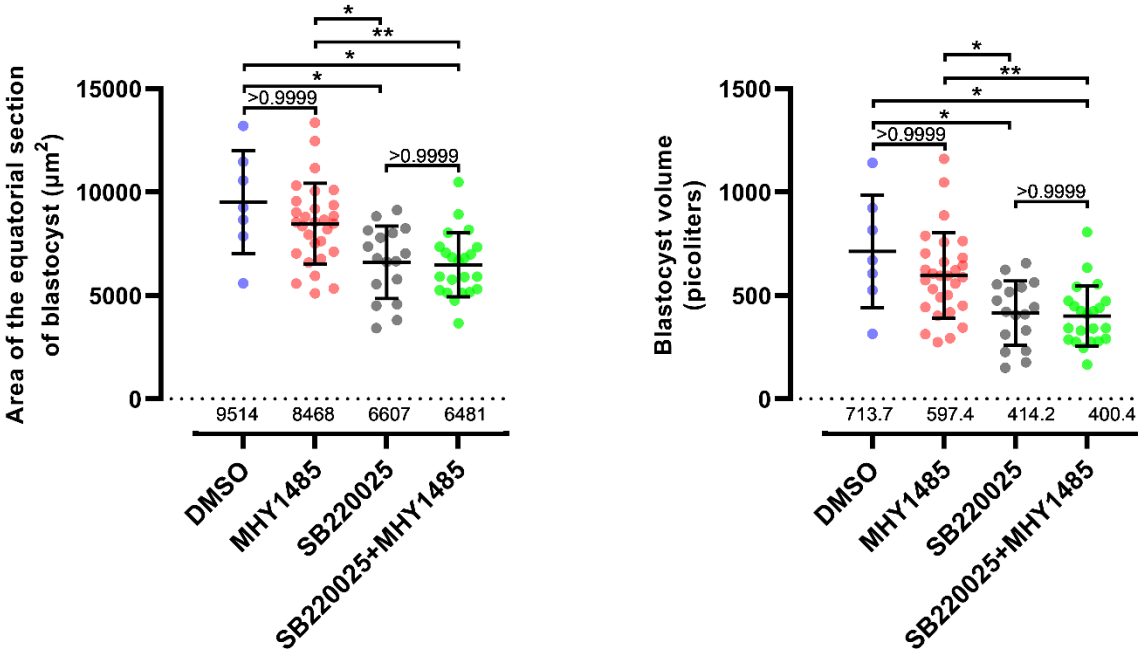

Quantification of blastocyst equatorial area (µm²) and volume (picoliters, pL) in fixed blastocysts cultured (E3.5-E4.5) in control (DMSO; n=7), mTORa (MHY1485; n=29), p38-MAPKi (SB220025; n=17) and p38-MAPKi + mTORa (SB220025+MHY1485; n=22) conditions.

Supplementary Table 1

Supplementary table with putative p38-MAPK consensus motifs and/or reported p38-MAPK interaction for phosphopeptides identified.

Uniprot_ID	gene_symbol	log_FC_Phos	FC	p-value	prot_FC	log2_FC_prot	Sequence_Modifications	phosphosite.org
A0A2I3BRL8	Gm7324	-4.11789652	0.057595643	9.05245E-05	0.96093	-0.057496754	RSTPSGPVR_Phospho (STY)	
Q3U9G9	Lbr	-4.053474318	0.060225809	0.002519767	0.536100027	-0.899425888	SVSASHEGDVK_Phospho (STY)	
Q6NXL1	Sec24d	-3.366174829	0.096979604	0.004411723	NaN	NaN	KHCASPSAASQLILPDSMKVLPVYMNSLLK_2 Oxidation (M),Phospho (STY),Deamidation (NQ)	
P13864	Dnmt1	-3.247056644	0.105326718	0.00030529	1.062320173	0.087218645	LEEVTAGTQLGPEEPCEQEDDNRSLRR_Phospho (STY)	
Q9R1M5	Nlrp5	-2.669340536	0.157198512	0.008762102	1.032506308	0.046150596	DQGPEQEQTSETLQSKEEDEVTEADK_Phospho (STY),Deamidation (NQ)	
P26231	Ctnna1	-2.187010999	0.219605943	0.003076975	0.974540588	-0.037205823	SRTSVQTEDDQLIAGQSAR_2 Phospho (STY)	SB202190
P07901	Hsp90aa1	-1.988197429	0.252053619	0.019429642	0.940131278	-0.089065869	ESDDKPEIEDVGSDEEEEEK_Phospho (STY)	SB202190 and p38-gamma (Mapk12)
P13864	Dnmt1	-1.951336966	0.258576493	0.001169949	1.062320173	0.087218645	LEEVTAGTQLGPEEPCEQEDDNRSLR_Phospho (STY)	
Q9WTQ5	Akap12	-1.824810104	0.282278254	0.032553285	0.83028907	-0.268314388	EGITPWASFKK_Phospho (STY)	
Q8BL97	Srsf7	-1.805034079	0.28617428	0.027099361	1.018575911	0.026553504	SASPERMD_Phospho (STY)	
Q8VDF2	Uhrf1	-1.751409042	0.297011554	0.048745748	0.991693952	-0.012033138	DSELSDSDSGYGVGHSESDKSSTHGEGAAEADDK_Phospho (STY)	
Q6B966	Nlrp14	-1.66770793	0.314753008	0.033262724	1.010889249	0.015624948	TEDDEMEYEASKEETVSEDKDFDDGIDYR_Phospho (STY)	
Q6P1G2	Kdm2b	-1.5866964	0.332932958	0.001973511	1.192898913	0.254471794	TPKPPTDDPTSPTSTPPEDQDSTGK_Phospho (STY)	
P97310	Mcm2	-1.412871424	0.375563451	0.012527339	0.903241178	-0.146816836	GLLYDSSEEDEERPAR_2 Phospho (STY)	
Q64012	Raly	-1.381679619	0.383771739	0.009794724	0.957779763	-0.062234141	LPAPQEDTASEAGTPQGEVQTR_Phospho (STY)	
Q80U70	Suz12	-1.327663036	0.398413093	0.003558826	0.9255625	-0.111597681	ASMSEFLESEDGEVEQQR_Phospho (STY)	
P62960	Ybx1	-1.326668164	0.39868793	0.001451431	0.929008362	-0.106236512	NYQQNYQNSESGEKNEGSESAPEGQAQQR_Phospho (STY)	SB202190
Q80W85	Npm2	-1.273898959	0.413540646	0.017924748	1.028928472	0.041142694	SRHSTSSVTETTAK_Acetyl (Protein N-term),3 Phospho (STY)	
Q6NS46	Pdcd11	-1.229850335	0.426361674	0.031576272	1.617573308	0.693831096	ERQESESEQELVNK_Phospho (STY)	
Q8BGD9	Eif4b	-1.229167662	0.426563473	0.0375903	0.885522439	-0.175399229	EEDCHSPTSKPPKPDQPLK_Phospho (STY)	SB202190 and SB203580
P24788	Cdk11b	-1.202618894	0.434485852	0.028946946	NaN	NaN	GTSPRPPEGGLGYSQLGDDDLK_Phospho (STY)	
Q8BK35	Nop53	-1.174227119	0.443121085	0.014163858	NaN	NaN	EMCEGLLEESDGEDEHEAGR_Phospho (STY)	
P43276	Hist1h1b	-1.14877749	0.451007244	0.002755721	1.174120405	0.231580363	SETAPAETAAPAPVEK_Acetyl (Protein N-term),Phospho (STY)	
Q6B966	Nlrp14	-1.091189165	0.469374326	0.013111684	1.010889249	0.015624948	EETVSEDKDFDDGIDYR_Phospho (STY)	
Q99MD9	Nasp	-1.058658095	0.480078391	0.019738881	1.057619162	0.080820221	GGREDMDISEPEEK_Phospho (STY)	
Q80XU3	Nucks1	-1.054856975	0.481344939	0.009325488	1.018087749	0.025861913	EMLLEDVGSEEEPEEDDEAPFQEK_Phospho (STY)	SB202190
O88738	Birc6	-1.028735481	0.490139567	0.045226094	NaN	NaN	LEGDSDDLLEDSDSEEHSR_Phospho (STY)	
Q9D7S7	Rpl22l1	-0.970038669	0.51049238	0.001943633	0.794534058	-0.331819033	YFQISQDEDGSESED_Phospho (STY)	
Q8K1J5	Sde2	-0.933422963	0.52361453	0.002778047	NaN	NaN	EDGIDAVEVAADRPGSPR_Phospho (STY)	
Q6NZJ6	Eif4g1	-0.92987576	0.524903543	0.001216142	0.983553192	-0.023925017	KAASLTEDR_Phospho (STY)	SB202190
Q99L45	Eif2s2	-0.904563404	0.53419434	0.034641922	1.008929594	0.012825502	SGDEMIFDPTMSK_Acetyl (Protein N-term),Phospho (STY)	
Q6NZE7	Fam122b	-0.899387932	0.536114131	0.026152933	NaN	NaN	RIDFTPVSPAPSPTR_2 Phospho (STY)	
Q6NZJ6	Eif4g1	-0.892168052	0.538803807	0.018739013	0.983553192	-0.023925017	AASLTEDR_Phospho (STY)	SB202190
Q61188	Ezh2	-0.885685089	0.541230449	0.00503181	NaN	NaN	ESSIIAPVPTEDVDTPPR_Phospho (STY)	p38-alpha (Mapk14) and SB203580
P11157	Rrm2	-0.859816491	0.551022643	0.02460188	0.825869752	-0.276013822	TPLATIADQQQLQLSPLKR_Phospho (STY)	SB203580
Q569Z6	Thrap3	-0.815989819	0.568018641	0.025926725	0.861227487	-0.21553373	ERSPALK_Phospho (STY)	
Q9D6Z1	Nop56	-0.798204878	0.575064276	0.009838901	0.923446884	-0.114899114	EELASDLEEMATSSAK_Phospho (STY)	
Q3TKT4	Smarca4	-0.766071995	0.588016281	0.036229471	0.674161203	-0.56883449	DSEAGSSTPTTSTR_Phospho (STY)	
Q61687	Atrx	-0.761796068	0.589761656	0.034141123	NaN	NaN	EEISDHENNVTILLEDSDLR_Phospho (STY)	
Q9CWE0	Mtfr1l	-0.760217456	0.590407332	0.027234246	NaN	NaN	NASVPNLR_Phospho (STY)	
Q3UJU9	Rmdn3	-0.750074983	0.594572654	0.029832402	0.975331179	-0.036035918	KDSLDLDVEAASSPAAAALEEDDSSGR_Phospho (STY)	
Q61687	Atrx	-0.745819043	0.596329229	0.047639842	NaN	NaN	YVESDDEKPTDENVNEK_Phospho (STY)	
Q61033	Tmpo	-0.714690501	0.609335838	0.016265336	1.175752853	0.233584833	SSTPLPTVSSSAENTR_Phospho (STY)	
Q9WTQ5	Akap12	-0.709249627	0.611638181	0.033309503	0.83028907	-0.268314388	RPSESDKEEELDK_Phospho (STY)	
O88874	Ccnk	-0.707620591	0.612329209	0.012982738	NaN	NaN	AVVVSPKEENK_Phospho (STY)	
Q8BTI8	Srrm2	-0.7051501	0.613378669	0.047349167	1.136278636	0.184316654	TSPLMLDR_Oxidation (M),Phospho (STY)	SB202190
Q6ZQ58	Larp1	-0.691205494	0.619336126	0.029079333	NaN	NaN	AVTPVPTK_Phospho (STY)	
Q64337	Sqstm1	-0.689794222	0.619942269	0.024293309	1.593884313	0.672546919	SRLTPTTPESSSTGTEDK_Phospho (STY)	p38-delta (Mapk13) and SB202190
Q7TPV4	Mybbp1a	-0.661105321	0.632393603	0.041462481	0.974867822	-0.036721471	LSQVNGATPVSPIEPESK_Phospho (STY)	
Q5F2E7	Nufip2	-0.63889789	0.642203356	0.024194805	0.97740286	-0.032974768	NDSWGSFDLR_Phospho (STY)	
Q6NXI6	Rprd2	-0.616916761	0.652062989	0.033824981	NaN	NaN	DVEDMELSDVEDDGSK_Phospho (STY)	SB202190
Q52KI8	Srrm1	-0.608684866	0.655794239	0.04021628	1.004383524	0.006310268	KETESEAEDDNLDDLER_Phospho (STY)	SB202190
Q6DID3	Scaf8	-0.586392677	0.666006112	0.041362549	NaN	NaN	ASEPVKEPVQTAQSPAPVEK_Phospho (STY)	SB202190
Q9WU40	Lemd3	-0.555294956	0.680517914	0.043625495	NaN	NaN	VLLGFSSDESDVEASPR_Phospho (STY)	
P26369	U2af2	-0.544382952	0.68568461	0.044510915	0.998966741	-0.001491448	SDFDEFER_Acetyl (Protein N-term),Phospho (STY)	
Q80WJ7	Mtdh	-0.481396369	0.716284005	0.038329268	1.148578762	0.199849791	SQEPISNDQKVSDDDKEK_Phospho (STY)	SB202190
Q52KI8	Srrm1	-0.466311801	0.723812636	0.048193016	1.004383524	0.006310268	AASPSPQSVR_Phospho (STY)	SB202190

The 51 proteins detected with at least one reduced phosphorylated polypeptide residue upon p38-MAPK inhibition. Proteins with more than one residue detected are highlighted in same colours. Putative p38-MAPK consensus motifs (serine or threonine followed by a proline; [S/T]P) detected in our study are highlighted within the phosphopeptide residues in letters coloured as such: TP and SP. Recorded instances of differential phosphorylation resulting from p38-MAPKs and/or specific inhibitors against p38-MAPKs as found in phosphosite database (www.phosphosite.org) are included against respective proteins. Data from phosphosite.org represent both mouse and human models and not necessarily specific to the sequence of phospho-modifications detected in our studies.

Supplementary Table 2

Additional phospho candidate KD

siRNA against Rpl22l1 (10uM)

#	TOTAL NUMBER OF CELLS			OUTER									ICM									RATIOS		
	Embryo Total	Embryo Total Non-Injected	Embryo Total Injected	Outer Nanog +ve	Outer Nanog +ve Injected	Outer Gata4 +ve	Outer Gata4 +ve Injected	Outer Double Negative	Outer Double Negative Injected	Total Outer	Total Outer Non-Injected	Total Outer Injected	Nanog +ve	Nanog +ve Non-Injected	Nanog +ve Injected	Gata4 +ve	Gata4 +ve Non-Injected	Gata4 +ve Injected	Nanog/ Gata4 double +ve	Nanog/ Gata4 double +ve Non-Injected	Nanog/ Gata4 double +ve Injected	Total ICM	Total ICM Non-Injected	Total ICM Injected	Overall ratio of PrE to ICM	Ratio of PrE to ICM among non-injected cells	Ratio of PrE to ICM among injected cells
1	60	33	27	0	0	0	0	44	19	44	25	19	9	4	5	4	3	1	3	1	2	16	8	8	0.25	0.38	0.13
2	73	38	35	6	4	0	0	52	26	58	28	30	7	4	3	8	6	2	0	0	0	15	10	5	0.53	0.60	0.40
3	65	34	31	0	0	0	0	48	21	48	27	21	9	0	9	7	7	0	1	0	1	17	7	10	0.41	1.00	0.00
4	65	23	42	4	1	2	0	48	34	54	19	35	9	4	5	2	0	2	0	0	0	11	4	7	0.18	0.00	0.29
5	78	44	34	0	0	0	0	63	32	63	31	32	7	6	1	8	7	1	0	0	0	15	13	2	0.53	0.54	0.50
6	70	33	37	3	3	0	0	52	22	55	30	25	7	2	5	5	1	4	3	0	3	15	3	12	0.33	0.33	0.33
7	72	36	36	0	0	0	0	63	31	63	32	31	3	1	2	5	3	2	1	0	1	9	4	5	0.56	0.75	0.40
8	64	26	38	2	1	0	0	40	26	42	15	27	10	5	5	8	4	4	4	2	2	22	11	11	0.36	0.36	0.36
9	71	38	33	0	0	0	0	57	26	57	31	26	5	0	5	9	7	2	0	0	0	14	7	7	0.64	1.00	0.29
10	66	33	33	3	0	0	0	45	21	48	27	21	12	5	7	5	1	4	1	0	1	18	6	12	0.28	0.17	0.33
11	80	42	38	0	0	0	0	57	29	57	28	29	9	5	4	11	7	4	3	2	1	23	14	9	0.48	0.50	0.44
12	80	36	44	2	0	0	0	62	36	64	28	36	8	7	1	8	1	7	0	0	0	16	8	8	0.50	0.13	0.88
13	75	47	28	2	1	0	0	52	21	54	32	22	9	7	2	12	8	4	0	0	0	21	15	6	0.57	0.53	0.67
14	71	44	27	2	0	0	0	61	24	63	39	24	5	2	3	3	3	0	0	0	0	8	5	3	0.38	0.60	0.67
15	65	35	30	0	0	0	0	49	24	49	25	24	16	10	6	0	0	0	0	0	0	16	10	6	0.00	0.00	0.00
16	74	39	35	7	4	0	0	59	28	66	34	32	7	5	2	1	0	1	0	0	0	8	5	3	0.13	0.00	0.33
17	76	42	34	6	5	0	0	59	24	65	36	29	7	2	5	2	2	0	2	2	0	11	6	5	0.18	0.33	0.00
18	90	45	45	2	2	0	0	76	34	78	42	36	5	2	3	7	1	6	0	0	0	12	3	9	0.58	0.33	0.67
19	75	50	25	0	0	0	0	65	23	65	42	23	2	0	2	5	5	0	3	3	0	10	8	2	0.50	0.63	0.00
20	78	40	38	0	0	0	0	67	36	67	31	36	6	5	1	5	4	1	0	0	0	11	9	2	0.45	0.44	0.50
21	66	26	40	1	1	0	0	48	26	49	22	27	16	4	12	1	0	1	0	0	0	17	4	13	0.06	0.00	0.08
22	64	25	39	5	2	0	0	45	30	50	18	32	8	3	5	5	4	1	1	0	1	14	7	7	0.36	0.57	0.14
23	100	44	56	7	7	0	0	78	37	85	41	44	7	1	6	8	2	6	0	0	0	15	3	12	0.53	0.67	0.50
24	104	58	46	3	1	0	0	87	41	90	48	42	6	4	2	8	6	2	0	0	0	14	10	4	0.57	0.60	0.50
Average	74.25	37.96	36.29	2.29	1.33	0.08	0.00	57.38	27.96	59.75	30.46	29.29	7.88	3.67	4.21	5.71	3.42	2.29	0.92	0.42	0.50	14.50	7.50	7.00	0.39	0.44	0.32

siRNA against Kdm2b (10uM)

#	TOTAL NUMBER OF CELLS			OUTER									ICM									RATIOS		
	Embryo Total	Embryo Total Non-Injected	Embryo Total Injected	Outer Nanog +ve	Outer Nanog +ve Injected	Outer Gata4 +ve	Outer Gata4 +ve Injected	Outer Double Negative	Outer Double Negative Injected	Total Outer	Total Outer Non-Injected	Total Outer Injected	Nanog +ve	Nanog +ve Non-Injected	Nanog +ve Injected	Gata4 +ve	Gata4 +ve Non-Injected	Gata4 +ve Injected	Nanog/ Gata4 double +ve	Nanog/ Gata4 double +ve Non-Injected	Nanog/ Gata4 double +ve Injected	Total ICM	Total ICM Non-Injected	Total ICM Injected	Overall ratio of PrE to ICM	Ratio of PrE to ICM among non-injected cells	Ratio of PrE to ICM among injected cells
1	97	64	33	8	7	0	0	66	23	74	44	30	6	6	0	17	14	3	0	0	0	23	20	3	0.74	0.70	1.00
2	95	48	47	2	2	0	0	75	39	77	36	41	10	7	3	8	5	3	0	0	0	18	12	6	0.44	0.42	0.50
3	96	52	44	10	6	0	0	69	29	79	44	35	15	0	9	2	2	0	0	0	0	17	8	9	0.12	0.25	0.00
4	57	39	18	0	0	0	0	45	17	45	28	17	3	2	1	8	8	0	1	1	0	12	11	1	0.67	0.73	0.00
5	122	69	53	1	1	0	0	93	49	94	44	50	9	6	3	19	19	0	0	0	0	28	25	3	0.68	0.76	0.00
6	110	45	65	0	0	0	0	90	50	90	40	50	3	1	2	17	4	13	0	0	0	20	5	15	0.85	0.80	0.87
7	42	26	16	14	10	0	0	18	2	32	20	12	10	6	4	0	0	0	0	0	0	10	6	4	0.00	0.00	0.00
8	113	51	62	0	0	0	0	86	57	86	29	57	6	3	3	21	19	2	0	0	0	27	22	5	0.78	0.86	0.40
9	65	25	40	28	19	0	0	36	21	64	24	40	0	0	0	1	1	0	0	0	0	1	1	0	1.00	1.00	0.00
10	102	52	50	0	0	0	0	77	43	77	34	43	10	8	2	14	9	5	1	1	0	25	18	7	0.56	0.50	0.71
11	90	38	52	6	5	0	0	50	31	56	20	36	21	13	8	9	4	5	4	1	3	34	18	16	0.26	0.22	0.31
12	66	42	24	2	1	0	0	49	21	51	29	22	9	9	0	2	2	0	4	2	2	15	13	2	0.13	0.15	0.00
13	74	46	28	0	0	0	0	42	23	42	19	23	21	16	5	11	11	0	0	0	0	32	27	5	0.34	0.41	0.00
14	94	53	41	0	0	0	0	74	40	74	34	40	10	9	1	10	10	0	0	0	0	20	19	1	0.50	0.53	0.00
Average	87.36	46.43	40.93	5.07	3.64	0.00	0.00	62.14	31.79	67.21	31.79	35.43	9.50	6.14	2.93	9.93	7.71	2.21	0.71	0.36	0.36	20.14	14.64	5.50	0.51	0.52	0.27

siRNA against Nolc1 (10uM)

#	TOTAL NUMBER OF CELLS			OUTER									ICM									RATIOS		
	Embryo Total	Embryo Total Non-Injected	Embryo Total Injected	Outer Nanog +ve	Outer Nanog +ve Injected	Outer Gata4 +ve	Outer Gata4 +ve Injected	Outer Double Negative	Outer Double Negative Injected	Total Outer	Total Outer Non-Injected	Total Outer Injected	Nanog +ve	Nanog +ve Non-Injected	Nanog +ve Injected	Gata4 +ve	Gata4 +ve Non-Injected	Gata4 +ve Injected	Nanog/ Gata4 double +ve	Nanog/ Gata4 double +ve Non-Injected	Nanog/ Gata4 double +ve Injected	Total ICM	Total ICM Non-Injected	Total ICM Injected	Overall ratio of PrE to ICM	Ratio of PrE to ICM among non-injected cells	Ratio of PrE to ICM among injected cells
1	117	79	38	0	0	0	0	91	30	91	61	30	9	9	0	17	9	8	0	0	0	26	18	8	0.65	0.50	1.00
2	96	47	49	1	0	0	0	81	43	82	39	43	7	7	0	7	1	6	0	0	0	14	8	6	0.50	0.13	1.00
3	98	66	32	0	0	0	0	76	27	76	49	27	9	0	0	12	7	5	1	1	0	22	17	5	0.55	0.41	1.00
4	87	53	34	5	0	0	0	66	32	71	39	32	6	5	1	10	9	1	0	0	0	16	14	2	0.63	0.64	0.50
5	95	54	41	2	0	0	0	73	34	75	41	34	7	7	0	13	6	7	0	0	0	20	13	7	0.65	0.46	1.00
6	67	30	37	1	0	0	0	49	28	50	22	28	13	4	9	4	4	0	0	0	0	17	8	9	0.24	0.50	0.00
7	56	18	38	2	1	0	0	33	22	35	12	23	20	6	14	1	0	1	0	0	0	21	6	15	0.05	0.00	0.07
8	77	36	41	0	0	0	0	68	36	68	32	36	9	4	5	0	0	0	0	0	0	9	4	5	0.00	0.00	0.00
9	55	35	20	9	3	0	0	39	11	48	34	14	6	1	5	1	0	1	0	0	0	7	1	6	0.14	0.00	0.17
Average	83.11	46.44	36.67	2.22	0.44	0.00	0.00	64.00	29.22	66.22	36.56	29.67	9.56	4.78	3.78	7.22	4.00	3.22	0.11	0.11	0.00	16.89	9.89	7.00	0.38	0.29	0.53

siRNA against Ybx1 (10uM)

#	TOTAL NUMBER OF CELLS			OUTER									ICM									RATIOS		
	Embryo Total	Embryo Total Non-Injected	Embryo Total Injected	Outer Nanog +ve	Outer Nanog +ve Injected	Outer Gata4 +ve	Outer Gata4 +ve Injected	Outer Double Negative	Outer Double Negative Injected	Total Outer	Total Outer Non-Injected	Total Outer Injected	Nanog +ve	Nanog +ve Non-Injected	Nanog +ve Injected	Gata4 +ve	Gata4 +ve Non-Injected	Gata4 +ve Injected	Nanog/ Gata4 double +ve	Nanog/ Gata4 double +ve Non-Injected	Nanog/ Gata4 double +ve Injected	Total ICM	Total ICM Non-Injected	Total ICM Injected	Overall ratio of PrE to ICM	Ratio of PrE to ICM among non-injected cells	Ratio of PrE to ICM among injected cells
1	83	49	34	0	0	0	0	65	26	65	39	26	12	4	8	5	5	0	1	1	0	18	10	8	0.28	0.50	0.00
2	56	28	28	17	9	0	0	31	17	48	22	26	8	6	2	0	0	0	0	0	0	8	6	2	0.00	0.00	0.00
3	90	44	46	8	7	0	0	60	24	68	37	31	11	0	6	9	2	7	2	0	2	22	7	15	0.41	0.29	0.47
4	90	48	42	1	1	0	0	66	36	67	30	37	10	9	1	10	8	2	3	1	2	23	18	5	0.43	0.44	0.40
5	63	31	32	3	1	0	0	38	23	41	17	24	17	10	7	4	3	1	1	1	0	22	14	8	0.18	0.21	0.13
6	68	30	38	8	7	0	0	41	16	49	26	23	16	4	12	3	0	3	0	0	0	19	4	15	0.16	0.00	0.20
7	77	35	42	30	21	0	0	27	11	57	25	32	13	9	4	6	0	6	1	1	0	20	10	10	0.30	0.00	0.60
8	72	32	40	4	4	0	0	50	28	54	22	32	6	2	4	11	7	4	1	1	0	18	10	8	0.61	0.70	0.50
Average	74.88	37.13	37.75	8.88	6.25	0.00	0.00	47.25	22.63	56.13	27.25	28.88	11.63	5.50	5.50	6.00	3.13	2.88	1.13	0.63	0.50	18.75	9.88	8.88	0.30	0.27	0.29

siRNA against Dnmt1 (10uM)

#	TOTAL NUMBER OF CELLS			OUTER									ICM									RATIOS		
	Embryo Total	Embryo Total Non-Injected	Embryo Total Injected	Outer Nanog +ve	Outer Nanog +ve Injected	Outer Gata4 +ve	Outer Gata4 +ve Injected	Outer Double Negative	Outer Double Negative Injected	Total Outer	Total Outer Non-Injected	Total Outer Injected	Nanog +ve	Nanog +ve Non-Injected	Nanog +ve Injected	Gata4 +ve	Gata4 +ve Non-Injected	Gata4 +ve Injected	Nanog/ Gata4 double +ve	Nanog/ Gata4 double +ve Non-Injected	Nanog/ Gata4 double +ve Injected	Total ICM	Total ICM Non-Injected	Total ICM Injected	Overall ratio of PrE to ICM	Ratio of PrE to ICM among non-injected cells	Ratio of PrE to ICM among injected cells
1	61									38			11			9			3			23			0.39		
2	61									48			12			0			1			13			0.00		
3	85									62			11			7			5			23			0.30		
4	78									57			11			8			2			21			0.38		
5	70									54			6			7			3			16			0.44		
6	86									64			9			13			0			22			0.59		
Average	73.50									53.83			10.00			7.33			2.33			19.67			0.35		

Supplementary Table 3

Atp1a1 proteome readout

Uniprot_ID	Gene Symbol	log2_FC	p-value	DMSO_1	DMSO_2	DMSO_3	p38i_1	p38i_2	p38i_3	DMSO_mean	p38i_mean
Q8VDN2	Atp1a1	0.01563491	0.891866342	25.98	25.99	25.84	25.8	25.96	26.1	25.94	25.95

Supplementary Table 4

Introns detected (as RPKM) for "translation" related genes; related to Fig. 3e

Sl. No.	Probe	Chromosome	Start	End	Probe Strand	Feature	E3.5 +7h (DMSO)	E3.5 +7h (SB220025)
1	Rps20	4	3831334	3835665	-	null	4.335468	5.4814467
2	Rps9	7	3703993	3706897	+	null	6.2938595	8.691212
3	Rps19	7	24884371	24889806	+	null	3.595584	4.8586073
4	Rps16	7	28350652	28353155	+	null	5.842512	5.757571
5	Rps17	7	81342732	81345254	-	null	5.08963	5.088256
6	Rps3	7	99477896	99483738	-	null	10.089131	10.129799
7	Rpsa	9	120127689	120132369	+	null	5.8119106	6.4425263
8	Rps26	10	128624534	128626747	-	null	7.9579744	8.017336
9	Rps29	12	69157722	69159186	-	null	6.3753366	7.874689
10	Rps23	13	90922958	90924950	+	null	4.6760044	5.5858107
11	Rpl30	15	34440505	34443640	-	null	4.1983867	4.612251
12	Rps18	17	33951999	33956001	-	null	5.2112346	7.1981916
13	Rps14	18	60774510	60778546	+	null	7.8575892	8.69915

Supplementary Table 5

Pharmacological agents used

Sl. No.	Name	Pharmacological activity	Working concentration	Manufacturer	Cat. No.	Embryonic stage	Duration	Figures
1	SB220025	p38-MAPK inhibitor	20µM	Calbiochem	559396	E3.5 to E4.5	24 hours	1c, d, e, & 5, supp. 5, 6
2						E3.5+4 hours to E3.5+7 hours	3 hours	1b
3						E3.5 to E3.5+3 hours	3 hours	1f
4						E3.5 to E3.5+6 hours	6 hours	1f
5						E3.5 to E3.5+9 hours	9 hours	1f
6						E3.5 to E3.5+12 hours (E4.0)	12 hours	1f
7						E3.5+2 hours to E3.5+9 hours	7 hours	2
8						E3.5 to E3.5+4 hours	4 hours	3
9						E3.5 to E3.5+7 hours	7 hours	3
10						E3.5 to E3.5+10 hours	10 hours	3, 4
11	TORIN1	mTORC1/2 inhibitor	20µM	SelleckChem	S2827	E3.5 to E4.5	24 hours	5d
12	MHY1485	mTOR activator	20µM	SelleckChem	S7811	E3.5 to E4.5	24 hours	5e, f, h, i, & supp. 7
13	PD0325901	MEK inhibitor	1µM	Sigma-Aldrich	PZ0162	E3.5 to E4.5	24 hours	5g, h, & supp. 6
14	mFGF4	Recombinant mouse FGF4 protein (activates FGF4-MEK/ERK pathway)	1000ng/ml	R&D Systems	5846-F4	E3.0 to E4.5 and E3.5 to E4.5	36 and 24 hours respectively	Supp. 5 & 6
15	Heparin sodium salt	Enhances receptor binding of FGF4	1µg/ml	Sigma-Aldrich	H3149	E3.0 to E4.5 and E3.5 to E4.5	36 and 24 hours respectively	Supp. 5 & 6

Supplementary Table 6

siRNA

Sl. No.	Target (siRNA)	Working concentration	Manufacturer	Cat. No.	Assay ID
1	Negative Control	10µM	QIAGEN GeneGlobe	SI03650318	
2	Mybbp1a	10µM	Thermo Scientific Silencer Select	AM16708	156950
3	Rpl22l1	10µM	Thermo Scientific Silencer Select	4390771	s86106
4	Kdm2b	10µM	Thermo Scientific Silencer Select	4390771	s78199
5	Nolc1	10µM	Thermo Scientific Silencer Select	AM16708	287747
6	Ybx1	10µM	Thermo Scientific Silencer Select	AM16708	187614
7	Dnmt1	10µM	Thermo Scientific Silencer Select	4390771	s65072

Supplementary Table 7

Antibodies

Sl. No.	Antibody against	Type	Target	Host / isotype	Manufacturer	Catalogue number	Dilution used
Immunofluorescence imaging							
1	Nanog (eBioMLC-51)	Primary; monoclonal	Mouse	Rat / IgG2a	Thermo Fisher Scientific Inc. (eBioscience™)	14-5761-80	1:200 in PBST (3% BSA)
2	GATA-4 (H-112)	Primary; polyclonal	Mouse, rat and human	Rabbit / IgG	Santa Cruz Biotechnology, Inc.	sc-9053	1:200 in PBST (3% BSA)
3	GATA-6	Primary; polyclonal	Human and mouse	Goat / IgG	R&D Systems™	AF1700	1:200 in PBST (3% BSA)
4	CDX2 (CDX2-88)	Primary; monoclonal	Conserved	Mouse / IgG1, kappa	BioGenex	MU392A-5UC	1:200 in PBST (3% BSA)
5	Acetyl-Histone H4 (Lys16)	Primary; polyclonal	Mouse, rat and human	Rabbit / IgG	Merck KGaA (Sigma-Aldrich, Inc.) (Upstate®)	07-329	1:100 in PBST (3% BSA)
6	RNA polymerase II CTD repeat YSPTSPS (phospho S2)	Primary; polyclonal	Mouse, rat, human etc.	Rabbit / IgG	Abcam plc.	ab5095	1:100 in PBST (3% BSA)
7	Donkey anti-Rat IgG (H+L) Highly Cross-Adsorbed Secondary Antibody, Alexa Fluor 488	Secondary; polyclonal	Rat	Donkey / IgG	Thermo Fisher Scientific Inc.	A-21208	1:500 in PBST (3% BSA)
8	Donkey anti-Rabbit IgG (H+L) Highly Cross-Adsorbed Secondary Antibody, Alexa Fluor 555	Secondary; polyclonal	Rabbit	Donkey / IgG	Thermo Fisher Scientific Inc.	A-31572	1:500 in PBST (3% BSA)
9	Donkey Anti-Goat IgG H&L (Alexa Fluor® 647)	Secondary; polyclonal	Goat	Donkey / IgG	Abcam plc.	ab150131	1:500 in PBST (3% BSA)
10	Donkey Anti-Rabbit IgG H&L (Alexa Fluor® 647)	Secondary; polyclonal	Rabbit	Donkey / IgG	Abcam plc.	ab150075	1:500 in PBST (3% BSA)
11	Goat Anti-Rat IgG H&L (Cy3 ®) preadsorbed	Secondary; polyclonal	Rat	Goat / IgG	Abcam plc.	ab98416	1:500 in PBST (3% BSA)
12	Donkey anti-Mouse IgG (H+L) Highly Cross-Adsorbed Secondary Antibody, Alexa Fluor 488	Secondary; polyclonal	Mouse	Donkey / IgG	Thermo Fisher Scientific Inc.	A-21202	1:500 in PBST (3% BSA)

Supplementary Table 8

Statistical tests	Unless otherwise stated within individual graphs as a specific P value (if statistically insignificant), the stated significance intervals were depicted as: P value < 0.0001 (****), 0.0001 to 0.001 (***), 0.001 to 0.01 (**) and 0.01 to 0.05 (*); error bars denote calculated standard deviations. Further details are provided within respective methods sections.

Figure				Test used
1	b			Unpaired t-test
	c			Unpaired t-test
	d			Mann-Whitney
	e		Time-lapse	One-way ANOVA with post-hoc Tukey HSD test
			Hatched vs. Unhatched	Chi-square test
			DMSO	Mann-Whitney
			SB220025	Mann-Whitney
			DMSO	Mann-Whitney
			SB220025	Mann-Whitney
			DMSO	Unpaired t-test
			SB220025	Mann-Whitney
4	b			Mann-Whitney
	d		Combined	Mann-Whitney
			18 and 28S	Mann-Whitney
	f			Unpaired t-test
	g			Mann-Whitney
	h			Mann-Whitney
5	j			One-way ANOVA (Kruskal-Wallis) and Dunn's test
	k			One-way ANOVA (Kruskal-Wallis) and Dunn's test
	l			One-way ANOVA (Kruskal-Wallis) and Dunn's test
	m			One-way ANOVA (Kruskal-Wallis) and Dunn's test
	n			One-way ANOVA (Kruskal-Wallis) and Dunn's test
	o			One-way ANOVA (Kruskal-Wallis) and Dunn's test
	p			One-way ANOVA (Brown-Forsythe and Welch's) and Dunnett's test
	q			One-way ANOVA (Kruskal-Wallis) and Dunn's test
6	f	Total	Combined	Welch's t-test
			Non-injected	Mann-Whitney
			Injected	Mann-Whitney
		NANOG	Combined	Mann-Whitney
			Non-injected	Mann-Whitney
			Injected	Unpaired t-test
		GATA4	Combined	Mann-Whitney
			Non-injected	Mann-Whitney
			Injected	Unpaired t-test

Supp. 4		i	Combined	Unpaired t-test
			Non-injected	Unpaired t-test
			Injected	Unpaired t-test
		ii	Combined	Unpaired t-test
			Non-injected	Unpaired t-test
			Injected	Unpaired t-test
		iii	Combined	Mann-Whitney
			Non-injected	Welch's t-test
			Injected	Welch's t-test
Supp. 5	a			Ordinary one-way ANOVA and Tukey's multiple comparisons test
	b			One-way ANOVA (Kruskal-Wallis) and Dunn's test
	c			One-way ANOVA (Kruskal-Wallis) and Dunn's test
	d			One-way ANOVA (Kruskal-Wallis) and Dunn's test
	e			One-way ANOVA (Kruskal-Wallis) and Dunn's test
			DMSO vs. SB220025 only (for GATA4 expressing inner cell number)	Mann-Whitney
	f			Ordinary one-way ANOVA and Tukey's multiple comparisons test
			DMSO vs. SB220025 only (for Ratio of PrE to ICM)	Unpaired t-test
	g			One-way ANOVA (Kruskal-Wallis) and Dunn's test
Supp. 6	a			One-way ANOVA (Kruskal-Wallis) and Dunn's test
	b			One-way ANOVA (Kruskal-Wallis) and Dunn's test
	c			One-way ANOVA (Kruskal-Wallis) and Dunn's test
	d			One-way ANOVA (Kruskal-Wallis) and Dunn's test
	e			One-way ANOVA (Kruskal-Wallis) and Dunn's test
	f			One-way ANOVA (Kruskal-Wallis) and Dunn's test
	g			One-way ANOVA (Kruskal-Wallis) and Dunn's test
Supp. 7				One-way ANOVA (Kruskal-Wallis) and Dunn's test

Supplementary Table 9

Primers used

Sl. No.	Primer	Sequence (5'->3') Sense	Antisense	Figures	Comments
1	Tbp	GAAGAACAATCCAGACTAGCAGCA	CCTTATAGGGAACTTCACATCACAG	1f	
2	H2afz	GCGCAGCCATCCTGGAGTA	CCGATCAGCGATTTGTGGA	4f, 6c	
3	Nanog	GGTTGAAGACTAGCAATGGTCTGA	TGCAATGGATGCTGGGATACTC	1f	
4	Gata4	CAAGCAGGACTCTTGGAACA	AGCAGGAATTTGAAGAGGGA	1f	
5	Mapk11	AATGTAGCGGTGAACGAGGA	CCAGATGTCCACTGTCTGGT	1f	Q-RTPCR
6	Mapk12	TATATCCATGCGGCTGGTGT	ATGTCCACTGTCTGCGTGTA	1f	
7	Mapk13	CAGCGAGGATAAGGTCCAGT	TCCAGGATCTTCAGCTCACA	1f	
8	Mapk14	ACATCGTGAAGTGCCAGAAG	CTAGGTTGCTGGGCTTTAGG	1f	
9	Mybbp1a	GTCTCTGCCGCTTCTGTCA	GGGATGATCTTAAATAGGTTTTGG	6c	
10	18S rRNA	CTCAACACGGGAAACCTCAC	CGCTCCACCAACTAAGAACG	4c, d	Q-RTPCR (SSP (from Masek et al. *Int. J. Mol. Sci.* 2020))
11	28S rRNA	CTAAATACCGGCACGAGACC	TTCACGCCCTCTTGAACTCT	4c, d	
12	45S pre-rRNA 5' ETS amplicon (1)	TCTCGCTTGTTTCTCCCGAT	GATGGGGTGGAGAGACGAG	4f	Q-RTPCR (rRNA processing (from Corsini et al. *Cell Stem Cell* (2018))
13	45S 5' ETS & 18S overlap amplicon (2)	GCGCTTCCTTACCTGGTTG	CCGTCGGCATGTATTAGCTC	4f	
14	18S rRNA amplicon (3)	CTGGATACCGCAGCTAGGAA	GAATTTCACCTCTAGCGGCG	4f	
15	ITS1 amplicon (4)	GTCTCGTTTCGTTCCTGCTG	TATTTCGGGTGTGAGCGAAC	4f	
16	5.8S rRNA amplicon (5)	GTGGATCACTCGGCTCGTG	GCAAGTGCGTTCGAAGTGTC	4f	
17	ITS2 amplicon (6)	TCCCGAAGTTCAGACGTGTG	AGAAAGACTGGTGAGGCAGC	4f	
18	45S ITS2 & 28S overlap amplicon (7)	CTCCTCGCTCTCTTCTTCCC	CTGTTCACTCGCCGTTACTG	4f	
19	28S rRNA amplicon (8)	AGTAACGGCGAGTGAACAGG	GATCAGAAGGACTTGGGCCC	4f	

Chapter II:

DDX21 is a p38-MAPK sensitive nucleolar protein necessary for mouse preimplantation embryo development and cell-fate specification.

Pablo Bora, Lenka Gahurova, Andrea Hauserova, Martina Stiborova, Rebecca Collier, David Potěšil, Zbyněk Zdráhal and Alexander W. Bruce.

(accepted at **Open Biology**)

bioRxiv 2021.04.13.439318

DDX21 is a p38-MAPK sensitive nucleolar protein necessary for mouse preimplantation embryo development and cell-fate specification.

Pablo Bora[1,*], Lenka Gahurova[1,2], Andrea Hauserova[1], Martina Stiborova[1], Rebecca Collier[1], David Potěšil[3], Zbyněk Zdráhal[3] and Alexander W. Bruce[1,*]

1. Laboratory of Early Mammalian Developmental Biology (LEMDB), Department of Molecular Biology & Genetics, Faculty of Science, University of South Bohemia, Branišovská 31, 37005 České Budějovice, Czech Republic.

2. Laboratory of Biochemistry and Molecular Biology of Germ Cells, Institute of Animal Physiology and Genetics, CAS, Rumburská 89, 27721 Liběchov, Czech Republic.

3. Central European Institute of Technology, Masaryk University, 62500 Brno, Czech Republic.

Correspondence:

* borapa00@prf.jcu.cz

* awbruce@prf.jcu.cz

Contributions:

P.B. and A.W.B. conceived the project, designed experiments, analysed results and wrote the manuscript. P.B. and L.G. prepared samples for mass spectrometry. P.B., A.H., M.S. and R.C. conducted experiments. A.H. also analysed some results. L.G. analysed proteomic and phosphoproteomic data. D.P. and Z.Z. performed phosphoproteomic mass spectrometry, did preliminary data analysis and wrote the associated methods.

Funding:

This work was supported by a project grant from the Czech Science Foundation/GAČR (18-02891S), a Marie Curie Individual Fellowship (MSC IF 708255) awarded to L.G. and a Ph.D. student award to P.B. by the Grant Agency of the University of South Bohemia (GAJU; 012/2019/P).

Availability of data and materials:

The mass spectrometry proteomics data have been deposited to the ProteomeXchange Consortium via the PRIDE partner repository with the dataset identifier PXD025754.

Competing interests:

The authors declare no competing interests.

Acknowledgements:

We acknowledge the Institute of Parasitology (Biology Centre of the Czech Academy of Sciences, in České Budějovice) for housing mice, Marta Gajewska (Institute of Oncology, Warsaw, Poland) and Anna Piliszek (Institute of Genetics and Animal Breeding, Polish Academy of Sciences, Jastrzębiec, Poland) for founder CBA/W mice, Alena Krejčí (Faculty of Science, University of South Bohemia, Czech Republic) for pooling resources and other members of our laboratory for valuable inputs and discussions. We also acknowledge the core facility Masaryk University, Brno, Czech Republic - Faculty of Informatics, supported by the MEYS CR (LM2018129 Czech-BioImaging) for assistance with image analysis. CIISB, Instruct-CZ Centre of Instruct-ERIC EU consortium, funded by MEYS CR infrastructure project LM2018127, is gratefully acknowledged for the financial support of the measurements at the CEITEC Proteomics Core Facility. Computational resources were supplied by the project "e-Infrastruktura CZ" (e-INFRA LM2018140) provided within the program Projects of Large Research, Development and Innovations Infrastructures.

Abstract:

Successful navigation of the mouse preimplantation stages of development, during which three distinct blastocyst lineages are derived, represents a prerequisite for continued development. We previously identified a role for p38-mitogen-activated kinases (p38-MAPK) regulating blastocyst inner cell mass (ICM) cell-fate, specifically primitive endoderm (PrE) differentiation, that is intimately linked to rRNA precursor processing, polysome formation and protein translation regulation. Here, we develop this work by assaying the role of DEAD-box RNA helicase 21 (DDX21), a known regulator of rRNA processing, in the context of p38-MAPK regulation of preimplantation mouse embryo development. We show nuclear DDX21 protein is robustly expressed from the 16-cell stage, becoming exclusively nucleolar during blastocyst maturation; a localisation dependent on active p38-MAPK. Efficient siRNA mediated clonal Ddx21 knockdown within developing embryos is associated with profound cell autonomous and non-autonomous proliferation defects and reduced blastocyst volume, by the equivalent peri-implantation blastocyst stage. Moreover, ICM residing Ddx21 knockdown clones express the EPI marker NANOG but rarely express the PrE differentiation marker GATA4. These data contribute extra significance to emerging importance of lineage specific translation regulation, as identified for p38-MAPK, during mouse preimplantation development.

Introduction:

Mammalian preimplantation embryonic development is the period between fertilisation and uterine implantation. This period encompasses zygotic genome activation (ZGA), cellular proliferation and lineage specification, culminating in a metabolically active outer trophectoderm (TE) cell layer, fluid-filled blastocoel cavity, epithelial primitive endoderm (PrE) layer and pluripotent epiblast cells (EPI) enveloped between the TE and PrE. Primary transcriptional regulators of cell-fate, such as TEAD4 and CDX2 (TE fate), GATA6, SOX17 and GATA4 (PrE fate) and NANOG and SOX2 (EPI fate), have been identified in the mouse model and are enabled by specific signalling networks; i.e., HIPPO-YAP for TE and FGF4-FGFR1/2-MEK/ERK for PrE (as extensively reviewed recently[1–4]). Furthermore, mechanical forces acting on the developing early embryo, on both cellular and embryonal levels, have been found to be significant in the spatial sorting and cell-fate specification of individual blastomeres[5–7]. Additionally, a more holistic view of preimplantation embryonic development is emerging by the incorporation of regulatory studies targeting global events, such as translation[8–11]. Indeed, regulation of translation is reported to be vital to modulating pluripotency around the peri-implantation stage[8], enabling embryonic diapause[9] and potentiating global transcriptional regulation[10].

In previous reports we have described an elementary role for p38 mitogen-activated protein kinase (p38-MAPK) signalling on PrE specification in the mouse blastocyst inner cell mass (ICM)[12], as well as a distinct function mitigating amino acid deprivation induced oxidative stress during blastocyst maturation[13]. Recently, we extended these investigations and described an early blastocyst functional role in regulating ribosomal RNA (rRNA) processing, translation and transcription required for correct mouse blastocyst expansion and PrE cell-fate specification and differentiation. Moreover, that this pathway appears largely independent of the quintessentially described FGF4-based PrE specification mechanisms and is at least partially upstream of the translation regulator mTOR[11]; itself independently implicated in PrE specific survival in late (E4.5) blastocysts[14]. p38-MAPK activity is also necessary for functional TE derivation prior to blastocyst formation, and its inhibition (p38-MAPKi) from the 16-cell stage (E3.0) specifically impairs fluid-filling of the blastocoel cavity by functionally impacting tight-junction proteins (TJP1), aquaporins (AQP3) and Na^+/K^+ pumps (such as ATP1); possibly as a result of p38-MAPKi induced translational and transcriptional deregulation[11,15,16]. Additionally, p38-MAPKi from the 8-cell stage (E2.5) is reported to cause developmental arrest, at the 8-16 cell stage transition, and is associated with defective embryo compaction and impaired filamentous actin formation[17].

In our recent publication describing the role of p38-MAPK in protein translation regulation and PrE differentiation, we reported the results of a phosphoproteomics screen for differentially expressed phosphoproteins in early mouse blastocysts ±p38-MAPKi; aimed at identifying relevant potential p38-MAPK effectors/substrates[11]. This analysis identified the Myb-binding protein 1A (MYBBP1A), a known regulator of rRNA transcription and processing[18] (shown by us

to be defective in p38-MAPKi blastocysts[11]). We showed siRNA induced clonal downregulation of *Mybbp1a* was associated with cell-autonomous proliferation defects and a strong bias against PrE differentiation within mouse blastocyst ICM[11]. The HIV Tat-specific factor 1 homolog (HTATSF1) protein, itself implicated in genetic knockout studies as regulating peri-implantation stage blastocyst EPI pluripotency[8], is a known functional interacting partner of MYBPP1A[8,19]. HTATSF1 also functionally associates with DEAD-box RNA helicase 21 (DDX21)[8,20]. Interestingly, although DDX21 was not specifically identified in our published ±p38-MAPKi early blastocyst screen[11] (falling outside the prescribed filters), we had previously observed it as a differentially phosphorylated protein in our preliminary optimisation trials (supplementary table S1 – derived from previously unpublished observations). Therefore, we decided to revisit the, to date uncharacterised, functional role of DDX21 during mouse preimplantation development within the context of p38-MAPK activity.

DDX21 (initially termed RNA helicase II/Guα) is primarily, but not exclusively, a nucleolar-localised RNA helicase (with ATPase activity) shown to be a regulator of rRNA processing; downregulation of which causes decreased production of both 18S and 28S rRNA and accumulation of unprocessed 20S pre-rRNA transcripts[21,22]. It co-fractionates as a protein complex consisting of pre-60S ribosomal subunits and other rRNA processing proteins, such as Pescadillo homolog 1 (PES1), Eukaryotic translation initiation factor 4E-binding protein 2 (EIF4EBP2) and Guanine nucleotide-binding protein-like 3 (GNL3; also known as Nucleostemin/NS)[23]. Recent detailed molecular studies have reported diverse DDX21 roles that range from rRNA metabolism and regulation of RNA polymerase (pol) I and II mediated transcription to nucleotide stress response and c-Jun activity[20,24–27]. Indeed, DDX21 regulates RNA pol II mediated transcription of mRNA and non-coding RNA components of ribonucleoprotein complexes[20]. According to another recent report, DDX21 interacts with a specific long non-coding (lnc) RNA, termed the 'small nucleolar RNA (snoRNA)-ended lncRNA that enhances pre-rRNA transcription' or SLERT, to reduce its inhibitory affinity for the RNA pol I complex[26]. Regulation of DDX21 activity itself is under the control of post-translational modification, with CREB-binding protein (CBP) mediated acetylation and Sirtuin7 (SIRT7) mediated deacetylation respectively decreasing or increasing its helicase activity[28]. Whilst some, rRNA metabolism related mouse genes, for example *Mybbp1a*[18], *Gnl3*[29] and potentially *Htatsf1* (homozygous knockout embryonic stem cells demonstrate reduced pluripotency[8]), are associated with embryonic lethal genetic knockout phenotypes, no similar *Ddx21* specific studies are reported. However, the Mouse Genome Informatics (MGI) database does catalogue evidence that N-ethyl-N-nitrosourea (ENU) induced mutagenesis of the *Ddx21* gene is embryonically lethal (http://www.informatics.jax.org/marker/MGI:1860494). Ribosomopathies, a collective term for varied human congenital developmental disorders, are mostly associated with heterozygous mutations in factors involved in ribosome biogenesis[30,31]. Interestingly, experimental perturbation of disease-causing candidate genes, such as those identified in Treacher Collins syndrome (TCS), Diamond–Blackfan anaemia (DBA) and

Shwachman–Diamond syndrome (SDS), have been reported to result in shifted localisation of DDX21 from nucleoli to the general nucleoplasm, with associated changes in DDX21 target chromatin interaction and rRNA processing[24]. Additionally, DDX21 can form a complex with the serine/threonine phosphoprotein phosphatase (PPP) family protein PP132, that along with other family members are well characterised late M-phase/cytokinesis cell cycle regulators[33].

Here, using pharmacological inhibition, siRNA mediated downregulation, confocal immuno-fluorescence microscopy and image analysis, we report our findings on the role of DDX21 during mouse preimplantation embryo development. We find basal levels of nuclear DDX21 protein expression until the 16-cell (E3.0) stage, when DDX21 levels begin to increase and become robustly expressed in the early (E3.5) blastocysts before becoming nucleolar by the late blastocyst stage. Moreover, that DDX21 protein expression is sensitive to p38-MAPKi during the period of blastocyst maturation (E3.5-E4.5), as evidenced by varying degrees of decreased nucleolar retention. Specific siRNA-mediated targeting of the *Ddx21* gene leads to efficient global mRNA knockdown and associated clonal cell-autonomous reductions in DDX21 protein expression that cause a 50% reduction in the volume of the late blastocyst. Intriguingly, such clonal *Ddx21* downregulation both cell autonomously (within the siRNA treated clone) and non-cell autonomously (affecting non-microinjected cells outside the *Ddx21* knockdown clone) impairs blastomere proliferation and results in severe defects in the numbers of EPI and PrE lineages by the late blastocyst stage; compared to equivalent stage non-specific control siRNA treated groups. These results complement our recent report on the general translational regulatory role of p38-MAPK during blastocyst development11 and identify DDX21 as a p38-MAPK effector with an apparently essential role in murine preimplantation embryonic development.

Results:

DDX21 localisation shifts from nuclear to nucleolar post-cavitation during preimplantation development.

We previously described an important role of p38-MAPK in coordinating an early blastocyst protein translation response necessary to promote PrE differentiation; identifying MYBPP1A, a known rRNA processing factor, as a p38-MAPK effector[11]. Whilst, there are mouse genetics-based evidences implicating some rRNA metabolism related genes (e.g. *Mybbp1a*[18], *Gnl3*[29] and *Htatsf*[18]) to critical roles in early development, no similar data exists for the RNA helicase encoding *Ddx21* gene. Therefore, given the precedents for early developmental functions of similar rRNA-related genes, and the fact we have detected differential phosphorylation of DDX21 protein in mouse blastocysts after p38-MAPKi (supplementary table S1), we decided to assay *Ddx21* gene expression throughout the preimplantation developmental stages. Data from recently published transcriptomic studies report *Ddx21* mRNA expression starting to rise from a low steady state

level at the 2-cell (E1.5) stage, peaking at the 8-cell stage and thereafter being maintained at a high level in all preimplantation embryonic cell lineages (supplementary Fig. S1)[34,35]. Immuno-fluorescent staining of DDX21 protein revealed expression at basal levels in the nuclei of 2-, 4-(E2.0) and 8-cell embryos and robust expression in a subset of 16-cell stage nuclei, that was found in all nuclei by the early through late blastocyst stages, correlating with formation of the blastocyst cavity (Fig. 1a). Interestingly, whereas in pre-cavitated embryos, DDX21 protein appeared to be either pan-nucleoplasmic or even adjacently localised to the nuclear membrane (Fig. 1b), post cavitation it was found to be exclusively nucleolar (Fig. 1d); suggesting a potential functional significance associated with the onset of blastocyst formation. Equally intriguing was the observation of similar differential DDX21 localisation behaviour regarding mitotic chromatin. DDX21 readily localised to condensed chromosomes prior to cavitation but appeared to be actively excluded from them post-cavitation (compare Figs. 1c & e); further suggesting functional adaptation of the role DDX21 as a response to blastocyst formation.

DDX21 localisation is sensitive to p38-MAPK signalling during blastocyst maturation.

Collectively, we have previously identified an early blastocyst developmental window of p38-MAPK activity (associated with protein translation regulation) required to support PrE differentiation[11], obtained evidence DDX21 is a candidate p38-MAPK substrate (supplementary table S1) and revealed blastocyst specific nucleolar restricted expression of DDX21 protein. We therefore sought to examine DDX21 protein expression and localisation (together with that of the functionally related and rRNA processing factor Nucleostemin/NS, also known as Guanine nucleotide-binding protein-like 3/GNL323; genetic nulls of which do not develop beyond E4.0[36,37].) in maturing mouse blastocysts ±p38-MAPKi (E3.5-E4.5 - Fig. 2a). In control E4.5 stage blastocysts, we observed expression of DDX21 and GLN3 in both inner and outer cell nuclei, that in respect to nucleolar structures was co-localised (Fig. 2b & b' insets). Nevertheless, respective protein expression quantitation revealed DDX21 to be more highly expressed in outer versus inner cell nuclei overall, with the inverse being true for GLN3 (compare Figs. 2 e & f, also alternatively expressed in supplementary Fig. S2). p38-MAPKi resulted in a clear reduction in both DDX21 and GNL3 protein expression that was evident in all blastocyst cells, comprising both inner and outer populations (Fig. 2c, d, e, f & supplementary Fig. S2). The percentage decrease upon p38-MAPKi in levels of GLN3 (56% decrease overall) was greater than DDX21 (30% decrease overall), nevertheless the values were statistically significant in both cases (Fig. 2c, d, e, f & supplementary Fig. S2). Apart from the changes in general DDX21 protein expression, we also note that p38-MAPKi was associated with a shift in DDX21 protein localisation. This was manifest in increased expression in the general nucleoplasm (Fig. 2c' & d') as opposed to exclusively nucleolar expression previously characterised in untreated (Fig. 1d) or control treated late blastocysts (Fig. 2b, b'). Interestingly, we did also observe the degree of p38-MAPKi dependent relocalisation of DDX21 protein away from the nucleolus was somewhat heterogeneous

(compare Figs 2c & c' with 2d & d'). This is possibly related to natural heterogeneity in the developmental timings of individual blastocysts at the point of administering p38-MAPKi. Notwithstanding, these data demonstrate the continued general expression of DDX21 and more profoundly GLN3 is sensitive to active p38-MAPK signalling during blastocyst maturation. Additionally, typical blastocyst stage nucleolar localisation of DDX21 protein is also regulated by active p38-MAPK. Collectively, these data lend support to the importance of p38-MAPK related regulation of translation, and particularly rRNA processing, as recently uncovered in early blastocyst maturation and eventual PrE differentiation[11].

Clonal downregulation of Ddx21 causes reduced embryo cell number and blastocyst expansion.

Given the revealed p38-MAPKi sensitivity of blastocyst DDX21 nucleolar localisation, we speculated what the effect of targeted dysregulation of the *Ddx21* gene expression would be on mouse preimplantation embryo development and, given our previously described reports[11–13], on blastocyst ICM cell fate derivation and specifically PrE differentiation. Accordingly, we devised a siRNA microinjection mediated scheme to downregulate *Ddx21* transcript levels (schematic described in Fig. 3a). To assess *Ddx21* specific siRNA efficiency, we microinjected both blastomeres of 2-cell stage embryos and quantified normalised *Ddx21* transcript levels at the late blastocyst stage. Compared to non-targeting control (NTC siRNA) microinjected embryos, at the equivalent stage, *Ddx21* specific siRNA elicited 42% decreased *Ddx21* mRNA expression (Fig. 3b). We next, created fluorescently marked embryonic clones by co-microinjecting one cell at the 2-cell stage with siRNA (either NTC or *Ddx21* specific) and mRNA encoding histone H2B-RFP reporter; thus, creating a clone initially comprising 50% of the embryo. Microinjected embryos were then cultured to the late blastocyst stage, fixed, immuno-fluorescently stained for DDX21 (and the outer trophectoderm marker protein CDX2[38]– to distinguish inner and outer cell populations) and the number of cells in the fluorescently marked siRNA microinjected clones, plus non-microinjected sister clones, and their spatial localisation within the embryo (outer or inner) recorded.

As shown in the confocal micrographs (Fig. 3f-g''), microinjected cell clones were clearly distinguishable by expression of the histone H2B-RFP reporter in both NTC and *Ddx21*-specific siRNA microinjection groups. However, whereas DDX21 protein was expressed in all cell nuclei (specifically nucleoli) in the NTC control group, it was only readily detected in cell nuclei derived from the non-microinjected clone in the *Ddx21* targeted group (although not always restricted to nucleoli) and appeared highly, if not completely, reduced in the marked microinjected clone (Fig. 3g, g' & g''). Indeed, normalised quantitation of DDX21 immuno-fluorescence confirmed a highly significant reduction in overall average expression per cell (encompassing both microinjected and non-microinjected cell clones) in the *Ddx21* siRNA treatment group versus the NTC control (Fig. 3c-e & alternatively presented in supplementary Fig. S3a-c). This was true of both outer and inner cell populations (note, DDX21 expression was higher in outer versus inner

cells in the NTC siRNA controls and was therefore consistent with observations made on similar late blastocysts treated with vehicle control DMSO – Fig. 2 & Fig. S2). The *Ddx21* siRNA induced reduction in DDX21 protein expression was most robust in the marked microinjected clone in both inner and outer cells (i.e. when compared to either the non-microinjected sister clones of the same embryos or the equivalent microinjected clone of the control NTC siRNA treatment group (Fig. 3e)); thus, confirming the anticipated cell autonomous effect of the microinjected *Ddx21* siRNA. However, it was also observed that clonal *Ddx21* knockdown also affected DDX21 protein expression in the non-microinjected clone, as it was also significantly reduced (in both inner and outer cells) in *Ddx21* versus NTC siRNA treatment groups (Fig. 3d and g''); confirming additional DDX21 related non-cell autonomous effects (that nevertheless did not affect every cell within that clone (Fig. 3d and g'). Notably, the microinjection of NTC siRNA had no statistically significant effect on DDX21 protein levels in either inner or outer cells and confirmed the absence of bias that could be attributable to the microinjection procedure. Hence, microinjection of *Ddx21* siRNA in one blastomere at the 2-cell stage causes highly efficient DDX21 protein knockdown within the clonal progeny of the microinjected cell but also results in reduced DDX21 expression in the accompanying non-microinjected sister clone, that is not restricted to the nucleolus by the late blastocyst stage.

Inspection of the embryos derived from the clonal NTC and *Ddx21* siRNA treatment groups also revealed profound morphological differences. Whereas, the NTC group comprised embryos with typical late blastocyst morphology (i.e. a mature CDX2 positive outer trophectoderm layer and large blastocyst cavity and ICM), the *Ddx21* siRNA microinjected embryos were typically smaller and appeared to comprise much fewer cells (although CDX2 protein expression was appropriately confined to outer cells only – compare Fig. 3f & g). Indeed, measuring the volume of the derived blastocysts, we observed a more than 50% reduction in *Ddx21* clonally downregulated embryos compared to control embryos (Fig. 3j). This result resonates with our recent report in which we revealed a similar blastocyst expansion defect, that is associated with significantly impaired PrE differentiation, upon p38-MAPKi (E3.5-E4.5)[11] and the fact we have identified DDX21 as a potential p38-MAPK effector (supplementary table S1). An analysis of the average number, relative spatial positioning and clonal origin of cells showed no significant differences between the NTC siRNA microinjected clone and its non-microinjected counterpart. However, in the *Ddx21* siRNA group only 27.45% of overall cell numbers originated from the microinjected blastomere (compared to 49.6% for NTC microinjected embryos), with comparative cell number deficits in the microinjected (versus non-microinjected) clone being highly significant in both outer and inner cell populations (on average 8.31 versus 20.85 and 2.27 versus 7.08, respectively) (Fig. 3h & I and supplementary Fig. S3d). The reduced contribution was particularly stark for inner cells, averaging at 24.3% of the total ICM (compared to 46.2% in controls), that in absolute numbers only represents an average of 2.27 inner cells. In addition to such *Ddx21* siRNA microinjected clone specific cell deficits, we also observed significantly reduced numbers of outer and inner

cells in the non-microinjected clone (when compared to the equivalent clone in the control NTC siRNA treatment group – on average 20.85 versus 26.67 and 7.08 versus 11.73, respectively) (Fig. 3h & i). These data confirm both cell autonomous and non-autonomous effects of clonal *Ddx21* knockdown in developing mouse embryos and agree with the atypical non-nucleolar localisation of DDX21 in the non-microinjected clone (see above). Thus, clonal downregulation of *Ddx21* results in a global effect on embryonic development, effecting cell proliferation and blastocyst volume.

Ddx21 downregulation results in defective blastocyst cell-fate specification.

Having previously confirmed a role for p38-MAPK during blastocyst maturation and PrE lineage differentiation[11–13] plus the effects of p38-MAPKi on DDX21 protein localisation (Fig. 2) and the remarkably reduced contribution of *Ddx21* siRNA injected blastomeres towards inner cells (Fig. 3), we wanted to assay the effect of clonal *Ddx21* knockdown on late blastocyst (E4.5) ICM cell fate. Accordingly, we repeated our clonal NTC/*Ddx21* siRNA 2-cell stage microinjection experiments (as described in Fig. 3a) and assayed the expression of NANOG and GATA4 protein as markers of the EPI and PrE. Consistently, we again observed robust and significant decreases in overall, outer and inner cell numbers in *Ddx21* siRNA microinjected embryos, that was most evident in the microinjected clone but also present in the non-microinjected clone (supplementary Fig. S4). We also observed significant and marked reductions in the overall number of ICM cells expressing either NANOG or GATA4, in both microinjected and non-microinjected clones, in *Ddx21* siRNA treated embryos (Fig. 4a, b & c). Whilst these reductions can reflect overall reduced cell number, it is notable the effect was stronger for GATA4 expressing PrE versus NANOG positive EPI-like cells, with an overall average of 1.0 GATA4 expressing cell in *Ddx21* downregulated embryos compared to 7.44 in control NTC siRNA embryos (Fig. 4c (ii) – the equivalent NANOG expressing EPI cell numbers being 3.47 and 9.0, respectively – Fig. 5c (i)). Moreover, among the *Ddx21* downregulated embryos, we observed an average of 0.93 GATA4 expressing cells originating from the non-injected blastomere and only 0.07 originating from the injected one (Fig. 4c (ii) - the equivalent NANOG expressing EPI cell numbers being 1.93 and 1.53, respectively - Fig. 4c (i)). Hence, despite the reduced number of overall, and specifically ICM, cells associated with clonal *Ddx21* downregulation, it is the derivation of GATA4 expressing PrE lineage that is more markedly impaired/blocked by the late blastocyst stage. This is further revealed by the significantly reduced ratio of GATA4 positive PrE cells versus total ICM cell number, in both the microinjected and non-microinjected clones, of *Ddx21* siRNA treated embryos (Fig. 4c (iii)); a trend not observed in the calculated ratio of NANOG positive EPI-like cells in the same embryos (Fig. S4 (iv)). These data support a role for DDX21, potentially regulated by p38-MAPK activity, in facilitating PrE differentiation in the mouse blastocyst.

Discussion:

The functional role of p38-MAPKs in preimplantation mouse embryos is a developing story and work from a few labs, including ours, have only just started to uncover the many facets of early development that this signalling pathway touches. In the earlier developmental stages, p38-MAPK activity is associated with formation of filamentous actin[17] and embryo compaction and subsequent appropriate functioning of the TE to enable expansion of the blastocoel cavity[15,16]. Our own p38-MAPK research has primarily focussed on the post E3.5 cavitated stages, thus specifically addressing blastocyst maturation and ICM specification towards EPI and PrE lineages[11–13]. In our recent work, we have identified a protein translation associated regulatory role for p38-MAPK that underpins PrE cell fate differentiation. This role appears to be functionally upstream of the mTOR pathway and largely independent of the classically described FGF4-ERK mediated mechanisms of PrE specification[11]. Whereas the upstream regulators/activators of this p38-MAPK pathway are the subject of informed speculation, potentially involving FGFR2, FGFR3 and/or PDGFRα[11], the downstream effectors can be many and encompass various mechanistic ontologies (reviewed here[39]). Hence the identification of known factors involved in rRNA metabolism and ribosome biogenesis (for example, MYBBP1A[11] and DDX21 described here) as being sensitive to p38-MAPK signalling and essential in appropriate preimplantation embryonic development, further reinforces the emerging importance of the broader hypotheses of germane regulation of protein translation.

To the best of our knowledge, we report the first observations of DDX21 protein expression and localisation during mouse preimplantation embryonic development (Fig. 1a). Expression of the *Ddx21* gene is reported to start around the 2-4 cell stage and peaks at the 8-cell stage in mouse embryos, subsequently remaining high across all cellular lineages; with close to nil expression in the maturing oocyte (supplementary Fig. S1)[34,35]. The protein appears to be expressed only after ZGA onset, and is thus not of maternal origin, becoming robustly observable in some 16-cell stage nuclei. Around blastocyst formation, all cells express DDX21 protein that then exhibits a typical nucleolar localisation as the blastocyst matures to the peri-implantation stage (Fig. 1a & d). Thus, the protein expression timeline closely follows that of the gene transcript. Moreover, the fact *Ddx21* knockdown clones only contribute an average of 11.69 cells to the late blastocyst, compared to 36.67 cells from the NTC siRNA microinjected blastomeres (Fig. 3h & i)), strongly suggests DDX21 expression is ordinarily necessary for transition beyond the 32-cell stage and in turn blastocyst formation. This is reinforced by the observation that such cell autonomous clonal cell number effects are also accompanied by non-cell autonomous effects within the non-microinjected clone; implying the existence of inter-blastomere proliferative signals that are impinged upon by functional DDX21. Moreover, the existence of such DDX21 related non-cell autonomous effects is also suggested by the fact DDX21 protein expression in the non-microinjected clone of *Ddx21* siRNA microinjected embryos does not always exhibit nucleoli restricted expression typical of the blastocyst stages. Nucleoli are sub-nuclear structures closely associated with ribosome biogenesis that gradually transit through extensive compositional,

functional and structural transformations between oogenesis and the embryonic morula stage (reviewed here[40,41]). Briefly, as developmentally competent oocytes slowly initiate inactivation of RNA pol I and II, their nucleoli gradually become denser and form atypical structures termed nucleolus-like-bodies (NLB); a process that is accompanied by reducing levels of component nucleolar proteins and correlates with paused ribosome biogenesis. After fertilisation, further atypical nucleolar bodies, termed nucleolus-precursor-bodies (NPB), emerge but are then replaced by somatic cell-type nucleoli after the morula to blastocyst transition. The functional significance of these atypical nucleolar bodies during early development is itself an interesting topic, with some reports suggesting their requirement during early ZGA and as gene regulatory structures in later stages[41]. However, it is interesting that our observations of exclusive nucleolar restricted DDX21 protein expression is concomitant with the emergence of somatic cell-type nucleoli during the earliest stages of blastocyst formation. Moreover, that such exclusive nucleolar expression is dependent on active p38-MAPK during blastocyst maturation, a time in which p38-MAPK mediated regulation of protein translation is required for PrE differentiation[11]. Thus, it is possible DDX21, potentially acting downstream of p38-MAPK regulation, is involved in the remodelling of early embryonic cell nucleoli, in order to sustain the morula to blastocyst transition and subsequent ICM maturation and PrE formation.

Related to the subject of DDX21 protein localisation, the observed differential association of DDX21 with condensed mitotic chromosomes as a function of developmental stage is intriguing (i.e. in association in pre-blastocyst stages and excluded in the blastocyst - Fig. 1c and e). There is a report suggesting DDX21 forms complexes with members of PPP family of phosphatases[32] and indeed PP1 and other members of PPP family are key cell cycle regulators[33]. Thus, this association may explain the observed DDX21 localisations in relation to mitotic chromatin but the stage specific differential nature of such localisation also implies any potential DDX21-PPP interaction is likely to be dynamically regulated during preimplantation development. Interestingly, it is during blastocyst formation that mouse embryo mitoses revert to centrosomal control, after previously being acentrosomally regulated since fertilisation (a murine specific characteristic amongst studied mammalian species[42]).

Post-translational modification by acetylation is reported to reduced DDX21 activity[28]. Here we report reduced phosphorylation of DDX21 at serine-218 (S218) in mouse blastocysts upon p38-MAPKi (supplementary table S1). According to the phosphosite.org database (an archive of all confirmed and predicted phosphorylation events in a host of model organisms[43]) this site is mouse specific and not conserved in either humans or rats; however, it does conform with the consensus [S/T]P dipeptide phosphorylation motif typical of the proline-directed mitogen-activated-kinase superfamily[44]. Direct experimental evidence of p38-MAPK phosphorylation mediated functional and/or locational regulation of DDX21 is lacking. However, based on our current observations this potential mechanism remains a strong possibility; as exemplified by the

shift to exclusively nucleolar DDX21 localisation upon blastocyst formation, that is itself sensitive to p38-MAPKi (Fig. 1 and Fig. 2). Such shifts in DDX21 localisation are also observed in genetic models of congenital ribosomopathies, such as TCS, DBA and SDS, and are interestingly present in the differentiated derivative of ES cells harbouring the specific genetic mutations but not the originating pluripotent parental ES cell lines themselves[24]. Thus, the p38-MAPKi phenotypes we observe during blastocyst maturation are, at least in the context of DDX21 localisation, similar to those translation defects underpinning described ribosomopathies. Moreover, coupled with our recent report of reduced translation and rRNA processing in blastocysts cultured under p38-MAPKi conditions[11], such ribosomopathy based insights[24] may be able to contribute to an expanded picture of the role of p38-MAPK signalling during blastocyst maturation and specifically ICM cell lineage and PrE derivation.

Our analysis of the contribution of *Ddx21* downregulated cell clones to late blastocyst (E4.5) ICM lineages is ostensibly an extension of our previous observations obtained under p38-MAPKi culture conditions[11–13], and is similarly characterised by a reduction in the number of GATA4 expressing PrE cells (Fig. 4). However, it is the severity of this deficit that distinguishes such *Ddx21* knockdown phenotypes, as almost no GATA4 expressing PrE cells were found to originate from *Ddx21* siRNA microinjected clone and moreover such GATA4 deficits were also non-cell autonomously observed in the non-microinjected sister clones (Fig. 4c (ii)). We similarly observed highly significant reductions in NANOG expressing EPI-like cells and outer TE cells in *Ddx21* siRNA microinjected embryos (Fig. 4c (i) and supplementary Fig. S4), although, compared to the almost complete block in PrE derivation, these lineages were less severely affected. In contrast, the p38-MAPKi (E3.5-E4.5) derived phenotype is more specifically centred on PrE cell differentiation (characterised by an uncommitted state of NANOG and GATA6 co-expression), with only limited and insignificant decreases in the quantity of other late blastocyst cell lineages[11–13]. Hence, these data suggest DDX21 likely plays a more fundamental role in regulating blastomere proliferation at the morula to blastocyst transition (supported by the increasing DDX21 protein expression data - Fig. 1) and developmentally precedes the previously studied period of p38-MAPKi during blastocyst maturation (E3.5-E4.5)[11–13]. Interestingly, it is not possible to study ultimate ICM cell fate in embryos exposed to p38-MAPKi before E3.5 (and the onset of cavitation and irreversible TE specification[45]) as embryos arrest development with around 32-cells and fail to cavitate[12]. This confirms the morula-blastocyst transition as acutely sensitive to p38-MAPKi and developmentally coincides with the observed apparent proliferative block of Ddx21 knockdown embryos (i.e. observed as more severe in the microinjected clone versus non-cell autonomous effects in the non-microinjected clone - Fig. 3 and Fig.4) and the observed transition of DDX21 protein expression to an exclusively nucleolar localisation (Fig. 1). Clonal *Ddx21* knockdown is still associated with cavity formation, albeit impaired in comparison to controls (Fig. 3j). This suggests that at least part of the pre-E3.5 administered p38-MAPKi 32-cell arrested development phenotype could have a DDX21 related root. In relation to p38-MAPKi phenotypes during

blastocyst maturation (E3.5-E4.5), it is likely any effect of p38-MAPK mediated regulation of DDX21 (e.g. potential direct phosphorylation leading to the observed loss of exclusively nucleolar expression – Fig. 2) will probably not be as drastic as efficient downregulation of the *Ddx21* derived mRNA and protein caused by RNAi. This leaves open the possibility active p38-MAPK regulation of DDX21 function is a contributing factor to our previously observed p38-MAPK role in protein translation, mouse blastocyst ICM maturation and PrE differentiation11. Much like our observations with *Ddx21* (this manuscript) and *Mybbp1a*[11] clonal downregulation in preimplantation embryos, *Mybbp1a*[18] and *Gnl3* (Nucleostemin)[29] homozygous gene knockouts also result defective development by the late blastocyst stage. These collective observations are bringing into focus the indispensable and potentially non-redundant role of various ribosome biogenesis related genes during the preimplantation stages of mouse development and the formation of the blastocyst ICM lineages in particular. Moreover, they also highlight the importance of the underpinning regulatory signalling mechanisms, such as the p38-MAPK pathway, responsible for their proper functioning.

Methods:

Mouse lines and embryo culture.

All mouse related experimental procedures (i.e. collecting preimplantation stage embryos for further study) complied with 'ARRIVE' guidelines and were carried out in accordance with EU directive 2010/63/EU (for animal experiments). Superovulation and strain mating regimen to produce experimental embryos; F1 hybrid (C57Bl6 x CBA/W) females injected sub-peritoneally with 7.5 IU pregnant mare serum gonadotrophin/PMSG (Folligon, MSD Animal Health, Boxmeer, Netherlands) and 48 hours later with 7.5 IU recombinant human chorionic gonadotrophin/hCG (Sigma-Aldrich, St. Louis, Missouri, USA; Cat. No. CG10), followed by overnight F1 male mating (successful mating confirmed by presence of vaginal plugs). E1.5 (2-cell) stage embryos were isolated from oviducts in M2 media (pre-warmed at 37˚C for at least 2-3 hours) and thereafter cultured in KSOM (Sigma-Aldrich, EmbryoMax KSOM Mouse Embryo Media; Cat. No. MR-020P-5F - pre-warmed and equilibrated in 5% CO2 and 37˚C) with amino acid (AA) supplementation; Gibco MEM Non-Essential Amino Acids Solution (100X) (Thermo Fisher Scientific, Paisley, Scotland; Cat. No. 11140035) and Gibco MEM Amino Acids Solution (50X) (Thermo Fisher Scientific; Cat. No. 11130036) were used to a working concentration of 0.5X. Embryos were cultured in micro-drops prepared in 35mm tissue culture dishes covered with light mineral oil (Irvine Scientific, Santa Ana, California, USA; Cat. No. 9305), in 5% CO2 incubators maintained at 37˚C until the appropriate stage. Pharmacological manipulations were performed by addition of chemical agents dissolved in dimethyl sulfoxide (Sigma-Aldrich; Cat. No. D4540) to KSOM+AA and equivalent volumes of DMSO were used as vehicle controls. Please note, the p38-MAPK (SB220025 – 20μM) inhibitor concentration used was derived by empirical titrations previously employed by ourselves[12] and literature based precedents[15,46]. All KSOM based culture media,

with or without additional chemicals (AAs, pharmacological agents), were pre-warmed and equilibrated in 5% CO2 and 37˚C for at least 3-4 hours prior to embryo transfer.

Sample collection for mass spectrometric analysis of differential (phospho)proteome.

2-cell (E1.5) stage embryos were cultured in normal KSOM+AA conditions until E3.5 +2h and thereafter 100 embryos each were moved to control or p38-MAPKi conditions and cultured for another 7 hours (E3.5 +9h). The embryos were then washed through pre-warmed (37˚C) Hank's balanced salt solution (HBSS, Sigma-Aldrich; Cat. No. H9269) and lysed by moving to a 1.5ml centrifuge tube containing about 15µl of SDT-lysis buffer (4% (w/v) SDS, 100 mM Tris-HCl pH 7.6, 0.1 M DTT). Cell lysis was performed by incubating the tubes in a 95˚C thermoblock for 12 minutes, brief centrifugation at 750 rpm, cooling to room temperature and storage at -80˚C.

Samples preparation for Liquid Chromatography–Mass Spectrometry (LC-MS) analysis.

Individual protein solutions were processed and analysed as described previously11. Briefly, protein lysates were processed by the filter-aided sample preparation (FASP) method. FASP eluates were used for phophopeptides enrichment using High-Select TiO2 Phosphopeptide Enrichment Kit (Thermo Fisher Scientific, Waltham, Massachusetts, USA). LC-MS/MS analyses of peptide mixtures (not enriched and enriched in phosphopeptides using TiO2 enrichment kit) were performed using a RSLCnano system connected to Orbitrap Fusion Lumos mass spectrometer (Thermo Fisher Scientific) as previously specified11. Analysis of the mass spectrometric RAW data files was performed using the MaxQuant software (version 1.6.1.0) using default settings. MS/MS ion searches were executed against modified cRAP database (based on http://www.thegpm.org/crap, 111 protein sequences) containing protein contaminants like keratin, trypsin etc., and UniProtKB protein database for Mus musculus (ftp://ftp.uniprot.org/pub/databases/uniprot/current_release/knowledgebase/reference_proteomes/Eukaryota/UP000000589_10090.fasta.gz; version from 20.6.2018, number of protein sequences: 22,297). Other conditions were the same as previously described[11]. Protein intensities reported in proteinGroups.txt file and evidence intensities reported in evidence.txt file (output of MaxQuant program) were further processed using the software container environment (https://github.com/OmicsWorkflows), version 3.5.3c. Processing workflow is available upon request. Protein and phosphopeptide candidates were selected based on the following criteria; Differential phospho-peptide candidates (exhibiting ≥1.5 fold differential abundance; note the cut-off was applied to acknowledge the potential sensitivity threshold limitations involved using such scare starting material) were selected based on the criteria described previously11.

Embryo manipulation by microinjections.

Single (for immuno-fluorescence confocal microscopy) or double (for qRT-PCR) blastomere microinjections of 2-cell (E1.5) stage embryos were performed using the FemtoJet 4i (Eppendorf, Hamburg, Germany; Cat. No. 5252000013) micro-injector, mechanical micro-manipulators (Leica, Wetzlar, Germany; Cat. No. ST0036714) and CellTram Vario (Eppendorf; Cat. No. 5176000033) pneumatic handler, under a negative capacitance enabled current controlled by an Electro 705 Electrometer (WPI, Sarasota, Florida, USA; Cat. No. SYS-705) and on the stage of an Olympus IX71 inverted fluorescence microscope. Embryos were pneumatically handled and immobilised for microinjection using a borosilicate glass capillary holder (without filament - Harvard Apparatus, Holliston, Massachusetts, USA; Cat. No. 30-0017). Micro-injectors were connected to needles prepared from filamented borosilicate glass capillaries (Harvard Apparatus; Cat. No. 30-0038) using a Narishige PC-10 capillary glass needle puller (Narishige Scientific Instrument Lab., Tokyo, Japan). siRNAs were co-microinjected at 10µM concentrations, with 50ng/µl H2b-RFP in vitro transcribed (mMESSAGE mMACHINE T3 IVT kit, Thermo Fisher Scientific; Cat. No. AM1348) and poly-A tailed (Poly(A) Tailing kit, ThermoFisher Scientific; Cat. No. AM1350) mRNA, in pre-warmed drops of M2 media overlaid with mineral oil, on the surface of concaved microscope slides. The non-targeting control siRNA (NTC) used was from Qiagen GeneGlobe (Qiagen, Hilden, Germany; Cat. No. SI03650318) and the Ddx21 siRNA used was from Thermo Fisher Scientific Silencer Select (Thermo Fisher Scientific; Cat. No. 4390771 & assay ID: s80158).

Immunofluorescence staining, confocal microscopy and image acquisition.

To remove the zona pellucida, preimplantation embryos at the appropriate developmental stage were quickly washed and pipetted in pre-warmed drops of acidic Tyrode's Solution (Sigma-Aldrich; Cat. No. T1788) until zona pellucidae were visually undetectable and then immediately washed through pre-warmed drops of M2 media. Embryos were fixed, in the dark, with 4% paraformaldehyde (Santa Cruz Biotechnology, Inc., Dallas, Texas, USA; Cat. No. sc-281692) for 20 minutes at room temperature. Permeabilisation was performed by transferring embryos to a 0.5% solution of Triton X-100 (Sigma-Aldrich; Cat. No. T8787), in phosphate buffered saline (PBS), for 20 minutes at room temperature. All washes post-fixation, permeabilisation and antibody staining were performed in PBS with 0.05% TWEEN 20 (Sigma-Aldrich; Cat. No. P9416) (PBST) by transferring embryos between two drops or wells (of 96-well micro-titre plates) of PBST, for 20 minutes at room temperature. Blocking and antibody staining was performed in 3% bovine serum albumin (BSA; Sigma-Aldrich; Cat. No. A7906) in PBST. Blocking incubations of 30 minutes at 4˚C were performed before both primary and secondary antibody incubation; primary antibody incubation (in blocking buffer) was performed overnight (~16 hours) at 4˚C and secondary antibody incubation carried out in the dark at room temperature for 70 minutes. Stained embryos were mounted in DAPI containing mounting medium (VECTASHIELD; Vector Laboratories, Inc., Burlingame, California, USA; Cat. No. H-1200), placed under cover slips on glass-bottomed 35mm culture plates and incubated at 4˚C for 30 minutes in the dark, prior to

confocal imaging. Details of the primary and secondary antibody combinations used can be found in supplementary table S2. Complete embryo confocal z-series images were acquired using a FV10i Confocal Laser Scanning Microscope and FV10i-SW image acquisition software (Olympus, Tokyo, Japan). Images were analysed using FV10-ASW 4.2 Viewer (Olympus) and Imaris X64 Microscopy Image Analysis Software (version 6.2.1; Bitplane AG - Oxford Instruments plc, Abingdon, United Kingdom). Cells were counted both manually and semi-automatically using Imaris X64 encoded functions.

Cell number quantification, statistics and graphical representation.

Total embryo cell number counts (plus outer and inner cell populations) from confocal acquired z-series micrographs (based on DAPI nuclei staining) were further subcategorised as inner or outer based on absence or presence of CDX2 expression respectively (Fig. 3). EPI or PrE cells were quantified based on detectable and exclusive expression of NANOG and GATA4 protein expression, respectively (Fig. 4). Cells not located within blastocyst ICMs that also did not stain for either GATA4 and/or NANOG, were designated as outer/TE cells. Initial recording and data accumulation was carried out using Microsoft Excel and further statistical analysis and graphical representations were performed with GraphPad Prism 8. Based on the normality and lognormality comparisons, appropriate statistical tests were used for the compared datasets (summarised in supplementary table S3). Unless otherwise stated within individual graphs as a specific p-value (if statistically insignificant), the stated significance intervals were as follows: p-value < 0.0001 (****), 0.0001 to 0.001 (***), 0.001 to 0.01 (**) and 0.01 to 0.05 (*). All graphs represent dot plots of the total sample size, with associated means and standard deviation error bars provided.

Fluorescence intensity quantification and statistical analysis.

Levels of DDX21 (Fig. 2e, 3c-e and supplementary Fig. S2a and S3a-c) and NUCLEOSTEMIN (GNL3) protein (Fig. 2f and supplementary Fig. S2b) were quantified, using Fiji (ImageJ)[47], as fluorescence intensity per cell nucleus and differentiated into inner and outer cells based on absence or presence of CDX2 immuno-fluorescence, respectively. The measurements settings for all of the above were as follows: Analyze>Set Measurements; and the following options were chosen: Area, Mean grey value and Integrated density. Using the “Polygon selections” tool, individual cell nuclei were demarcated and the aforementioned measurements recorded. The selected area was then moved so as to encompass an area excluding that of the embryo or cell nucleus, respectively, and background measurements were recorded. This process was continued for all the embryos analysed, under both control and p38-MAPKi conditions and the results were transferred to a spreadsheet for further calculations. The Corrected Total Cell Fluorescence (CTCF), in arbitrary units, for each embryo was measured as such: CTCF = Integrated Density – (Area of selected cell X Mean fluorescence of background readings)[48,49] – supplementary tables

S4 & 5. The calculated CTCF are plotted as scatters, with mean and standard deviations marked. The CTCF differences were statistically tested using appropriate statistical tests (supplementary table S3) based on normality and lognormality comparisons and the results, unless otherwise stated within individual graphs as a specific p-value (if statistically insignificant), are stated as following significance intervals: p-value < 0.0001 (****), 0.0001 to 0.001 (***), 0.001 to 0.01 (**) and 0.01 to 0.05 (*).

Blastocyst size and volume calculations.

Equatorial outer circumference and total volume measurements for the blastocyst as a whole were carried out by measuring the embryo outer circumference of the centrally located widest Z-stack using Fiji (ImageJ)[47]. The measurements were set as follows: Analyze>Set Measurements; and the "Perimeter" option was selected; using the "Polygon selections" tool, the outer circumference was traced and measured. The radius of the measured circumference was deduced and that value was used to calculate an approximate volume for all the embryos analysed under both control (NTC) and *Ddx21* siRNA injected conditions. The calculated volume in picoliters (pL) (tabulated in supplementary table S6 is plotted as a scatter, with mean and standard deviations marked. The differences were statistically tested using Mann-Whitney test and the results, unless otherwise stated within individual graphs as a specific p-value (if statistically insignificant), are stated at the following significance intervals: p-value < 0.0001 (****), 0.0001 to 0.001 (***), 0.001 to 0.01 (**) and 0.01 to 0.05 (*).

Quantitative real-time PCR (qRT-PCR).

20 embryos per condition (control (NTC) and *Ddx21* siRNA injected) from global microinjection experiments, were collected at E4.5 and immediately processed for RNA extraction and isolation using the ARCTURUS PicoPure RNA Isolation Kit (Thermo Fisher Scientific; Cat. No. KIT0204), following the manufacturer's protocol. The entire eluted volume of total RNA was immediately DNase treated with TURBO DNase ((Thermo Fisher Scientific; Cat. No. AM2238) according to the manufacturer provided protocol. The whole sample was then subject to cDNA synthesis using SuperScript III Reverse Transcriptase (Thermo Fisher Scientific; Cat. No. 18080044), as directed by the manufacturer and employing oligo d(T)16 (Thermo Fisher Scientific; Cat. No. N8080128), dNTP Mix (Thermo Fisher Scientific; Cat. No. R0192) and RNase Inhibitor (Thermo Fisher Scientific; Cat. No. N8080119). The synthesized cDNA was diluted as required with nuclease free water and 1µl was used in 10µl individual final SYBR-green based qRT-PCR reaction volumes (PCR Biosystems Ltd., London, United Kingdom; Cat. No. PB20.11) with oligonucleotide primers at a final concentration of 300nM each. A Bio-Rad CFX96 Touch Real-Time PCR Detection System apparatus, employing standard settings, was used for data accumulation and initial analysis was performed with the accompanying Bio-Rad CFX Manager software. Triplicate measurements per gene were assayed from one experiment that were each technically replicated. The sequence of

oligonucleotide primers (5’ to 3’) used were: i) Tbp - GAAGAACAATCCAGACTAGCAGCA (sense) and CCTTATAGGGAACTTCACATCACAG (anti-sense) and ii) - Ddx21: TTCCTTCTGCAACGGAAATAA (sense) and GAGGCACAGAATCCAAGAGC (anti-sense). The average transcript levels of the Ddx21 gene were derived after internal normalisation against Tbp mRNA levels. Data was acquired and initially analysed with CFX Manager, then processed in Microsoft Excel (biological and technical replicate averaging) and GraphPad Prism 9 (graphical output).

Figure legends:

1. Figure 1: DDX21 protein expression and localisation in developing preimplantation mouse embryos.

a) From left to right, Z-projection confocal micrographs of 2-cell, 4-cell, 8-cell, 16-cell, E3.5 and E4.5 embryos stained for the nucleus (DAPI), DDX21 (also displayed as an inverted grayscale image) and a merge of the two (DAPI pseudo-coloured blue, DDX21 in grayscale).

b) to e) Single z-section confocal micrograph of an 8-cell stage embryo immuno-stained for DDX21 with magnified inlay showing (b) nucleoplasmic/nuclear membrane localisation in interphase cells and (c) condensed chromatin localisation in a mitotic cell. d) Single z-section confocal micrograph of a cavitated blastocyst-stage embryo immuno-stained for DDX21 with magnified image showing nucleolar localisation in interphase cells and (e) excluded localisation from condensed chromatin in a mitotic cell. DAPI and DDX2 signal is pseudo-coloured cyan and yellow in the merged images (panels b-e) and scale bar (panels a-e) = 20µm.

2. Figure 2: Effect of p38-MAPK inhibition on DDX21 and NUCLEOSTEMIN (GNL3) protein expression and localisation during blastocyst maturation.

a) Scheme illustrating experimental protocol of p38-MAPK inhibition (p38-MAPKi) during blastocyst maturation (E3.5-4.5; previously reported by us to be a period during which p38-MAPK signalling is required for PrE specification and blastocyst maturation11–13).

b) d) Confocal microscopy z-projections of (b) control (DMSO treated; n=7) and (c, d) p38-MAPKi (SB220025 treated; n=5) embryos immuno-stained for DDX21 and NUCLEOSTEMIN (GNL3) (both displayed as inverted grayscale images). In DAPI (blue) merged images, DDX21 and NUCLEOSTEMIN signal is pseudo-coloured yellow and red, respectively; in DDX21 and NUCLEOSTEMIN merges, respective cyan and red pseudo-colour pallets are used.

b') Single confocal z-sections, with magnified inlays, of DAPI, DDX21 & NUCLEOSTEMIN immuno-stained nuclei of control (DMSO treated) blastocysts. Green dotted enclosure demarcates nucleolar localisation of DDX21 and the region is superimposed on DAPI and NUCELOSTEMIN images highlighting co-localisation.

c') & d') Magnified single confocal z-sections, with magnified inlays of DDX21 immuno-stained nuclei (co-stained with DAPI) of p38-MAPKi (SB220025 treated) blastocysts. In merged images, DAPI and DDX21 signals are pseudo-coloured blue and yellow, respectively. Scale bar (panels b-d) = 20µm.

e) & f) Scatter plot quantifications of per cell nuclei Corrected Total Cell Fluorescence (CTCF) of e) DDX21 and f) NUCLEOSTEMIN (GNL3) immuno-staining in control (DMSO treated) and p38-MAPKi (SB220025 treated) embryos, as expressed for all cells, outer cells and inner cells. DDX21: DMSO from n=16 embryos (outer cells=271, inner cells=122) & SB220025 from n=15 embryos (outer cells=190, inner cells=67) and NUCLEOSTEMIN: DMSO from n=7 embryos (outer cells=205, inner cells=97) & SB220025 from n=5 embryos (outer cells=100, inner cells=40). Collated individual nuclei CTCF quantifications for (e) and (f) are provided in supplementary table S4. (Alternative comparative representations of these data are provided in supplementary Fig. S2)

3. Figure 3: Clonal knockdown of *Ddx21* and effect on late-blastocyst morphology and cell numbers.

a) Experimental design to determine the efficiency of siRNA mediated *Ddx21* gene mRNA knockdown in microinjected embryos cultured to the equivalent late blastocyst (E4.5) stage (right panel) and to assay the contribution of marked *Ddx21* knockdown clones to late blastocyst cell lineages (left panel)

b) qRT-PCR derived relative *Ddx21* transcript levels (normalised to *Tbp* mRNA levels) between embryos injected with non-targeting control (NTC) siRNA and siRNA specific for *Ddx21* mRNA at E4.5.

c)-e) Scatter plot quantifications of per cell CTCF values for DDX21 expression in control (NTC siRNA injected n=15 embryos; non-injected cells outer n=151 & inner n=108, injected cells outer n=153 & inner n=112) and *Ddx21* downregulated (*Ddx21* siRNA injected n=26; non-injected cells outer n=225 & inner n=125, injected cells outer n=157 & inner n=59) embryos, comparing c) all inner and outer cells, between NTC and *Ddx21* siRNA injected embryos, d) only non-injected cells between inner and outer cells for both sets of embryos, and e) only injected cells between inner and outer cells for both sets of embryos (Collated individual nuclei CTCF quantifications for (c), (d) and (e) are provided in supplementary table S5).

f) & g) Confocal micrograph z-projections of representative late (E4.5) stage blastocysts initially microinjected (in one blastomere at the 2-cell stage) with (f) NTC siRNA (n=15) and (g) *Ddx21* siRNA (n=26), plus recombinant H2b-RFP fluorescent reporter mRNA (identifying the clonal progeny of the injected cell). Individual DAPI (grayscale pan-nuclear stain; total number of cells), DDX21 (grayscale) and CDX2 (grayscale; TE cells) channel micrographs, plus merged DDX21 (cyan), CDX2 (magenta) and H2B- RFP (red; microinjected clone) images are shown.

g') & g'') Magnified single z-section confocal micrograph of clonal *Ddx21* downregulated embryo with DDX21 immuno-stained nuclei representative for both autonomous and non-autonomous effects (and DAPI counterstain). In merged image H2B-RFP and DDX21 signal is pseudo-coloured red and cyan, respectively. Red arrowheads mark progeny of *Ddx21* siRNA microinjected cells (discernible by H2B-RFP fluorescence – detailing cell autonomous DDX21 protein knockdown) and cyan arrowhead marks non-microinjected cells (detailing in g') continued but reduced DDX21 expression, or g'') non-autonomous DDX21 protein knockdown). Scale bar (panels f-g'') = 20µm.

h) & i) Scatter plot quantification of cell numbers in (h) NTC siRNA and (i) *Ddx21* siRNA microinjected embryos, categorised into total, inner and outer cell populations, based on combined CDX2 expression and DAPI fluorescence. Collated individual embryo cell number quantifications are provided in supplementary table S7. (Alternative comparative representations of these data are provided in supplementary Fig. S3)

j) Quantification of blastocyst volume (pL). Collated individual embryo volume quantifications are provided in supplementary table S6.

4. Figure 4: Effect of *Ddx21* knockdown on Epiblast (EPI) and Primitive Endoderm (PrE) lineage specification at E4.5.

a) & b) Confocal microscopy z-series projections of late blastocyst (E4.5) stage embryos derived from clonal microinjections (one blastomere at the 2-cell stage) of a) control NTC siRNA (n=9) and b) *Ddx21* siRNA (n=15) embryos immuno-stained for EPI (NANOG) and PrE (GATA4) lineage markers; note H2B-RFP distinguished microinjected and non-microinjected cell clones (experimental design in Fig. 3a). In merged images, NANOG, GATA4 and H2B-RFP signals are pseudo-coloured cyan, yellow and red respectively. Scale bar = 20µm.

c) Scatter plot quantification of (i) EPI cell numbers (only expressing NANOG), (ii) PrE cell numbers (only expressing GATA4) and (iii) the PrE to total ICM ratio, of clonal NTC siRNA and *Ddx21* siRNA microinjected injected embryos, as observed in either the microinjected or non-injected clones and both clones combined. Collated individual embryo cell number quantifications are provided in supplementary table S8. (Alternative comparative representations of these data are provided in supplementary Fig. S4)

Supplementary figure legends:

1. Figure S1: Gene expression profile of *Ddx21*

Gene expression profile of *Ddx21* mRNA in oocyte, preimplantation embryos and early embryonic cell lineages. Data collected from (a) Zhang, B., Zheng, H., Huang, B. et al. Allelic reprogramming

of the histone modification H3K4me3 in early mammalian development. Nature 537, 553–557 (2016) and (b) Wang, C., Liu, X., Gao, Y. et al. Reprogramming of H3K9me3-dependent heterochromatin during mammalian embryo development. Nat Cell Biol 20, 620–631 (2018).

2. Figure S2: Supplementary to Figure 2. Effect of p38-MAPK inhibition on DDX21 and NUCLEOSTEMIN (GNL3) protein expression.

Comparing per nucleus corrected fluorescence (CTCF) of (a) DDX21 and (b) NUCLEOSTEMIN (GNL3) between inner and outer cells (based on CDX2 expression) at E4.5 after 24 hours (from E3.5) of treatment in both control (DMSO) and p38-MAPKi (SB220025) conditions.

3. Figure S3: Supplementary to Figure 3. Clonal knockdown of *Ddx21* and effect on late-blastocyst morphology and cell numbers.

Scatter plot quantification of per cell CTCF of DDX21 expression in control (NTC *siRNA* injected n=15 embryos; non-injected cells outer n=151 & inner n=108, injected cells outer n=153 & inner n=112) and *Ddx21* downregulated (*Ddx21* siRNA injected n=26; non-injected cells outer n=225 & inner n=125, injected cells outer n=157 & inner n=59) embryos,

a) Combined for cells from embryos injected with NTC and *Ddx21* siRNA

b) Only outer cells, comparing injected and non-injected cell clones between NTC and *Ddx21* siRNA.

c) Only inner cells, comparing injected and non-injected cell clones s between NTC and *Ddx21* siRNA.

d) Scatter plot quantification of cell numbers comparing NTC siRNA and *Ddx21* siRNA microinjected embryos, categorised between microinjected, non-microinjected clones and combined cell number and further divided between (i) total, (ii) outer and (iii) inner cell populations.

4. Figure S4: Supplementary to Figure 4. Effect of *Ddx21* knockdown on Epiblast (EPI) and Primitive Endoderm (PrE) lineage specification at E4.5.

Scatter plot quantification of (i) total cell numbers (DAPI nuclear stain), (ii) outer cell numbers, (iii) inner cell numbers, (iv) ratio of EPI to ICM, (v) number of NANOG-GATA4 co-negative inner cells and (vi) ratio of NANOG-GATA4 co-negative inner cells to ICM of clonal NTC siRNA and *Ddx21* siRNA microinjected injected embryos, as observed in either the microinjected or non-injected clones and both clones combined.

Supplementary table legends:

1. Table S1: Phosphoproteomic mass spectrometry result regarding detection of DDX21 in DMSO (control) vs. p38-MAPKi (SB220025) conditions.

2. Table S2: List of antibodies used.

3. Table S3: List of statistical tests used for respective data analysis.

4. Table S4: Collated individual nuclei CTCF quantifications for DDX21 and NUCLEOSTEMIN (GNL3) in DMSO (control) vs. p38-MAPKi (SB220025) conditions. (Supplementary to Fig. 2e, f & S2a, b). Available online along with the preprint at bioRxiv.

5. Table S5: Collated individual nuclei CTCF quantifications for DDX21 in control (NTC siRNA injected) and *Ddx21* downregulated embryos (*Ddx21* siRNA). (Supplementary to Fig. 3c-e & S3a-c). Available online along with the preprint at bioRxiv.

6. Table S6: Collated individual embryo volume (in picoliter (pL)). (Supplementary to Fig. 3j)

7. Table S7: Collated individual embryo cell number quantifications in control (NTC siRNA injected) and *Ddx21* downregulated embryos (*Ddx21* siRNA). Cells are divided into inner and outer based on absence or presence of CDX2 expression respectively and non-injected or injected based on absence or presence of RFP respectively (Supplementary to Fig. 3f-i & S3d).

8. Table S8: Collated individual embryo cell number quantifications in control (NTC siRNA injected) and *Ddx21* downregulated embryos (*Ddx21* siRNA). Cells are divided based on physical location (inner and outer) and on NANOG and GATA4 expression. Non-injected or injected demarcations are based on absence or presence of RFP respectively (Supplementary to Fig. 4 & S4). Available online along with the preprint at bioRxiv.

References:

1. Chazaud, C. & Yamanaka, Y. Lineage specification in the mouse preimplantation embryo. Development 143, 1063–1074 (2016).

2. Płusa, B. & Piliszek, A. Common principles of early mammalian embryo self-organisation. Development 147, dev183079 (2020).

3. Shahbazi, M. N. Mechanisms of human embryo development: from cell fate to tissue shape and back. Development 147, dev190629 (2020).

4. Alberio, R. Regulation of Cell Fate Decisions in Early Mammalian Embryos. Annu. Rev. Anim. Biosci. 8, 377–393 (2020).

5. Ryan, A. Q., Chan, C. J., Graner, F. & Hiiragi, T. Lumen Expansion Facilitates Epiblast-Primitive Endoderm Fate Specification during Mouse Blastocyst Formation. Dev. Cell 51, 684-697.e4 (2019).

6. Maître, J.-L., Niwayama, R., Turlier, H., Nédélec, F. & Hiiragi, T. Pulsatile cell-autonomous contractility drives compaction in the mouse embryo. Nat. Cell Biol. 17, 849–55 (2015).

7. Chan, C. J. et al. Hydraulic control of mammalian embryo size and cell fate. Nature 571, 112–116 (2019).

8. Corsini, N. S. et al. Coordinated Control of mRNA and rRNA Processing Controls Embryonic Stem Cell Pluripotency and Differentiation. Cell Stem Cell 22, 543-558.e12 (2018).

9. Bulut-Karslioglu, A. et al. Inhibition of mTOR induces a paused pluripotent state. Nature 540, 119–123 (2016).

10. Bulut-Karslioglu, A. et al. The Transcriptionally Permissive Chromatin State of Embryonic Stem Cells Is Acutely Tuned to Translational Output. Cell Stem Cell 22, 369-383.e8 (2018).

11. Bora, P. et al. p38-MAPK mediated rRNA processing and translation regulation enables PrE differentiation during mouse blastocyst maturation. bioRxiv 2020.11.30.403931 (2020) doi:10.1101/2020.11.30.403931.

12. Thamodaran, V. & Bruce, A. W. p38 (Mapk14/11) occupies a regulatory node governing entry into primitive endoderm differentiation during preimplantation mouse embryo development. Open Biol. 6, 15034 (2016).

13. Bora, P., Thamodaran, V., Šušor, A. & Bruce, A. W. p38-Mitogen Activated Kinases Mediate a Developmental Regulatory Response to Amino Acid Depletion and Associated Oxidative Stress in Mouse Blastocyst Embryos. Front. cell Dev. Biol. 7, 276 (2019).

14. Bessonnard, S., Vandormael-Pournin, S., Coqueran, S., Cohen-Tannoudji, M. & Artus, J. PDGF Signaling in Primitive Endoderm Cell Survival Is Mediated by PI3K-mTOR Through p53-Independent Mechanism. Stem Cells 37, 888–898 (2019).

15. Natale, D. R., Paliga, A. J. M., Beier, F., D'Souza, S. J. A. & Watson, A. J. p38 MAPK signaling during murine preimplantation development. Dev. Biol. 268, 76–88 (2004).

16. Bell, C. E. & Watson, A. J. p38 MAPK Regulates Cavitation and Tight Junction Function in the Mouse Blastocyst. PLoS One 8, e59528 (2013).

17. Paliga, A. J. M., Natale, D. R. & Watson, A. J. p38 mitogen-activated protein kinase (MAPK) first regulates filamentous actin at the 8-16-cell stage during preimplantation development. Biol. cell 97, 629–40 (2005).

18. Mori, S. et al. Myb-Binding Protein 1A (MYBBP1A) Is Essential for Early Embryonic Development, Controls Cell Cycle and Mitosis, and Acts as a Tumor Suppressor. PLoS One 7, e39723 (2012).

19. Hochstatter, J. et al. Myb-binding Protein 1a (Mybbp1a) Regulates Levels and Processing of Pre-ribosomal RNA. J. Biol. Chem. 287, 24365–24377 (2012).

20. Calo, E. et al. RNA helicase DDX21 coordinates transcription and ribosomal RNA processing. Nature 518, 249–253 (2015).

21. Yang, H. et al. Down-regulation of RNA helicase II/Gu results in the depletion of 18 and 28 S rRNAs in Xenopus oocyte. J. Biol. Chem. 278, 38847–59 (2003).

22. Henning, D., So, R. B., Jin, R., Lau, L. F. & Valdez, B. C. Silencing of RNA helicase II/Gualpha inhibits mammalian ribosomal RNA production. J. Biol. Chem. 278, 52307–14 (2003).

23. Romanova, L. et al. Critical Role of Nucleostemin in Pre-rRNA Processing. J. Biol. Chem. 284, 4968–4977 (2009).

24. Calo, E. et al. Tissue-selective effects of nucleolar stress and rDNA damage in developmental disorders. Nature 554, 112–117 (2018).

25. Santoriello, C. et al. RNA helicase DDX21 mediates nucleotide stress responses in neural crest and melanoma cells. Nat. Cell Biol. 22, 372–379 (2020).

26. Xing, Y.-H. et al. SLERT Regulates DDX21 Rings Associated with Pol I Transcription. Cell 169, 664-678.e16 (2017).

27. Zhang, Y., Baysac, K. C., Yee, L.-F., Saporita, A. J. & Weber, J. D. Elevated DDX21 regulates c-Jun activity and rRNA processing in human breast cancers. Breast Cancer Res. 16, 449 (2014).

28. Song, C., Hotz-Wagenblatt, A., Voit, R. & Grummt, I. SIRT7 and the DEAD-box helicase DDX21 cooperate to resolve genomic R loops and safeguard genome stability. Genes Dev. 31, 1370–1381 (2017).

29. Qu, J. & Bishop, J. M. Nucleostemin maintains self-renewal of embryonic stem cells and promotes reprogramming of somatic cells to pluripotency. J. Cell Biol. 197, 731–45 (2012).

30. Farley-Barnes, K. I., Ogawa, L. M. & Baserga, S. J. Ribosomopathies: Old Concepts, New Controversies. Trends Genet. 35, 754–767 (2019).

31. Mills, E. W. & Green, R. Ribosomopathies: There's strength in numbers. Science 358, (2017).

32. De Wever, V. et al. Isolation of human mitotic protein phosphatase complexes: identification of a complex between protein phosphatase 1 and the RNA helicase Ddx21. PLoS One 7, e39510 (2012).

33. Holder, J., Poser, E. & Barr, F. A. Getting out of mitosis: spatial and temporal control of mitotic exit and cytokinesis by PP1 and PP2A. FEBS Lett. 593, 2908–2924 (2019).

34. Zhang, B. et al. Allelic reprogramming of the histone modification H3K4me3 in early mammalian development. Nature 537, 553–557 (2016).

35. Wang, C. et al. Reprogramming of H3K9me3-dependent heterochromatin during mammalian embryo development. Nat. Cell Biol. 20, 620–631 (2018).

36. Beekman, C. et al. Evolutionarily Conserved Role of Nucleostemin: Controlling Proliferation of Stem/Progenitor Cells during Early Vertebrate Development. Mol. Cell. Biol. 26, 9291–9301 (2006).

37. Zhu, Q., Yasumoto, H. & Tsai, R. Y. L. Nucleostemin delays cellular senescence and negatively regulates TRF1 protein stability. Mol. Cell. Biol. 26, 9279–90 (2006).

38. Strumpf, D. et al. Cdx2 is required for correct cell fate specification and differentiation of trophectoderm in the mouse blastocyst. Development 132, 2093–102 (2005).

39. Canovas, B. & Nebreda, A. R. Diversity and versatility of p38 kinase signalling in health and disease. Nat. Rev. Mol. Cell Biol. 6, (2021).

40. van Sluis, M. & McStay, B. Nucleolar DNA Double-Strand Break Responses Underpinning rDNA Genomic Stability. Trends Genet. 35, 743–753 (2019).

41. Fulka, H. & Aoki, F. Nucleolus Precursor Bodies and Ribosome Biogenesis in Early Mammalian Embryos: Old Theories and New Discoveries. Biol. Reprod. 94, 143 (2016).

42. Courtois, A., Schuh, M., Ellenberg, J. & Hiiragi, T. The transition from meiotic to mitotic spindle assembly is gradual during early mammalian development. J. Cell Biol. 198, 357–70 (2012).

43. Hornbeck, P. V et al. PhosphoSitePlus, 2014: mutations, PTMs and recalibrations. Nucleic Acids Res. 43, D512-20 (2015).

44. Bardwell, L. Mechanisms of MAPK signalling specificity. Biochem. Soc. Trans. 34, 837–41 (2006).

45. Posfai, E. et al. Position- and Hippo signaling-dependent plasticity during lineage segregation in the early mouse embryo. Elife 6, 1–24 (2017).

46. Bessonnard, S. et al. ICM conversion to epiblast by FGF/ERK inhibition is limited in time and requires transcription and protein degradation. Sci. Rep. 7, 12285 (2017).

47. Schindelin, J. et al. Fiji: an open-source platform for biological-image analysis. Nat. Methods 9, 676–82 (2012).

48. McCloy, R. A. et al. Partial inhibition of Cdk1 in G 2 phase overrides the SAC and decouples mitotic events. Cell Cycle 13, 1400–1412 (2014).

49. Potapova, T. A., Sivakumar, S., Flynn, J. N., Li, R. & Gorbsky, G. J. Mitotic progression becomes irreversible in prometaphase and collapses when Wee1 and Cdc25 are inhibited. Mol. Biol. Cell 22, 1191–1206 (2011).

Fig 1 (DDX21 expression)

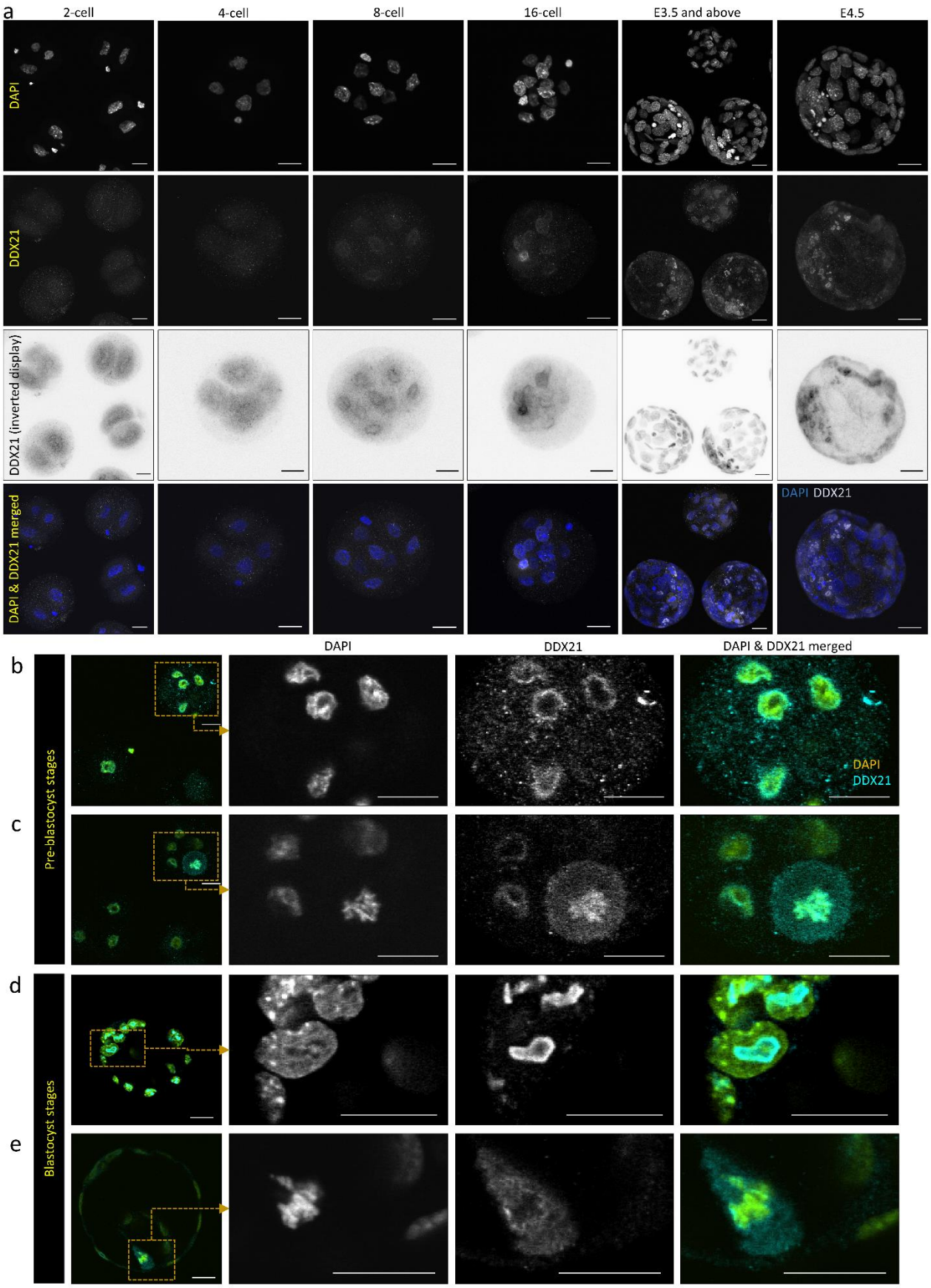

Fig 2 (DMSO vs p38i; Ddx21 and Nucleostemin fluorescence)

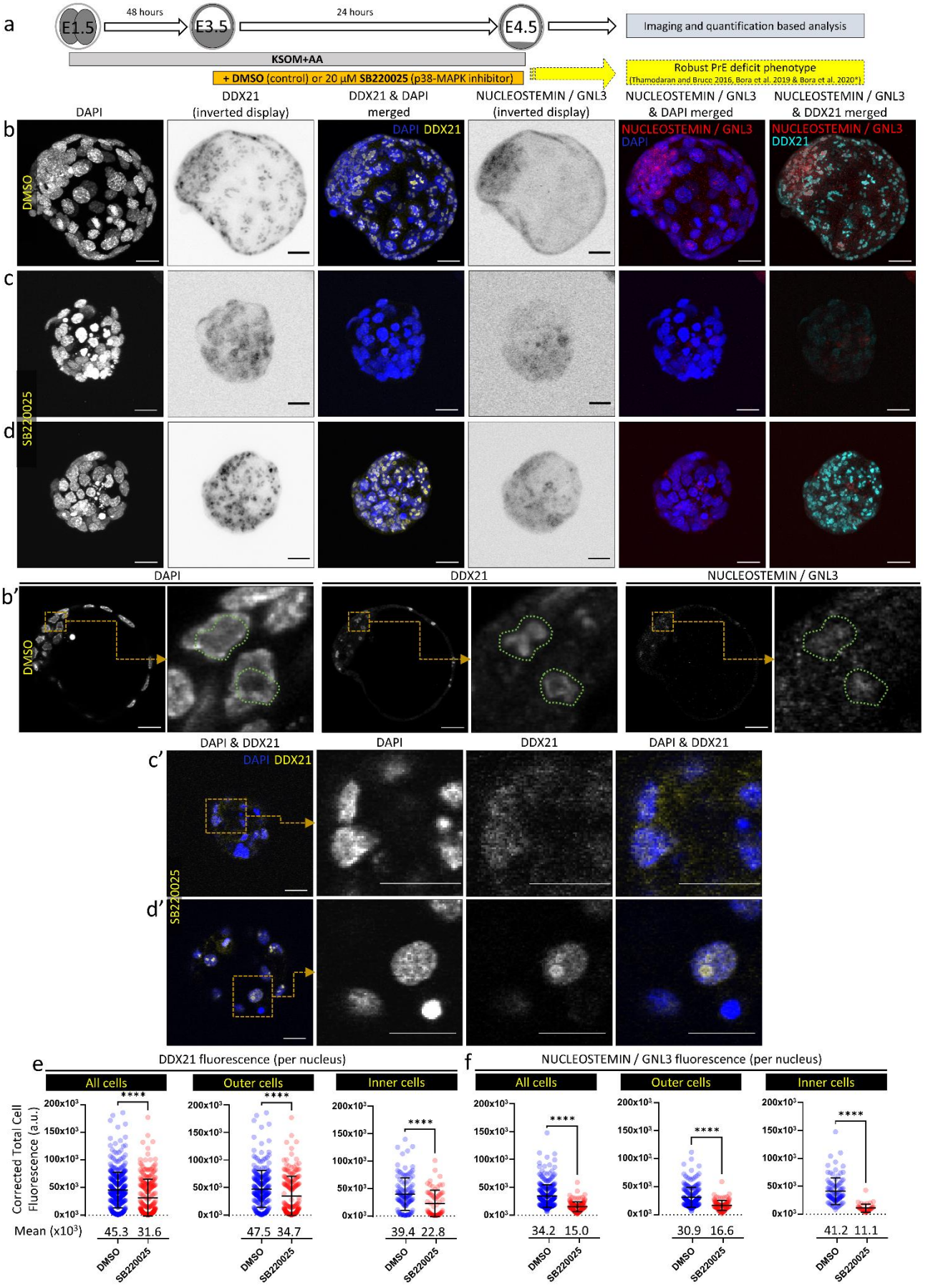

Fig 3 (Ddx21 KD; CTCF, cell numbers and embryo morphology)

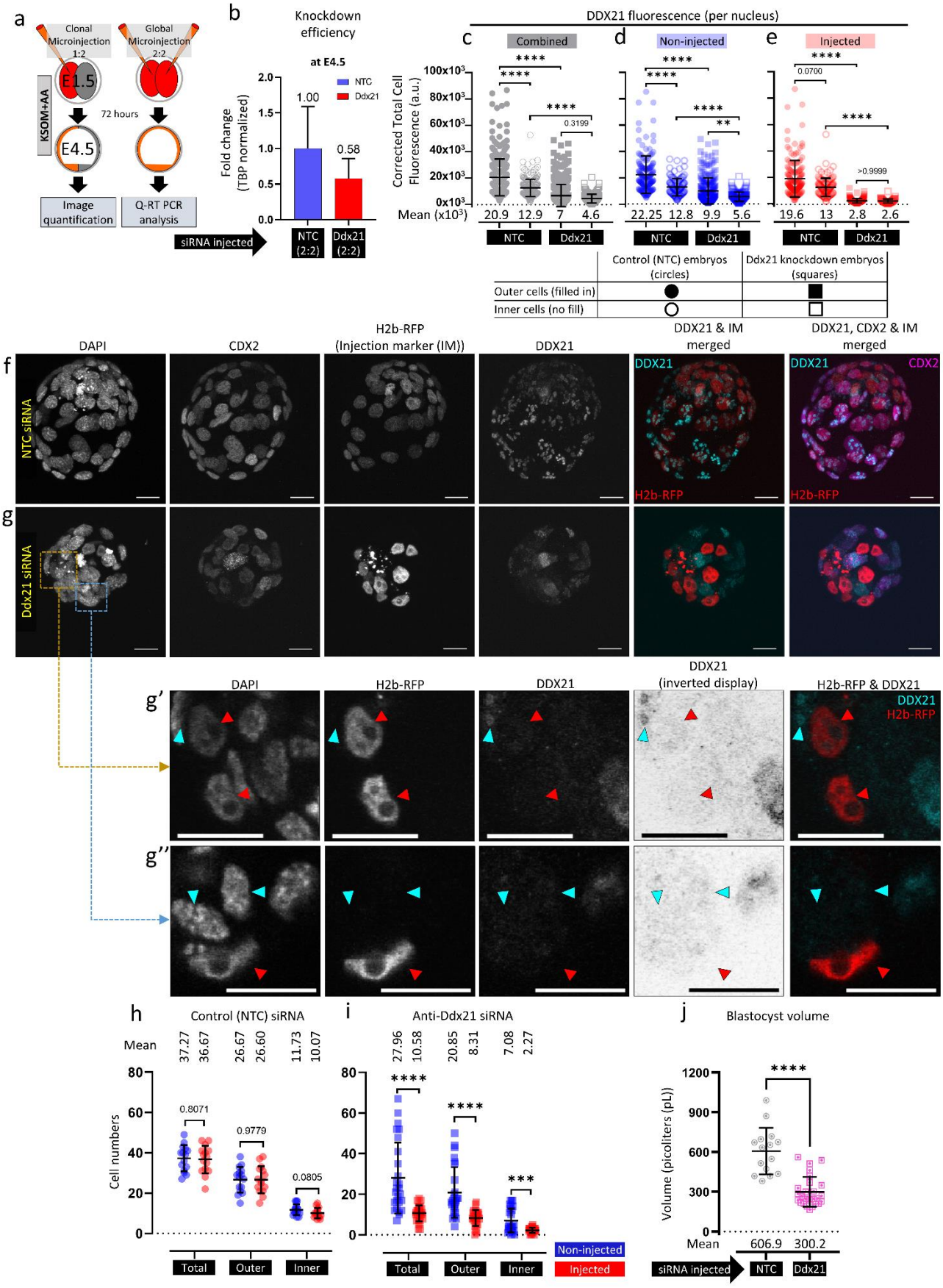

Fig 4 (Ddx21 KD and lineage markers)

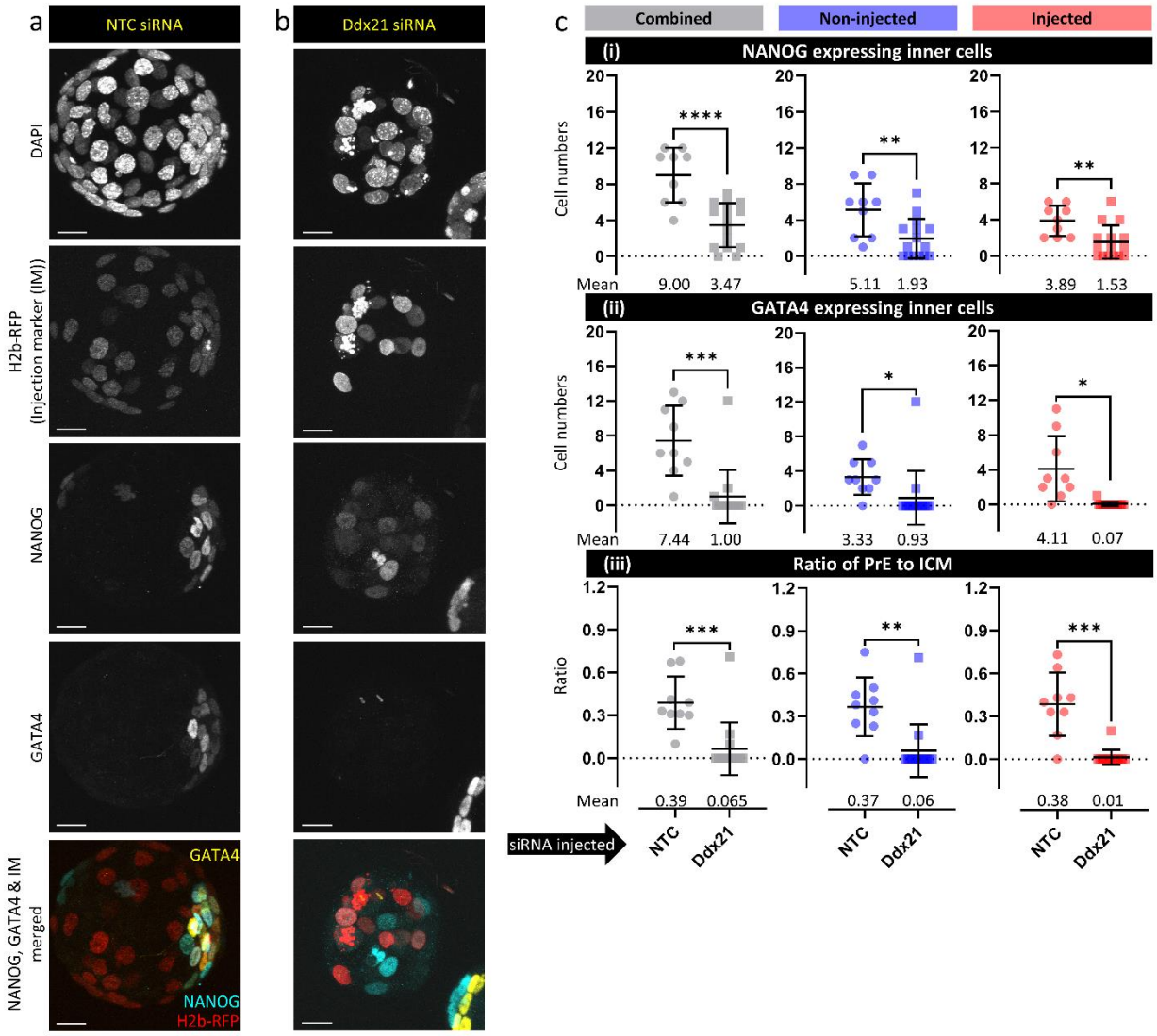

Fig S1

a Gene expression profile of *Ddx21* from *Zhang et al. Nature 537, 553–557 (2016)*

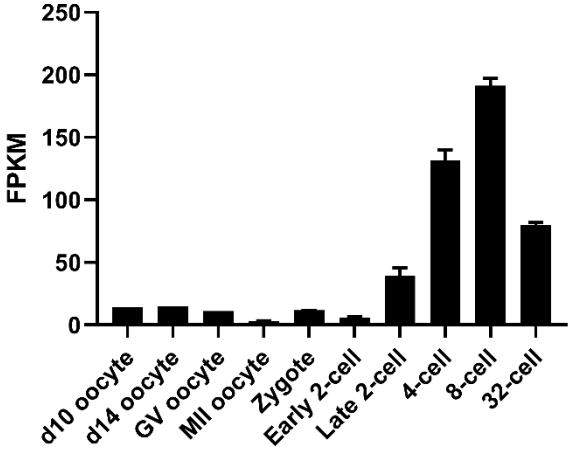

b Gene expression profile of *Ddx21* from *Wang et al. Nat Cell Biol 20, 620–631 (2018)*

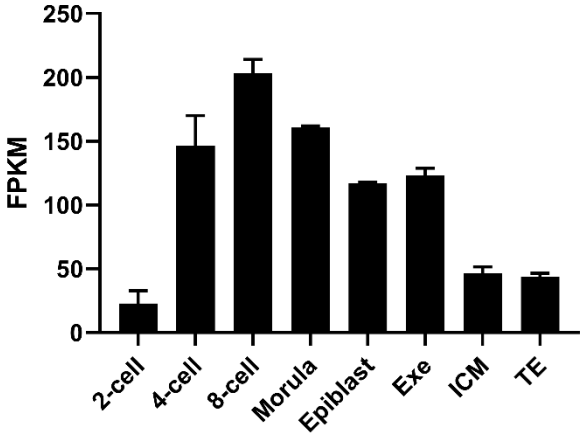

Gene expression profile of *Ddx21* in oocyte, preimplantation embryos and early embryonic cellular lineages. Data collected from *Zhang, B., Zheng, H., Huang, B. et al. Allelic reprogramming of the histone modification H3K4me3 in early mammalian development. Nature 537, 553–557 (2016)* and *Wang, C., Liu, X., Gao, Y. et al. Reprogramming of H3K9me3-dependent heterochromatin during mammalian embryo development. Nat Cell Biol 20, 620–631 (2018)*.

Fig S2

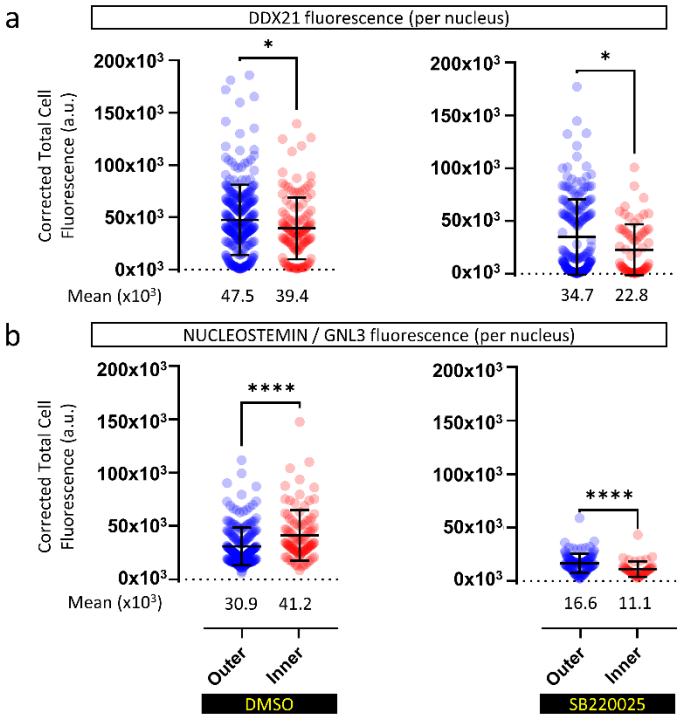

Supplementary to Figure 2. Effect of p38-MAPK inhibition on DDX21 and NUCLEOSTEMIN (GNL3) protein expression.

Comparing per nucleus corrected fluorescence (CTCF) of (a) DDX21 and (b) NUCLEOSTEMIN (GNL3) between inner and outer cells (based on CDX2 expression) at E4.5 after 24 hours (from E3.5) of treatment in both control (DMSO) and p38-MAPKi (SB220025) conditions.

Fig S3

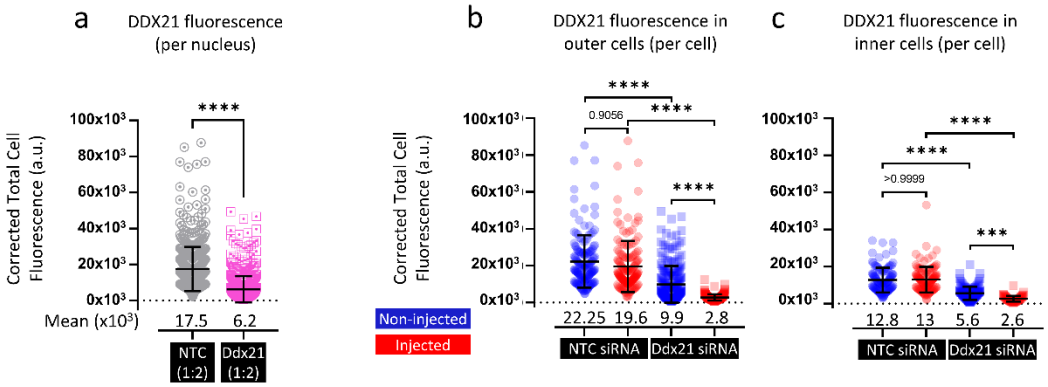

Supplementary to Fig. 3c-e.

Scatter plot quantification of per cell CTCF of DDX21 expression in control (NTC siRNA injected n=15 embryos; non-injected cells outer n=151 & inner n=108, injected cells outer n=153 & inner n=112) and Ddx21 downregulated (Ddx21 siRNA injected n=26; non-injected cells outer n=225 & inner n=125, injected cells outer n=157 & inner n=59) embryos,

a) Combined for cells from embryos injected with NTC and Ddx21 siRNA

b) Only outer cells, comparing injected and non-injected cell clones between NTC and Ddx21 siRNA.

c) Only inner cells, comparing injected and non-injected cell clones s between NTC and Ddx21 siRNA.

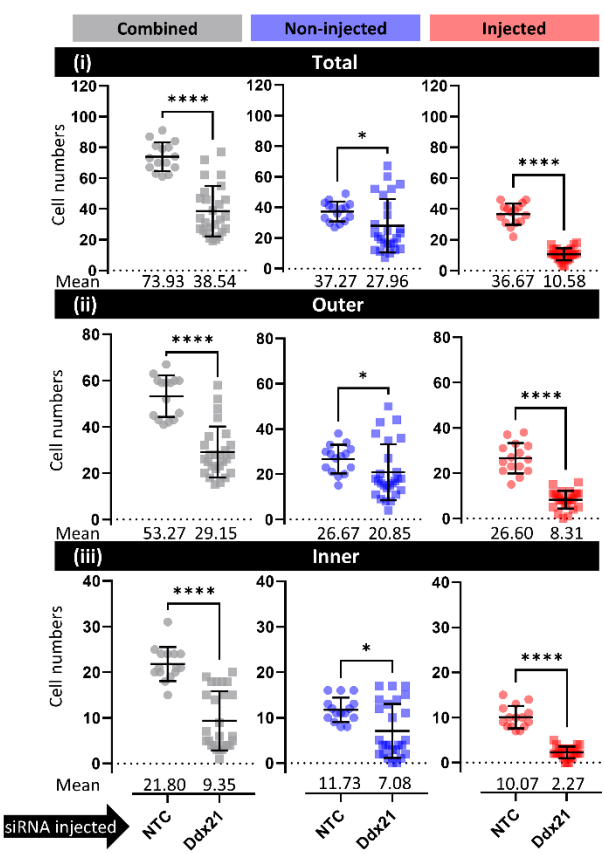

Supplementary to Fig. 3h, i.

d) Scatter plot quantification of cell numbers comparing NTC siRNA and Ddx21 siRNA microinjected embryos, categorised between microinjected, non-microinjected clones and combined cell number and further divided between (i) total, (ii) outer and (iii) inner cell populations.

Fig S4

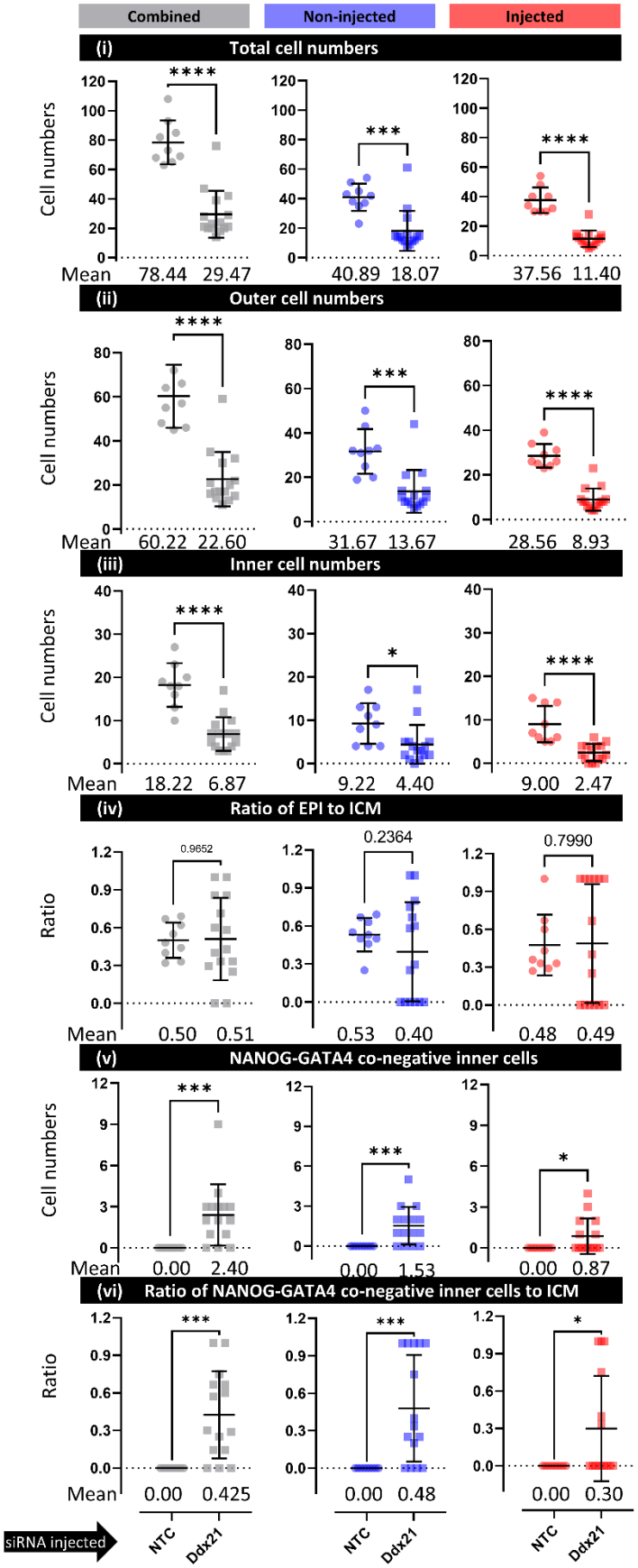

Supplementary to Fig. 4
Scatter plot quantification of (i) total cell numbers (DAPI nuclear stain), (ii) outer cell numbers, (iii) inner cell numbers, (iv) ratio of EPI to ICM, (v) number of NANOG-GATA4 co-negative inner cells and (vi) ratio of NANOG-GATA4 co-negative inner cells to ICM of clonal NTC siRNA and Ddx21 siRNA microinjected injected embryos, as observed in either the microinjected or non-injected clones and both clones combined.

Supplementary table 1 (Mass spec result for DDX21)

protein	code	adj. p-value	non-adj. p-value	logFC 2/-2	change in p38 vs control	FC_peptide	FC_protein	Peptide_sequence	cont_1	cont_2	cont_3	p38_1	p38_2	p38_3
Ddx21	Q9JIK5	no	yes	yes	down	0.14	1.33	EASGDAGEKSPR_Phospho (ST)	17.88	16.66				14.45

Supplementary table 2 (Antibodies used)
Antibodies

Sl. No.	Antibody against	Type	Target	Host / isotype	Manufacturer	Catalogue number	Dilution used
			Immunofluorescence imaging				
1	DDX21	Primary; polyclonal	Conserved	Rabbit / IgG	Novus Biologicals	NB100-1718	1:100 in PBST (3% BSA)
2	NUCLEOSTEMIN	Primary; monoclonal	Mouse, rat and human	Mouse / IgG1, kappa	Santa Cruz Biotechnology, Inc.	sc-398978	1:100 in PBST (3% BSA)
3	CDX2 (CDX2-88)	Primary; monoclonal	Conserved	Mouse / IgG1, kappa	BioGenex	MU392A-5UC	1:200 in PBST (3% BSA)
4	NANOG (eBioMLC-51)	Primary; monoclonal	Mouse	Rat / IgG2a	Thermo Fisher Scientific Inc. (eBioscience™)	14-5761-80	1:200 in PBST (3% BSA)
5	GATA-4 (H-112)	Primary; polyclonal	Mouse, rat and human	Rabbit / IgG	Santa Cruz Biotechnology, Inc.	sc-9053	1:200 in PBST (3% BSA)
6	Donkey anti-Rat IgG (H+L) Highly Cross-Adsorbed Secondary Antibody, Alexa Fluor 488	Secondary; polyclonal	Rat	Donkey / IgG	Thermo Fisher Scientific Inc.	A-21208	1:500 in PBST (3% BSA)
7	Donkey anti-Rabbit IgG (H+L) Highly Cross-Adsorbed Secondary Antibody, Alexa Fluor 555	Secondary; polyclonal	Rabbit	Donkey / IgG	Thermo Fisher Scientific Inc.	A-31572	1:500 in PBST (3% BSA)
8	Donkey Anti-Rabbit IgG H&L (Alexa Fluor® 647)	Secondary; polyclonal	Rabbit	Donkey / IgG	Abcam plc.	ab150075	1:500 in PBST (3% BSA)
9	Donkey anti-Mouse IgG (H+L) Highly Cross-Adsorbed Secondary Antibody, Alexa Fluor 488	Secondary; polyclonal	Mouse	Donkey / IgG	Thermo Fisher Scientific Inc.	A-21202	1:500 in PBST (3% BSA)

Supplementary table 3 (Statistical tests used)

Statistical tests	Unless otherwise stated within individual graphs as a specific P value (if statistically insignificant), the stated significance intervals were depicted as: P value < 0.0001 (****), 0.0001 to 0.001 (***), 0.001 to 0.01 (**) and 0.01 to 0.05 (*); error bars denote calculated standard deviations. Further details are provided within respective methods sections.

Figure				Test used
2	e			Mann-Whitney
	f			Mann-Whitney
3	c			One-way ANOVA (Kruskal-Wallis) and Dunn's test
	d			One-way ANOVA (Kruskal-Wallis) and Dunn's test
	e			One-way ANOVA (Kruskal-Wallis) and Dunn's test
	h			Unaired t-tests (for "Total" and "Outer") & Mann-Whitney (for "Inner")
	i			Mann-Whitney (for "Total" and "Outer") & Welch's t-test (for "Inner")
	j			Mann-Whitney
4	c	i	Combined	Unpaired t-test
			Non-injected	Unpaired t-test
			Injected	Mann-Whitney
		ii	Combined	Unpaired t-test
			Non-injected	Welch's t-test
			Injected	Welch's t-test
		iii	Combined	Unpaired t-test
			Non-injected	Unpaired t-test
			Injected	Welch's t-test

S2	a		DMSO	Unpaired t-test
			SB220025	Mann-Whitney
	b		DMSO	Mann-Whitney
			SB220025	Mann-Whitney
S3	a			Mann-Whitney
	b			One-way ANOVA (Kruskal-Wallis) and Dunn's test
	c			One-way ANOVA (Kruskal-Wallis) and Dunn's test
	d	i	Combined	Mann-Whitney
			Non-injected	Mann-Whitney
			Injected	Welch's t-test
		ii	Combined	Mann-Whitney
			Non-injected	Mann-Whitney
			Injected	Welch's t-test
		iii	Combined	Mann-Whitney
			Non-injected	Mann-Whitney
			Injected	Mann-Whitney
S4		i	Combined	Mann-Whitney
			Non-injected	Mann-Whitney
			Injected	Mann-Whitney
		ii	Combined	Mann-Whitney
			Non-injected	Mann-Whitney
			Injected	Mann-Whitney
		iii	Combined	Mann-Whitney
			Non-injected	Mann-Whitney
			Injected	Mann-Whitney
		iv	Combined	Mann-Whitney
			Non-injected	Welch's t-test
			Injected	Mann-Whitney
		v	Combined	Welch's t-test
			Non-injected	Welch's t-test
			Injected	Welch's t-test
		vi	Combined	Welch's t-test
			Non-injected	Welch's t-test
			Injected	Welch's t-test

Supplementary table 6 (Volume)

Supplementary to Fig. 3j

	Control (NTC) siRNA	*Ddx21* siRNA
N	**Volme of blastocyst embryo (in picoliters)**	**Volme of blastocyst embryo (in picoliters)**
1	675.34	370.47
2	653.86	187.23
3	435.87	347.98
4	872.17	303.50
5	990.20	210.99
6	633.85	269.24
7	672.66	242.03
8	418.48	247.14
9	696.90	165.57
10	381.42	285.26
11	719.08	512.70
12	418.31	250.62
13	472.18	218.74
14	515.55	538.24
15	547.90	266.19
16		419.83
17		236.92
18		207.50
19		209.48
20		328.10
21		560.44
22		226.80
23		247.10
24		190.49
25		300.41
26		462.48
Average	606.92	300.21

Supplementary table 7 (Cell numbers)

Supplementary to Fig. 3f-I & S3d

NTC siRNA (10uM)

#	TOTAL NUMBER OF CELLS											
				OUTER						ICM		
	Embryo Total	Embryo Total Non-Injected	Embryo Total Injected	Outer Cdx2 +ve Non-Injected	Outer Cdx2 +ve Injected	Outer Cdx2 +ve	Total Outer Non-Injected	Total Outer Injected	Total Outer	Total ICM Non-Injected	Total ICM Injected	Total ICM
1	80	39	41	27	32	59	27	32	59	12	9	21
2	81	40	41	31	29	60	31	29	60	9	12	21
3	61	33	28	23	18	41	23	18	41	10	10	20
4	74	42	32	34	25	59	34	25	59	8	7	15
5	87	43	44	30	33	63	30	33	63	13	11	24
6	67	36	31	38	21	59	38	21	59	8	10	18
7	91	45	46	29	38	67	29	38	67	16	8	24
8	62	31	31	21	21	42	21	21	42	10	10	20
9	79	40	39	29	31	60	29	31	60	11	8	19
10	67	29	38	20	23	43	20	23	43	16	15	31
11	84	49	35	33	27	60	33	27	60	16	8	24
12	63	41	22	28	15	43	28	15	43	13	7	20
13	73	27	46	15	37	52	15	37	52	12	9	21
14	70	30	40	19	26	45	19	26	45	11	14	25
15	70	34	36	23	23	46	23	23	46	11	13	24
Average	73.93	37.27	36.67	26.67	26.60	53.27	26.67	26.60	53.27	11.73	10.07	21.80

Ddx21 siRNA (10uM)

#	TOTAL NUMBER OF CELLS											
				OUTER						ICM		
	Embryo Total	Embryo Total Non-Injected	Embryo Total Injected	Outer Cdx2 +ve Non-Injected	Outer Cdx2 +ve Injected	Outer Cdx2 +ve	Total Outer Non-Injected	Total Outer Injected	Total Outer	Total ICM Non-Injected	Total ICM Injected	Total ICM
1	55	52	3	35	2	37	35	2	37	17	1	18
2	34	17	17	15	15	30	15	15	30	2	2	4
3	51	48	3	36	0	36	36	0	36	12	3	15
4	35	23	12	18	8	26	18	8	26	5	4	9
5	20	10	10	8	8	16	8	8	16	1	2	3
6	27	20	7	18	5	23	18	5	23	2	2	4
7	39	25	14	21	11	32	21	11	32	4	3	7
8	21	7	14	4	11	15	4	11	15	3	3	6
9	26	19	7	15	5	20	15	5	20	4	2	6
10	27	16	11	14	9	23	14	9	23	2	2	4
11	72	60	12	43	9	52	43	9	52	17	3	20
12	33	21	12	17	11	28	17	11	28	4	1	5
13	24	13	11	9	11	20	9	11	20	4	0	4
14	77	67	10	50	8	58	50	8	58	17	2	19
15	46	35	11	20	8	28	20	8	28	15	3	18
16	25	12	13	11	11	22	11	11	22	1	2	3
17	30	16	14	13	12	25	13	12	25	3	2	5
18	31	23	8	18	8	26	18	8	26	5	0	5
19	22	12	10	8	10	18	8	10	18	4	0	4
20	47	29	18	16	16	32	16	16	32	13	2	15
21	62	52	10	38	6	44	38	6	44	14	4	18
22	46	41	5	27	1	28	27	1	28	14	4	18
23	43	26	17	16	12	28	16	12	28	10	5	15
24	19	11	8	11	7	18	11	7	18	0	1	1
25	28	17	11	17	8	25	17	8	25	0	3	3
26	62	55	7	44	4	48	44	4	48	11	3	14
Average	38.54	27.96	10.58	20.85	8.31	29.15	20.85	8.31	29.15	7.08	2.27	9.35

Chapter III:

p38-mitogen activated kinases mediate a developmental regulatory response to amino acid depletion and associated oxidative stress in mouse blastocyst embryos.

Pablo Bora, Vasanth Thamodaran, Andrej Susor and Alexander W. Bruce.

Front. Cell Dev. Biol., 2019, **7**, 276. (PubMed ID: 31788473)

frontiers in Cell and Developmental Biology

BRIEF RESEARCH REPORT
published: 08 November 2019
doi: 10.3389/fcell.2019.00276

p38-Mitogen Activated Kinases Mediate a Developmental Regulatory Response to Amino Acid Depletion and Associated Oxidative Stress in Mouse Blastocyst Embryos

Pablo Bora[1], Vasanth Thamodaran[1†], Andrej Šušor[2] and Alexander W. Bruce[1]*

[1] Laboratory of Early Mammalian Developmental Biology, Department of Molecular Biology and Genetics, Faculty of Science, University of South Bohemia, České Budějovice, Czechia, [2] Laboratory of Biochemistry and Molecular Biology of Germ Cells, Institute of Animal Physiology and Genetics CAS, v. v. i., Liběchov, Czechia

OPEN ACCESS

Edited by:
Karin Lykke-Hartmann,
Aarhus University, Denmark

Reviewed by:
Berenika Plusa,
The University of Manchester, United Kingdom
Elizabeth R. Smith,
University of Miami, United States
Mary Familari,
The University of Melbourne, Australia

***Correspondence:**
Alexander W. Bruce
awbruce@prf.jcu.cz

†Present address:
Vasanth Thamodaran,
Centre for Stem Cell Research (a unit of 'inStem', Bengaluru), Christian Medical College Campus, Vellore, India

Specialty section:
This article was submitted to Cell Growth and Division, a section of the journal Frontiers in Cell and Developmental Biology

Received: 08 July 2019
Accepted: 25 October 2019
Published: 08 November 2019

Citation:
Bora P, Thamodaran V, Šušor A and Bruce AW (2019) p38-Mitogen Activated Kinases Mediate a Developmental Regulatory Response to Amino Acid Depletion and Associated Oxidative Stress in Mouse Blastocyst Embryos. Front. Cell Dev. Biol. 7:276. doi: 10.3389/fcell.2019.00276

Maternal starvation coincident with preimplantation development has profound consequences for placental-fetal development, with various identified pathologies persisting/manifest in adulthood; the 'Developmental Origin of Health and Disease' (DOHaD) hypothesis/model. Despite evidence describing DOHaD-related incidence, supporting mechanistic and molecular data relating to preimplantation embryos themselves are comparatively meager. We recently identified the classically recognized stress-related p38-mitogen activated kinases (p38-MAPK) as regulating formation of the extraembryonic primitive endoderm (PrE) lineage within mouse blastocyst inner cell mass (ICM). Thus, we wanted to assay if PrE differentiation is sensitive to amino acid availability, in a manner regulated by p38-MAPK. Although blastocysts appropriately mature, without developmental/morphological or cell fate defects, irrespective of amino acid supplementation status, we found the extent of p38-MAPK inhibition induced phenotypes was more severe in the absence of amino acid supplementation. Specifically, both PrE and epiblast (EPI) ICM progenitor populations remained unspecified and there were fewer cells and smaller blastocyst cavities. Such phenotypes could be ameliorated, to resemble those observed in groups supplemented with amino acids, by addition of the anti-oxidant NAC (*N*-acetyl-cysteine), although PrE differentiation deficits remained. Therefore, p38-MAPK performs a hitherto unrecognized homeostatic early developmental regulatory role (in addition to direct specification of PrE), by buffering blastocyst cell number and ICM cell lineage specification (relating to EPI) in response to amino acid availability, partly by counteracting induced oxidative stress; with clear implications for the DOHaD model.

Keywords: p38-mitogen activated kinases, mouse blastocyst, cell fate, oxidative stress, primitive endoderm, developmental origin of health and disease (DOHaD)

Abbreviations: AA, amino acid; EPI, epiblast; ERK1/2, extra-cellular regulated kinases 1/2; DOHaD, developmental origin of health and disease; ICM, inner cell mass; KSOM, potassium simplex optimization media; NAC, *N*-acetyl-cysteine; p38-MAPK, p38-mitogen activated kinases (specifically p38α&β/MAPK14/11); PrE, primitive endoderm; ROS, reactive oxygen species; TE, trophectoderm.

INTRODUCTION

The formation of the peri-implantation stage mouse blastocyst (by embryonic day 4.5/E4.5) represents the culmination of the preimplantation period in which three distinct cell lineages emerge. Two lineages are differentiating and will ultimately yield supportive extraembryonic tissues; the outer-residing and epithelized trophectoderm (TE) that gives rise to the placenta, and the mono-layered primitive endoderm (PrE), occupying the interface between the fluid filled cavity and underlying ICM, that contributes to the yolk sac. The third lineage, represented by the pluripotent epiblast (EPI), residing deep within the ICM, serves as a progenitor pool for all subsequent tissues of the fetus; extensively reviewed (Frum and Ralston, 2015; Chazaud and Yamanaka, 2016; Rossant, 2016). We have previously reported a role for p38-mitogen activated kinases a/β (herein referred to as p38-MAPK), employing pharmacological inhibition, in regulating primitive endoderm (PrE) differentiation within mouse blastocyst ICM (Thamodaran and Bruce, 2016). p38-MAPK was found to act during the early stages of ICM maturation (the period between E3.5–E4.0), downstream of fibroblast growth factor (FGF) signaling, permitting PrE progenitors to resolve their uncommitted fate [as is characteristic of the majority of nascent ICM cells at E3.5 (Chazaud et al., 2006)] and thus, functionally diverge and segregate from the EPI lineage (Thamodaran and Bruce, 2016). Although, p38-MAPK (and their related paralogs, p38γ/δ) belong to the wider family of serine-threonine and tyrosine kinases, regulating a wide variety of cellular functions (Cargnello and Roux, 2011), they differ from the other family members, such as extra-cellular regulated kinases [e.g., ERK1/2 – themselves implicated in FGF-mediated PrE differentiation at a developmental point succeeding that identified for p38-MAPK (Nichols et al., 2009; Yamanaka et al., 2010; Frankenberg et al., 2011; Kang et al., 2013; Thamodaran and Bruce, 2016)] in that they are classically known to be activated by extracellular stress stimuli; for example pro-inflammatory cytokines, U.V. radiation and physical stress, rather than liganded growth-factor associated receptor tyrosine kinases (Remy et al., 2010). It is estimated activated p38-mitogen activated kinases in general are able to phosphorylate and regulate between 200 and 300 cellular substrates (Cuadrado and Nebreda, 2010; Trempolec et al., 2013; Hornbeck et al., 2019). In the context of this study, there is precedent for the involvement of active p38-MAPK in amino acid (AA) signaling (Casas-Terradellas et al., 2008) and regulation of autophagy (Webber, 2010), in other non-embryo models.

The 'Developmental Origin of Health and Disease' (DOHaD) model hypothesizes environmental cues, particularly nutrient availability, during the peri-conceptual days of development manifests changes in embryonic metabolism and development, with potential pathological consequences extending into adulthood (O'Brien et al., 1999). Rodent pups born to mothers exposed to low protein diets during preimplantation stages of development are reported to have significantly increased birth weight, elevated systolic blood pressure, liver hypertrophy, cardiovascular and metabolic disorders, aberrant establishment of gene imprints plus hyperactive behavior and poor memory (Kwong et al., 2000, 2006; Fleming et al., 2015, 2018). Such observations are indicative of adaptive and persistent changes in early embryo physiology/metabolism; indeed, similar studies report increased endocytosis and nutrient uptake in the extraembryonic TE and PrE lineages, arising from altered epigenetic gene regulation (Sun et al., 2014, 2015). Thus, mounting evidence corroborates the incidence of the DOHaD model, yet there is a comparative dearth of detailed and supportive molecular mechanistic data that could underpin how preimplantation stage embryos react and develop under conditions of nutrient deprivation.

Accordingly, we have examined our previously identified p38-MAPK inhibition induced defective PrE phenotypes, themselves associated with reduced blastocyst cell number (Thamodaran and Bruce, 2016), to ascertain if p38-MAPK not only regulates PrE differentiation *per se*, but also perform a dual regulative/homeostatic role in mediating preimplantation mouse embryo/blastocyst development in response to limited amino acid (AA) availability, as could be inferred from earlier studies (Kwong et al., 2000, 2006; Sun et al., 2014, 2015; Fleming et al., 2015, 2018) addressing DOHaD.

MATERIALS AND METHODS

Mouse Lines and Embryo Culture

All experimental procedures relating to mice (i.e., derivation of preimplantation stage embryos for further study) complied with 'ARRIVE' guidelines and were carried out in accordance with EU Directive 2010/63/EU (for animal experiments). Superovulation and strain mating regime to produce embryos for the experiments are shown in the figures and are as previously described (Mihajlovic et al., 2015). E1.5 (i.e., 2-cell) stage embryos were isolated from the oviducts of the females in M2 media (pre-warmed at 37°C for at least 2–3 h) and thereafter cultured in KSOM (EmbryoMax® KSOM Mouse Embryo Media; cat. # MR-020P-5F – pre-warmed and equilibrated in 5% CO_2 and 37°C), either with or without amino acid supplementation. For KSOM + AA condition, Gibco™ MEM Non-Essential Amino Acids Solution (100X) (cat. # 11140035) and Gibco MEM™ Amino Acids Solution (50X) (cat. # 11130036) were used to a working concentration of 0.5X. Embryos were cultured in micro-drops prepared in 35 mm tissue culture dishes covered with light mineral oil (Irvine Scientific. cat. # 9305), in 5% CO_2 incubators maintained at 37°C until the appropriate stage and thereafter were analyzed according to the experimental design. Chemical inhibition of p38-MAPKs was carried out using SB220025 (Calbiochem® cat. # 559396; dissolved in dimethyl sulfoxide/DMSO) at 20 μM working concentration in the respective culture medium, as described previously (Thamodaran and Bruce, 2016). DMSO (Sigma-Aldrich® cat. # D4540) of equivalent volume was used as solvent control to a final working concentration of 0.2% by volume. Embryos with a blastocoel cavity occupying approximately 50% of the volume of the embryo at 12.00 h on E3.5 were moved to either inhibitory or control culture conditions and cultured for a further 24 h (i.e., E4.5). Rescue experiments were similarly performed by further addition

of *N*-Acetyl-L-cysteine (NAC, dissolved in water; Sigma-Aldrich® cat. # A7250) to a final working concentration of 1 or 10 mM in respective culture medium. All KSOM based culture media, with or without additional chemicals (AAs, inhibitors or anti-oxidants), was pre-warmed and equilibrated in 5% CO_2 and 37°C for at least 3–4 h prior to embryo transfer.

Bright-Field Microscopy, Immunofluorescence Staining, Confocal Microscopy, and Image Analysis

Bright-field images were captured using Olympus IX71 inverted fluorescence microscope and Optika TCB3.0 imaging unit along with the associated Optika Vision Lite 2.1 software. To remove the *zona pellucida*, blastocysts were quickly washed and pipetted in pre-warmed drops of Tyrode's Solution, Acidic (Sigma-Aldrich® cat. # T1788), until the *zona* was visually undetectable, immediately followed by washes through pre-warmed drops of M2 media. Thereafter embryos were fixed, in dark, at appropriate stages with 4% paraformaldehyde (Santa Cruz Biotechnology, Inc., cat. # sc-281692) for 20 min at room temperature. Permeabilization was performed by transferring embryos to a 0.5% solution of Triton X-100 (Sigma-Aldrich® cat. # T8787), in phosphate buffered saline (PBS), for 20 min at room temperature. Washes post-fixation, permeabilization and antibody staining were performed in PBS with 0.05% of TWEEN® 20 (Sigma-Aldrich® cat. # P9416) (PBST) by transferring embryos between two drops or wells (of 96-well micro-titer plates) of PBST, for 20 min at room temperature. Blocking and antibody staining was performed in 3% bovine serum albumin (BSA; Sigma-Aldrich® cat. # A7906) in PBST. Blocking incubations of 30 min at 4°C were performed before both primary and secondary antibody staining; primary antibody staining (in blocking buffer) was incubated overnight (∼16 h) at 4°C and secondary antibody staining carried out in the dark at room temperature for 70 min. Stained embryos were mounted in DAPI containing mounting medium VECTASHIELD® (Vector Laboratories, Inc., cat. # H-1200), placed on cover slips and incubated at 4°C for 30 min in the dark, prior to confocal imaging. Details of the primary and secondary antibody combinations used can be found in **Supplementary Table S4**. Confocal images were acquired using a FV10i Confocal Laser Scanning Microscope and FV10i-SW image acquisition software (Olympus)®. Images were analyzed using FV10-ASW 4.2 Viewer (Olympus)® and Imaris X64 Microscopy Image Analysis Software [version 6.2.1; Bitplane AG (Oxford Instruments plc)]. Cells were counted manually and automatically using Imaris X64.

Cell Number Quantification, Statistics, and Graphical Representation

Total cell number counts (based on DAPI nuclei staining) were further sub categorized as EPI or PrE cells based on detectable and exclusive NANOG and GATA4 (confocal images in **Figure 1** and graphs in **Figures 2**, **4**, **5**) or GATA6 (confocal images and graphs in **Figure 5**) double immuno-staining, respectively. Cells not located within blastocyst ICMs that also did not stain for either GATA4 and/or NANOG, were designated as outer/TE cells. Specifically relating to **Figure 5**, ICM cells that were positively stained for both GATA6 and NANOG at E4.5 were designated as uncommitted in terms of cell fate. Initial recording and data accumulation was carried out using Microsoft Excel and further statistical analysis and graphical representations performed with GraphPad Prism 8. A Mann–Whitney pairwise statistical test was employed. Unless otherwise stated within individual graphs as a specific *P*-value (if statistically insignificant), the stated significance intervals were depicted as such: *P*-value < 0.0001 (****), 0.0001 to 0.001 (***), 0.001 to 0.01 (**), and 0.01 to 0.05 (*). All graphs represent dot plots of the total sample size, with associated means and the standard error bars highlighted. **Supplementary Table S5** summarizes the results of additional Welch's ANOVA tests performed across DMSO and p38-MAPK inhibited conditions in which either no NAC, 1 mM NAC and 10 mM NAC, was supplemented to both KSOM and KSOM + AA conditions. Analysis was performed using GraphPad Prism 8, *P*-values are numerically stated, and significance intervals are depicted as such: *P*-value < 0.0001 (****), 0.0001 to 0.001 (***), 0.001 to 0.01 (**), and 0.01 to 0.05 (*).

Quantitative Real-Time PCR (Q-RTPCR)

Two-cell stage (E1.5) embryos were collected and cultured in KSOM + AA until E3.5 (i.e., at 12:00 h) stage and then equally distributed in to four experimental pre-equilibrated media conditions [i.e., (i) KSOM + DMSO, (ii) KSOM + SB220025, (iii) KSOM + AA + DMSO, and (iv) KSOM + AA + SB220025]. At 22:00 h (i.e., 10 h of treatment), 25 embryos from each condition were collected immediately processed for RNA extraction and isolation using the ARCTURUS® PicoPure® RNA Isolation Kit (Applied Biosystems™; cat. KIT0204), following the manufacturer's protocol. The entire eluted volume of total RNA was immediately DNase treated with Invitrogen™ TURBO™ DNase (cat. AM2238) according to the manufacturer provided protocol. The whole sample was then subject to cDNA synthesis using Invitrogen™ SuperScript™ III Reverse Transcriptase (cat. 18080044), as directed by the manufacturer and employing Invitrogen Oligo™ d(T)16 (cat. N8080128), ThermoScientific™ dNTP Mix (cat. R0192) and Applied Biosystems™ RNase Inhibitor (cat. N8080119). The final cDNA volume of 30 μl was diluted to 45 μl with nuclease free water and 1 μl used in 10 μl individual final SYBR-green based Q-RT-PCR reaction volumes (qPCRBIO SyGreen Mix Lo-ROX – cat. PB20.11). A Bio-Rad CFX96 Touch Real-Time PCR Detection System apparatus, employing standard settings, was employed for data accumulation and initial analysis was performed with the accompanying Bio-Rad CFX Manager™ software. Triplicate measurements per gene (the sequence of individual oligonucleotide primers, used at a final concentration of 300 nM, are provided in **Supplementary Table S6**) were assayed from two biological replicates that were each technically replicated. The averaged transcript levels of analyzed genes (i.e., *Cat*, *Sod1,* and *Sod2*) were derived after internal normalization

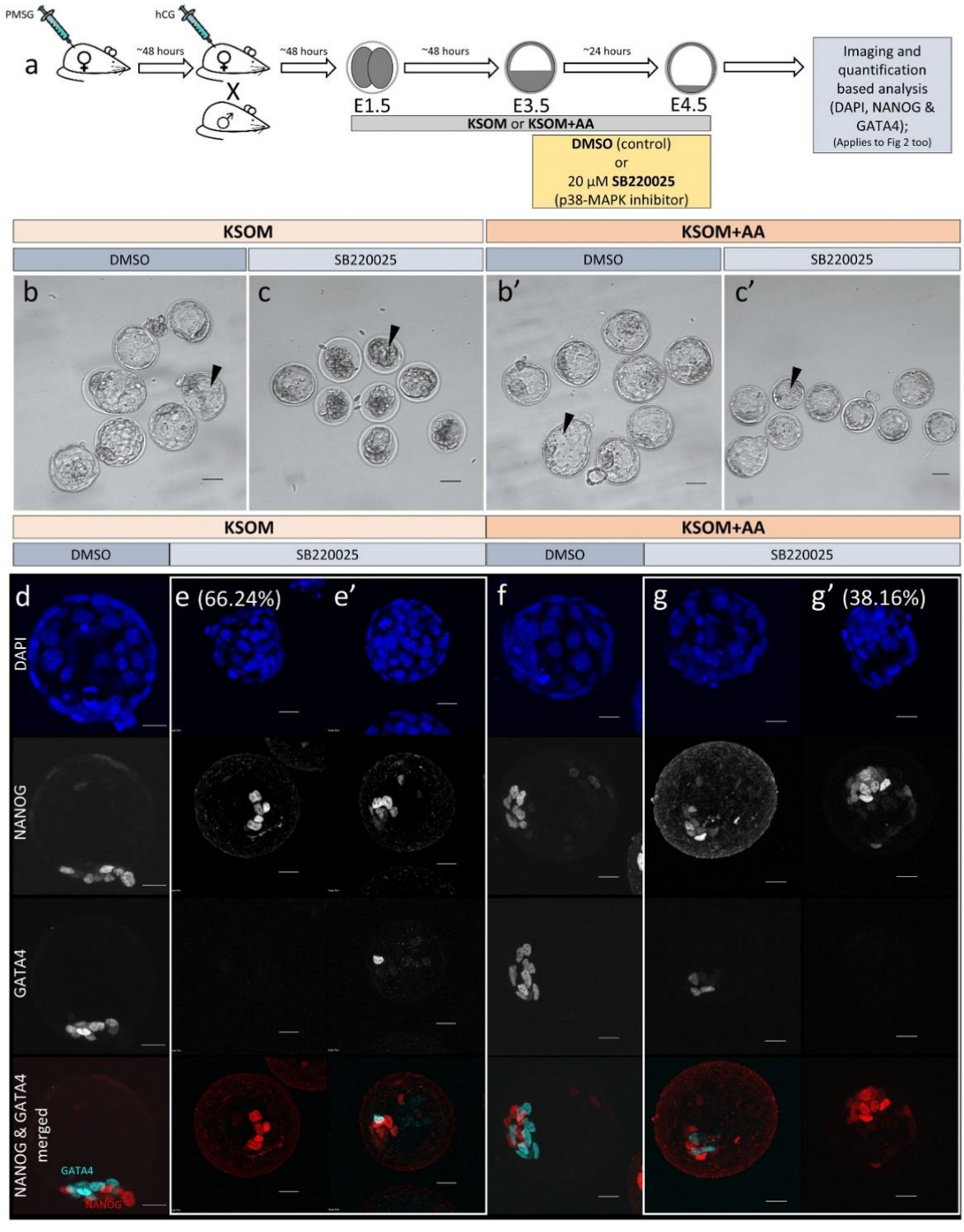

FIGURE 1 | Continued

FIGURE 1 | Effect of p38-MAPK inhibition on mouse blastocyst morphology and ICM cell fate derivation in culture conditions ± exogenous amino acid supplementation. **(a)** Experimental design: embryos were collected at E1.5 (2-cell stage) and *in vitro* cultured to E3.5 in media without (KSOM) or with amino acid supplementation (KSOM + AA) and transferred to respective control (DMSO) or p38-MAPK inhibitory conditions (SB220025) until E4.5. Embryos were then fixed, immuno-stained and imaged as described in materials and methods. **(b–c′)** Bright-field micrographs of mouse blastocysts at E4.5; all treatments were carried out from E3.5 to E4.5, i.e., 24 h. Panels, from left to right, represent KSOM + DMSO **(b)**, KSOM + p38-MAPK inhibition **(c)**, KSOM + AA + DMSO **(b′)** and KSOM + AA + p38-MAPK inhibition **(c′)**. Black arrowheads notify presence, absence, and relative volumes of the blastocyst cavities. In KSOM + p38-MAPK inhibition **(c)**, blastocoel cavities are markedly smaller and/or collapsed, whereas mostly intact cavities are observed in all other conditions. Scale bar = 40 μm. **(d–g′)** Z-stack projection confocal images of embryos at E4.5 under the conditions and treatments as depicted above/panel **(a)**; stained for, from top to bottom, nucleus/DNA (DAPI), epiblast (NANOG), primitive endoderm (GATA4) and total ICM (NANOG and GATA4 merged) under, KSOM + DMSO **(d)**, KSOM + p38-MAPK inhibition, with no GATA4 positive cells (66% of analyzed embryos) **(e)** and with one or more GATA4 positive cells (34% of analyzed embryos) **(e′)**, KSOM + AA + DMSO **(f)** and KSOM + AA + p38-MAPK inhibition with one or more GATA4 positive cells (65% of analyzed embryos) **(g)** and with no GATA4 positive cells (35% of analyzed embryos) **(g′)** culture conditions. All images in one vertical panel are of the same embryo at the same magnification. Scale bar = 20 μm.

against *H2afz* mRNA levels, in four experimental culture conditions assayed. As such data was acquired and initially analyzed with CFX Manager™, then processed in Microsoft Excel (biological and technical replicate averaging) and GraphPad Prism 8 (graphical output). Welch's ANOVA statistical significance test followed by Dunnett's T3 multiple comparisons test were employed. Unless otherwise stated within individual graphs as a specific *P*-value (if statistically insignificant), the stated significance intervals were depicted as: *P*-value < 0.0001 (****), 0.0001 to 0.001 (***), 0.001 to 0.01 (**), and 0.01 to 0.05 (*); error bars denote calculated standard deviations.

Blastocyst Reactive Oxygen Species (ROS) Staining

Collected 2-cell stage embryos were cultured in KSOM until E3.5 (12:00 h) then moved to either KSOM + DMSO or KSOM + SB220025 (pre-equilibrated for 3 h prior) and cultured for another 6 h (i.e., E3.75; alternatively expressed as 18:00 h on the same day) or to E4.25 (i.e., until 06:00 h the next day). Thereafter embryos were transferred to M2 media containing 5 μM Invitrogen™ CellROX™ Green Reagent (a ROS specific reporter dye; cat. C10444), that had been pre-equilibrated in the dark at 37°C for 30 min, and incubated under the same conditions for 30 min before being washed through two drops of regular M2 media. Whereas E3.75 (n = 2 per experimental group) embryos were immediately live mounted in M2 drops and imaged under the confocal microscope (FV10i, Olympus®, using appropriate preparatory CellROX™ Green filter settings), those ROS stained embryos collected at E4.25 (KSOM + DMSO, n = 14; KSOM + SB220025, n = 15) were fixed in 4% paraformaldehyde prior to confocal microscopic imaging. Confocal images are depicted as projections of individual z-stack images using the FV10i-SW image acquisition software (Olympus®) rainbow spectral intensity palette (from blue to white, representing lowest to highest signal intensities). All the images in each group (i.e., E3.75 and E4.25) were acquired at equal laser intensity and detector sensitivity. The number of ROX-positive/staining foci in the z-stack projections of individual embryos fixed at E4.25 were quantified using Image J[1], by first subtracting background (using a rolling ball radius of 50 pixels) and invoking the 'finding maxima tool' (prominence > 5). The counted number of foci were statistically verified and graphically depicted using GraphPad Prism 8; statistical test employed was an unpaired, two-tailed *t*-tests. Unless otherwise stated within individual graphs as a specific *P*-value (if statistically insignificant), the stated significance intervals are depicted: *P*-value < 0.0001 (****), 0.0001 to 0.001 (***), 0.001 to 0.01 (**), and 0.01 to 0.05 (*). The graphs represent dot plot of total sample size together with mean and the standard deviation bars indicated.

Phosphorylated/Activated p38-MAPK Western Blotting and Quantification

Collected 2-cell stage embryos were cultured in either KSOM or KSOM + AA until E3.5 (12:00 h) or E3.75 (18.00 h) and 20–40 embryos processed for western/immunoblotting per culture condition; briefly embryos were washed through two drops of Dulbecco's PBS (Sigma-Aldrich; cat. BSS-1005-B), transferred to 1.5 ml microfuge tubes (removing excess PBS) and flash frozen in liquid nitrogen. To prepared samples 10 mL of 10X SDS reducing agent/loading buffer (NuPAGE buffer, Thermo Fisher Scientific, NP 0004, Thermo Fisher Scientific) was added and then boiled at 100°C for 5 min. Loaded proteins were then electrophoretically separated on gradient precast 4–12% SDS-PAGE gels (Thermo Fisher Scientific, NP0323) and transferred to Immobilon P membranes (Merck group, IVPD00010) using a semi-dry blotting system (Biometra/Analytik Jena) for 25 min at 5 mA/cm^2. Blotted membranes were blocked in 5% skimmed milk powder dissolved in 0.05% Tween-Tris pH 7.4 buffered saline (TTBS), for 1 h, briefly rinsed in TTBS and then incubated overnight at 4°C overnight in 1% milk/TTBS containing primary antibody (against phosphorylated p38-MAPK). Membranes were washed in three changes of TTBS buffer (20 min each at room temperature) and anti-immunoglobulin-species-specific-peroxidase conjugated secondary antibody added to the blot in 1% milk/TTBS, for 1 h (room temperature). Immuno-detected proteins were visualized by chemiluminescent photographic film exposure (ECL kit; GE Life Sciences, RPN2232) and digitally scanned using a GS-800 calibrated densitometer (Bio-Rad Laboratories) and quantified using ImageJ[1]. Antibody stripped membrane blots were re-probed and quantified, for loading controls (detecting GADPH), in an identical manner. Note, presented quantified data (**Figure 3f**) of GAPDH normalized phosphorylated p38-MAPK levels are taken from two independent biological replicates. **Supplementary Table S4**

[1]http://rsbweb.nih.gov/ij/

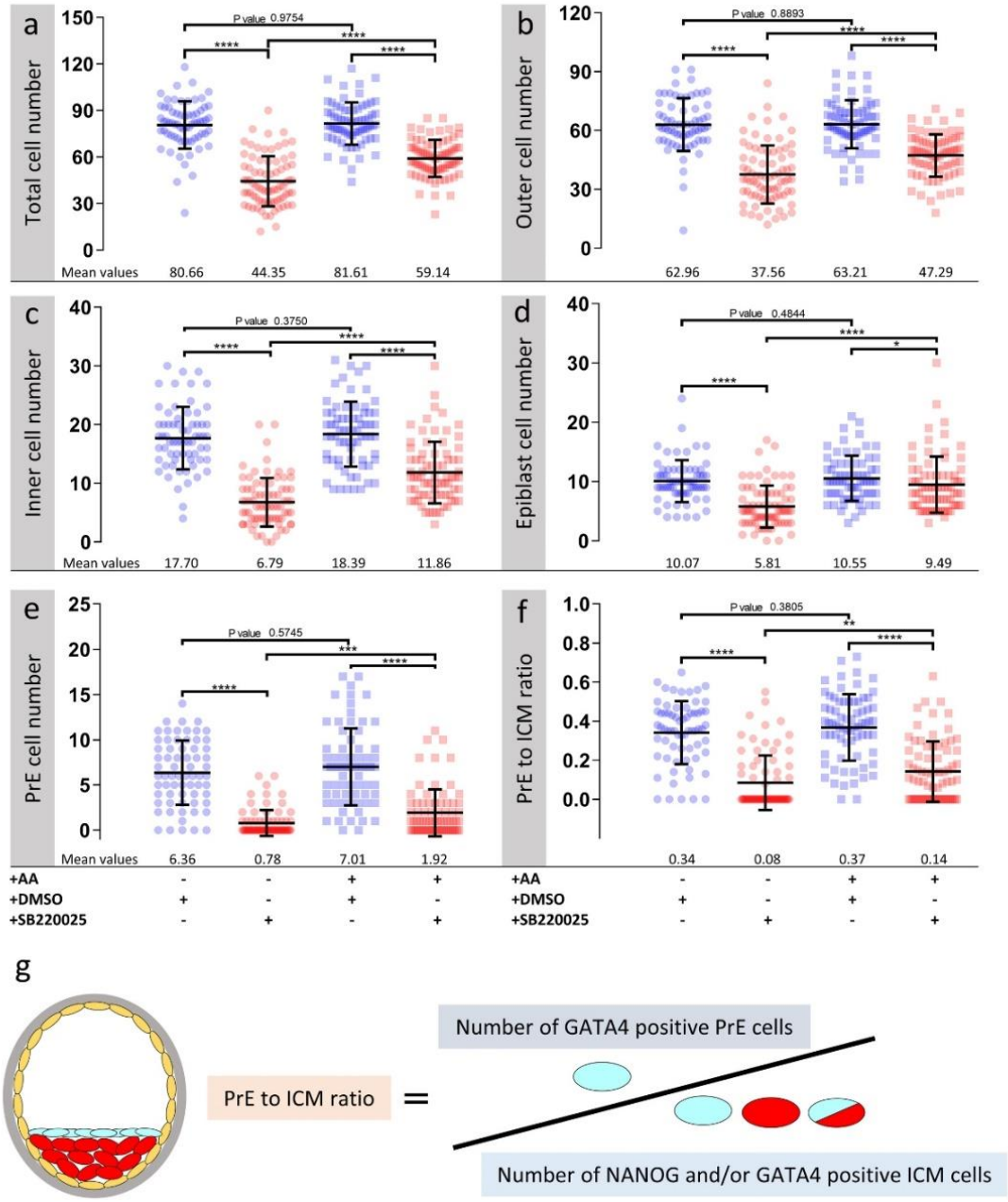

FIGURE 2 | Effect of p38-MAPK inhibition on blastocyst cell numbers, based on DAPI, NANOG and GATA4 staining and confocal microscopy, in culture conditions ± exogenous amino acid supplementation. Culture conditions in relation to amino acid supplementation status and presence of DMSO or p38-MAPK inhibitor (SB220025), from E3.5 to E4.5 (as shown **Figure 1**) are also shown at the bottom of the individual charts; from left to right; KSOM + DMSO (n = 67), KSOM + p38i (n = 77), KSOM + AA + DMSO (n = 71), and KSOM + AA + p38i (n = 76). **(a)** Quantification of total cell number based on counting DAPI stained blastomere nuclei. **(b)** Quantification of outer cell number based on subtracting NANOG and/or GATA4 positive inner cells from the DAPI stained total cell number (plus position within the embryo). **(c)** Quantification of inner cell number based on NANOG and/or GATA4 stained inner cells (plus position within the embryo). **(d)** Quantification of epiblast (EPI) cell number based on NANOG alone stained inner cells. **(e)** Quantification of primitive endoderm (PrE) cell number based on GATA4 alone stained inner cells. **(f)** Contribution of GATA4 stained primitive endoderm cells as a ratio of the total inner cells (NANOG and/or GATA4 stained cells). **(g)** Explanatory scheme of method employed to calculate PrE:ICM ratio values depicted in this image. Statistical test employed: Mann–Whitney test (GraphPad Prism 8). Unless otherwise stated, within the graphs as a distinct P-value (if statistically insignificant), the significance intervals are denoted: P-value < 0.0001 (****), 0.0001 to 0.001 (***), 0.001 to 0.01 (**) and 0.01 to 0.05 (*). Data relating to each individual embryo assayed are detailed in **Supplementary Table S1**.

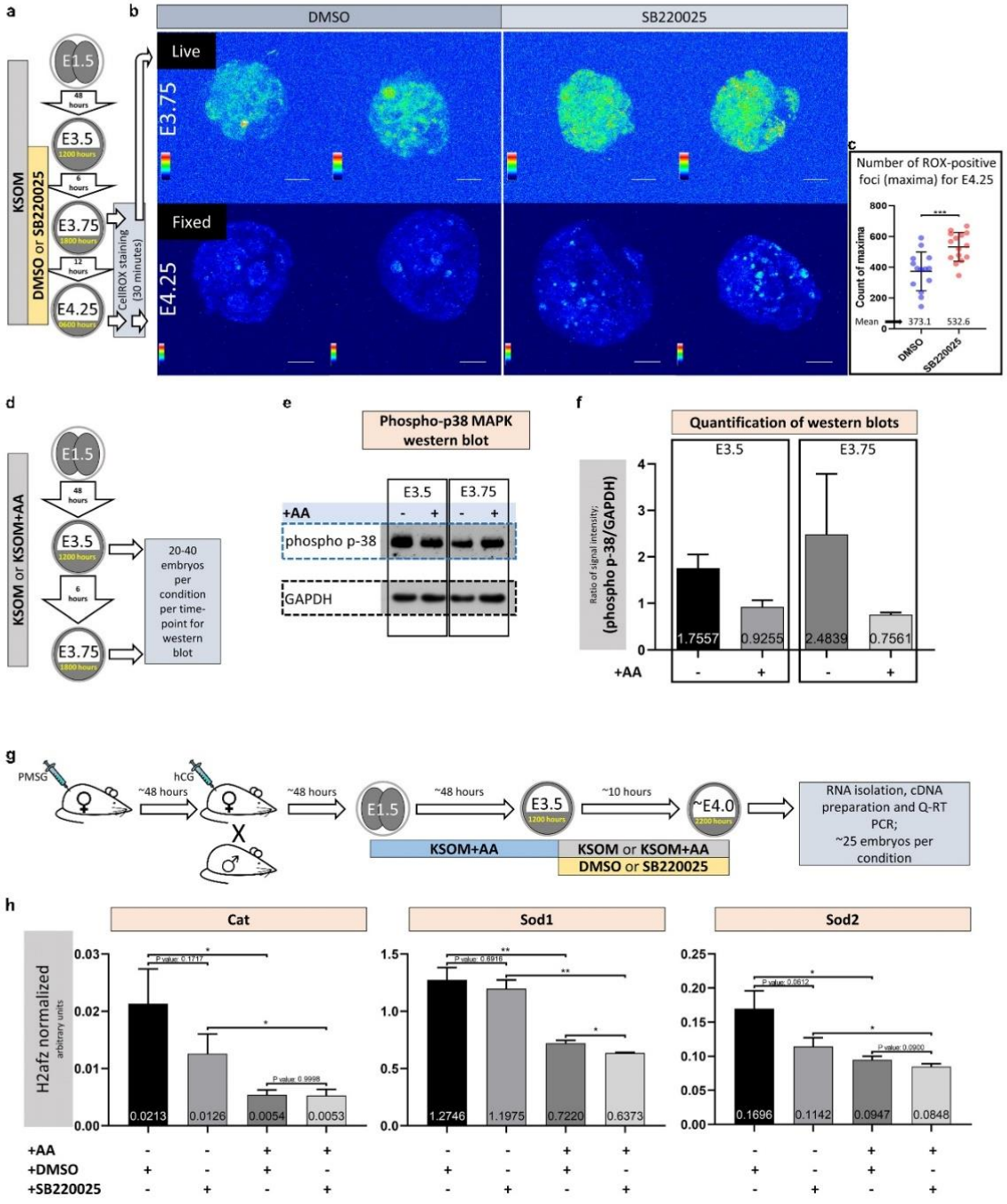

FIGURE 3 | Amino acid starvation coupled with p38-MAPK inhibition induces increased blastocyst ROS levels whereas amino acid starvation alone is sufficient to induce increased phosphorylation/activation of p38-MAPK and transcription of genes with enzymatic anti-oxidant properties. **(a)** Experimental design detailing culture conditions for embryos and sampling time points used to visualize and quantify blastocyst ROS levels. **(b)** Projected confocal z-stack images of blastocyst embryos stained with CellROX Green at E3.75 and 4.25 and were respectively imaged live or after fixation. A spectral rainbow palette is used to denote signal intensity levels (blue representing lowest to white denoting highest signal intensity); scale bar = 20 μm. **(c)** Quantification of the average per embryo incidence of ROX-positive foci (maxima) for the E4.25 assayed and fixed embryo groups cultured in KSOM plus DMSO and SB220025; as described in **(a,b)**. The statistical test

(Continued)

FIGURE 3 | Continued
employed was an unpaired, two-tailed Student's *t*-test. The stated significance intervals are depicted as: *P*-value < 0.0001 (****), 0.0001 to 0.001 (***), 0.001 to 0.01 (**), and 0.01 to 0.05 (*). The graphs represent dot plots of total sample size together with stated experimental group means and the standard deviations (error bars). **(d)** Experimental design detailing culture conditions for embryos and sampling time points used in western blotting based assay of activated and phosphorylated p38-MAPK protein expression in blastocyst embryos cultured in KSOM ± AA. **(e)** Representative western blot of phosphorylated p38-MAPK and GAPDH (as control) blastocyst protein levels, after culture in KSOM and KSOM + AA, at E3.5 and E3.75. Note, uneven sample loading (GAPDH) and hence need for normalized quantitation **(f)**. **(f)** Relative signal intensity quantification data of the GAPDH normalized levels of phosphorylated p38-MAPK protein expression (judged by western blot) in blastocysts (at E3.5 and E3.75) after culture in KSOM and KSOM + AA (from two independent biological replicates). **(g)** Experimental design detailing culture conditions for embryos used in Q-RTPCR based quantification of enzymatic anti-oxidant gene mRNA expression in blastocysts (at E4.0) cultured in KSOM ± AA treated with DMSO or p38-MAPK inhibitor (SB220025). **(h)** Quantification of the relative transcript expression levels of *Cat*, *Sod1* and *Sod2*, internally normalized to *H2afz* levels, across the four conditions. The statistical test employed were Welch's ANOVA tests followed by Dunnett's T3 multiple comparisons test (GraphPad Prism 8). Unless otherwise stated within individual charts as a specific *P*-value (if statistically insignificant), the stated significance intervals are as follows: *P*-value < 0.0001 (****), 0.0001 to 0.001 (***), 0.001 to 0.01 (**), and 0.01 to 0.05 (*); error bars denote standard deviation and mean *H2afz* normalized expression levels are numerically stated.

details the identity and utilized concentrations of the primary and peroxidase-conjugated antibodies used.

RESULTS AND DISCUSSION

p38-MAPK Activity Buffers Amino Acid Availability to Ensure Germane Blastocyst Maturation and Appropriate ICM Cell Lineage Derivation

As outlined above, we assayed the effect of exogenous AA supplementation on *in vitro* mouse blastocyst formation, assaying total, outer/TE, overall ICM, pluripotent EPI and PrE cell numbers. Concomitantly, we analyzed the effect of pharmacological p38-MAPK inhibition [using SB220025 (Jackson et al., 1998)], given our previously identified role for p38-MAPK in regulating PrE specification and formation during the blastocyst maturation developmental window [E3.5–E4.5 (Thamodaran and Bruce, 2016)]. Accordingly, 2-cell stage mouse embryos were *in vitro* cultured until the early blastocyst stage (E3.5) in a commonly utilized and chemically defined commercial growth media lacking AAs (except L-glutamine; KSOM) or the identical media supplemented with essential and non-essential AAs (KSOM + AA). Embryos were then switched to the equivalent media containing either SB220025 or DMSO (vehicle control), further cultured to the late blastocyst stage (E4.5), fixed and immuno-fluorescently stained for EPI (NANOG) or PrE (GATA4) marker protein expression. Irrespective of AA supplementation status, we did not observe any morphological differences between the DMSO control treated groups; each yielding hatching blastocysts with appropriately large cavities (**Figures 1b,b′**) and ICMs consisting a NANOG positive (NANOG +) EPI compartment overlaid with mono-layered GATA4 positive (GATA4 +) PrE cells (**Figures 1d,f**). Neither the average number of total, outer and inner (including PrE and EPI) cells, nor the PrE:total ICM cell number ratio, were significantly different between each of the DMSO treated control groups (**Figure 2**). Thus, exogenous AA supplementation did not overtly affect embryonic/blastocyst development or ICM lineage derivation during the preimplantation period (notwithstanding possible undetectable changes, possibly epigenetic in origin, that may potentially underpin any subsequent DOHaD phenotypes).

Similar inspection of the p38-MAPK inhibited groups confirmed our previously reported data (Thamodaran and Bruce, 2016), whereby blastocysts were morphologically smaller (particularly the KSOM group) (**Figures 1c,c′**) and had a robust PrE deficit (note lack of GATA4 + cells **Figures 1e,e′,g,g′**). Indeed, a detailed analysis of cell numbers (**Figure 2**) revealed the p38-MAPK inhibited embryos that were cultured in KSOM were significantly more adversely affected than those cultured in KSOM + AA, comprising fewer overall, outer and inner cells, although both inhibited groups had significantly fewer cells than their equivalent DMSO controls. Furthermore, p38-MAPK inhibited embryos cultured in KSOM also had significantly fewer EPI cells (5.81 cells) than either p38-MAPK inhibited blastocysts cultured in KSOM + AA (9.49 cells) or the appropriate DMSO treated KSOM control groups (10.07 cells) (**Figure 2d**). This trend was also observed in the PrE, albeit representing a small difference in the overall magnitude; i.e., an average difference of 1.14 cells between the KSOM + AA and KSOM conditions under p38-MAPK inhibition (0.78 cells in KSOM and 1.92 in KSOM + AA, compared with 6.36 and 7.01 in the respective control DMSO conditions – **Figure 2e**). p38-MAPK inhibition, thus, severely attenuated PrE differentiation irrespective of AA supplementation status, with the magnitude of the effect being marginally greater, yet reaching statistical significance, in blastocysts matured in KSOM media. Interestingly, there was no similar robust reduction in EPI cells in p38-MAPK inhibited embryos from the KSOM + AA cultured group (10.55 cells in control vs. 9.49 in inhibited conditions), in line with our previous observations (Thamodaran and Bruce, 2016). Collectively, these data confirm maximally reduced cell number phenotypes associated with p38-MAPK inhibition under non-supplemented KSOM culture conditions, and indicate a developmental buffering capacity of active p38-MAPK (that potentially ensures required AA availability) that is necessary for appropriate blastocyst development/maturation. However, the fact that exogenous AA supplementation is able to elicit a near complete rescue in EPI cell number deficits caused by p38-MAPK inhibition but only has a marginal effect on robustly impaired PrE differentiation, demonstrates such a regulative AA-related homeostatic role of p38-MAPK to be distinct and independent of that it fulfils in potentiating PrE differentiation (Thamodaran and Bruce, 2016).

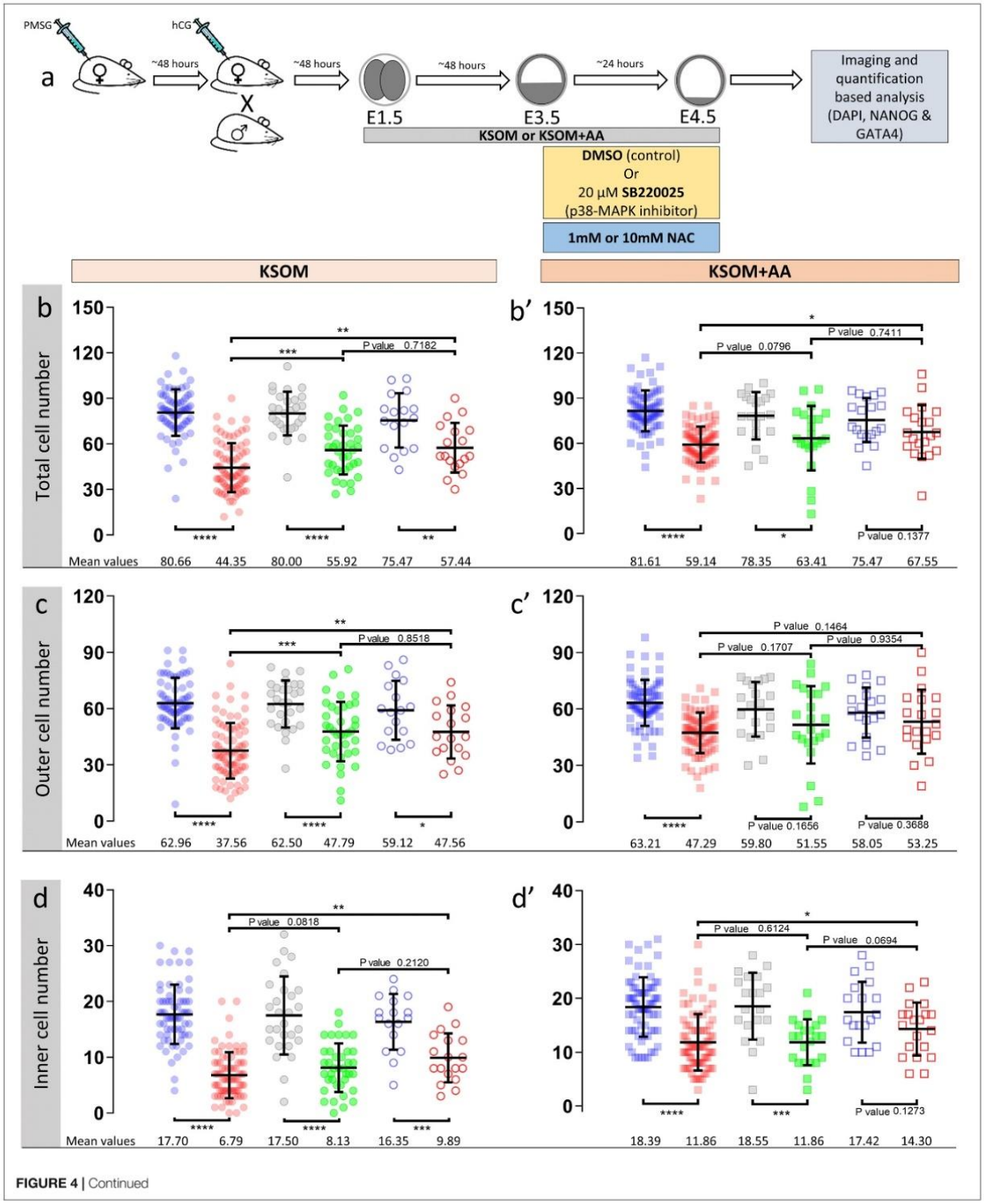

FIGURE 4 | Continued

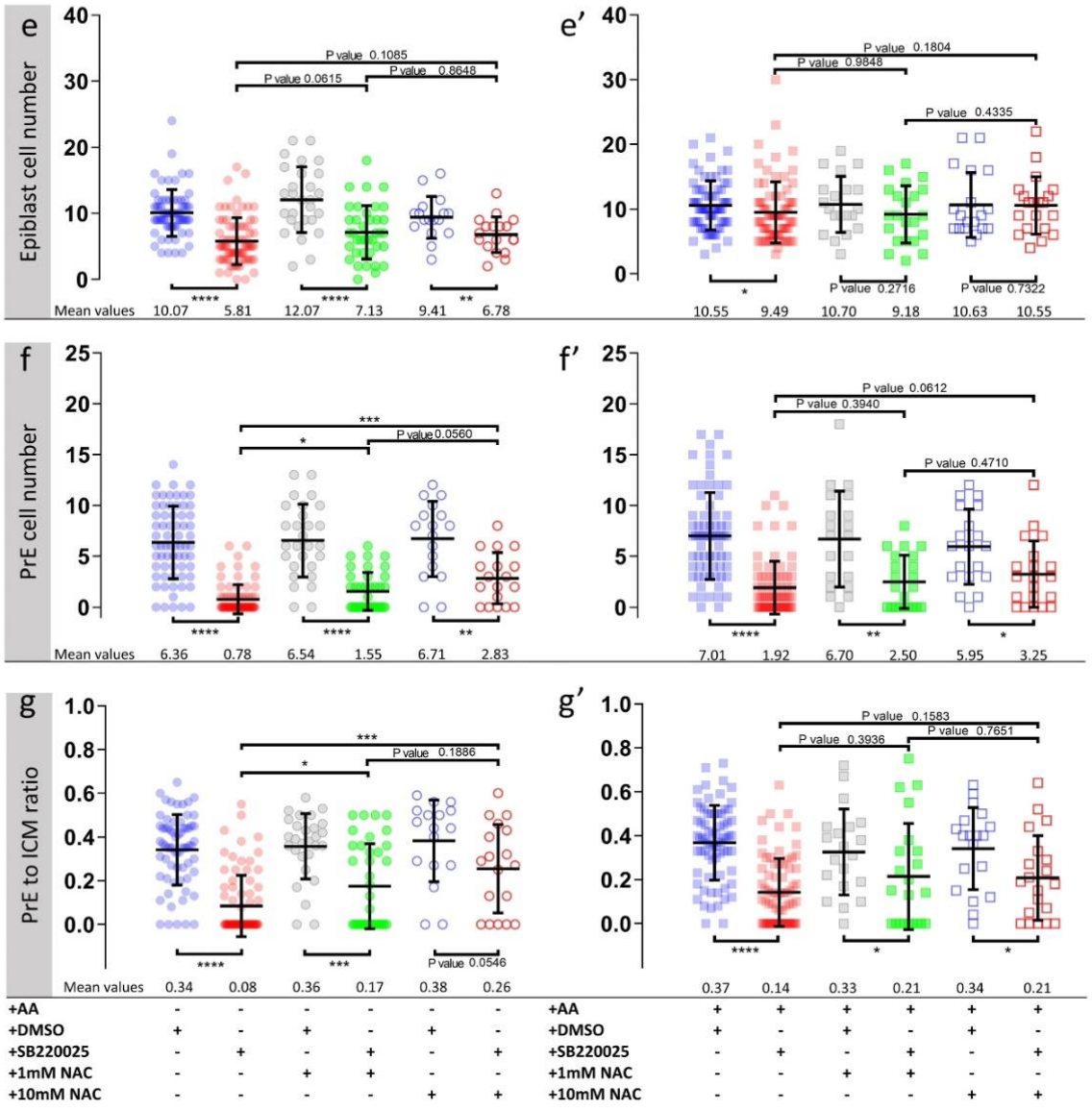

FIGURE 4 | Effect of anti-oxidant (NAC) treatment on p38-MAPK inhibited blastocyst cell numbers, based on DAPI, NANOG and GATA4 staining and confocal microscopy, in culture conditions ± exogenous amino acid supplementation. **(a)** Experimental design detailing culture conditions of embryos recovered at the 2-cell (E1.5) stage, in regard to culture media amino acid supplementation status and the possible combined regimes of NAC plus DMSO or p38-MAPK inhibitor (SB220025) treatment from E3.5-E4.5. KSOM group **(b–g)**, left to right: DMSO (n = 67), p38-MAPK inhibition (n = 77), DMSO + 1 mM NAC (n = 28), p38-MAPK inhibition + 1 mM NAC (n = 38), DMSO + 10 mM NAC (n = 17) and p38-MAPK inhibition + 10 mM NAC (n = 18). KSOM + AA group **(b′–g′)**, left to right: DMSO (n = 71), p38-MAPK inhibition (n = 76), DMSO + 1 mM NAC (n = 20), p38-MAPK inhibition + 1 mM NAC (n = 22), DMSO + 10 mM NAC (n = 19) and p38-MAPK inhibition + 10 mM NAC (n = 20). An explanatory matrix of the composition of each experimental condition is present beneath the relevant charts, at the base of the whole figure. **(bb′)** Quantification of total cell number based on counting DAPI stained nuclei of the blastomeres. **(c,c′)** Quantification of outer cell number based on subtracting NANOG and/or GATA4 positive inner cells from the DAPI stained total cell number (plus position within the embryo). **(d,d′)** Quantification of inner cell number based on NANOG and/or GATA4 stained inner cells number (plus position within the embryo). **(e,e′)** Quantification of epiblast cell number based on NANOG alone stained inner cells. **(f,f′)** Quantification of primitive endoderm cell number based on GATA4 alone stained inner cells. **(g,g′)** Quantification of the contribution of GATA4 stained primitive endoderm cells as a ratio of the total inner cells (NANOG and/or GATA4 stained cells). Statistical test employed: Mann–Whitney test (GraphPad Prism 8). Unless otherwise stated, within the graphs as a distinct P-value (if statistically insignificant), the significance intervals are as follows: P-value < 0.0001 (****), 0.0001 to 0.001 (***), 0.001 to 0.01 (**), and 0.01 to 0.05 (*). Note, data relating to DMSO and p38-MAPK inhibition conditions in KSOM and KSOM + AA media are reproduced from **Figure 2** to aid comparison with NAC treated groups. Data relating to each individual embryo assayed are detailed in **Supplementary Table S2**. A Welch's ANOVA statistical analysis of the data presented in this figure is presented in **Supplementary Table S5**.

How active p38-MAPK executes this homeostatic role in the absence of exogenous AAs (see KSOM + DMSO conditions **Figures 1**, **2**) is unclear but may involve sequestration of intracellular sources of AA via regulated autophagy, as reported in other non-embryo-related models/systems (Corcelle et al., 2007; Webber, 2010; Webber and Tooze, 2010; Henson et al., 2014). Consistently, p38-MAPK has also been reported to regulate mTOR containing complexes, involved in balanced metabolism, cell growth/proliferation control and autophagy (Casas-Terradellas et al., 2008; Cully et al., 2010; Wu et al., 2011; Gutierrez-Uzquiza et al., 2012; Linares et al., 2015). Moreover, partial mTOR inhibition in mouse blastocysts is known to induce a state of developmental diapause (Bulut-Karslioglu et al., 2016), whilst relative differences in mTOR activity (linked to p53 activity) have been reported as a mechanism by which cells exiting the naive pluripotent state compete and are potentially eliminated from early post-implantation embryonic tissues (Bowling et al., 2018). It would be interesting to investigate further the potential regulation of mTOR via p38-MAPK. Interestingly, there also exists precedent from cell line models for atypical glucose induced autophagy, which is independent of mTOR and relies on p38-MAPK. This mechanism of glucose induced and p38-MAPK dependant autophagy is however only operative under conditions of nutrient deprivation, such as depletion of exogenously provided AAs (Moruno-Manchon et al., 2013). Given the base media (i.e., KSOM) used in this study contains glucose, it is possible a similar mechanism of induced and p38-MAPK dependent autophagy is responsible for the overtly normal blastocyst maturation observed in DMSO treated control embryos cultured in the AA-free non-supplemented KSOM.

p38-MAPK Counteracts Amino Acid Depletion Induced Oxidative Stress During Blastocyst Maturation

Amino acid starvation is closely linked to increased oxidative stress (Harding et al., 2003), whereby induced anti-oxidant mechanisms, involving *de novo* protein expression, are impaired (Vucetic et al., 2017). Additionally, activated p38-MAPK (specifically p38α/MAPK14) has been reported to orchestrate the induced/stabilized expression of enzymatic antioxidants (Gutierrez-Uzquiza et al., 2012). Therefore, given the morula to blastocyst transition in mouse preimplantation development is accompanied by a large increase in glucose utilization and oxygen consumption (Brown and Whittingham, 1991; Leese, 2012), with the potential to contribute elevated levels of ROS (Murphy, 2009; Harvey, 2019), we hypothesized the observed aggravated effect of p38-MAPK inhibition in the absence of AA supplementation was contributed by increased oxidative stress. In support of this model, we could directly detect increased levels of ROS (using a ROX-dye) in blastocysts under p38-MAPK inhibited conditions in both live E3.75 (**Figures 3a,b**, upper panels) and fixed E4.25 (**Figures 3a,b**, lower panels and **Figure 3c**, detailing quantification of the average number of ROX-positive foci per embryo) stage embryos, cultured in non-supplemented KSOM (see also **Supplementary Figure S1**, detailing projected z-section confocal micrographs of all ROX stained E4.25 stage fixed embryos used in ROS quantification). Additionally, a comparative and quantitative assay of the levels of functionally active phosphorylated p38-MAPK protein in blastocysts derived after culture in either KSOM or KSOM + AA, reported enhanced levels of active p38-MAPK in the KSOM cultured group condition at both E3.5 and E3.75 (**Figures 3d–f**); i.e., the culture condition, with AA supplementation, already shown to be most sensitive to the effects of p38-MAPK inhibition (**Figures 1**, **2**). In further support of the model, we could also detect significantly enhanced expression of recognized mRNA transcripts for enzymatic antioxidants [i.e., Catalase/*Cat* and Superoxide-dismutases 1 and 2/*Sod1* and *Sod2* (Gutierrez-Uzquiza et al., 2012)] in control DMSO treated blastocysts cultured in un-supplemented KSOM versus KSOM + AA. Moreover, in the case of *Cat* and *Sod2* expression, such comparatively enhanced levels could be attenuated by p38-MAPK inhibition, although not to levels observed in blastocysts cultured in KSOM + AA (**Figures 3g,h** – note all blastocysts were initially cultured in KSOM + AA until E3.5, before being transferred to one of the four assayed media conditions). Collectively, these data support the hypothesis that increased oxidative stress caused by a lack of exogenous AA media supplementation is buffered by active p38-MAPK to ensure germane blastocyst development and the potential to adopt appropriate ICM cell fates.

Accordingly, we therefore tested if blastocyst cell number deficits caused by p38-MAPK inhibition could be ameliorated by providing exogenous anti-oxidants to the culture media. Thus, we repeated the cell counting experiments described above, including extra conditions in which cultured blastocysts (E3.5–E4.5), under control (DMSO) and p38-MAPK inhibited conditions, were provided the antioxidant *N*-acetyl-cysteine (NAC; either 1 or 10 mM – **Figure 4**). Focusing on the non-supplemented (KSOM) group, we observed that NAC addition to control DMSO treated embryo groups had no significant effect on average total, outer or inner cell number; nor EPI/PrE derivation (*n.b.* PrE:ICM ratio; **Figures 4b–g** and **Supplementary Table S5**: Welch's-ANOVA test), suggesting a lack of significant oxidative stress under control conditions. However, under p38-MAPK inhibited conditions, NAC supplementation caused significant increases (i.e., 'rescues') in all but EPI cell numbers (**Figures 4b–g** and **Supplementary Table S5**), when compared with p38-MAPK inhibition in the absence of NAC; indicating a role for p38-MAPK in mitigating depleted AA induced oxidative stress. A marked divergent effect was indeed observed in respect to the two ICM cell lineages. Whilst, NAC treatment did not significantly alter the average number of EPI (NANOG +) cells under p38-MAPK inhibition (5.81, 7.13, and 6.78 in non-supplemented, 1 and 10 mM NAC conditions respectively; **Figure 4e**), the number of PrE cells (GATA4 +) was significantly increased (0.78, 1.55, and 2.83 in non-supplemented, 1 and 10 mM NAC conditions respectively; **Figure 4f**), with an improving trend toward higher concentrations of NAC (**Figures 4f,g**). Therefore, these data strongly imply that under conditions of exogenous AA depletion, p38-MAPK activity specifically supports the development of differentiating extraembryonic lineages (TE and PrE) by combating induced oxidative stress (as revealed by

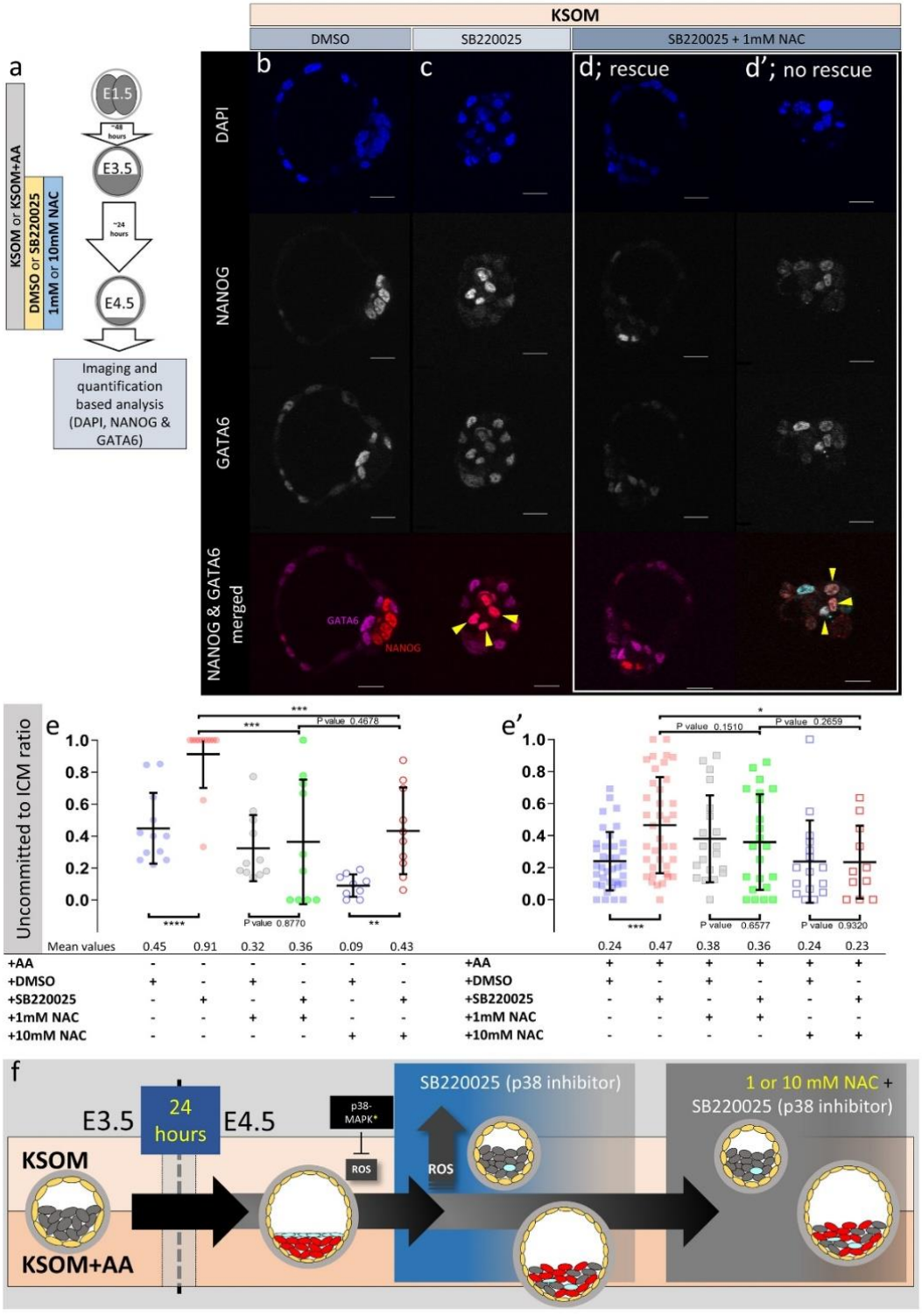

FIGURE 5 | Continued

FIGURE 5 | Effect of anti-oxidant (NAC) treatment on uncommitted ICM cells in p38-MAPK inhibited blastocysts, based on DAPI, NANOG, and GATA6 staining and confocal microscopy, in culture conditions ± exogenous amino acid supplementation. **(a)** Experimental design detailing culture conditions of embryos recovered at the 2-cell (E1.5) stage, in regard to culture media amino acid supplementation status and the possible combined regimes of NAC plus DMSO or p38-MAPK inhibitor (SB220025) treatment from E3.5 to E4.5. **(b–d′)** Single confocal microscopy z-sections of representative E4.5 embryos, cultured in KSOM (plus indicated combined regimes of DMSO/SB220025 and NAC from E3.5-E4.5) stained for, from top to bottom, nucleus/DNA (DAPI), epiblast (NANOG), primitive endoderm (GATA6) and uncommitted cells (NANOG and GATA6 co-staining – see pseudo-colored merged image). Yellow arrowheads highlight ICM cells co-expressing both markers (i.e., uncommitted cells); **(d,d′)** show examples of embryos in which addition of 1 mM NAC was able to either rescue, or not rescue, ICM cells from the p38-MAPK inhibition induced uncommitted cell fate, respectively. All images in one vertical panel are of the same embryo at same magnification. Scale bar = 20 μm. **(e,e′)** Contribution of GATA6 and NANOG co-stained (i.e., uncommitted) cells, shown as a ratio of the averaged total of inner cells (NANOG and/or GATA6 inner stained cells), in embryos cultured in KSOM **(e)** or KSOM + AA **(e′)** under indicated (see explanatory matrix, as in **Figure 4**) combined regimes of DMSO/SB220025 and NAC treatment from E3.5 to E4.5; KSOM **(e)**, left to right: DMSO (n = 12), p38-MAPK inhibition (n = 12), DMSO + 1 mM NAC (n = 11), p38-MAPK inhibition + 1 mM NAC (n = 10), DMSO + 10 mM NAC (n = 9) and p38-MAPK inhibition + 10 mM NAC (n = 10); KSOM + AA **(e′)**, left to right: DMSO (n = 37), p38-MAPK inhibition (n = 38), DMSO + 1 mM NAC (n = 20), p38-MAPK inhibition + 1 mM NAC (n = 22), DMSO + 10 mM NAC (n = 16) and p38-MAPK inhibition + 10 mM NAC (n = 11). Statistical test employed: Mann–Whitney test (GraphPad Prism 8). Unless otherwise stated, within the graphs as a distinct P-value (if statistically insignificant), the significance intervals are: P-value < 0.0001 (****), 0.0001 to 0.001 (***), 0.001 to 0.01 (**), and 0.01 to 0.05 (*). Data relating to each individual embryo assayed are detailed in **Supplementary Table S3**. A Welch's ANOVA statistical analysis of the data presented in this figure is presented in **Supplementary Table S5**. **(f)** Model: irrespective of exogenous AA media supplementation (i.e., KSOM ± AA), early (E3.5) stage blastocysts are able to appropriately specify and segregate ICM cell lineages (red EPI and blue PrE) by the late blastocyst (E4.5) stage. However, inhibition of p38-MAPK reveals derivation of ICM lineages from initially uncommitted progenitors (shown in gray) is differentially impaired in a manner dependent on exogenous AA media supplementation. Whereas in the presence of exogenous AA (KSOM + AA) it is only the PrE (and not EPI) that fails to specify, a complete absence of provided AA (KSOM) is associated with the majority of ICM cells (i.e., EPI and PrE progenitors) being retained in the uncommitted state by the late blastocyst (E4.5) stage, with reduced cell number and smaller cavities. Further supplementation of the anti-oxidant NAC is able to partially rescue the more severe phenotype associated with p38-MAPK inhibition in a subset of embryos cultured in KSOM media (to a point resembling p38-MAPK inhibition in KSOM + AA media; i.e., specified EPI, unspecified PrE), whereas NAC addition had no effect on the milder p38-MAPK inhibition phenotype observed in embryos cultured in KSOM + AA. Collectively, such data indicate a requirement for p38-MAPK to homeostatically buffer, AA depletion induced oxidative stress (caused by increased ROS levels), to allow germane blastocyst development and conditions conducive to EPI specification; however PrE specification and ultimate differentiation is governed by an, as yet unknown, but independent p38-MAPK mediated mechanism [downstream of FGF-signaling, as previously described (Thamodaran and Bruce, 2016)].

the described rescue phenotypes associated with concomitant p38-MAPK inhibition and NAC supplementation). Moreover, the data also suggest this anti-oxidant role is not extended to the pluripotent EPI and confirm that PrE differentiation, *per se,* is sensitive to oxidative stress. These data accord with our previous observations that p38-MAPK inhibition specifically impairs PrE cell-fate derivation, by preventing resolution of initially uncommitted cell fate states within early blastocyst ICMs, without significantly influencing EPI formation (Thamodaran and Bruce, 2016) (recapitulated here; KSOM + AA – **Figures 2**, **4**). However, the observed NAC-derived rescue effects were only partial when compared to average cell numbers recorded in the appropriate DMSO control groups, and with the exception of GATA4 + PrE derivation, were not further enhanced by the higher (10 mM) NAC concentration. Indeed, increased/rescued total, outer and PrE cell numbers in NAC treated p38-MAPK inhibited embryos, in the KSOM group, were only equivalent to those observed in the corresponding KSOM + AA conditions (**Figure 4**). This suggests further, as yet unknown, p38-MAPK regulated mechanisms (unrelated to oxidative stress) must also contribute to ensure appropriate numbers of total, outer (TE) and PrE cells during blastocyst maturation. However, the present data confirm the existence of at least a dual role of p38-MAPK during blastocyst maturation. Firstly, that concerned with homeostatic regulation of AA availability and associated oxidative stress and secondly, that by which p38-MAPK directly regulates PrE specification/differentiation, as previously described (Thamodaran and Bruce, 2016).

It is noteworthy that a study employing cancer cell line models reports p38-MAPK as elevating glucose uptake but shunting its metabolism away from glycolysis in favor of the pentose phosphate pathway to generate increased levels of NADPH that are required to counteract ROS (Desideri et al., 2014). Thus, it is tempting to speculate a similar mechanism to counteract ROS, under depleted AA conditions, may also be operative in the blastocyst. Interestingly, recently available preprint study data compellingly report the importance of blastocyst cavity expansion for PrE specification[2]; given such expansion requires a functioning TE (Madan et al., 2007), it is possible any impairment in TE cell number/function could negatively impact this process. Consistently, we have observed the blastocyst cavities of p38-MAPK inhibited blastocysts to be visibly smaller than controls (**Figures 1b–c′**; highlighted by black arrowheads), irrespective of AA supplementation status. Reports relating to glioblastoma cancer models have also clearly uncovered p38-MAPK dependant mechanisms of cell survival, involving induction of the *Cox2* gene (catalyzing the committed step in prostaglandin synthesis) (Parente et al., 2013) and that have been linked to AA starvation (Li et al., 2017). However, it is improbable p38-MAPK exerts a similar role in the mouse blastocyst ICM, as we were unable to detect any basal or induced, as the recognized mechanism of regulated expression (Smith et al., 2000), *Cox2* derived mRNA transcripts in either the control or experimental conditions (data not provided), again irrespective of KSOM media AA supplementation status. Lastly, we found the addition of NAC to p38-MAPK inhibited blastocysts under KSOM + AA culture conditions had no significant effects (**Figures 4b′–g′** and **Supplementary Table S5**), suggesting AA supplementation alone is sufficient to mitigate deleterious oxidative stresses (potentially caused by increased ROS production) associated with p38-MAPK inhibition. However, the fact p38-MAPK inhibition was still associated with significantly reduced total, outer and

[2]https://doi.org/10.1101/575282

PrE cell numbers further supports the existence of additional uncharacterized, yet p38-MAPK mediated, mechanism(s) of supporting appropriate blastocyst cell number.

p38-MAPK Dependent Homeostatic Regulation of Amino Acid Availability, and Associated Depletion Induced Oxidative Stress, Facilitates PrE Progenitor Specification From an Initially Uncommitted State of Cell Fate, During Blastocyst Maturation

Cells of maturing mouse blastocysts ICM (E3.5–E4.5) transit from an initially uncommitted state, expressing both NANOG (EPI) and GATA6 (PrE), via an intermediate stage whereby progenitors of each lineage express either marker in a randomly distributed and mutually exclusive manner (the so-called 'salt and pepper' pattern), culminating in the separated late blastocyst tissue layers [PrE having initiated further marker protein expression; e.g., SOX17 and GATA4 (Kuo et al., 1997; Chazaud et al., 2006; Niakan et al., 2010)]. We previously reported p38-MAPK inhibition during this developmental window significantly impairs PrE (GATA4 +), but not EPI (NANOG +), formation by retaining PrE progenitor cells in the uncommitted state (Thamodaran and Bruce, 2016). Given such experiments were performed in KSOM + AA, we now decided to also assay PrE specification from the uncommitted state in KSOM cultured blastocysts, in the presence/absence of NAC. Consistent with our previous study (Thamodaran and Bruce, 2016), the inhibition of p38-MAPK in blastocysts cultured in KSOM + AA was associated with increased numbers of uncommitted/PrE progenitor ICM cells (co-expressing NANOG and GATA6 – illustrated by an increase in the uncommitted cell:total ICM ratio – **Figure 5e′**). However, NAC supplementation resolved this uncommitted state to levels observed in corresponding DMSO treated controls (reaching significance at 10 mM NAC). These data suggest p38-MAPK inhibition in KSOM + AA media is associated with levels of oxidative stress, that represent an impediment to PrE progenitor specification in the blastocyst (i.e., *a* resolution of the uncommitted state by downregulating NANOG and maintaining GATA6 expression). Moreover, they invoke an endogenous anti-oxidant role for p38-MAPK that promotes PrE specification, although crucially such a role is not alone sufficient to ensure full differentiation as marked by GATA4 expression (discussed above – **Figure 4**). Whereas in KSOM cultured p38-MAPK inhibited blastocysts, the observed uncommitted ICM phenotype (NANOG and GATA6 co-expression) was much more robust (affecting virtually all ICM cells – i.e., progenitors of PrE and EPI alike; **Figures 5c,e**). Such data suggest a lack of AA supplementation itself, coupled with p38-MAPK inhibition, severely impairs resolution of the uncommitted state toward either PrE or EPI (even if some very limited initiation of GATA4 expression can occur later – **Figures 1**, **2**, **4**). This is opposed to the effect of p38-MAPK inhibition in KSOM + AA, whereby only resolution of uncommitted cells to PrE is impaired [**Figure 5e′** (Thamodaran and Bruce, 2016)]. Addition of NAC to DMSO treated control KSOM culture groups revealed that the antioxidant alone, in the absence of supplemented AAs, promotes resolution of the uncommitted state (reaching significance at 10 mM NAC), although as reference above this is not translated to full PrE differentiation (as marked by GATA4 expression – **Figures 1**, **2**, **4**). However, the effect is blunted under p38-MAPK inhibited conditions with only a sub-population of embryos resolving NANOG and GATA6 co-expression patterns (**Figures 5d,d′**).

Therefore, AA supplementation can ameliorate developmentally persistent, p38-MAPK inhibition associated, uncommitted ICM/PrE cell fates that can be further augmented by additional anti-oxidant treatment using NAC. As NAC mediated resolution of such p38-MAPK inhibition induced uncommitted states (affecting EPI and PrE progenitors) is not as efficient in the absence of exogenous AA, a PrE specification/differentiation promoting role of p38-MAPK, regulating appropriate amino acid homeostasis and counteracting oxidative stress, is further supported.

CONCLUSION

Our data reveal novel AA sensing and regulative/homeostatic buffering mechanisms, centered on p38-MAPK, that counteract oxidative stress and ensure germane mouse blastocyst development; manifest in appropriate cell number and resolution of uncommitted EPI/PrE progenitors within the ICM (summarized in **Figure 5f**). These findings resonate with DOHaD models, illustrating how varying nutritional status can place regulatory/metabolic burdens upon the early embryo, with consequences for the differentiation of an extraembryonic tissue, later relied upon during *in utero* development of the fetus. The results also provide important considerations for improved assisted reproductive technologies that necessitate *in vitro* human embryo culture.

DATA AVAILABILITY STATEMENT

All datasets generated for this study are included in the article/**Supplementary Material**.

ETHICS STATEMENT

The animal study was reviewed and approved by ethics committee of the Biology Centre (in České Budějovice) of the Czech Academy of Sciences and by the responsible committee of the Czech Academy of Sciences on the national level, in accordance with the Czech and European Union law.

AUTHOR CONTRIBUTIONS

PB, VT, and AB: project contributions and experimental design. PB and VT: practical research. PB and AŠ: western

blotting experiments. PB and AB: data analysis and manuscript preparation.

FUNDING

This work was supported by grants from the Czech Science Foundation/GAČR (18-02891S) and Grant Agency of the University of South Bohemia (GAJU; 012/2019/P).

ACKNOWLEDGMENTS

We acknowledge Institute of Parasitology, Biology Centre (in České Budějovice), Czech Academy of Sciences for housing mice, Marta Gajewska (Institute of Oncology, Warsaw, Poland) and Anna Piliszek (Institute of Genetics and Animal Breeding, Polish Academy of Sciences, Jastrzębiec, Poland) for founder CBA/W mice, Alena Krejčí (Faculty of Science, University of South Bohemia, Czechia) for pooling resources, and other members of our laboratory (LEMDB – particularly Lenka Gahurová) for valuable inputs and discussions.

SUPPLEMENTARY MATERIAL

The Supplementary Material for this article can be found online at: https://www.frontiersin.org/articles/10.3389/fcell.2019.00276/full#supplementary-material

FIGURE S1 | Projected confocal z-stack images of all blastocyst embryos stained with CellROX Green at E4.25 and imaged after fixation.

TABLE S1 | Quantification of total and NANOG and/or GATA4 expressing cell numbers for all analyzed embryos in KSOM +/− amino acids + DMSO or SB220025.

TABLE S2 | Quantification of total and NANOG and/or GATA4 expressing cell numbers for all analyzed embryos in KSOM +/− amino acids + DMSO or SB220025 + 1 or 10 mM NAC.

TABLE S3 | Quantification of total and NANOG and/or GATA6 expressing cell numbers for all analyzed embryos in KSOM +/− amino acids + DMSO or SB220025 + 1 or 10 mM NAC.

TABLE S4 | Antibodies used for immunofluorescence staining and western blotting.

TABLE S5 | Welch's ANOVA test results (corresponding to **Figures 4**, **5e,e'**).

TABLE S6 | Oligonucleotide primers used for Q-RT PCR (corresponding to **Figure 3h**).

REFERENCES

Bowling, S., Di Gregorio, A., Sancho, M., Pozzi, S., Aarts, M., Signore, M., et al. (2018). P53 and mTOR signalling determine fitness selection through cell competition during early mouse embryonic development. *Nat. Commun.* 9:1763. doi: 10.1038/s41467-018-04167-y

Brown, J. J., and Whittingham, D. G. (1991). The roles of pyruvate, lactate and glucose during preimplantation development of embryos from F1 hybrid mice in vitro. *Development* 112, 99–105.

Bulut-Karslioglu, A., Biechele, S., Jin, H., Macrae, T. A., Hejna, M., Gertsenstein, M., et al. (2016). Inhibition of mTOR induces a paused pluripotent state. *Nature* 540, 119–123. doi: 10.1038/nature20578

Cargnello, M., and Roux, P. P. (2011). Activation and function of the MAPKs and their substrates, the MAPK-activated protein kinases. *Microbiol. Mol. Biol. Rev.* 75, 50–83. doi: 10.1128/MMBR.00031-10

Casas-Terradellas, E., Tato, I., Bartrons, R., Ventura, F., and Rosa, J. L. (2008). ERK and p38 pathways regulate amino acid signalling. *Biochim. Biophys. Acta* 1783, 2241–2254. doi: 10.1016/j.bbamcr.2008.08.011

Chazaud, C., and Yamanaka, Y. (2016). Lineage specification in the mouse preimplantation embryo. *Development* 143, 1063–1074. doi: 10.1242/dev.128314

Chazaud, C., Yamanaka, Y., Pawson, T., and Rossant, J. (2006). Early lineage segregation between epiblast and primitive endoderm in mouse blastocysts through the Grb2-MAPK pathway. *Dev. Cell* 10, 615–624. doi: 10.1016/j.devcel.2006.02.020

Corcelle, E., Djerbi, N., Mari, M., Nebout, M., Fiorini, C., Fenichel, P., et al. (2007). Control of the autophagy maturation step by the MAPK ERK and p38: lessons from environmental carcinogens. *Autophagy* 3, 57–59. doi: 10.4161/auto.3424

Cuadrado, A., and Nebreda, A. R. (2010). Mechanisms and functions of p38 MAPK signalling. *Biochem. J.* 429, 403–417. doi: 10.1042/BJ20100323

Cully, M., Genevet, A., Warne, P., Treins, C., Liu, T., Bastien, J., et al. (2010). A role for p38 stress-activated protein kinase in regulation of cell growth via TORC1. *Mol. Cell. Biol.* 30, 481–495. doi: 10.1128/MCB.00688-09

Desideri, E., Vegliante, R., Cardaci, S., Nepravishta, R., Paci, M., and Ciriolo, M. R. (2014). MAPK14/p38alpha-dependent modulation of glucose metabolism affects ROS levels and autophagy during starvation. *Autophagy* 10, 1652–1665. doi: 10.4161/auto.29456

Fleming, T. P., Watkins, A. J., Sun, C., Velazquez, M. A., Smyth, N. R., and Eckert, J. J. (2015). Do little embryos make big decisions? How maternal dietary protein restriction can permanently change an embryo's potential, affecting adult health. *Reprod. Fertil. Dev.* 27, 684–692. doi: 10.1071/RD14455

Fleming, T. P., Watkins, A. J., Velazquez, M. A., Mathers, J. C., Prentice, A. M., Stephenson, J., et al. (2018). Origins of lifetime health around the time of conception: causes and consequences. *Lancet* 391, 1842–1852. doi: 10.1016/S0140-6736(18)30312-X

Frankenberg, S., Gerbe, F., Bessonnard, S., Belville, C., Pouchin, P., Bardot, O., et al. (2011). Primitive endoderm differentiates via a three-step mechanism involving Nanog and RTK signaling. *Dev. Cell* 21, 1005–1013. doi: 10.1016/j.devcel.2011.10.019

Frum, T., and Ralston, A. (2015). Cell signaling and transcription factors regulating cell fate during formation of the mouse blastocyst. *Trends Genet.* 31, 402–410. doi: 10.1016/j.tig.2015.04.002

Gutierrez-Uzquiza, A., Arechederra, M., Bragado, P., Aguirre-Ghiso, J. A., and Porras, A. (2012). p38alpha mediates cell survival in response to oxidative stress via induction of antioxidant genes: effect on the p70S6K pathway. *J. Biol. Chem.* 287, 2632–2642. doi: 10.1074/jbc.M111.323709

Harding, H. P., Zhang, Y., Zeng, H., Novoa, I., Lu, P. D., Calfon, M., et al. (2003). An integrated stress response regulates amino acid metabolism and resistance to oxidative stress. *Mol. Cell.* 11, 619–633. doi: 10.1016/s1097-2765(03)00105-9

Harvey, A. J. (2019). Mitochondria in early development: linking the microenvironment, metabolism and the epigenome. *Reproduction* 157, R159–R179. doi: 10.1530/REP-18-0431

Henson, S. M., Lanna, A., Riddell, N. E., Franzese, O., Macaulay, R., Griffiths, S. J., et al. (2014). p38 signaling inhibits mTORC1-independent autophagy in senescent human CD8(+) T cells. *J. Clin. Invest.* 124, 4004–4016. doi: 10.1172/JCI75051

Hornbeck, P. V., Kornhauser, J. M., Latham, V., Murray, B., Nandhikonda, V., Nord, A., et al. (2019). 15 years of PhosphoSitePlus(R): integrating post-translationally modified sites, disease variants and isoforms. *Nucleic Acids Res.* 47, D433–D441. doi: 10.1093/nar/gky1159

Jackson, J. R., Bolognese, B., Hillegass, L., Kassis, S., Adams, J., Griswold, D. E., et al. (1998). Pharmacological effects of SB 220025, a selective inhibitor of P38 mitogen-activated protein kinase, in angiogenesis and chronic inflammatory disease models. *J. Pharmacol. Exp. Ther.* 284, 687–692.

Kang, M., Piliszek, A., Artus, J., and Hadjantonakis, A. K. (2013). FGF4 is required for lineage restriction and salt-and-pepper distribution of primitive endoderm factors but not their initial expression in the mouse. *Development* 140, 267–279. doi: 10.1242/dev.084996

Kuo, C. T., Morrisey, E. E., Anandappa, R., Sigrist, K., Lu, M. M., Parmacek, M. S., et al. (1997). GATA4 transcription factor is required for ventral morphogenesis and heart tube formation. *Genes Dev.* 11, 1048–1060. doi: 10.1101/gad.11.8.1048

Kwong, W. Y., Miller, D. J., Ursell, E., Wild, A. E., Wilkins, A. P., Osmond, C., et al. (2006). Imprinted gene expression in the rat embryo-fetal axis is altered in response to periconceptional maternal low protein diet. *Reproduction* 132, 265–277. doi: 10.1530/rep.1.01038

Kwong, W. Y., Wild, A. E., Roberts, P., Willis, A. C., and Fleming, T. P. (2000). Maternal undernutrition during the preimplantation period of rat development causes blastocyst abnormalities and programming of postnatal hypertension. *Development* 127, 4195–4202.

Leese, H. J. (2012). Metabolism of the preimplantation embryo: 40 years on. *Reproduction* 143, 417–427. doi: 10.1530/REP-11-0484

Li, Z., Chang, C. M., Wang, L., Zhang, P., and Shu, H. G. (2017). Cyclooxygenase-2 induction by amino acid deprivation requires p38 mitogen-activated protein kinase in human glioma cells. *Cancer Invest.* 35, 237–247. doi: 10.1080/07357907.2017.1292517

Linares, J. F., Duran, A., Reina-Campos, M., Aza-Blanc, P., Campos, A., Moscat, J., et al. (2015). Amino acid activation of mtorc1 by a pb1-domain-driven kinase complex cascade. *Cell Rep.* 12, 1339–1352. doi: 10.1016/j.celrep.2015.07.045

Madan, P., Rose, K., and Watson, A. J. (2007). Na/K-ATPase beta1 subunit expression is required for blastocyst formation and normal assembly of trophectoderm tight junction-associated proteins. *J. Biol. Chem.* 282, 12127–12134. doi: 10.1074/jbc.m700696200

Mihajlovic, A. I., Thamodaran, V., and Bruce, A. W. (2015). The first two cell-fate decisions of preimplantation mouse embryo development are not functionally independent. *Sci. Rep.* 5:15034.

Moruno-Manchon, J. F., Perez-Jimenez, E., and Knecht, E. (2013). Glucose induces autophagy under starvation conditions by a p38 MAPK-dependent pathway. *Biochem. J.* 449, 497–506. doi: 10.1042/BJ20121122

Murphy, M. P. (2009). How mitochondria produce reactive oxygen species. *Biochem. J.* 417, 1–13. doi: 10.1042/BJ20081386

Niakan, K. K., Ji, H., Maehr, R., Vokes, S. A., Rodolfa, K. T., Sherwood, R. I., et al. (2010). Sox17 promotes differentiation in mouse embryonic stem cells by directly regulating extraembryonic gene expression and indirectly antagonizing self-renewal. *Genes Dev.* 24, 312–326. doi: 10.1101/gad.1833510

Nichols, J., Silva, J., Roode, M., and Smith, A. (2009). Suppression of Erk signalling promotes ground state pluripotency in the mouse embryo. *Development* 136, 3215–3222. doi: 10.1242/dev.038893

O'Brien, P. M. S., Wheeler, T., and Barker, D. J. P. (1999). *Fetal Programming: Influences on Development and Disease in Later Life*. London: RCOG Press, 414–421.

Parente, R., Trifiro, E., Cuozzo, F., Valia, S., Cirone, M., and Di Renzo, L. (2013). Cyclooxygenase-2 is induced by p38 MAPK and promotes cell survival. *Oncol. Rep.* 29, 1999–2004. doi: 10.3892/or.2013.2308

Remy, G., Risco, A. M., Inesta-Vaquera, F. A., Gonzalez-Teran, B., Sabio, G., Davis, R. J., et al. (2010). Differential activation of p38MAPK isoforms by MKK6 and MKK3. *Cell. Signal.* 22, 660–667. doi: 10.1016/j.cellsig.2009.11.020

Rossant, J. (2016). Making the mouse blastocyst: past, present, and future. *Curr. Top. Dev. Biol.* 117, 275–288. doi: 10.1016/bs.ctdb.2015.11.015

Smith, W. L., Dewitt, D. L., and Garavito, R. M. (2000). Cyclooxygenases: structural, cellular, and molecular biology. *Annu. Rev. Biochem.* 69, 145–182. doi: 10.1146/annurev.biochem.69.1.145

Sun, C., Denisenko, O., Sheth, B., Cox, A., Lucas, E. S., Smyth, N. R., et al. (2015). Epigenetic regulation of histone modifications and Gata6 gene expression induced by maternal diet in mouse embryoid bodies in a model of developmental programming. *BMC Dev. Biol.* 15:3. doi: 10.1186/s12861-015-0053-1

Sun, C., Velazquez, M. A., Marfy-Smith, S., Sheth, B., Cox, A., Johnston, D. A., et al. (2014). Mouse early extra-embryonic lineages activate compensatory endocytosis in response to poor maternal nutrition. *Development* 141, 1140–1150. doi: 10.1242/dev.103952

Thamodaran, V., and Bruce, A. W. (2016). p38 (Mapk14/11) occupies a regulatory node governing entry into primitive endoderm differentiation during preimplantation mouse embryo development. *Open Biol.* 6:160190. doi: 10.1098/rsob.160190

Trempolec, N., Dave-Coll, N., and Nebreda, A. R. (2013). SnapShot: p38 MAPK substrates. *Cell* 152:924-924.e1.

Vucetic, M., Cormerais, Y., Parks, S. K., and Pouyssegur, J. (2017). The central role of amino acids in cancer redox homeostasis: vulnerability points of the cancer redox code. *Front. Oncol.* 7:319. doi: 10.3389/fonc.2017.00319

Webber, J. L. (2010). Regulation of autophagy by p38alpha MAPK. *Autophagy* 6, 292–293. doi: 10.4161/auto.6.2.11128

Webber, J. L., and Tooze, S. A. (2010). Coordinated regulation of autophagy by p38alpha MAPK through mAtg9 and p38IP. *EMBO J.* 29, 27–40. doi: 10.1038/emboj.2009.321

Wu, X. N., Wang, X. K., Wu, S. Q., Lu, J., Zheng, M., Wang, Y. H., et al. (2011). Phosphorylation of raptor by p38beta participates in arsenite-induced mammalian target of rapamycin complex 1 (mTORC1) activation. *J. Biol. Chem.* 286, 31501–31511. doi: 10.1074/jbc.M111.233122

Yamanaka, Y., Lanner, F., and Rossant, J. (2010). FGF signal-dependent segregation of primitive endoderm and epiblast in the mouse blastocyst. *Development* 137, 715–724. doi: 10.1242/dev.043471

Conflict of Interest: The authors declare that the research was conducted in the absence of any commercial or financial relationships that could be construed as a potential conflict of interest.

Supplementary table S1: Quantification of total and NANOG and/or GATA4 expressing cell numbers for all analysed embryos in KSOM +/- amino acids + DMSO or SB220025

KSOM

DMSO

#	TOTAL NUMBER OF CELLS							Ratio of PrE/Total ICM	Ratio of Inner/ Outer cells
	Embryo	Double Negative	ICM						
			NANOG +ve	GATA4 +ve	NANOG/ GATA4 double +ve	PrE	Total		
1	55	51	4	0	0	0	4	0.00	0.08
2	74	55	10	2	7	2	19	0.11	0.35
3	97	77	11	9	0	9	20	0.45	0.26
4	85	65	12	7	1	7	20	0.35	0.31
5	73	58	12	3	0	3	15	0.20	0.26
6	77	57	13	7	0	7	20	0.35	0.35
7	86	72	6	5	3	5	14	0.36	0.19
8	78	58	9	10	1	10	20	0.50	0.34
9	88	59	19	6	4	6	29	0.21	0.49
10	96	84	12	0	0	0	12	0.00	0.14
11	96	78	8	10	0	10	18	0.56	0.23
12	93	79	10	3	1	3	14	0.21	0.18
13	81	58	16	6	1	6	23	0.26	0.40
14	102	91	7	4	0	4	11	0.36	0.12
15	98	77	9	12	0	12	21	0.57	0.27
16	72	55	11	4	2	4	17	0.24	0.31
17	85	58	13	12	2	12	27	0.44	0.47
18	24	9	10	4	1	4	15	0.27	1.67
19	87	67	11	6	3	6	20	0.30	0.30
20	83	65	9	5	4	5	18	0.28	0.28
21	61	45	7	3	6	3	16	0.19	0.36
22	87	71	9	6	1	6	16	0.38	0.23
23	90	74	9	7	0	7	16	0.44	0.22
24	72	55	9	8	0	8	17	0.47	0.31
25	79	62	8	8	1	8	17	0.47	0.27
26	97	79	9	9	0	9	18	0.50	0.23
27	83	61	10	11	1	11	22	0.50	0.36
28	70	53	10	6	1	6	17	0.35	0.32
29	83	63	9	11	0	11	20	0.55	0.32
30	81	63	10	8	0	8	18	0.44	0.29
31	63	48	9	5	1	5	15	0.33	0.31
32	82	62	11	9	0	9	20	0.45	0.32
33	84	70	8	6	0	6	14	0.43	0.20
34	77	60	11	6	0	6	17	0.35	0.28
35	82	65	6	11	0	11	17	0.65	0.26
36	106	86	9	11	0	11	20	0.55	0.23
37	92	68	9	14	1	14	24	0.58	0.35
38	101	79	12	10	0	10	22	0.45	0.28
39	118	91	15	12	0	12	27	0.44	0.30
40	75	63	4	5	3	5	12	0.42	0.19
41	65	51	12	2	0	2	14	0.14	0.27
42	70	60	5	3	2	3	10	0.30	0.17
43	65	52	6	2	5	2	13	0.15	0.25
44	77	63	8	5	1	5	14	0.36	0.22
45	92	79	8	4	1	4	13	0.31	0.16
46	48	39	4	0	5	0	9	0.00	0.23
47	79	61	9	8	1	8	18	0.44	0.30
48	81	61	12	8	0	8	20	0.40	0.33
49	67	55	7	5	0	5	12	0.42	0.22
50	83	66	11	6	0	6	17	0.35	0.26
51	60	54	4	2	0	2	6	0.33	0.11
52	44	31	12	0	1	0	13	0.00	0.42
53	108	79	16	11	2	11	29	0.38	0.37
54	75	53	10	9	3	9	22	0.41	0.42
55	70	59	10	0	1	0	11	0.00	0.19
56	75	60	5	9	1	9	15	0.60	0.25
57	73	50	15	8	0	8	23	0.35	0.46
58	93	63	16	10	4	10	30	0.33	0.48
59	79	61	12	4	2	4	18	0.22	0.30
60	70	52	8	10	0	10	18	0.56	0.35
61	97	78	11	5	3	5	19	0.26	0.24
62	89	73	9	7	0	7	16	0.44	0.22
63	82	67	11	2	2	2	15	0.13	0.22
64	92	80	10	1	1	1	12	0.08	0.15
65	82	55	15	10	2	10	27	0.37	0.49
66	87	60	24	3	0	3	27	0.11	0.45
67	88	65	9	11	3	11	23	0.48	0.35
68									
69									
70									
71									
72									
73									
74									
75									
76									
77									
78									
79									
80									
TOTAL	5404	4218	675	426	85	426	1186	22.89	20.48
AVERAGE	80.7	63.0	10.1	6.4	1.3	6.4	17.7	0.34	0.31
SEM	1.9	1.6	0.4	0.4	0.2	0.4	0.6	0.02	0.02

p38 Inhibited

#	TOTAL NUMBER OF CELLS							Ratio of PrE/Total ICM	Ratio of Inner/ Outer cells
	Embryo	Double Negative	ICM						
			NANOG +ve	GATA4 +ve	NANOG/ GATA4 double +ve	PrE	Total		
1	15	15	0	0	0	0	0	0.00	0.00
2	28	27	1	0	0	0	1	0.00	0.04
3	45	40	4	1	0	1	5	0.20	0.13
4	65	53	8	3	1	3	12	0.25	0.23
5	41	37	4	0	0	0	4	0.00	0.11
6	38	35	3	0	0	0	3	0.00	0.09
7	35	25	9	1	0	1	10	0.10	0.40
8	49	41	7	1	0	1	8	0.13	0.20
9	29	26	3	0	0	0	3	0.00	0.12
10	27	22	5	0	0	0	5	0.00	0.23
11	34	29	5	0	0	0	5	0.00	0.17
12	32	30	2	0	0	0	2	0.00	0.07
13	69	49	16	4	0	4	20	0.20	0.41
14	61	51	6	4	0	4	10	0.40	0.20
15	78	67	5	6	0	6	11	0.55	0.16
16	41	40	1	0	0	0	1	0.00	0.03
17	37	31	4	0	2	0	6	0.00	0.19
18	54	45	5	3	1	3	9	0.33	0.20
19	41	37	3	0	1	0	4	0.00	0.11
20	37	34	2	0	1	0	3	0.00	0.09
21	31	19	11	1	0	1	12	0.08	0.63
22	31	29	2	0	0	0	2	0.00	0.07
23	27	17	10	0	0	0	10	0.00	0.59
24	22	18	4	0	0	0	4	0.00	0.22
25	36	30	6	0	0	0	6	0.00	0.20
26	59	50	8	1	0	1	9	0.11	0.18
27	53	46	5	1	1	1	7	0.14	0.15
28	49	36	9	4	0	4	13	0.31	0.36
29	57	51	4	2	0	2	6	0.33	0.12
30	70	56	8	6	0	6	14	0.43	0.25
31	62	50	12	0	0	0	12	0.00	0.24
32	43	36	5	2	0	2	7	0.29	0.19
33	33	27	5	1	0	1	6	0.17	0.22
34	22	19	3	0	0	0	3	0.00	0.16
35	39	33	5	1	0	1	6	0.17	0.18
36	67	60	3	2	2	2	7	0.29	0.12
37	60	40	15	5	0	5	20	0.25	0.50
38	45	41	4	0	0	0	4	0.00	0.10
39	30	26	3	1	0	1	4	0.25	0.15
40	65	56	6	1	2	1	9	0.11	0.16
41	68	60	8	0	0	0	8	0.00	0.13
42	45	34	11	0	0	0	11	0.00	0.32
43	58	54	4	0	0	0	4	0.00	0.07
44	57	49	5	3	0	3	8	0.38	0.16
45	70	65	3	0	2	0	5	0.00	0.08
46	37	35	2	0	0	0	2	0.00	0.06
47	75	67	6	2	0	2	8	0.25	0.12
48	29	18	11	0	0	0	11	0.00	0.61
49	50	43	6	1	0	1	7	0.14	0.16
50	25	16	9	0	0	0	9	0.00	0.56
51	32	29	3	0	0	0	3	0.00	0.10
52	25	22	3	0	0	0	3	0.00	0.14
53	29	25	4	0	0	0	4	0.00	0.16
54	54	48	6	0	0	0	6	0.00	0.13
55	37	30	7	0	0	0	7	0.00	0.23
56	28	27	1	0	0	0	1	0.00	0.04
57	12	12	0	0	0	0	0	0.00	0.00
58	31	27	2	2	0	2	4	0.50	0.15
59	50	38	11	0	1	0	12	0.00	0.32
60	66	58	8	0	0	0	8	0.00	0.14
61	44	38	6	0	0	0	6	0.00	0.16
62	50	46	4	0	0	0	4	0.00	0.09
63	39	35	4	0	0	0	4	0.00	0.11
64	76	72	4	0	0	0	4	0.00	0.06
65	34	31	3	0	0	0	3	0.00	0.10
66	55	52	3	0	0	0	3	0.00	0.06
67	39	34	5	0	0	0	5	0.00	0.15
68	31	24	7	0	0	0	7	0.00	0.29
69	38	21	17	0	0	0	17	0.00	0.81
70	38	29	9	0	0	0	9	0.00	0.31
71	90	84	5	1	0	1	6	0.17	0.07
72	45	37	8	0	0	0	8	0.00	0.22
73	27	16	11	0	0	0	11	0.00	0.69
74	40	35	5	0	0	0	5	0.00	0.14
75	37	30	5	0	2	0	7	0.00	0.23
76	52	43	9	0	0	0	9	0.00	0.21
77	45	34	11	0	0	0	11	0.00	0.32
78									
79									
80									
TOTAL	3415	2892	447	60	16	60	523	6.51	15.63
AVERAGE	44.4	37.6	5.8	0.8	0.2	0.8	6.8	0.08	0.20
SEM	1.8	1.7	0.4	0.2	0.1	0.2	0.5	0.02	0.02

Supplementary table S1 (contd.)

KSOM with amino acids

DMSO

#	TOTAL NUMBER OF CELLS							Ratio of PrE/Total ICM	Ratio of Inner/ Outer cells
	Embryo	Double Negative	ICM						
			NANOG +ve	GATA4 +ve	NANOG/ GATA4 double +ve	PrE	Total		
1	52	34	17	0	1	0	18	0.00	0.53
2	84	67	9	8	0	8	17	0.47	0.25
3	68	51	15	2	0	2	17	0.12	0.33
4	83	69	7	7	0	7	14	0.50	0.20
5	66	57	8	1	0	1	9	0.11	0.16
6	87	73	9	5	0	5	14	0.36	0.19
7	59	50	8	1	0	1	9	0.11	0.18
8	74	62	11	1	0	1	12	0.08	0.19
9	81	59	16	4	2	4	22	0.18	0.37
10	66	48	10	7	1	7	18	0.39	0.38
11	75	61	7	7	0	7	14	0.50	0.23
12	61	48	7	6	0	6	13	0.46	0.27
13	78	64	10	3	1	3	14	0.21	0.22
14	74	60	6	8	0	8	14	0.57	0.23
15	71	48	11	12	0	12	23	0.52	0.48
16	78	62	7	8	1	8	16	0.50	0.26
17	79	66	6	4	3	4	13	0.31	0.20
18	84	61	10	12	1	12	23	0.52	0.38
19	44	35	4	3	2	3	9	0.33	0.26
20	91	70	14	7	0	7	21	0.33	0.30
21	76	67	5	3	1	3	9	0.33	0.13
22	78	63	10	5	0	5	15	0.33	0.24
23	93	75	10	7	1	7	18	0.39	0.24
24	96	66	16	14	0	14	30	0.47	0.45
25	76	48	11	17	0	17	28	0.61	0.58
26	80	59	8	13	0	13	21	0.62	0.36
27	90	80	5	5	0	5	10	0.50	0.13
28	72	57	10	5	0	5	15	0.33	0.26
29	83	64	12	7	0	7	19	0.37	0.30
30	95	69	13	12	1	12	26	0.46	0.38
31	82	62	10	9	1	9	20	0.45	0.32
32	69	58	8	2	1	2	11	0.18	0.19
33	88	71	13	4	0	4	17	0.24	0.24
34	77	66	3	8	0	8	11	0.73	0.17
35	84	60	9	15	0	15	24	0.63	0.40
36	86	62	14	9	1	9	24	0.38	0.39
37	89	70	13	6	0	6	19	0.32	0.27
38	72	58	11	1	2	1	14	0.07	0.24
39	58	48	6	4	0	4	10	0.40	0.21
40	73	52	6	15	0	15	21	0.71	0.40
41	85	63	15	5	2	5	22	0.23	0.35
42	90	67	7	15	1	15	23	0.65	0.34
43	85	67	9	7	2	7	18	0.39	0.27
44	117	98	11	7	1	7	19	0.37	0.19
45	84	74	6	4	0	4	10	0.40	0.14
46	88	69	10	8	1	8	19	0.42	0.28
47	107	89	11	7	0	7	18	0.39	0.20
48	98	68	12	16	2	16	30	0.53	0.44
49	94	81	11	1	1	1	13	0.08	0.16
50	90	67	16	7	0	7	23	0.30	0.34
51	80	60	10	8	2	8	20	0.40	0.33
52	79	57	8	12	2	12	22	0.55	0.39
53	93	71	19	3	0	3	22	0.14	0.31
54	66	45	18	3	0	3	21	0.14	0.47
55	101	74	14	11	2	11	27	0.41	0.36
56	72	55	12	5	0	5	17	0.29	0.31
57	83	57	15	9	2	9	26	0.35	0.46
58	71	40	21	5	5	5	31	0.16	0.78
59	92	73	8	7	4	7	19	0.37	0.26
60	78	58	11	3	6	3	20	0.15	0.34
61	80	60	13	7	0	7	20	0.35	0.33
62	77	56	10	11	0	11	21	0.52	0.38
63	60	40	20	0	0	0	20	0.00	0.50
64	78	69	6	3	0	3	9	0.33	0.13
65	95	75	8	9	3	9	20	0.45	0.27
66	106	88	13	4	1	4	18	0.22	0.20
67	80	62	8	8	2	8	18	0.44	0.29
68	111	82	12	17	0	17	29	0.59	0.35
69	110	88	10	12	0	12	22	0.55	0.25
70	76	59	10	7	0	7	17	0.41	0.29
71	96	76	10	10	0	10	20	0.50	0.26
72									
73									
74									
75									
76									
77									
78									
79									
80									
TOTAL	5794	4488	749	498	59	498	1306	26.17	21.48
AVERAGE	81.6	63.2	10.5	7.0	0.8	7.0	18.4	0.37	0.30
SEM	1.6	1.5	0.4	0.5	0.1	0.5	0.7	0.02	0.01

p38 Inhibited

#	TOTAL NUMBER OF CELLS							Ratio of PrE/Total ICM	Ratio of Inner/ Outer cells
	Embryo	Double Negative	ICM						
			NANOG +ve	GATA4 +ve	NANOG/ GATA4 double +ve	PrE	Total		
1	79	71	7	0	1	0	8	0.00	0.11
2	66	55	8	3	0	3	11	0.27	0.20
3	63	49	11	3	0	3	14	0.21	0.29
4	59	53	5	0	1	0	6	0.00	0.11
5	52	45	6	1	0	1	7	0.14	0.16
6	54	47	5	0	2	0	7	0.00	0.15
7	56	49	6	1	0	1	7	0.14	0.14
8	46	38	8	0	0	0	8	0.00	0.21
9	47	42	5	0	0	0	5	0.00	0.12
10	53	43	6	3	1	3	10	0.30	0.23
11	36	27	6	1	2	1	9	0.11	0.33
12	70	56	10	3	1	3	14	0.21	0.25
13	55	46	7	2	0	2	9	0.22	0.20
14	46	38	5	0	3	0	8	0.00	0.21
15	56	49	5	1	1	1	7	0.14	0.14
16	47	37	9	1	0	1	10	0.10	0.27
17	62	52	7	3	0	3	10	0.30	0.19
18	57	42	14	1	0	1	15	0.07	0.36
19	55	44	9	1	1	1	11	0.09	0.25
20	51	42	9	0	0	0	9	0.00	0.21
21	53	42	8	2	1	2	11	0.18	0.26
22	78	60	9	8	1	8	18	0.44	0.30
23	61	56	5	0	0	0	5	0.00	0.09
24	45	40	5	0	0	0	5	0.00	0.13
25	51	37	14	0	0	0	14	0.00	0.38
26	45	34	10	1	0	1	11	0.09	0.32
27	53	46	5	1	1	1	7	0.14	0.15
28	62	51	8	3	0	3	11	0.27	0.22
29	55	40	9	5	1	5	15	0.33	0.38
30	58	50	6	2	0	2	8	0.25	0.16
31	64	54	7	0	3	0	10	0.00	0.19
32	78	65	11	2	0	2	13	0.15	0.20
33	65	48	9	8	0	8	17	0.47	0.35
34	35	29	6	0	0	0	6	0.00	0.21
35	73	53	15	5	0	5	20	0.25	0.38
36	71	48	23	0	0	0	23	0.00	0.48
37	77	57	10	10	0	10	20	0.50	0.35
38	61	50	10	1	0	1	11	0.09	0.22
39	75	65	7	3	0	3	10	0.30	0.15
40	62	43	16	3	0	3	19	0.16	0.44
41	61	47	12	2	0	2	14	0.14	0.30
42	79	66	9	4	0	4	13	0.31	0.20
43	23	18	5	0	0	0	5	0.00	0.28
44	68	54	9	4	1	4	14	0.29	0.26
45	68	59	5	4	0	4	9	0.44	0.15
46	57	43	9	5	0	5	14	0.36	0.33
47	63	50	13	0	0	0	13	0.00	0.26
48	64	59	5	0	0	0	5	0.00	0.08
49	66	55	10	1	0	1	11	0.09	0.20
50	52	44	4	3	1	3	8	0.38	0.18
51	68	61	7	0	0	0	7	0.00	0.11
52	66	50	15	1	0	1	16	0.06	0.32
53	60	49	7	2	2	2	11	0.18	0.22
54	49	37	12	0	0	0	12	0.00	0.32
55	57	50	7	0	0	0	7	0.00	0.14
56	85	60	16	8	1	8	25	0.32	0.42
57	63	54	8	0	1	0	9	0.00	0.17
58	71	60	11	0	0	0	11	0.00	0.18
59	53	34	18	0	1	0	19	0.00	0.56
60	51	48	3	0	0	0	3	0.00	0.06
61	49	39	9	1	0	1	10	0.10	0.26
62	35	27	7	1	0	1	8	0.13	0.30
63	45	28	17	0	0	0	17	0.00	0.61
64	71	59	8	1	3	1	12	0.08	0.20
65	55	49	5	1	0	1	6	0.17	0.12
66	59	29	30	0	0	0	30	0.00	1.03
67	43	24	19	0	0	0	19	0.00	0.79
68	52	44	5	2	1	2	8	0.25	0.18
69	55	34	20	0	1	0	21	0.00	0.62
70	66	56	10	0	0	0	10	0.00	0.18
71	65	50	11	4	0	4	15	0.27	0.30
72	62	49	11	2	0	2	13	0.15	0.27
73	48	36	12	0	0	0	12	0.00	0.33
74	85	69	6	10	0	10	16	0.63	0.23
75	73	56	14	1	2	1	17	0.06	0.30
76	76	54	11	11	0	11	22	0.50	0.41
77									
78									
79									
80									
TOTAL	4495	3594	721	146	34	146	901	10.86	20.37
AVERAGE	59.1	47.3	9.5	1.9	0.4	1.9	11.9	0.14	0.27
SEM	1.4	1.2	0.5	0.3	0.1	0.3	0.6	0.02	0.02

Supplementary table S2: Quantification of total and NANOG and/or GATA4 expressing cell numbers for all analysed embryos in KSOM +/- amino acids + DMSO or SB220025 + 1 or 10mM NAC

KSOM + 1mM NAC

DMSO

#	TOTAL NUMBER OF CELLS							Ratio of PrE/Total ICM	Ratio of Inner/ Outer cells
			ICM						
	Embryo	Double Negative	NANOG +ve	GATA4 +ve	NANOG/ GATA4 double +ve	PrE	Total		
1	82	63	8	11	0	11	19	0.58	0.30
2	65	63	2	0	0	0	2	0.00	0.03
3	38	28	9	0	1	0	10	0.00	0.36
4	70	49	11	10	0	10	21	0.48	0.43
5	70	60	6	4	0	4	10	0.40	0.17
6	71	53	10	8	0	8	18	0.44	0.34
7	89	73	10	6	0	6	16	0.38	0.22
8	83	70	5	6	2	6	13	0.46	0.19
9	95	80	7	8	0	8	15	0.53	0.19
10	96	82	9	5	0	5	14	0.36	0.17
11	88	73	9	6	0	6	15	0.40	0.21
12	74	68	3	3	0	3	6	0.50	0.09
13	85	60	12	13	0	13	25	0.52	0.42
14	98	69	16	13	0	13	29	0.45	0.42
15	111	79	21	11	0	11	32	0.34	0.41
16	80	65	12	3	0	3	15	0.20	0.23
17	77	57	14	5	1	5	20	0.25	0.35
18	97	75	13	8	1	8	22	0.36	0.29
19	73	51	17	2	3	2	22	0.09	0.43
20	70	43	14	10	3	10	27	0.37	0.63
21	91	68	13	10	0	10	23	0.43	0.34
22	62	50	7	2	3	2	12	0.17	0.24
23	75	47	18	9	1	9	28	0.32	0.60
24	91	73	10	7	1	7	18	0.39	0.25
25	64	52	6	6	0	6	12	0.50	0.23
26	84	71	8	4	1	4	13	0.31	0.18
27	77	58	11	8	0	8	19	0.42	0.33
28	84	70	9	5	0	5	14	0.36	0.20
29									
30									
31									
32									
33									
34									
35									
36									
37									
38									
39									
40									
TOTAL	2240	1750	290	183	17	183	490	10.01	8.22
AVERAGE	80.0	62.5	10.4	6.5	0.6	6.5	17.5	0.36	0.29
SEM	2.7	2.4	0.8	0.7	0.2	0.7	1.3	0.03	0.03

p38 Inhibited

#	TOTAL NUMBER OF CELLS							Ratio of PrE/Total ICM	Ratio of Inner/ Outer cells
			ICM						
	Embryo	Double Negative	NANOG +ve	GATA4 +ve	NANOG/ GATA4 double +ve	PrE	Total		
1	43	41	2	0	0	0	2	0.00	0.05
2	42	36	4	2	0	2	6	0.33	0.17
3	46	43	3	0	0	0	3	0.00	0.07
4	63	56	5	2	0	2	7	0.29	0.13
5	58	48	10	0	0	0	10	0.00	0.21
6	27	16	11	0	0	0	11	0.00	0.69
7	38	36	2	0	0	0	2	0.00	0.06
8	56	48	8	0	0	0	8	0.00	0.17
9	34	25	6	3	0	3	9	0.33	0.36
10	51	37	9	5	0	5	14	0.36	0.38
11	29	11	18	0	0	0	18	0.00	1.64
12	48	43	3	2	0	2	5	0.40	0.12
13	34	30	4	0	0	0	4	0.00	0.13
14	35	29	6	0	0	0	6	0.00	0.21
15	52	46	2	3	1	3	6	0.50	0.13
16	58	47	9	2	0	2	11	0.18	0.23
17	41	34	5	2	0	2	7	0.29	0.21
18	67	53	8	6	0	6	14	0.43	0.26
19	67	62	5	0	0	0	5	0.00	0.08
20	70	54	14	2	0	2	16	0.13	0.30
21	77	63	9	5	0	5	14	0.36	0.22
22	43	29	11	1	2	1	14	0.07	0.48
23	58	50	6	0	2	0	8	0.00	0.16
24	92	78	9	4	1	4	14	0.29	0.18
25	71	61	5	5	0	5	10	0.50	0.16
26	55	46	7	2	0	2	9	0.22	0.20
27	47	40	6	0	1	0	7	0.00	0.18
28	78	67	11	0	0	0	11	0.00	0.16
29	83	81	2	0	0	0	2	0.00	0.02
30	81	70	7	4	0	4	11	0.36	0.16
31	47	46	1	0	0	0	1	0.00	0.02
32	45	38	7	0	0	0	7	0.00	0.18
33	75	67	4	4	0	4	8	0.50	0.12
34	65	61	2	2	0	2	4	0.50	0.07
35	60	51	9	0	0	0	9	0.00	0.18
36	70	63	4	3	0	3	7	0.43	0.11
37	60	51	9	0	0	0	9	0.00	0.18
38	59	59	0	0	0	0	0	0.00	0.00
39									
40									
TOTAL	2125	1816	243	59	7	59	309	6.46	8.35
AVERAGE	55.9	47.8	6.4	1.6	0.2	1.6	8.1	0.17	0.22
SEM	2.6	2.6	0.6	0.3	0.1	0.3	0.7	0.03	0.04

KSOM + 10mM NAC

DMSO

#	TOTAL NUMBER OF CELLS							Ratio of PrE/Total ICM	Ratio of Inner/ Outer cells
			ICM						
	Embryo	Double Negative	NANOG +ve	GATA4 +ve	NANOG/ GATA4 double +ve	PrE	Total		
1	57	39	10	8	0	8	18	0.44	0.46
2	75	53	16	6	0	6	22	0.27	0.42
3	74	58	9	7	0	7	16	0.44	0.28
4	77	59	15	3	0	3	18	0.17	0.31
5	43	38	5	0	0	0	5	0.00	0.13
6	57	48	3	5	1	5	9	0.56	0.19
7	51	40	11	0	0	0	11	0.00	0.28
8	55	41	10	4	0	4	14	0.29	0.34
9	103	83	10	8	2	8	20	0.40	0.24
10	81	60	10	11	0	11	21	0.52	0.35
11	82	61	9	11	1	11	21	0.52	0.34
12	95	78	7	10	0	10	17	0.59	0.22
13	83	72	8	3	0	3	11	0.27	0.15
14	93	75	9	9	0	9	18	0.50	0.24
15	83	66	9	8	0	8	17	0.47	0.26
16	102	86	7	9	0	9	16	0.56	0.19
17	72	48	12	12	0	12	24	0.50	0.50
18									
19									
20									
TOTAL	1283	1005	160	114	4	114	278	6.50	4.88
AVERAGE	75.5	59.1	9.4	6.7	0.2	6.7	16.4	0.38	0.29
SEM	4.3	3.8	0.8	0.9	0.1	0.9	1.2	0.05	0.03

p38 Inhibited

#	TOTAL NUMBER OF CELLS							Ratio of PrE/Total ICM	Ratio of Inner/ Outer cells
			ICM						
	Embryo	Double Negative	NANOG +ve	GATA4 +ve	NANOG/ GATA4 double +ve	PrE	Total		
1	30	27	3	0	0	0	3	0.00	0.11
2	61	56	2	3	0	3	5	0.60	0.09
3	45	35	6	4	0	4	10	0.40	0.29
4	52	37	9	2	4	2	15	0.13	0.41
5	40	32	4	4	0	4	8	0.50	0.25
6	50	44	6	0	0	0	6	0.00	0.14
7	49	45	4	0	0	0	4	0.00	0.09
8	52	39	6	6	1	6	13	0.46	0.33
9	68	55	9	4	0	4	13	0.31	0.24
10	90	74	8	8	0	8	16	0.50	0.22
11	69	61	8	0	0	0	8	0.00	0.13
12	78	59	13	6	0	6	19	0.32	0.32
13	62	52	10	0	0	0	10	0.00	0.19
14	47	39	6	2	0	2	8	0.25	0.21
15	81	67	8	6	0	6	14	0.43	0.21
16	72	64	7	1	0	1	8	0.13	0.13
17	52	45	5	2	0	2	7	0.29	0.16
18	36	25	8	3	0	3	11	0.27	0.44
19									
20									
TOTAL	1034	856	122	51	5	51	178	4.58	3.93
AVERAGE	57.4	47.6	6.8	2.8	0.3	2.8	9.9	0.25	0.22
SEM	3.8	3.3	0.6	0.6	0.2	0.6	1.0	0.05	0.02

Supplementary table S2 (contd.)

KSOM+AA + 1mM NAC

DMSO

#	TOTAL NUMBER OF CELLS							Ratio of PrE/Total ICM	Ratio of Inner/ Outer cells
	Embryo	Double Negative	ICM						
			NANOG +ve	GATA4 +ve	NANOG/ GATA4 double +ve	PrE	Total		
1	97	75	12	9	1	9	22	0.41	0.29
2	87	77	7	1	2	1	10	0.10	0.13
3	49	33	10	3	3	3	16	0.19	0.48
4	45	30	11	1	3	1	15	0.07	0.50
5	68	56	9	2	1	2	12	0.17	0.21
6	78	50	17	11	0	11	28	0.39	0.56
7	78	62	10	5	1	5	16	0.31	0.26
8	56	53	3	0	0	0	3	0.00	0.06
9	68	45	16	5	2	5	23	0.22	0.51
10	91	73	6	12	0	12	18	0.67	0.25
11	78	57	13	8	0	8	21	0.38	0.37
12	89	68	5	12	4	12	21	0.57	0.31
13	93	77	9	7	0	7	16	0.44	0.21
14	88	63	6	18	1	18	25	0.72	0.40
15	73	47	13	9	4	9	26	0.35	0.55
16	67	46	19	2	0	2	21	0.10	0.46
17	79	67	9	3	0	3	12	0.25	0.18
18	100	76	13	11	0	11	24	0.46	0.32
19	93	75	9	8	1	8	18	0.44	0.24
20	90	66	17	7	0	7	24	0.29	0.36
21									
22									
23									
24									
25									
26									
27									
28									
29									
30									
31									
32									
33									
34									
35									
36									
37									
38									
39									
40									
TOTAL	1567	1196	214	134	23	134	371	6.52	6.64
AVERAGE	78.4	59.8	10.7	6.7	1.2	6.7	18.6	0.33	0.33
SEM	3.5	3.2	1.0	1.1	0.3	1.1	1.4	0.04	0.03

p38 Inhibited

#	TOTAL NUMBER OF CELLS							Ratio of PrE/Total ICM	Ratio of Inner/ Outer cells
	Embryo	Double Negative	ICM						
			NANOG +ve	GATA4 +ve	NANOG/ GATA4 double +ve	PrE	Total		
1	79	68	5	6	0	6	11	0.55	0.16
2	57	43	12	2	0	2	14	0.14	0.33
3	63	42	15	5	1	5	21	0.24	0.50
4	66	57	9	0	0	0	9	0.00	0.16
5	60	45	12	3	0	3	15	0.20	0.33
6	81	73	2	6	0	6	8	0.75	0.11
7	95	79	9	6	1	6	16	0.38	0.20
8	59	46	13	0	0	0	13	0.00	0.28
9	13	8	5	0	0	0	5	0.00	0.63
10	76	68	3	5	0	5	8	0.63	0.12
11	28	11	17	0	0	0	17	0.00	1.55
12	96	84	8	4	0	4	12	0.33	0.14
13	76	61	9	4	2	4	15	0.27	0.25
14	71	55	16	0	0	0	16	0.00	0.29
15	45	37	8	0	0	0	8	0.00	0.22
16	58	44	14	0	0	0	14	0.00	0.32
17	85	72	13	0	0	0	13	0.00	0.18
18	60	47	11	2	0	2	13	0.15	0.28
19	80	71	6	3	0	3	9	0.33	0.13
20	63	55	7	1	0	1	8	0.13	0.15
21	62	49	5	8	0	8	13	0.62	0.27
22	22	19	3	0	0	0	3	0.00	0.16
23									
24									
25									
26									
27									
28									
29									
30									
31									
32									
33									
34									
35									
36									
37									
38									
39									
40									
TOTAL	1395	1134	202	55	4	55	261	4.70	6.73
AVERAGE	63.4	51.5	9.2	2.5	0.2	2.5	11.9	0.21	0.31
SEM	4.6	4.4	0.9	0.6	0.1	0.6	0.9	0.05	0.06

KSOM+AA + 10mM NAC

DMSO

#	TOTAL NUMBER OF CELLS							Ratio of PrE/Total ICM	Ratio of Inner/ Outer cells
	Embryo	Double Negative	ICM						
			NANOG +ve	GATA4 +ve	NANOG/ GATA4 double +ve	PrE	Total		
1	84	61	17	6	0	6	23	0.26	0.38
2	64	54	9	1	0	1	10	0.10	0.19
3	66	41	21	3	1	3	25	0.12	0.61
4	66	40	21	1	4	1	26	0.04	0.65
5	95	67	16	12	0	12	28	0.43	0.42
6	58	38	16	3	1	3	20	0.15	0.53
7	82	65	7	10	0	10	17	0.59	0.26
8	92	76	6	10	0	10	16	0.63	0.21
9	45	35	5	4	1	4	10	0.40	0.29
10	70	55	7	7	1	7	15	0.47	0.27
11	68	57	7	4	0	4	11	0.36	0.19
12	57	45	7	3	2	3	12	0.25	0.27
13	91	75	9	7	0	7	16	0.44	0.21
14	93	78	8	6	1	6	15	0.40	0.19
15	84	64	8	11	1	11	20	0.55	0.31
16	85	65	10	8	2	8	20	0.40	0.31
17	69	59	10	0	0	0	10	0.00	0.17
18	71	56	7	6	2	6	15	0.40	0.27
19	94	72	11	11	0	11	22	0.50	0.31
20									
TOTAL	1434	1103	202	113	16	113	331	6.48	6.03
AVERAGE	75.5	58.1	10.6	5.9	0.8	5.9	17.4	0.34	0.32
SEM	3.4	3.0	1.2	0.8	0.2	0.8	1.3	0.04	0.03

p38 Inhibited

#	TOTAL NUMBER OF CELLS							Ratio of PrE/Total ICM	Ratio of Inner/ Outer cells
	Embryo	Double Negative	ICM						
			NANOG +ve	GATA4 +ve	NANOG/ GATA4 double +ve	PrE	Total		
1	52	30	22	0	0	0	22	0.00	0.73
2	51	32	15	4	0	4	19	0.21	0.59
3	67	48	18	1	0	1	19	0.05	0.40
4	58	52	6	0	0	0	6	0.00	0.12
5	55	41	11	1	2	1	14	0.07	0.34
6	77	66	4	7	0	7	11	0.64	0.17
7	84	71	7	2	4	2	13	0.15	0.18
8	61	45	13	3	0	3	16	0.19	0.36
9	65	48	12	5	0	5	17	0.29	0.35
10	25	19	6	0	0	0	6	0.00	0.32
11	53	44	5	3	1	3	9	0.33	0.20
12	63	46	12	3	2	3	17	0.18	0.37
13	97	80	9	8	0	8	17	0.47	0.21
14	60	49	11	0	0	0	11	0.00	0.22
15	81	66	11	4	0	4	15	0.27	0.23
16	74	57	13	4	0	4	17	0.24	0.30
17	67	58	9	0	0	0	9	0.00	0.16
18	81	58	11	12	0	12	23	0.52	0.40
19	74	65	7	1	1	1	9	0.11	0.14
20	106	90	9	7	0	7	16	0.44	0.18
TOTAL	1351	1065	211	65	10	65	286	4.16	5.96
AVERAGE	67.6	53.3	10.6	3.3	0.5	3.3	14.3	0.21	0.30
SEM	4.0	3.8	1.0	0.7	0.2	0.7	1.1	0.04	0.03

Supplementary table S3: Quantification of total and NANOG and/or GATA6 expressing cell numbers for all analysed embryos in KSOM +/- amino acids + DMSO or SB220025 + 1 or 10mM NAC

KSOM

DMSO

#	TOTAL NUMBER OF CELLS		ICM				Ratio of NANOG-GATA6 double +ve/Total ICM
	Embryo	Double Negative	NANOG +ve	NANOG-GATA6 double +ve	PrE	Total	
1	75	63	4	6	5	12	0.50
2	65	51	12	9	2	14	0.64
3	70	60	5	4	3	10	0.40
4	65	52	6	11	2	13	0.85
5	70	52	8	4	10	18	0.22
6	97	78	11	8	5	19	0.42
7	89	73	9	4	7	16	0.25
8	82	67	11	6	2	15	0.40
9	92	80	10	3	1	12	0.25
10	82	55	15	8	10	27	0.30
11	87	60	24	23	3	27	0.85
12	88	65	9	7	11	23	0.30
13							
14							
15							
TOTAL	962	756	124	93	61	206	5.38
AVERAGE	80.2	63.0	10.3	7.8	5.1	17.2	0.45
SEM	3.1	2.9	1.5	1.5	1.0	1.7	0.06

p38 Inhibited

#	TOTAL NUMBER OF CELLS		ICM				Ratio of NANOG-GATA6 double +ve/Total ICM
	Embryo	Double Negative	NANOG +ve	NANOG-GATA6 double +ve	PrE	Total	
1	70	65	3	5	0	5	1.00
2	37	35	2	2	0	2	1.00
3	75	67	6	5	2	8	0.63
4	38	21	17	17	0	17	1.00
5	38	29	9	9	0	9	1.00
6	90	84	5	2	1	6	0.33
7	45	37	8	8	0	8	1.00
8	27	16	11	11	0	11	1.00
9	40	35	5	5	0	5	1.00
10	37	30	5	7	0	7	1.00
11	52	43	9	9	0	9	1.00
12	45	34	11	11	0	11	1.00
13							
14							
15							
TOTAL	594	496	91	91	3	98	10.96
AVERAGE	49.5	41.3	7.6	7.6	0.3	8.2	0.91
SEM	5.5	5.9	1.2	1.2	0.2	1.1	0.06

KSOM with amino acids

DMSO

#	TOTAL NUMBER OF CELLS		ICM				Ratio of NANOG-GATA6 double +ve/Total ICM
	Embryo	Double Negative	NANOG +ve	NANOG-GATA6 double +ve	PrE	Total	
1	84	60	9	0	15	24	0.00
2	86	62	14	11	9	24	0.46
3	89	70	13	4	6	19	0.21
4	72	58	11	8	1	14	0.57
5	58	48	6	2	4	10	0.20
6	73	52	6	2	15	21	0.10
7	85	63	15	7	5	22	0.32
8	90	67	7	2	15	23	0.09
9	85	67	9	6	7	18	0.33
10	117	98	11	4	7	19	0.21
11	84	74	6	2	4	10	0.20
12	88	69	10	3	8	19	0.16
13	107	89	11	2	7	18	0.11
14	98	68	12	3	16	30	0.10
15	94	81	11	9	1	13	0.69
16	90	67	16	6	7	23	0.26
17	80	60	10	7	8	20	0.35
18	79	57	8	3	12	22	0.14
19	93	71	19	14	3	22	0.64
20	66	45	18	4	3	21	0.19
21	101	74	14	2	11	27	0.07
22	72	55	12	3	5	17	0.18
23	83	57	15	7	9	26	0.27
24	71	40	21	14	5	31	0.45
25	92	73	8	5	7	19	0.26
26	78	58	11	8	3	20	0.40
27	80	60	13	0	7	20	0.00
28	77	56	10	2	11	21	0.10
29	60	40	20	11	0	20	0.55
30	78	69	6	0	3	9	0.00
31	95	75	8	6	9	20	0.30
32	106	88	13	6	4	18	0.33
33	80	62	8	2	8	18	0.11
34	111	82	12	0	17	29	0.00
35	110	88	10	1	12	22	0.05
36	76	59	10	6	7	17	0.35
37	96	76	10	3	10	20	0.15
38							
39							
40							
TOTAL	3184	2438	423	175	281	746	8.89
AVERAGE	86.1	65.9	11.4	4.7	7.6	20.2	0.24
SEM	2.3	2.2	0.6	0.6	0.7	0.8	0.03

p38 Inhibited

#	TOTAL NUMBER OF CELLS		ICM				Ratio of NANOG-GATA6 double +ve/Total ICM
	Embryo	Double Negative	NANOG +ve	NANOG-GATA6 double +ve	PrE	Total	
1	75	65	7	1	3	10	0.10
2	62	43	16	4	3	19	0.21
3	61	47	12	7	2	14	0.50
4	79	66	9	2	4	13	0.15
5	23	18	5	5	0	5	1.00
6	68	54	9	2	4	14	0.14
7	68	59	5	1	4	9	0.11
8	57	43	9	2	5	14	0.14
9	63	50	13	4	0	13	0.31
10	64	59	5	5	0	5	1.00
11	66	55	10	9	1	11	0.82
12	52	44	4	2	3	8	0.25
13	68	61	7	6	0	7	0.86
14	66	50	15	11	1	16	0.69
15	60	49	7	8	2	11	0.73
16	49	37	12	3	0	12	0.25
17	57	50	7	1	0	7	0.14
18	85	60	16	4	8	25	0.16
19	63	54	8	8	0	9	0.89
20	71	60	11	7	0	11	0.64
21	53	34	18	10	0	19	0.53
22	51	48	3	1	0	3	0.33
23	49	39	9	6	1	10	0.60
24	35	27	7	7	1	8	0.88
25	45	28	17	9	0	17	0.53
26	71	59	8	4	1	12	0.33
27	55	49	5	2	1	6	0.33
28	59	29	30	27	0	30	0.90
29	43	24	19	17	0	19	0.89
30	52	44	5	2	2	8	0.25
31	55	34	20	8	0	21	0.38
32	66	56	10	2	0	10	0.20
33	65	50	11	9	4	15	0.60
34	62	49	11	6	2	13	0.46
35	48	36	12	9	0	12	0.75
36	85	69	6	0	10	16	0.00
37	73	56	14	9	1	17	0.53
38	76	54	11	2	11	22	0.09
39							
40							
TOTAL	2300	1809	403	222	74	491	17.68
AVERAGE	60.5	47.6	10.6	5.8	1.9	12.9	0.47
SEM	2.1	2.0	0.9	0.8	0.4	0.9	0.05

Supplementary table S3 (contd.)

KSOM + 1mM NAC

DMSO

#	TOTAL NUMBER OF CELLS						Ratio of NANOG-GATA6 double +ve/Total ICM
	Embryo	Double Negative	ICM				
			NANOG +ve	NANOG-GATA6 double +ve	PrE	Total	
1	97	75	13	4	8	22	0.18
2	73	51	17	17	2	22	0.77
3	70	43	14	5	10	27	0.19
4	91	68	13	4	10	23	0.17
5	62	50	7	5	2	12	0.42
6	75	47	18	7	9	28	0.25
7	91	73	10	10	7	18	0.56
8	64	52	6	6	6	12	0.50
9	84	71	8	3	4	13	0.23
10	77	58	11	3	8	19	0.16
11	84	70	9	2	5	14	0.14
12							
TOTAL	**868**	**658**	**126**	**66**	**71**	**210**	3.57
AVERAGE	**78.9**	**59.8**	**11.5**	**6.0**	**6.5**	**19.1**	0.32
SEM	**3.5**	**3.5**	**1.2**	**1.3**	**0.9**	**1.8**	0.06

p38 Inhibited

#	TOTAL NUMBER OF CELLS						Ratio of NANOG-GATA6 double +ve/Total ICM
	Embryo	Double Negative	ICM				
			NANOG +ve	NANOG-GATA6 double +ve	PrE	Total	
1	78	67	11	8	0	11	0.73
2	83	81	2	0	0	2	0.00
3	81	70	7	2	4	11	0.18
4	47	46	1	0	0	1	0.00
5	45	38	7	7	0	7	1.00
6	75	67	4	0	4	8	0.00
7	65	61	2	0	2	4	0.00
8	60	51	9	6	0	9	0.67
9	70	63	4	2	3	7	0.29
10	60	51	9	7	0	9	0.78
11							
12							
TOTAL	**664**	**595**	**56**	**32**	**13**	**69**	3.64
AVERAGE	**66.4**	**59.5**	**5.6**	**3.2**	**1.3**	**6.9**	0.36
SEM	**4.3**	**4.1**	**1.1**	**1.1**	**0.6**	**1.1**	0.12

KSOM + 10mM NAC

DMSO

#	TOTAL NUMBER OF CELLS						Ratio of NANOG-GATA6 double +ve/Total ICM
	Embryo	Double Negative	ICM				
			NANOG +ve	NANOG-GATA6 double +ve	PrE	Total	
1	103	83	10	2	8	20	0.10
2	81	60	10	3	11	21	0.14
3	82	61	9	4	11	21	0.19
4	95	78	7	2	10	17	0.12
5	83	72	8	0	3	11	0.00
6	93	75	9	3	9	18	0.17
7	83	66	9	1	8	17	0.06
8	102	86	7	0	9	16	0.00
9	72	48	12	1	12	24	0.04
10							
TOTAL	**794**	**629**	**81**	**16**	**81**	**165**	0.82
AVERAGE	**88.2**	**69.9**	**9.0**	**1.8**	**9.0**	**18.3**	0.09
SEM	**3.5**	**4.1**	**0.5**	**0.5**	**0.9**	**1.2**	0.02

p38 Inhibited

#	TOTAL NUMBER OF CELLS						Ratio of NANOG-GATA6 double +ve/Total ICM
	Embryo	Double Negative	ICM				
			NANOG +ve	NANOG-GATA6 double +ve	PrE	Total	
1	68	55	9	3	4	13	0.23
2	90	74	8	1	8	16	0.06
3	69	61	8	6	0	8	0.75
4	78	59	13	7	6	19	0.37
5	62	52	10	7	0	10	0.70
6	47	39	6	4	2	8	0.50
7	81	67	8	2	6	14	0.14
8	72	64	7	7	1	8	0.88
9	52	45	5	3	2	7	0.43
10	36	25	8	3	3	11	0.27
TOTAL	**655**	**541**	**82**	**43**	**32**	**114**	4.33
AVERAGE	**65.5**	**54.1**	**8.2**	**4.3**	**3.2**	**11.4**	0.43
SEM	**5.2**	**4.6**	**0.7**	**0.7**	**0.9**	**1.3**	0.09

Supplementary table S3 (contd.)

KSOM + 1mM NAC

DMSO

#	TOTAL NUMBER OF CELLS						Ratio of NANOG-GATA6 double +ve/Total ICM
	Embryo	Double Negative	ICM				
			NANOG +ve	NANOG-GATA6 double +ve	PrE	Total	
1	97	75	13	4	8	22	0.18
2	73	51	17	17	2	22	0.77
3	70	43	14	5	10	27	0.19
4	91	68	13	4	10	23	0.17
5	62	50	7	5	2	12	0.42
6	75	47	18	7	9	28	0.25
7	91	73	10	10	7	18	0.56
8	64	52	6	6	6	12	0.50
9	84	71	8	3	4	13	0.23
10	77	58	11	3	8	19	0.16
11	84	70	9	2	5	14	0.14
12							
TOTAL	**868**	**658**	**126**	**66**	**71**	**210**	3.57
AVERAGE	**78.9**	**59.8**	**11.5**	**6.0**	**6.5**	**19.1**	0.32
SEM	**3.5**	**3.5**	**1.2**	**1.3**	**0.9**	**1.8**	0.06

p38 Inhibited

#	TOTAL NUMBER OF CELLS						Ratio of NANOG-GATA6 double +ve/Total ICM
	Embryo	Double Negative	ICM				
			NANOG +ve	NANOG-GATA6 double +ve	PrE	Total	
1	78	67	11	8	0	11	0.73
2	83	81	2	0	0	2	0.00
3	81	70	7	2	4	11	0.18
4	47	46	1	0	0	1	0.00
5	45	38	7	7	0	7	1.00
6	75	67	4	0	4	8	0.00
7	65	61	2	0	2	4	0.00
8	60	51	9	6	0	9	0.67
9	70	63	4	2	3	7	0.29
10	60	51	9	7	0	9	0.78
11							
12							
TOTAL	**664**	**595**	**56**	**32**	**13**	**69**	3.64
AVERAGE	**66.4**	**59.5**	**5.6**	**3.2**	**1.3**	**6.9**	0.36
SEM	**4.3**	**4.1**	**1.1**	**1.1**	**0.6**	**1.1**	0.12

KSOM + 10mM NAC

DMSO

#	TOTAL NUMBER OF CELLS						Ratio of NANOG-GATA6 double +ve/Total ICM
	Embryo	Double Negative	ICM				
			NANOG +ve	NANOG-GATA6 double +ve	PrE	Total	
1	103	83	10	2	8	20	0.10
2	81	60	10	3	11	21	0.14
3	82	61	9	4	11	21	0.19
4	95	78	7	2	10	17	0.12
5	83	72	8	0	3	11	0.00
6	93	75	9	3	9	18	0.17
7	83	66	9	1	8	17	0.06
8	102	86	7	0	9	16	0.00
9	72	48	12	1	12	24	0.04
10							
TOTAL	**794**	**629**	**81**	**16**	**81**	**165**	0.82
AVERAGE	**88.2**	**69.9**	**9.0**	**1.8**	**9.0**	**18.3**	0.09
SEM	**3.5**	**4.1**	**0.5**	**0.5**	**0.9**	**1.2**	0.02

p38 Inhibited

#	TOTAL NUMBER OF CELLS						Ratio of NANOG-GATA6 double +ve/Total ICM
	Embryo	Double Negative	ICM				
			NANOG +ve	NANOG-GATA6 double +ve	PrE	Total	
1	68	55	9	3	4	13	0.23
2	90	74	8	1	8	16	0.06
3	69	61	8	6	0	8	0.75
4	78	59	13	7	6	19	0.37
5	62	52	10	7	0	10	0.70
6	47	39	6	4	2	8	0.50
7	81	67	8	2	6	14	0.14
8	72	64	7	7	1	8	0.88
9	52	45	5	3	2	7	0.43
10	36	25	8	3	3	11	0.27
TOTAL	**655**	**541**	**82**	**43**	**32**	**114**	4.33
AVERAGE	**65.5**	**54.1**	**8.2**	**4.3**	**3.2**	**11.4**	0.43
SEM	**5.2**	**4.6**	**0.7**	**0.7**	**0.9**	**1.3**	0.09

Supplementary table S3 (contd. 2)

KSOM+AA + 1mM NAC

DMSO

#	TOTAL NUMBER OF CELLS						Ratio of NANOG-GATA6 double +ve/Total ICM
			ICM				
	Embryo	Double Negative	NANOG +ve	NANOG-GATA6 double +ve	PrE	Total	
1	97	75	12	3	9	22	0.14
2	87	77	7	9	1	10	0.90
3	49	33	10	13	3	16	0.81
4	45	30	11	13	1	15	0.87
5	68	56	9	9	2	12	0.75
6	78	50	17	6	11	28	0.21
7	78	62	10	3	5	16	0.19
8	56	53	3	1	0	3	0.33
9	68	45	16	12	5	23	0.52
10	91	73	6	0	12	18	0.00
11	78	57	13	6	8	21	0.29
12	89	68	5	4	12	21	0.19
13	93	77	9	2	7	16	0.13
14	88	63	6	3	18	25	0.12
15	73	47	13	11	9	26	0.42
16	67	46	19	12	2	21	0.57
17	79	67	9	3	3	12	0.25
18	100	76	13	4	11	24	0.17
19	93	75	9	6	8	18	0.33
20	90	66	17	10	7	24	0.42
21							
22							
23							
24							
25							
TOTAL	1567	1196	214	130	134	371	7.60
AVERAGE	78.4	59.8	10.7	6.5	6.7	18.6	0.38
SEM	3.5	3.2	1.0	1.0	1.1	1.4	0.06

p38 Inhibited

#	TOTAL NUMBER OF CELLS						Ratio of NANOG-GATA6 double +ve/Total ICM
			ICM				
	Embryo	Double Negative	NANOG +ve	NANOG-GATA6 double +ve	PrE	Total	
1	79	68	5	0	6	11	0.00
2	57	43	12	2	2	14	0.14
3	63	42	15	3	5	21	0.14
4	66	57	9	4	0	9	0.44
5	60	45	12	5	3	15	0.33
6	81	73	2	0	6	8	0.00
7	95	79	9	1	6	16	0.06
8	59	46	13	5	0	13	0.38
9	13	8	5	0	0	5	0.00
10	76	68	3	0	5	8	0.00
11	28	11	17	14	0	17	0.82
12	96	84	8	3	4	12	0.25
13	76	61	9	2	4	15	0.13
14	71	55	16	8	0	16	0.50
15	45	37	8	6	0	8	0.75
16	58	44	14	12	0	14	0.86
17	85	72	13	9	0	13	0.69
18	60	47	11	9	2	13	0.69
19	80	71	6	3	3	9	0.33
20	63	55	7	5	1	8	0.63
21	62	49	5	1	8	13	0.08
22	22	19	3	2	0	3	0.67
23							
24							
25							
TOTAL	1395	1134	202	94	55	261	7.91
AVERAGE	63.4	51.5	9.2	4.3	2.5	11.9	0.36
SEM	4.6	4.4	0.9	0.8	0.6	0.9	0.06

KSOM+AA + 10mM NAC

DMSO

#	TOTAL NUMBER OF CELLS						Ratio of NANOG-GATA6 double +ve/Total ICM
			ICM				
	Embryo	Double Negative	NANOG +ve	NANOG-GATA6 double +ve	PrE	Total	
1	84	61	17	4	6	23	0.17
2	64	54	9	4	1	10	0.40
3	66	41	21	9	3	25	0.36
4	66	40	21	8	1	26	0.31
5	95	67	16	1	12	28	0.04
6	58	38	16	11	3	20	0.55
7	92	76	6	0	10	16	0.00
8	45	35	5	1	4	10	0.10
9	70	55	7	1	7	15	0.07
10	91	75	9	0	7	16	0.00
11	93	78	8	4	6	15	0.27
12	84	64	8	2	11	20	0.10
13	85	65	10	4	8	20	0.20
14	69	59	10	10	0	10	1.00
15	71	56	7	3	6	15	0.20
16	94	72	11	1	11	22	0.05
17							
18							
19							
20							
TOTAL	1227	936	181	63	96	291	3.81
AVERAGE	76.7	58.5	11.3	3.9	6.0	18.2	0.24
SEM	3.8	3.5	1.3	0.9	0.9	1.4	0.06

p38 Inhibited

#	TOTAL NUMBER OF CELLS						Ratio of NANOG-GATA6 double +ve/Total ICM
			ICM				
	Embryo	Double Negative	NANOG +ve	NANOG-GATA6 double +ve	PrE	Total	
1	25	19	6	2	0	6	0.33
2	53	44	5	1	3	9	0.11
3	63	46	12	3	3	17	0.18
4	97	80	9	0	8	17	0.00
5	60	49	11	7	0	11	0.64
6	81	66	11	3	4	15	0.20
7	74	57	13	2	4	17	0.12
8	67	58	9	5	0	9	0.56
9	81	58	11	0	12	23	0.00
10	74	65	7	4	1	9	0.44
11	106	90	9	0	7	16	0.00
12							
13							
14							
15							
16							
17							
18							
19							
20							
TOTAL	781	632	103	27	42	149	2.57
AVERAGE	71.0	57.5	9.4	2.5	3.8	13.5	0.23
SEM	6.6	5.7	0.8	0.7	1.2	1.5	0.07

Supplementary table S4 (antibodies used): Antibodies used for immunofluorescence staining and western blotting

Sl. No.	Antibody	Type	Target	Host / isotype	Manufacturer	Catalogue number	Dilution used
Immunofluorescence imaging							
1	Nanog (eBioMLC-51)	Primary; monoclonal	Mouse	Rat / IgG2a	Thermo Fisher Scientific Inc. (eBioscience™)	14-5761-80	1:200 in PBST (3% BSA)
2	GATA-4 (H-112)	Primary; polyclonal	Mouse, rat and human	Rabbit / IgG	Santa Cruz Biotechnology, Inc.	sc-9053	1:200 in PBST (3% BSA)
3	GATA-6	Primary; polyclonal	Human and mouse	Goat / IgG	R&D Systems™	AF1700	1:200 in PBST (3% BSA)
4	Donkey anti-Rat IgG (H+L) Highly Cross-Adsorbed Secondary Antibody, Alexa Fluor 488	Secondary; polyclonal	Rat	Donkey / IgG	Thermo Fisher Scientific Inc.	A-21208	1:500 in PBST (3% BSA)
5	Donkey anti-Rabbit IgG (H+L) Highly Cross-Adsorbed Secondary Antibody, Alexa Fluor 555	Secondary; polyclonal	Rabbit	Donkey / IgG	Thermo Fisher Scientific Inc.	A-31572	1:500 in PBST (3% BSA)
6	Donkey Anti-Goat IgG H&L (Alexa Fluor® 647)	Secondary; polyclonal	Goat	Donkey / IgG	Abcam plc.	ab150131	1:500 in PBST (3% BSA)
7	Donkey Anti-Rabbit IgG H&L (Alexa Fluor® 647)	Secondary; polyclonal	Rabbit	Donkey / IgG	Abcam plc.	ab150075	1:500 in PBST (3% BSA)
8	Goat Anti-Rat IgG H&L (Cy3 ®) preadsorbed	Secondary; polyclonal	Rat	Goat / IgG	Abcam plc.	ab98416	1:500 in PBST (3% BSA)
Immunoblotting							
9	Phospho-p38 MAPK (Thr180/Tyr182) (28B10)	Primary; monoclonal	Mouse, rat and human	Mouse / IgG1	Cell Signaling Technology, Inc.	9216S	1:500 in 1% milk
10	GAPDH	Primary; polyclonal	Mouse, rat and human	Rabbit	Merck KGaA (Sigma-Aldrich, Inc.)	G9545	1:20,000 in 1% milk
11	Peroxidase AffiniPure Goat Anti-Mouse IgG (H+L)	Secondary; polyclonal	Mouse	Goat / IgG	Jackson ImmunoResearch Europe Ltd.	115-035-003	1:10,000 in 1% milk
12	Peroxidase AffiniPure Donkey Anti-Rabbit IgG (H+L)	Secondary; polyclonal	Rabbit	Donkey / IgG	Jackson ImmunoResearch Europe Ltd.	711-035-152	1:10,000 in 1% milk

Supplementary table S5 (ANOVA results for figures 4 and 5e & e'):
Welch's ANOVA test results (corresponding to figures 4, 5e and e')

Welch's ANOVA test

	KSOM		KSOM+AA	
	DMSO	**SB220025 (p38i)**	**DMSO**	**SB220025 (p38i)**
Total cell number	0.5568 (ns)	0.0005 (***)	0.2422 (ns)	0.1291 (ns)
Outer cell number	0.6594 (ns)	0.0019 (**)	0.2643 (ns)	0.2595 (ns)
Inner cell number	0.6266 (ns)	0.0229 (*)	0.7817 (ns)	0.1476 (ns)
Epiblast cell number	0.0959 (ns)	0.1745 (ns)	0.9893 (ns)	0.5693 (ns)
PrE cell number	0.9329 (ns)	0.0022 (**)	0.5677 (ns)	0.2169 (ns)
PrE to ICM ratio	0.6893 (ns)	0.0015 (**)	0.6342 (ns)	0.2126 (ns)
Uncommitted to ICM ratio	<0.0001 (****)	0.0002 (***)	0.1308 (ns)	0.0348 (*)

Supplementary table S6 (oligonucleotide primers used for Q-RT PCR; Fig 3h):
Oligonucleotide primers used for Q-RT PCR (corresponding to figure 3h)

Sequences of oligonucleotide primer pairs used for Q-RT PCR			
Sl. No.	**Gene**	**Forward primer (5'-3')**	**Reverse primer (5'-3')**
1	H2afz	GCGCAGCCATCCTGGAGTA	CCGATCAGCGATTTGTGGA
2	Cat	TCCTCGTTCAGGATGTGGTT	TGCGTGTACCACTCTCTCAG
3	Sod1	CGGTGAACCAGTTGTGTTGT	GGTCTCCAACATGCCTCTCT
4	Sod2	CAAGCACAGCCTCCCAGA	ATCTGCGCGTTAATGTGTGG

Supplementary Fig. S1 (supplementary to Fig 3 b (fixed))

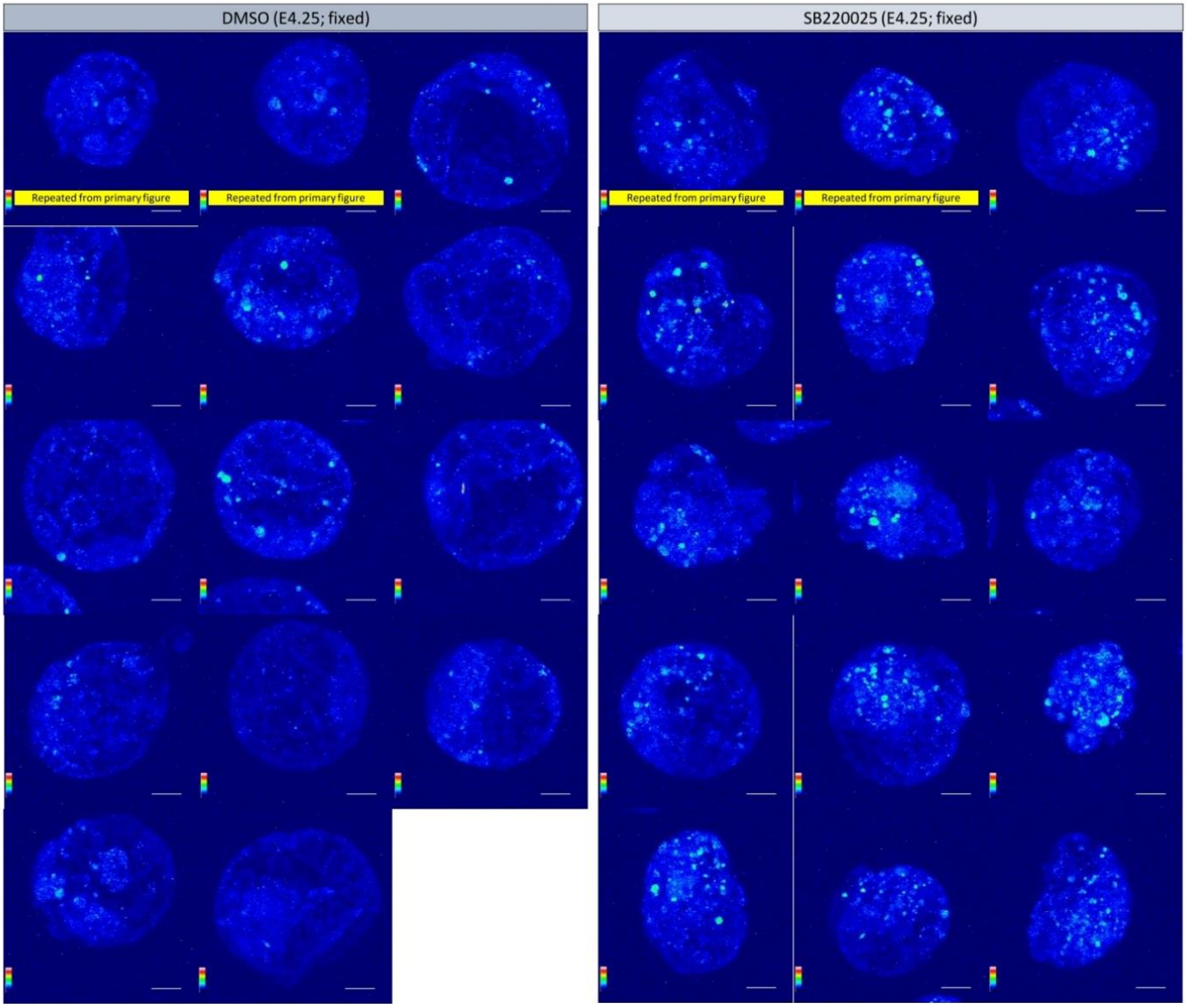

(Supplementary table to Fig 3 c)

Count of ROX-positive foci (maxima) for E4.25

	KSOM	
	DMSO	SB220025
	204	442
	291	422
	314	466
	456	462
	543	617
	423	541
	393	589
	591	623
	385	478
	393	520
	144	668
	461	608
	389	640
	237	346
		567
Average	373.14	532.60

Results & discussion:

The work presented in this thesis arose from the aim of gaining a better understanding of the role of p38-MAPK signalling in mouse preimplantation embryos, particularly during the period of blastocyst maturation (i.e. E3.5 to E4.5). Two discernible features can define this period: formation and expansion of the blastocoel cavity and specification of the inner ICM cells towards EPI and PrE lineages. Previous observations, both from this laboratory and others, have reported that inhibition of p38-MAPK signalling influences both of those features[65,70]. Work from the group of Professor Andrew J. Watson (University of Western Ontario, Canada) was the earliest to shed light on this less studied signalling pathway in preimplantation embryonic development, particularly prior to E3.5. They have reported the requirement of functional p38-MAPK in development of the embryos beyond the 8-16-cell stage[69], regulation of filamentous F-actin[69,71], and in the blastocyst for integrity of certain factors, like TJP1 and AQP3, necessary for fluid-filling of the blastocoel cavity[70]. Deformed and/or smaller cavities in mouse blastocysts treated with p38-MAPK inhibitors were also reported by the group of Professor Eisuke Nishida (RIKEN and Kyoto University, Japan)[62], though, to the best of current knowledge, they did not follow up on the observations reported. Prior work from the laboratory found that inhibition of p38-MAPK from E3.5 resulted in fewer GATA4 expressing PrE cells at E4.5[65]. This was the first report of the influence of active p38-MAPK on cell fate specification in the ICM. The manuscripts that comprise this thesis are an attempt to uncover some of the molecular mechanisms, which connects p38-MAPK activity and preimplantation development, particularly focussing on blastocyst maturation and accompanying lineage specification of ICM cells.

The first chapter, derived from the manuscript entitled "*p38-MAPK-mediated translation regulation during early blastocyst development is required for primitive endoderm differentiation in mice*", presents a comprehensive examination of the effect of p38-MAPK inhibition starting from E3.5, by using live imaging, phospho(proteomic) mass spectrometry, multi-time-point transcriptome sequencing, rRNA and polysome profiling, embryo siRNA microinjection, immunofluorescence confocal imaging and image analysis[66]. Previous work from the laboratory, on p38-MAPK activity and preimplantation development, reported that inhibition of p38-MAPK (p38-MAPKi) between E3.5 and E4.5, and specifically prior to E3.75, results in decrease in number of GATA4 expressing PrE cells by the late blastocyst stage[65]. Work reported in this chapter was able to further narrow the window of required p38-MAPK activity towards proper PrE specification to a three-hour period (i.e. E3.5+4 hours to E3.5+7 hours). Though the observed phenotype was not as robust as the one following 24-hours of p38-MAPKi, the results were statistically significant and indicate p38-MAPK activity during early portion of blastocyst maturation as important. Live embryo imaging demonstrated an inability of p38-MAPKi embryos to expand following the normally observed pulsatile motion of a maturing blastocyst, with differences in embryo size becoming apparent around the E3.5+5 hour mark. Furthermore, p38-

MAPKi embryos, though demonstrating the pulses, fail to expand at all beyond the E3.5+10 hour mark and fewer of those embryos hatched. Together with observations from gene expression data for the four p38-MAPK paralogs, *Nanog*, and *Gata4*, the E3.5+7(±3) hour mark appears to be significant in the functioning of p38-MAPKs towards blastocyst maturation and typical ICM cell fate specification.

Taking cues from the aforementioned time-points and other experimental observations, embryos with p38-MAPKi between E3.5+2 hours and E3.5+9 hours (i.e. 7 hour inhibition) were used to identify differentially phosphorylated and differentially expressed proteins, as compared to controls (DMSO treated). Phospho(proteomic) mass-spectrometry results for differentially expressed proteins were particularly enriched for "translation" and "ribosome biogenesis", whereas differentially phosphorylated proteins were largely related to RNA metabolism, transcription regulation, chromatin organisation among others. The "translation" related differentially expressed proteins primarily demonstrated reduced expression upon p38-MAPKi and this indicated to us that p38-MAPK might be regulating the global translational landscape in the developing blastocyst. Further examination of the global regulatory landscape was carried out by sequencing the transcriptome (mRNA) to identify differentially expressed genes between control (DMSO) and p38-MAPKi treated blastocysts at E3.5+4 hours, E3.5+7 hours and E3.5+10 hours, with inhibition starting at E3.5+0 hours. The number of differentially expressed genes increased from 34 at the +4 hour point, to 1240 at the +7 hour point and then decreased to 480 at the +10 hour point. Considering the higher quantity of differentially expressed genes at the +7 hour point and observations stated in the last paragraph, the transcriptome was comparatively analysed with respect to the +4 hour and the +10 hour points. Three distinct clusters arose and are presented in figure 3 of the manuscript. Cluster I represented genes down-regulated upon p38-MAPKi at +7 hour point, that appeared to begin the descent at the +4 hour point, but returned to control levels by the +10 hour point. Cluster III represents genes expressed in the exactly opposite manner (i.e. up-regulated at +7 hours but returned to control levels by the +10 hour point). The smallest cluster (cluster II) represented up-regulated genes that did not recuperate to the control levels by the +10 hour point. Thus, the overall picture detailed a larger cluster of differentially regulated genes around the +7 hour point, which though normalises by +10 hour mark, might lead to forthcoming phenotypic changes. Whereas a small group of genes are effected for a longer duration, which might also presage a prolonged phenotypic effect. The dynamic nature of the p38-MAPKi phenotype and data observed from the multi-omics studies opens up potential future research avenues, probably utilising experimental systems and approaches to precisely manipulate and analyse the role of multiple genes.

Gene ontology analysis of differentially expressed gene transcripts at the E3.5+7 hour point revealed enrichment of translation and RNA-splicing related genes, much like what was observed in the (phospho)proteomemics data. Another enriched section related to mitochondrial

respiration, which is relevant both in respect to previously reported observations about blastocyst metabolism and p38-MAPK[72] and unpublished observations from the laboratory. Morula to blastocyst transition is accompanied with metabolic changes at various levels, including, increased oxygen consumption[112], glucose metabolism[113], ATP turnover[114] and detrimental ROS levels[115]. Indeed all biochemical metabolic pathways are connected to mitochondrial activity (see comprehensive review of metabolism in preimplantation embryos[116]). p38-MAPKi results in impaired glucose uptake around the early blastocyst stage[72], in elevated ROS levels[67] and also in impaired mitochondrial activity particularly in the TE cells (unpublished observations from the lab). Thus, the enrichment of mitochondrial respiration related terms in the transcriptomics data, comparing control to p38-MAPKi, is another interesting aspect of p38-MAPK activity in the developing blastocyst and can be explored as a follow-up to this thesis.

Analysing the transcriptomic read-out of those "translation" related proteins identified in the mass spectrometry analysis to be down-regulated upon p38-MAPKi, it was discovered their respective mRNA transcripts were primarily up-regulated at the +7 hour point and normalised to control levels by the +10 hour point. Two important conclusions can be derived from this observation; firstly, there is either a general over expression of those genes or an accumulation of their transcripts, but since these proteins are also down-regulated it indicates a hampered ribosome biogenesis pathway and/or decreased overall translation, which can indeed be related (possibly indicative of a feedback regulatory loop). Secondly, any p38-MAPKi induced change in translation-related transcript accumulation appears to normalise by the +10 hour point, thus indicating either a RNA-turn-over mechanism at play or that ribosome biogenesis and resultant translation returns to "normal" by the 10 hour point. The subsequent set of experimental observations suggest that the depressed translational landscape indeed continues up to the +10 hour point, thus the normalising of the aforementioned transcripts most likely represents an inherent "house-keeping" mechanism to get rid of accumulated RNAs, *per se*.

The global translational landscape was analysed at E3.5+10 hour time point (i.e. after 10 hours of p38-MAPKi). Firstly, using an O-Propargyl-puromycin incorporation based florescence assay to quantify newly synthesised proteins, a nearly 50% decrease in *de novo* protein synthesis was observed in the p38-MAPKi embryos. A polysome-profiling assay specifically developed for low-input samples[117], such as preimplantation embryos, enabled us to quantify the proportion of ribosome subunits (based on 18s and 28s rRNA) as originating from either polysomic fractions or non-polysomic fractions. In the p38-MAPKi condition, higher proportions of ribosomes were from the non-polysomic fraction (i.e. not actively translating ribosomes) as compared to the controls. The ratios indicate the decrease to be across both 18s and 28s rRNA analysed, thus the results were not skewed and demonstrated an actual decrease in polysomic fractions and consequently provided further proof of reduced active translation.

The phosphoproteomic analysis was also used to identify potential downstream effectors of p38-MAPK in the blastocyst; candidates were determined based on increased and/or decreased detection of individual protein phosphorylation coupled with less than 1.3-fold change in protein abundance, and then further refined based on information from available literature. A couple of these identified candidates, MYBBP1A and DDX21, were experimentally verified in this thesis and shown to be involved in blastocyst maturation and lineage-specification. Potential MAPK consensus motifs in both these proteins, which have not previously been reported as targets of p38-MAPK, were detected to harbour decreased phosphorylation in p38-MAPKi embryos. These proteins are also known to be involved in processes related to ribosome biogenesis, like rRNA transcription and processing[118–122]. Whereas the effect of MYBBP1A was further analysed in this manuscript, the observations regarding DDX21 formed the basis of a separate manuscript and was thus discussed in chapter II. Nevertheless, based on the reported rRNA regulatory roles of potential p38-MAPK effectors, the 45s pre-rRNA was examined in p38-MAPKi embryos and an accumulation of unprocessed pre-rRNA intermediates was observed. The p38-MAPKi induced processing defects were particularly focussed upon impaired removal of the ITS2 site, which is flanked by the 5.8s and 28s rRNA on either side. These observations further associate p38-MAPK activity to ribosome biogenesis and subsequent regulation of the translation landscape in developing mouse blastocysts.

Emerging evidence of co-regulatory events connects global gene regulation mechanisms and based on observations reported in recently published papers[122–124], the state of active transcription was analysed. Along with a decrease in translation, p38-MAPKi was found to also lead to a globally decreased levels of H4K16-acetylation (H4K16ac – a mark of actively transcribed chromatin[125]) and actively transcribing RNA pol II phosphorylated at S2[126] (Pol II S2p). Thus, these observations indicate that p38-MAPKi also results in decreased global transcription, in addition to reduced translation[122–124].

Analysing *Mybbp1a* by loss-of-function studies gene knockdown (i.e. siRNA mediated clonal down-regulation of the mRNA by microinjecting one cell of two-cell stage embryos), was reported to result in a robust reduction in total cell numbers by E4.5, significantly within the cell clone originating from the microinjected blastomere. A decrease was also noted for NANOG expressing EPI cells and GATA4 expressing PrE cells, with an average of 1.29 GATA4 expressing injected cells in embryos injected with *Mybbp1a* siRNA (compared to 4.67 GATA4 expressing injected cells in embryos injected with control (NTC) siRNA). Thus, MYBBP1A, which was identified via phosphoproteomics as a potential effector of p38-MAPK during blastocyst maturation, is necessary for proper ICM lineage specification, with particular impact on PrE cells.

Since translation regulation was identified as a target of p38-MAPK, potentially working via effectors such as MYBBP1A, the of the best-studied translation regulatory signalling pathway (i.e. mTOR) was further analysed. mTOR inhibition (mTORi, using TORIN1) from the early

blastocyst stage onwards (E3.5) has been reported to induce embryonic diapause, which was a result of depressed translation and co-transcriptional events[124]. Inhibition of mTOR resulted in fewer GATA4 expressing PrE cells (akin to p38-MAPKi) but also fewer overall cell numbers and NANOG expressing EPI cells. This is what might be expected in a diapaused state, and thus the observations reported here validate and add another layer to the initial report of mTORi induced embryonic diapause. The p38-MAPKi and mTORi phenotypes further differ in that the former leads to death of all the embryos around E5.5 to E6.5, whereas the latter appears to permit diapaused blastocyst survival until E13.5. Pharmaceutically activating mTOR (mTORa; using MHY1485) under conditions of p38-MAPKi in the E3.5 to E4.5 period was found to result in a partial "rescue" of GATA4 expressing PrE cell numbers. The "rescue" was also observed in all the cell-types, though nowhere was it a complete rescue to control levels.

The well-defined and primary signalling pathway necessary for ICM lineage specification is the FGF4-FGFR1/2-MEK/ERK pathway. NANOG expressing cells also produce FGF4, which, via binding with receptors FGFR1/2, can activate the MEK/ERK pathway in neighbouring cells, leading to sustained expression of GATA6 and down-regulation of NANOG and resulting PrE differentiation. Inhibiting MEK1/2 from E3.5 (using the small molecule inhibitor PD0325901) results in all the inner cells expressing NANOG at E4.5, and thus no PrE specification[78]. Combining MEK inhibition with mTORa too results in an exclusively EPI populated ICM, thus mTOR activation cannot "rescue" GATA4 expression in MEK inhibited embryos, unlike that of the p38-MAPKi embryos. Contrary to the effect of MEK inhibition, exogenous FGF4 supplementation during blastocyst maturation results in an ICM exclusively of GATA4 expressing PrE cells, with no NANOG expressing cells, by E4.5[78]. Supplementation of FGF4 coupled with p38-MAPKi resulted in lack of any NANOG expressing cells at E4.5. Thus, p38-MAPK potentially lies downstream of FGF4 and MEK and upstream of mTOR in the cascade of signalling molecules functioning towards proper ICM specification and survival.

Summarising chapter I, p38-MAPK, acting via effectors such as MYBBP1A, was found to influence rRNA regulation and ribosome biogenesis and in turn global translation and co-transcriptional events. p38-MAPK activity in the first 10-hours post E3.5 is of particular importance towards normal blastocyst maturation and inner cell lineage specification and the timing can be further refined to a 3-hour period around E3.75. Finally, p38-MAPK potentially acts downstream of the FGF4-FGFR1/2-MEK/ERK pathway but upstream of mTOR, towards generating a viable population of GATA4 expressing PrE cells at E4.5.

Chapter II, covering the manuscript entitled, "*DDX21 is a p38-MAPK sensitive nucleolar protein necessary for mouse preimplantation embryo development and cell-fate specification*", attempts to focus on one particular p38-MAPK effector (i.e. DDX21) and reports on its expression dynamics during preimplantation embryonic development and its connection with p38-MAPK and normal blastocyst maturation[68]. DDX21 was initially identified in a preliminary phosphoproteomic screen

to detect differentially phosphorylated proteins, much as described for chapter I. The only difference was the number of embryos used, which stood at 100 embryos per repeat (and three repeats) per condition as compared to 300 embryos for the screen described in chapter I. In the process of completing the manuscript described in chapter I, the reported functional similarity between MYBBP1A and DDX21 was realised and consequently DDX21 was further investigated. Much like MYBBP1A, DDX21 is also a primarily nucleolar protein, and similar to many other factors that occupy the nucleoli, DDX21 and MYBBP1A partake in mechanisms associated with rRNA processing and ribosome biogenesis.

Aided by availability of an immunocytochemistry-verified antibody against DDX21, expression and localisation of DDX21 protein was reported, possibly for the first time, across the preimplantation developmental time-line. Published single-cell transcriptomics of early embryos indicated the expression of *Ddx21* gene starts around the 4-cell stage, peaking at 8-cell stage and thereafter being consistently high across subsequent preimplantation embryonic cellular lineages[127,128]. DDX21 protein expression appears to closely follow that of the gene transcript and is clearly visible around the 8-16-cell stage. While the level of protein expression continues increasing as development progresses, the subcellular localisation changes. In the earlier stages, prior to blastocyst (E3.5) stage, DDX21 has a pan-nuclear localisation, and co-localises with condensed mitotic chromosomes. In the blastocyst embryo, DDX21 takes up a somatic-type nucleolar localisation, and appears to be excluded from mitotically condensed chromosomes. Thus, expression of the DDX21 protein appears temporally and spatially dynamic in the preimplantation embryo. Moreover, DDX21 localisation appears to follow the reported structural and functional transition of nucleoli during preimplantation development (reviewed here[129]), that leads to the formation of somatic-type nucleoli around E3.5. DDX21 also appeared to be more abundantly expressed in the outer cells compared to inner cells of the blastocyst.

As previously established, p38-MAPKi from E3.5 to E4.5 is detrimental to typical blastocyst maturation and lineage specification. Therefore, because DDX21 was a potential p38-MAPK effector, the impact of p38-MAPKi on DDX21 expression in that period was examined. Indeed, DDX21 protein localisation and expression level were sensitive to p38-MAPKi between E3.5 and E4.5. Accordingly, there was a global decrease in quantified DDX21 protein in both inner and outer cells, upon p38-MAPKi. DDX21 protein also appeared to lose the exclusively nucleolar localisation and appeared more nuceoplasmic in the p38-MAPKi embryos, though the degree of mislocalisation was not consistent across the analysed embryos, probably indicative of general biological heterogeneity. GNL3 (NUCLEOSTEMIN), a known co-factor of DDX21 that is also involved in rRNA transcription and processing, was also analysed in the same period. GNL3 and DDX21 appeared to largely co-localise in nucleoli at E4.5, and contrary to levels of DDX21, GNL3 expression was enriched in the inner cells as compared to the outer cells. After p38-MAPKi (from E3.5 to E4.5) there was a more drastic effect on GNL3 expression levels, with almost no

discernible GNL3 expression detected in the inhibited embryo groups; confirming an acute sensitivity of GLN3 expression on active p38-MAPK.

Clonal loss-of-function analyses were also performed by microinjecting *Ddx21* siRNA in one cell of a two-cell stage embryos and examining the blastocysts at E4.5. Confirmed down-regulation of *Ddx21* mRNA resulted in decrease of DDX21 protein expression in both the injected and non-injected cells, and across inner and outer cell populations, thus indicating the existence of non-cell-autonomous effects of *Ddx21* gene down-regulation (not previously observed after similar down-regulation of the *Mybpp1a* gene). Cell numbers too were sharply reduced in *Ddx21* siRNA injected embryos compared to control (NTC siRNA) injected embryos. On an average, *Ddx21* siRNA injected blastomeres gave rise to only 10.58 cells at E4.5 (compared to 36.67 cells in NTC siRNA injected blastomeres). This represented 8.31 outer cells and 2.27 inner cells (compared to 26.60 and 10.07 respectively, in controls). Furthermore, *Ddx21* siRNA injected embryos at E4.5 also had smaller and malformed blastocoel cavities, with the volume of the blastocyst being about 50% of that of the control NTC siRNA injected embryos. Expanding the loss-of-function analysis to assay the formation of late blastocyst inner cell lineages, *Ddx21* siRNA injected blastomeres were found to contribute towards fewer NANOG (*Ddx21* siRNA: 1.53 and NTC siRNA: 3.89) and GATA4 (*Ddx21* siRNA: 0.07 and NTC siRNA: 4.11) expressing inner cells, representive of the EPI and PrE lineages respectively. Once again, this effect was non-cell-autonomous, thus even the non-injected blastomeres in the *Ddx21* siRNA injected embryos gave rise to fewer cells of either lineage (NANOG- *Ddx21* KD: 1.93 and control: 5.11; GATA4- *Ddx21* KD: 0.93 and control: 3.33). In both instances (i.e. cell-autonomous and non-cell-autonomous) the effect was much more pronounced in case of GATA4 expressing PrE cells compared to EPI cells (indeed, in the case of the *Ddx21* siRNA microinjected cell clone, GATA4 expressing PrE ICM cells were almost never observed).

Identifying potential p38-MAPK effectors with a role in blastocyst maturation and inner cell lineage specification was one of the primary aims of the project, and in DDX21 and MYBBP1A, not only were two such factors identified, but also resulted in a broader picture of p38-MAPK regulating ribosome biogenesis and a permissive translational landscape towards normal developmental cellular differentiation[66,68]. DDX21 protein also demonstrates a p38-MAPK sensitivity and appears less likely to be to retained in cell nucleoli, site of ribosome biosynthesis[130,131], and observed being nucleoplasmic upon p38-MAPKi[68]. Interestingly, similar localisations are also observed in a cell-type specific manners with regards to genetic mutations corresponding to recognised ribosomopathies[120].

Summarising chapter II, evidence was reported for DDX21 as a novel p38-MAPK effector, which exhibits a dynamic spatio-temporal expression pattern during preimplantation mouse embryo development. The expression of DDX21 and its co-factor GNL3 is sensitive to p38-MAPK activity during blastocyst maturation. Furthermore, DDX21 appears to play a significant role in ensuring

proper blastocyst maturation and ICM lineage specification, as *Ddx21* specific siRNA-injected embryos have significantly fewer cells, and in particular inner cells of either lineage.

The first two chapters explore the protein translation regulatory role of p38-MAPKs, that seem to act, at least partially, via regulation of rRNA processing utilising factors such as MYBBP1A, DDX21 and GNL3. The functional role of p38-MAPKs in early embryos (prior to E3.5), and particularly in proper functioning of TE cells, has been established by reports from other laboratories[70,74], and inhibition even at later stages (E3.5 to E4.5) continues to result in fewer TE cells[65–67]. p38-MAPKi induced global attenuation of translational and co-transcriptional landscape can have a cell-lineage-independent effects on survival during blastocyst maturation too, and may also be responsible for the observed decrease in number of TE cells. Relating to the blastocyst inner cell lineages, the effect of p38-MAPKi is most discernible in the quantity of GATA4 expressing PrE cells, whereas the number of NANOG expressing EPI cells remains largely steady. Furthermore, regulation and/or maintenance of an appropriate translational and transcriptional landscape has been reported to be vital towards typical cellular lineage specification and embryonic development[122–124].

As discussed previously, mTOR inhibition alters the translational landscape such that the blastocyst remains in a state of diapause[124], whereas loss-of-function of rRNA processing factors such as HTATSF1 results in altered protein synthesis and consequently developmental cell fate specification[122]. p38-MAPKi, starting from 2-cell stage, arrests typical development beyond the 16-cell stage[71], at the same time no blastocyst stage embryos are derived from genetic knockout of *Mybbp1a*[132], *Gnl3*[133] and possibly *Ddx21* too (http://www.informatics.jax.org/marker/MGI:1860494). Observations reported here, that siRNA-mediated knockdown of *Mybbp1a* and *Ddx21* results in about 16 and 10 cells from the microinjected blastomere at E4.5, respectively, along with the aforementioned points suggests requirement of the genes for progress of embryonic development to the blastocyst stage and beyond. It can be speculated that p38-MAPK helps to functionally regulate multiple ribosome biogenesis related genes, which though have similar molecular functions, are nevertheless non-redundant and individually vital for embryonic survival and development, particularly around the 32-cell-stage. These aspects of p38-MAPK activity towards translation regulation, enabling an appropriate global gene regulatory landscape, appears to be also important in development and cell lineage specification beyond the 32-cell stage (i.e. blastocyst maturation). However, unlike mTOR inhibition, p38-MAPK inhibition from E3.5 results in death of embryos by 48-hours of treatment, thus indicating a role of p38-MAPK in embryonic cell survival too.

Recent studies have indicated a two-staged regulation of PrE lineage generation, wherein the first stage i.e. the specification is enabled by the quintessential ICM lineage specification signalling pathway of FGF4-FGFR1/2-MEK/ERK[78], the second stage is PrE survival and being mediated by FGFR2-PDGFRα-PI3K-mTOR[84,85]. This point is discussed in more details within the

manuscript in chapter I, the short summary is that since p38-MAPK appears to be upstream of mTOR and potentially independent of FGF4-FGFR1/2-MEK/ERK mediated pathway, it might be playing a more direct role in the process of PrE survival. Chapter III provides glimpses of the role of p38-MAPK in regulating nutrient and consequent oxidative stress, towards cell survival, proliferation and developmental differentiation, thus implcating p38-MAPKs as a part of embryonic cell survival mechanism.

Whereas phosphoproteomic mass spectrometric analysis has revealed potential downstream effectors of p38-MAPKs, the upstream activator and/or activating signals leading to p38-MAPK activation in the blastocyst are yet to be experimentally verified. As mentioned above, there is indirect experimental evidence suggesting FGFR2 and/or PDGFRα as being the membrane bound ligand-receptors possibly activating p38-MAPK, though informed speculation can also be made about FGFR3 as having a role to play. *Fgfr3*, from demonstrating no expression at E3.5, appears to be specifically expressed in E4.5 PrE cells, and does so in a *Fgf4*-dependent manner[82]. Coupled with reports of FGFR3 enabled p38-MAPK activation[97], such a mechanism can be at play in the developing blastocyst, working towards survival and maintenance of a viable PrE population. Examination of the potential upstream regulator of p38-MAPK will be another vital piece in the mechanistic understanding of p38-MAPKs in blastocyst maturation and component cellular lineage specification and survival.

The manuscript entitled "*p38-mitogen activated kinases mediate a developmental regulatory response to amino acid depletion and associated oxidative stress in mouse blastocyst embryos*" constitutes chapter III and describes the role of p38-MAPKs as an alleviator of nutrient-constraint induced oxidative stress during blastocyst maturation. Preimplantation embryo culture is usually performed in KSOM media, which may or may not be supplemented with amino acids. Whereas embryos are recorded to develop appropriately in either condition, absence of amino acids can be considered equivalent to lower nutrient availability. p38-MAPKi between E3.5 and E4.5 under conditions of amino acid availability has been previously reported to be detrimental to proper blastocyst maturation and cell fate specification[65]. The p38-MAPKi phenotypes reported in the manuscripts within this thesis are primarily from experiments under conditions of amino acid supplementation, and report fewer blastocyst cells in general and particularly fewer GATA4 expressing PrE cells. As p38-MAPK is a recognised stress-activated kinase[134], it was hypothesised p38-MAPK activity may be functionally important for cell survival under conditions of stress, including amino acid deprivation. In this manuscript, the originally observed phenotypes of p38-MAPKi between E3.5 and E4.5 are reported to be more severe in the absence of amino acids. Whereas in presence of amino acids, p38-MAPKi does result in the classical phenotype of fewer overall and ICM cells (with profound reductions in GATA4 expressing PrE cells but only a mild effect on NANOG expressing EPI cells), in absence of amino acids the decreases in total and ICM cell number approaches 50%. Such p38-MAPKi profoundly affects cell numbers of both ICM lineages compared to the controls. Although, with an average of less than one GATA4 expressing

cell observed under such conditions, PrE differentiation is markedly more affected than EPI. The severity of the phenotype under conditions of amino acid deprivation were also observed in a near complete lack of blastocoel cavities and cells appearing to be darker in appearance and apoptotic. Notably, there were no significant differences in total, ICM, PrE or EPI cell number, nor cavity size, in control embryos cultured in either the presence or absence of amino acids. This demonstrates the developing blastocysts' capacity to buffer the potential stress condition of amino acid starvation and an active involvement/role for p38-MAPK mediated signalling under conditions of amino acid deprivation.

p38-MAPKi in absence of amino acids (E3.5 to E4.5) also resulted in a quantifiable increase in the levels of reactive oxygen species (ROS), potentially resulting in oxidative damage and detrimental developmental potential of the blastocyst (as observed). Indeed, levels of phosphorylated p38-MAPK (thus, enzymatically active protein), were higher in embryos cultured (without p38-MAPKi) in absence of amino acids compared to those cultured in presence of amino acids, during the early blastocyst maturation period. Furthermore, the absence of amino acids also resulted in increased blastocyst expression of enzymes known to catalyse the removal of ROS, like *Cat*, *Sod1* and *Sod2*. p38-MAPKi in the absence of amino acids also resulted in a decrease in the expression of *Cat* and *Sod2* transcripts, whereas in case of embryos cultured in presence of amino acids, there were no such changes (except for a statistically significant but small decrease in *Sod1* expression). Overall the data demonstrate that the absence of supplemented amino acids in the culture media of developing blastocyst, results in increased phosphorylation (and activity) of p38-MAPK and promotes increased gene expression of ROS catalysing enzymes that is associated with normal development and ICM lineage specification.

N-acetyl cysteine (NAC) is a widely used anti-oxidant[135] that when added to blastocysts cultured in media devoid of supplemented amino acids but containing p38-MAPK inhibitor (E3.5 to E4.5 – i.e. normally associated with the comparatively more severe phenotypes) demonstrated a "rescue" of p38-MAPKi induced cell numbers deficits in all but NANOG expressing EPI cells. Such increases in blastocyst cell numbers correlated with increasing the concentration of NAC used from 1mM to 10mM. Moreover, the observed increase in number of GATA4 expressing PrE cells was to a level equivalent to that in p38-MAPKi blastocysts cultured in the presence of amino acids (but were still lower than in control groups irrespective of amino acid supplementation status – i.e. the original reported p38-MAPKi phenotype[65]). Importantly, similar addition of NAC had no major impact on cell numbers in p38-MAPKi embryos cultured under amino acid supplemented conditions. NAC supplementation in absence of amino acids and presence of p38-MAPK inhibitor also demonstrated a decrease in number of uncommitted inner cells (i.e. co-expressing NANOG and GATA6) compared to the embryos cultured with no NAC supplementation, indicating improved developmental potential and progression.

Thus, chapter III describes a role for p38-MAPK in mitigating amino acid deprivation induced oxidative stress in the developing blastocyst, potentially via regulating expression of enzymes catalysing the removal of ROS. Furthermore, it is also a demonstration of the remarkably robust developmental capacity of the preimplantation mouse embryo, and specifically the blastocyst.

Conclusion:

Taken together, the studies described in this thesis, indicate a multi-pronged mode of action for p38-MAPKs in blastocyst maturation and cell fate specification. p38-MAPKs are generally known to have a wide-array of effectors, influencing a seemingly wider spectrum of molecular pathways[61]. Similarly, in murine preimplantation embryonic development too, multiple mechanisms and phenotypes are observed to be associated with p38-MAPK activity.

Thus, from the manuscripts contained within this thesis and published literature, a role of p38-MAPK can be deduced, in both enabling maintenance of a metabolic landscape necessary for cell survival and maintenance of a global translational and transcriptional landscapes that enables typical development and cell lineage specification during blastocyst maturation (graphically summarised in Figure 23).

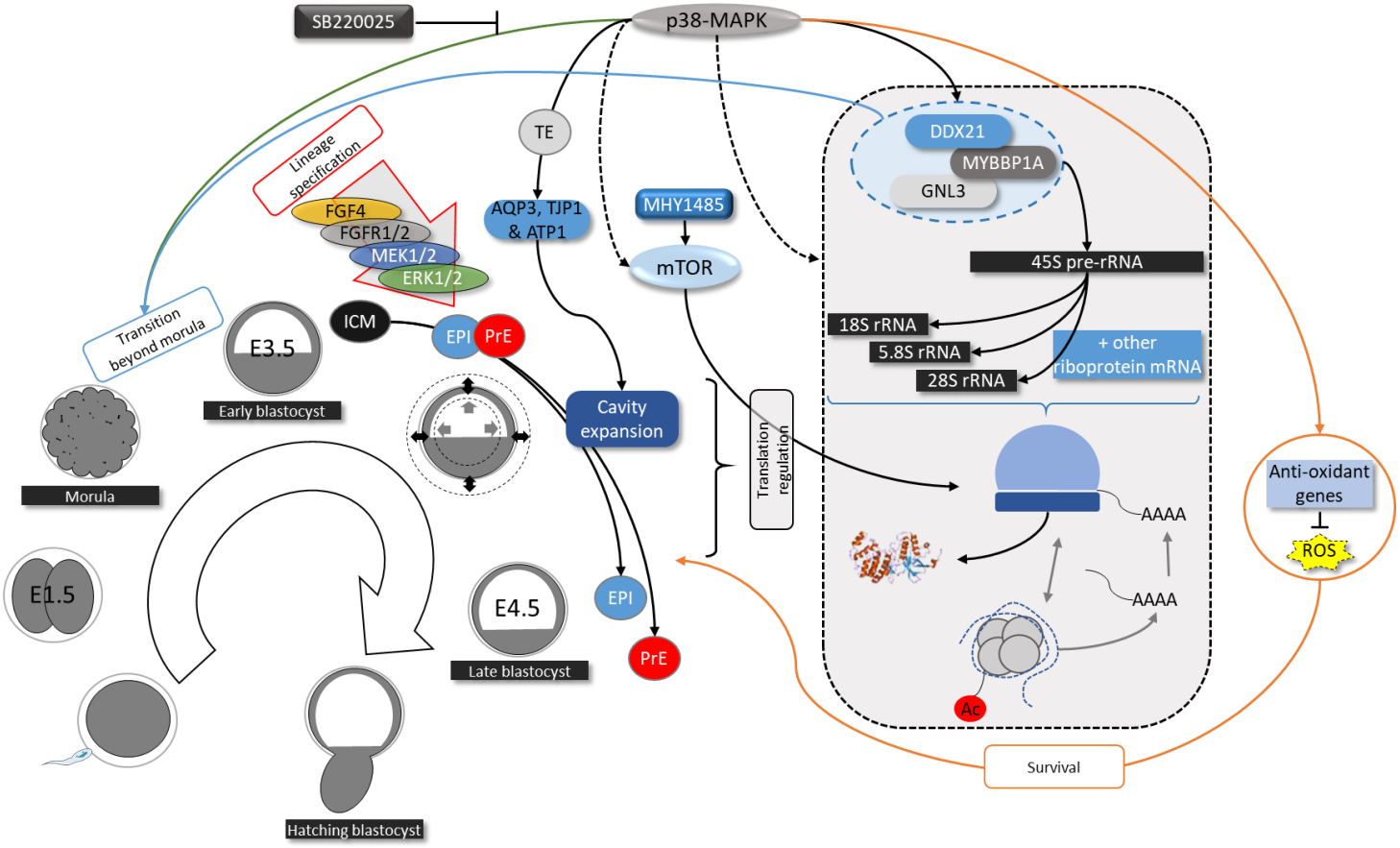

Figure 23: **Working model: The multi-faceted roles played by p38-MAPK in preimplantation embryonic development and cell fate specification**. (Adapted from Bora et al. accepted at Communications Biology, 2021)

References:

1 R. Alberio, Regulation of Cell Fate Decisions in Early Mammalian Embryos., *Annu. Rev. Anim. Biosci.*, 2020, **8**, 377–393.

2 P. Svoboda, Mammalian zygotic genome activation., *Semin. Cell Dev. Biol.*, 2018, **84**, 118–126.

3 K. N. Schulz and M. M. Harrison, Mechanisms regulating zygotic genome activation., *Nat. Rev. Genet.*, 2019, **20**, 221–234.

4 D. Jukam, S. A. M. Shariati and J. M. Skotheim, Zygotic Genome Activation in Vertebrates, *Dev. Cell*, 2017, **42**, 316–332.

5 V. Yartseva and A. J. Giraldez, The Maternal-to-Zygotic Transition During Vertebrate Development: A Model for Reprogramming., *Curr. Top. Dev. Biol.*, 2015, **113**, 191–232.

6 A. K. Tarkowski, Experiments on the development of isolated blastomers of mouse eggs., *Nature*, 1959, **184**, 1286–7.

7 M.-E. Torres-Padilla, On transposons and totipotency, *Philos. Trans. R. Soc. B Biol. Sci.*, 2020, **375**, 20190339.

8 A. K. Tarkowski and J. Wróblewska, Development of blastomeres of mouse eggs isolated at the 4- and 8-cell stage., *J. Embryol. Exp. Morphol.*, 1967, **18**, 155–80.

9 C. Chazaud and Y. Yamanaka, Lineage specification in the mouse preimplantation embryo, *Development*, 2016, **143**, 1063–1074.

10 M. Zhu and M. Zernicka-Goetz, Principles of Self-Organization of the Mammalian Embryo, *Cell*, 2020, **183**, 1467–1478.

11 J. Fiorentino, M.-E. Torres-Padilla and A. Scialdone, Measuring and Modeling Single-Cell Heterogeneity and Fate Decision in Mouse Embryos, *Annu. Rev. Genet.*, 2020, **54**, annurev-genet-021920-110200.

12 M. D. White, J. Zenker, S. Bissiere and N. Plachta, Instructions for Assembling the Early Mammalian Embryo, *Dev. Cell*, 2018, **45**, 667–679.

13 J. Wang, L. Wang, G. Feng, Y. Wang, Y. Li, X. Li, C. Liu, G. Jiao, C. Huang, J. Shi, T. Zhou, Q. Chen, Z. Liu, W. Li and Q. Zhou, Asymmetric Expression of LincGET Biases Cell Fate in Two-Cell Mouse Embryos, *Cell*, 2018, **175**, 1887-1901.e18.

14 A. Hupalowska, A. Jedrusik, M. Zhu, M. T. Bedford, D. M. Glover and M. Zernicka-Goetz, CARM1 and Paraspeckles Regulate Pre-implantation Mouse Embryo Development, *Cell*, 2018, **175**, 1902-1916.e13.

15 M.-E. Torres-Padilla, D. Parfitt, T. Kouzarides and M. Zernicka-Goetz, Histone arginine methylation regulates pluripotency in the early mouse embryo, *Nature*, 2007, **445**, 214–218.

16 M. D. White, J. F. Angiolini, Y. D. Alvarez, G. Kaur, Z. W. Zhao, E. Mocskos, L. Bruno, S. Bissiere, V. Levi and N. Plachta, Long-Lived Binding of Sox2 to DNA Predicts Cell Fate in the Four-Cell Mouse Embryo, *Cell*, 2016, **165**, 75–87.

17 H. Y. G. Lim, Y. D. Alvarez, M. Gasnier, Y. Wang, P. Tetlak, S. Bissiere, H. Wang, M. Biro and N. Plachta, Keratins are asymmetrically inherited fate determinants in the mammalian embryo, *Nature*, , DOI:10.1038/s41586-020-2647-4.

18 S. Louvet, J. Aghion, A. Santa-Maria, P. Mangeat and B. Maro, Ezrin becomes restricted to outer cells following asymmetrical division in the preimplantation mouse embryo., *Dev. Biol.*, 1996, **177**, 568–79.

19 S. Vinot, T. Le, S. Ohno, T. Pawson, B. Maro and S. Louvet-Vallée, Asymmetric distribution of PAR proteins in the mouse embryo begins at the 8-cell stage during compaction., *Dev. Biol.*, 2005, **282**, 307–19.

20 D. Vestweber, A. Gossler, K. Boller and R. Kemler, Expression and distribution of cell adhesion molecule uvomorulin in mouse preimplantation embryos., *Dev. Biol.*, 1987, **124**, 451–6.

21 A. J. Watson and G. M. Kidder, Immunofluorescence assessment of the timing of appearance and cellular distribution of Na/K-ATPase during mouse embryogenesis., *Dev. Biol.*, 1988, **126**, 80–90.

22 G. M. Kidder and A. J. Watson, Roles of Na,K-ATPase in Early Development and Trophectoderm Differentiation, *Semin. Nephrol.*, 2005, **25**, 352–355.

23 E. Korotkevich, R. Niwayama, A. Courtois, S. Friese, N. Berger, F. Buchholz and T. Hiiragi, The Apical Domain Is Required and Sufficient for the First Lineage Segregation in the Mouse Embryo, *Dev. Cell*, 2017, **40**, 235-247.e7.

24 S. Anani, S. Bhat, N. Honma-Yamanaka, D. Krawchuk and Y. Yamanaka, Initiation of Hippo signaling is linked to polarity rather than to cell position in the pre-implantation mouse embryo., *Development*, 2014, **141**, 2813–24.

25 A. I. Mihajlović and A. W. Bruce, The first cell-fate decision of mouse preimplantation embryo development: integrating cell position and polarity., *Open Biol.*, , DOI:10.1098/rsob.170210.

26 H. Sasaki, Position- and polarity-dependent Hippo signaling regulates cell fates in preimplantation mouse embryos., *Semin. Cell Dev. Biol.*, 2015, **48**, 1–8.

27 P. Home, R. P. Kumar, A. Ganguly, B. Saha, J. Milano-Foster, B. Bhattacharya, S. Ray, S. Gunewardena, A. Paul, S. A. Camper, P. E. Fields and S. Paul, Genetic redundancy of GATA factors in the extraembryonic trophoblast lineage ensures the progression of preimplantation and postimplantation mammalian development., *Development*, 2017, **144**, 876–888.

28 A. Ralston, B. J. Cox, N. Nishioka, H. Sasaki, E. Chea, P. Rugg-Gunn, G. Guo, P. Robson, J. S.

Draper and J. Rossant, Gata3 regulates trophoblast development downstream of Tead4 and in parallel to Cdx2., *Development*, 2010, **137**, 395–403.

29 J. G. Dumortier, M. Le Verge-Serandour, A.-F. F. Tortorelli, A. Mielke, L. de Plater, H. Turlier and J.-L. Maître, Hydraulic fracturing and active coarsening position the lumen of the mouse blastocyst., *Science*, 2019, **365**, 465–468.

30 P. Madan, K. Rose and A. J. Watson, Na/K-ATPase β1 Subunit Expression Is Required for Blastocyst Formation and Normal Assembly of Trophectoderm Tight Junction-associated Proteins, *J. Biol. Chem.*, 2007, **282**, 12127–12134.

31 L. C. Barcroft, H. Offenberg, P. Thomsen and A. J. Watson, Aquaporin proteins in murine trophectoderm mediate transepithelial water movements during cavitation, *Dev. Biol.*, 2003, **256**, 342–354.

32 C. Chazaud, Y. Yamanaka, T. Pawson and J. Rossant, Early Lineage Segregation between Epiblast and Primitive Endoderm in Mouse Blastocysts through the Grb2-MAPK Pathway, *Dev. Cell*, 2006, **10**, 615–624.

33 A. Q. Ryan, C. J. Chan, F. Graner and T. Hiiragi, Lumen Expansion Facilitates Epiblast-Primitive Endoderm Fate Specification during Mouse Blastocyst Formation., *Dev. Cell*, 2019, **51**, 684-697.e4.

34 J. Artus, A. Piliszek and A.-K. Hadjantonakis, The primitive endoderm lineage of the mouse blastocyst: Sequential transcription factor activation and regulation of differentiation by Sox17, *Dev. Biol.*, 2011, **350**, 393–404.

35 A. A. Avilion, S. K. Nicolis, L. H. Pevny, L. Perez, N. Vivian and R. Lovell-Badge, Multipotent cell lineages in early mouse development depend on SOX2 function., *Genes Dev.*, 2003, **17**, 126–40.

36 G. Guo, M. Huss, G. Q. Tong, C. Wang, L. Li Sun, N. D. Clarke and P. Robson, Resolution of cell fate decisions revealed by single-cell gene expression analysis from zygote to blastocyst., *Dev. Cell*, 2010, **18**, 675–85.

37 S. Menchero, T. Rayon, M. J. Andreu and M. Manzanares, Signaling pathways in mammalian preimplantation development: Linking cellular phenotypes to lineage decisions, *Dev. Dyn.*, 2017, **246**, 245–261.

38 N. Plachta, T. Bollenbach, S. Pease, S. E. Fraser and P. Pantazis, Oct4 kinetics predict cell lineage patterning in the early mammalian embryo, *Nat. Cell Biol.*, 2011, **13**, 117–123.

39 Y. Watanabe, K. Y. Miyasaka, A. Kubo, Y. S. Kida, O. Nakagawa, Y. Hirate, H. Sasaki and T. Ogura, Notch and Hippo signaling converge on Strawberry Notch 1 (Sbno1) to synergistically activate Cdx2 during specification of the trophectoderm, *Sci. Rep.*, 2017, **7**, 46135.

40 T. Rayon, S. Menchero, A. Nieto, P. Xenopoulos, M. Crespo, K. Cockburn, S. Cañon, H. Sasaki, A.-K. Hadjantonakis, J. L. de la Pompa, J. Rossant and M. Manzanares, Notch and

Hippo Converge on Cdx2 to Specify the Trophectoderm Lineage in the Mouse Blastocyst, *Dev. Cell*, 2014, **30**, 410–422.

41 B. Arabadjiev, R. Petkova, A. Momchilova, S. Chakarov and R. Pankov, Of mice and men – differential mechanisms of maintaining the undifferentiated state in mESC and hESC, *Biodiscovery*, 2012, 1–13.

42 S. M. Morgani and J. M. Brickman, LIF supports primitive endoderm expansion during pre-implantation development, *Development*, 2015, **142**, 3488–3499.

43 S. Pauklin and L. Vallier, Activin/Nodal signalling in stem cells, *Development*, 2015, **142**, 607–619.

44 D. B. Constam and E. J. Robertson, SPC4/PACE4 regulates a TGFbeta signaling network during axis formation., *Genes Dev.*, 2000, **14**, 1146–55.

45 Y. Shi and J. Massagué, Mechanisms of TGF-beta signaling from cell membrane to the nucleus., *Cell*, 2003, **113**, 685–700.

46 K. Tsuchida, M. Nakatani, N. Yamakawa, O. Hashimoto, Y. Hasegawa and H. Sugino, Activin isoforms signal through type I receptor serine/threonine kinase ALK7., *Mol. Cell. Endocrinol.*, 2004, **220**, 59–65.

47 J. L. Wrana, L. Attisano, R. Wieser, F. Ventura and J. Massagué, Mechanism of activation of the TGF-beta receptor., *Nature*, 1994, **370**, 341–7.

48 M. M. Matzuk, T. R. Kumar and A. Bradley, Different phenotypes for mice deficient in either activins or activin receptor type II., *Nature*, 1995, **374**, 356–60.

49 M. M. Matzuk, T. R. Kumar, A. Vassalli, J. R. Bickenbach, D. R. Roop, R. Jaenisch and A. Bradley, Functional analysis of activins during mammalian development., *Nature*, 1995, **374**, 354–6.

50 R. Z. Lu, S. Matsuyama, M. Nishihara and M. Takahashi, Developmental expression of activin/inhibin beta A, beta B, and alpha subunits, and activin receptor-IIB genes in preimplantation mouse embryos., *Biol. Reprod.*, 1993, **49**, 1163–9.

51 R. M. Albano, N. Groome and J. C. Smith, Activins are expressed in preimplantation mouse embryos and in ES and EC cells and are regulated on their differentiation., *Development*, 1993, **117**, 711–23.

52 C. Granier, V. Gurchenkov, A. Perea-Gomez, A. Camus, S. Ott, C. Papanayotou, J. Iranzo, A. Moreau, J. Reid, G. Koentges, D. Sabéran-Djoneidi and J. Collignon, Nodal cis-regulatory elements reveal epiblast and primitive endoderm heterogeneity in the peri-implantation mouse embryo., *Dev. Biol.*, 2011, **349**, 350–62.

53 K. Takaoka, M. Yamamoto, H. Shiratori, C. Meno, J. Rossant, Y. Saijoh and H. Hamada, The mouse embryo autonomously acquires anterior-posterior polarity at implantation., *Dev. Cell*, 2006, **10**, 451–9.

54 E. Coucouvanis and G. R. Martin, BMP signaling plays a role in visceral endoderm differentiation and cavitation in the early mouse embryo., *Development*, 1999, **126**, 535–46.

55 S. J. L. Graham, K. B. Wicher, A. Jedrusik, G. Guo, W. Herath, P. Robson and M. Zernicka-Goetz, BMP signalling regulates the pre-implantation development of extra-embryonic cell lineages in the mouse embryo., *Nat. Commun.*, 2014, **5**, 5667.

56 N. S. Reyes de Mochel, M. Luong, M. Chiang, A. L. Javier, E. Luu, F. Toshihiko, G. R. MacGregor, O. Cinquin and K. W. Y. Cho, BMP signaling is required for cell cleavage in preimplantation-mouse embryos., *Dev. Biol.*, 2015, **397**, 45–55.

57 M. A. Lemmon and J. Schlessinger, Cell signaling by receptor tyrosine kinases., *Cell*, 2010, **141**, 1117–34.

58 R. Trenker and N. Jura, Receptor tyrosine kinase activation: From the ligand perspective., *Curr. Opin. Cell Biol.*, 2020, **63**, 174–185.

59 D. K. Morrison, MAP kinase pathways., *Cold Spring Harb. Perspect. Biol.*, 2012, **4**, 1–5.

60 Y. Zhang and C. Dong, Regulatory mechanisms of mitogen-activated kinase signaling., *Cell. Mol. Life Sci.*, 2007, **64**, 2771–89.

61 B. Canovas and A. R. Nebreda, Diversity and versatility of p38 kinase signalling in health and disease., *Nat. Rev. Mol. Cell Biol.*, , DOI:10.1038/s41580-020-00322-w.

62 M. Maekawa, T. Yamamoto, T. Tanoue, Y. Yuasa, O. Chisaka and E. Nishida, Requirement of the MAP kinase signaling pathways for mouse preimplantation development., *Development*, 2005, **132**, 1773–83.

63 Y. Wang, E. E. Puscheck, J. J. Lewis, A. B. Trostinskaia, F. Wang and D. A. Rappolee, Increases in phosphorylation of SAPK/JNK and p38MAPK correlate negatively with mouse embryo development after culture in different media., *Fertil. Steril.*, 2005, **83 Suppl 1**, 1144–54.

64 Y. Xie, E. E. Puscheck and D. A. Rappolee, Effects of SAPK/JNK inhibitors on preimplantation mouse embryo development are influenced greatly by the amount of stress induced by the media., *Mol. Hum. Reprod.*, 2006, **12**, 217–24.

65 V. Thamodaran and A. W. Bruce, p38 (Mapk14/11) occupies a regulatory node governing entry into primitive endoderm differentiation during preimplantation mouse embryo development., *Open Biol.*, 2016, **6**, 15034.

66 P. Bora, L. Gahurova, T. Mašek, A. Hauserova, D. Potěšil, D. Jansova, A. Susor, Z. Zdráhal, A. Ajduk, M. Pospíšek and A. W. Bruce, p38-MAPK mediated rRNA processing and translation regulation enables PrE differentiation during mouse blastocyst maturation, *bioRxiv*, 2020, 2020.11.30.403931.

67 P. Bora, V. Thamodaran, A. Šušor and A. W. Bruce, p38-Mitogen Activated Kinases Mediate a Developmental Regulatory Response to Amino Acid Depletion and Associated Oxidative Stress in Mouse Blastocyst Embryos., *Front. cell Dev. Biol.*, 2019, **7**, 276.

68 P. Bora, L. Gahurova, A. Hauserova, M. Stiborova, R. Collier, D. Potěšil, Z. Zdráhal and A. W. Bruce, DDX21 is a p38-MAPK sensitive nucleolar protein necessary for mouse preimplantation embryo development and cell-fate specification, *bioRxiv*, 2021, 2021.04.13.439318.

69 D. R. Natale, A. J. M. Paliga, F. Beier, S. J. A. D'Souza and A. J. Watson, p38 MAPK signaling during murine preimplantation development., *Dev. Biol.*, 2004, **268**, 76–88.

70 C. E. Bell and A. J. Watson, p38 MAPK Regulates Cavitation and Tight Junction Function in the Mouse Blastocyst, *PLoS One*, 2013, **8**, e59528.

71 A. J. M. Paliga, D. R. Natale and A. J. Watson, p38 mitogen-activated protein kinase (MAPK) first regulates filamentous actin at the 8-16-cell stage during preimplantation development., *Biol. cell*, 2005, **97**, 629–40.

72 B. Sozen, S. Ozturk, A. Yaba and N. Demir, The p38 MAPK signalling pathway is required for glucose metabolism, lineage specification and embryo survival during mouse preimplantation development, *Mech. Dev.*, 2015, **138**, 375–398.

73 C.-W. Lu, A. Yabuuchi, L. Chen, S. Viswanathan, K. Kim and G. Q. Daley, Ras-MAPK signaling promotes trophectoderm formation from embryonic stem cells and mouse embryos, *Nat. Genet.*, 2008, **40**, 921–926.

74 J. Yang, D. Zhang, Y. Yu, R.-J. Zhang, X.-L. Hu, H.-F. Huang and Y.-C. Lu, Binding of FGF2 to FGFR2 in an autocrine mode in trophectoderm cells is indispensable for mouse blastocyst formation through PKC-p38 pathway, *Cell Cycle*, 2015, **14**, 3318–3330.

75 E. Arman, R. Haffner-Krausz, Y. Chen, J. K. Heath and P. Lonai, Targeted disruption of fibroblast growth factor (FGF) receptor 2 suggests a role for FGF signaling in pregastrulation mammalian development, *Proc. Natl. Acad. Sci.*, 1998, **95**, 5082–5087.

76 B. Feldman, W. Poueymirou, V. Papaioannou, T. DeChiara and M. Goldfarb, Requirement of FGF-4 for postimplantation mouse development, *Science (80-.).*, 1995, **267**, 246–249.

77 M. Kang, A. Piliszek, J. Artus and A.-K. Hadjantonakis, FGF4 is required for lineage restriction and salt-and-pepper distribution of primitive endoderm factors but not their initial expression in the mouse, *Development*, 2013, **140**, 267–279.

78 Y. Yamanaka, F. Lanner and J. Rossant, FGF signal-dependent segregation of primitive endoderm and epiblast in the mouse blastocyst, *Development*, 2010, **137**, 715–724.

79 D. Krawchuk, N. Honma-Yamanaka, S. Anani and Y. Yamanaka, FGF4 is a limiting factor controlling the proportions of primitive endoderm and epiblast in the ICM of the mouse blastocyst., *Dev. Biol.*, 2013, **384**, 65–71.

80 M. Kang, V. Garg and A. Hadjantonakis, Lineage Establishment and Progression within the Inner Cell Mass of the Mouse Blastocyst Requires FGFR1 and FGFR2, *Dev. Cell*, 2017, **41**, 496-510.e5.

81 A. Molotkov, P. Mazot, J. R. Brewer, R. M. Cinalli and P. Soriano, Distinct Requirements for

FGFR1 and FGFR2 in Primitive Endoderm Development and Exit from Pluripotency, *Dev. Cell*, 2017, **41**, 511-526.e4.

82 Y. Ohnishi, W. Huber, A. Tsumura, M. Kang, P. Xenopoulos, K. Kurimoto, A. K. Oleś, M. J. Araúzo-Bravo, M. Saitou, A.-K. Hadjantonakis and T. Hiiragi, Cell-to-cell expression variability followed by signal reinforcement progressively segregates early mouse lineages, *Nat. Cell Biol.*, 2014, **16**, 27–37.

83 N. Schrode, N. Saiz, S. Di Talia and A.-K. Hadjantonakis, GATA6 Levels Modulate Primitive Endoderm Cell Fate Choice and Timing in the Mouse Blastocyst, *Dev. Cell*, 2014, **29**, 454–467.

84 A. Molotkov and P. Soriano, Distinct mechanisms for PDGF and FGF signaling in primitive endoderm development, *Dev. Biol.*, 2018, **442**, 155–161.

85 S. Bessonnard, S. Vandormael-Pournin, S. Coqueran, M. Cohen-Tannoudji and J. Artus, PDGF Signaling in Primitive Endoderm Cell Survival Is Mediated by PI3K-mTOR Through p53-Independent Mechanism., *Stem Cells*, 2019, **37**, 888–898.

86 B. Plusa, A. Piliszek, S. Frankenberg, J. Artus and A.-K. Hadjantonakis, Distinct sequential cell behaviours direct primitive endoderm formation in the mouse blastocyst, *Development*, 2008, **135**, 3081–3091.

87 J. Artus, J.-J. Panthier and A.-K. Hadjantonakis, A role for PDGF signaling in expansion of the extra-embryonic endoderm lineage of the mouse blastocyst, *Development*, 2010, **137**, 3361–3372.

88 A. Cuadrado and A. R. Nebreda, Mechanisms and functions of p38 MAPK signalling, *Biochem. J.*, 2010, **429**, 403–417.

89 T. Zarubin and J. Han, Activation and signaling of the p38 MAP kinase pathway, *Cell Res.*, 2005, **15**, 11–18.

90 L. K. Petersen, P. Blakskjær, A. Chaikuad, A. B. Christensen, J. Dietvorst, J. Holmkvist, S. Knapp, M. Kořínek, L. K. Larsen, A. E. Pedersen, S. Röhm, F. A. Sløk and N. J. V. Hansen, Novel p38α MAP kinase inhibitors identified from yoctoReactor DNA-encoded small molecule library, *Medchemcomm*, 2016, **7**, 1332–1339.

91 J. M. Salvador, P. R. Mittelstadt, T. Guszczynski, T. D. Copeland, H. Yamaguchi, E. Appella, A. J. Fornace and J. D. Ashwell, Alternative p38 activation pathway mediated by T cell receptor-proximal tyrosine kinases., *Nat. Immunol.*, 2005, **6**, 390–5.

92 P. R. Mittelstadt, H. Yamaguchi, E. Appella and J. D. Ashwell, T cell receptor-mediated activation of p38{alpha} by mono-phosphorylation of the activation loop results in altered substrate specificity., *J. Biol. Chem.*, 2009, **284**, 15469–74.

93 L. Jirmanova, D. N. Sarma, D. Jankovic, P. R. Mittelstadt and J. D. Ashwell, Genetic disruption of p38alpha Tyr323 phosphorylation prevents T-cell receptor-mediated p38alpha activation and impairs interferon-gamma production., *Blood*, 2009, **113**, 2229–

37.

94 B. Ge, H. Gram, F. Di Padova, B. Huang, L. New, R. J. Ulevitch, Y. Luo and J. Han, MAPKK-independent activation of p38alpha mediated by TAB1-dependent autophosphorylation of p38alpha., *Science*, 2002, **295**, 1291–4.

95 Y. Wang, X. Zhou, K. Oberoi, R. Phelps, R. Couwenhoven, M. Sun, A. Rezza, G. Holmes, C. J. Percival, J. Friedenthal, P. Krejci, J. T. Richtsmeier, D. L. Huso, M. Rendl and E. W. Jabs, p38 inhibition ameliorates skin and skull abnormalities in Fgfr2 Beare-Stevenson mice, *J. Clin. Invest.*, 2012, **122**, 2153–2164.

96 Y. Wang, M. Sun, V. L. Uhlhorn, X. Zhou, I. Peter, N. Martinez-Abadias, C. A. Hill, C. J. Percival, J. T. Richtsmeier, D. L. Huso and E. W. Jabs, Activation of p38 MAPK pathway in the skull abnormalities of Apert syndrome Fgfr2(+P253R) mice., *BMC Dev. Biol.*, 2010, **10**, 22.

97 M. Mahe, F. Dufour, H. Neyret-Kahn, A. Moreno-Vega, C. Beraud, M. Shi, I. Hamaidi, V. Sanchez-Quiles, C. Krucker, M. Dorland-Galliot, E. Chapeaublanc, R. Nicolle, H. Lang, C. Pouponnot, T. Massfelder, F. Radvanyi and I. Bernard-Pierrot, An FGFR3/MYC positive feedback loop provides new opportunities for targeted therapies in bladder cancers., *EMBO Mol. Med.*, 2018, **10**, 1–18.

98 V. Lafarga, A. Cuadrado, I. Lopez de Silanes, R. Bengoechea, O. Fernandez-Capetillo and A. R. Nebreda, p38 Mitogen-activated protein kinase- and HuR-dependent stabilization of p21(Cip1) mRNA mediates the G(1)/S checkpoint., *Mol. Cell. Biol.*, 2009, **29**, 4341–51.

99 Y. Zeng, H. Sankala, X. Zhang and P. R. Graves, Phosphorylation of Argonaute 2 at serine-387 facilitates its localization to processing bodies., *Biochem. J.*, 2008, **413**, 429–36.

100 T. Ueda, R. Watanabe-Fukunaga, H. Fukuyama, S. Nagata and R. Fukunaga, Mnk2 and Mnk1 Are Essential for Constitutive and Inducible Phosphorylation of Eukaryotic Initiation Factor 4E but Not for Cell Growth or Development, *Mol. Cell. Biol.*, 2004, **24**, 6539–6549.

101 V. Sørensen, Y. Zhen, M. Zakrzewska, E. M. Haugsten, S. Wälchli, T. Nilsen, S. Olsnes and A. Wiedlocha, Phosphorylation of fibroblast growth factor (FGF) receptor 1 at Ser777 by p38 mitogen-activated protein kinase regulates translocation of exogenous FGF1 to the cytosol and nucleus., *Mol. Cell. Biol.*, 2008, **28**, 4129–41.

102 E. F. Wagner and Á. R. Nebreda, Signal integration by JNK and p38 MAPK pathways in cancer development, *Nat. Rev. Cancer*, 2009, **9**, 537–549.

103 R. H. Adams, A. Porras, G. Alonso, M. Jones, K. Vintersten, S. Panelli, A. Valladares, L. Perez, R. Klein and A. R. Nebreda, Essential Role of p38α MAP Kinase in Placental but Not Embryonic Cardiovascular Development, *Mol. Cell*, 2000, **6**, 109–116.

104 J. S. Mudgett, J. Ding, L. Guh-Siesel, N. A. Chartrain, L. Yang, S. Gopal and M. M. Shen, Essential role for p38alpha mitogen-activated protein kinase in placental angiogenesis, *Proc. Natl. Acad. Sci.*, 2000, **97**, 10454–10459.

105 A. Cuenda and S. Rousseau, p38 MAP-Kinases pathway regulation, function and role in human diseases, *Biochim. Biophys. Acta - Mol. Cell Res.*, 2007, **1773**, 1358–1375.

106 G. Sabio, J. S. C. Arthur, Y. Kuma, M. Peggie, J. Carr, V. Murray-Tait, F. Centeno, M. Goedert, N. A. Morrice and A. Cuenda, p38γ regulates the localisation of SAP97 in the cytoskeleton by modulating its interaction with GKAP, *EMBO J.*, 2005, **24**, 1134–1145.

107 V. A. Beardmore, H. J. Hinton, C. Eftychi, M. Apostolaki, M. Armaka, J. Darragh, J. McIlrath, J. M. Carr, L. J. Armit, C. Clacher, L. Malone, G. Kollias and J. S. C. Arthur, Generation and Characterization of p38β (MAPK11) Gene-Targeted Mice, *Mol. Cell. Biol.*, 2005, **25**, 10454–10464.

108 J. Desai, V. Holt-Shore, R. J. Torry, M. R. Caudle and D. S. Torry, Signal Transduction and Biological Function of Placenta Growth Factor in Primary Human Trophoblast1, *Biol. Reprod.*, 1999, **60**, 887–892.

109 T. Morooka and E. Nishida, Requirement of p38 Mitogen-activated Protein Kinase for Neuronal Differentiation in PC12 Cells, *J. Biol. Chem.*, 1998, **273**, 24285–24288.

110 R. K. Bikkavilli, M. E. Feigin and C. C. Malbon, p38 mitogen-activated protein kinase regulates canonical Wnt- -catenin signaling by inactivation of GSK3, *J. Cell Sci.*, 2008, **121**, 3598–3607.

111 K. Brown, S. Legros, J. Artus, M. X. Doss, R. Khanin, A.-K. Hadjantonakis and A. Foley, A Comparative Analysis of Extra-Embryonic Endoderm Cell Lines, *PLoS One*, 2010, **5**, e12016.

112 F. D. Houghton, J. G. Thompson, C. J. Kennedy and H. J. Leese, Oxygen consumption and energy metabolism of the early mouse embryo., *Mol. Reprod. Dev.*, 1996, **44**, 476–85.

113 M. Lane and D. K. Gardner, Amino acids and vitamins prevent culture-induced metabolic perturbations and associated loss of viability of mouse blastocysts., *Hum. Reprod.*, 1998, **13**, 991–7.

114 H. J. Leese, Metabolism of the preimplantation mammalian embryo., *Oxf. Rev. Reprod. Biol.*, 1991, **13**, 35–72.

115 N. M. Orsi and H. J. Leese, Protection against reactive oxygen species during mouse preimplantation embryo development: role of EDTA, oxygen tension, catalase, superoxide dismutase and pyruvate., *Mol. Reprod. Dev.*, 2001, **59**, 44–53.

116 H. J. Leese, Metabolism of the preimplantation embryo: 40 years on, *Reproduction*, 2012, **143**, 417–427.

117 T. Masek, E. del Llano, L. Gahurova, M. Kubelka, A. Susor, K. Roucova, C. Lin, A. W. Bruce and M. Pospisek, Identifying the Translatome of Mouse NEBD-Stage Oocytes via SSP-Profiling; A Novel Polysome Fractionation Method, *Int. J. Mol. Sci.*, 2020, **21**, 1254.

118 H. Yang, J. Zhou, R. L. Ochs, D. Henning, R. Jin and B. C. Valdez, Down-regulation of RNA helicase II/Gu results in the depletion of 18 and 28 S rRNAs in Xenopus oocyte., *J. Biol. Chem.*, 2003, **278**, 38847–59.

119 Y. Zhang, K. C. Baysac, L.-F. Yee, A. J. Saporita and J. D. Weber, Elevated DDX21 regulates c-Jun activity and rRNA processing in human breast cancers, *Breast Cancer Res.*, 2014, **16**, 449.

120 E. Calo, R. A. Flynn, L. Martin, R. C. Spitale, H. Y. Chang and J. Wysocka, RNA helicase DDX21 coordinates transcription and ribosomal RNA processing, *Nature*, 2015, **518**, 249–253.

121 J. Hochstatter, M. Hölzel, M. Rohrmoser, L. Schermelleh, H. Leonhardt, R. Keough, T. J. Gonda, A. Imhof, D. Eick, G. Längst and A. Németh, Myb-binding Protein 1a (Mybbp1a) Regulates Levels and Processing of Pre-ribosomal RNA, *J. Biol. Chem.*, 2012, **287**, 24365–24377.

122 N. S. Corsini, A. M. Peer, P. Moeseneder, M. Roiuk, T. R. Burkard, H.-C. Theussl, I. Moll and J. A. Knoblich, Coordinated Control of mRNA and rRNA Processing Controls Embryonic Stem Cell Pluripotency and Differentiation, *Cell Stem Cell*, 2018, **22**, 543-558.e12.

123 A. Bulut-Karslioglu, T. A. Macrae, J. A. Oses-Prieto, S. Covarrubias, M. Percharde, G. Ku, A. Diaz, M. T. McManus, A. L. Burlingame and M. Ramalho-Santos, The Transcriptionally Permissive Chromatin State of Embryonic Stem Cells Is Acutely Tuned to Translational Output, *Cell Stem Cell*, 2018, **22**, 369-383.e8.

124 A. Bulut-Karslioglu, S. Biechele, H. Jin, T. A. Macrae, M. Hejna, M. Gertsenstein, J. S. Song and M. Ramalho-Santos, Inhibition of mTOR induces a paused pluripotent state, *Nature*, 2016, **540**, 119–123.

125 G. C. A. Taylor, R. Eskeland, B. Hekimoglu-Balkan, M. M. Pradeepa and W. A. Bickmore, H4K16 acetylation marks active genes and enhancers of embryonic stem cells, but does not alter chromatin compaction., *Genome Res.*, 2013, **23**, 2053–65.

126 P. Komarnitsky, E. J. Cho and S. Buratowski, Different phosphorylated forms of RNA polymerase II and associated mRNA processing factors during transcription., *Genes Dev.*, 2000, **14**, 2452–60.

127 B. Zhang, H. Zheng, B. Huang, W. Li, Y. Xiang, X. Peng, J. Ming, X. Wu, Y. Zhang, Q. Xu, W. Liu, X. Kou, Y. Zhao, W. He, C. Li, B. Chen, Y. Li, Q. Wang, J. Ma, Q. Yin, K. Kee, A. Meng, S. Gao, F. Xu, J. Na and W. Xie, Allelic reprogramming of the histone modification H3K4me3 in early mammalian development., *Nature*, 2016, **537**, 553–557.

128 C. Wang, X. Liu, Y. Gao, L. Yang, C. Li, W. Liu, C. Chen, X. Kou, Y. Zhao, J. Chen, Y. Wang, R. Le, H. Wang, T. Duan, Y. Zhang and S. Gao, Reprogramming of H3K9me3-dependent heterochromatin during mammalian embryo development., *Nat. Cell Biol.*, 2018, **20**, 620–631.

129 H. Fulka and F. Aoki, Nucleolus Precursor Bodies and Ribosome Biogenesis in Early Mammalian Embryos: Old Theories and New Discoveries., *Biol. Reprod.*, 2016, **94**, 143.

130 M. Piazzi, A. Bavelloni, A. Gallo, I. Faenza and W. L. Blalock, Signal Transduction in Ribosome Biogenesis: A Recipe to Avoid Disaster., *Int. J. Mol. Sci.*, , DOI:10.3390/ijms20112718.

131 J. Kresoja-Rakic and R. Santoro, Nucleolus and rRNA Gene Chromatin in Early Embryo Development., *Trends Genet.*, 2019, **35**, 868–879.

132 S. Mori, R. Bernardi, A. Laurent, M. Resnati, A. Crippa, A. Gabrieli, R. Keough, T. J. Gonda and F. Blasi, Myb-Binding Protein 1A (MYBBP1A) Is Essential for Early Embryonic Development, Controls Cell Cycle and Mitosis, and Acts as a Tumor Suppressor, *PLoS One*, 2012, **7**, e39723.

133 J. Qu and J. M. Bishop, Nucleostemin maintains self-renewal of embryonic stem cells and promotes reprogramming of somatic cells to pluripotency., *J. Cell Biol.*, 2012, **197**, 731–45.

134 J. Han, J. D. Lee, L. Bibbs and R. J. Ulevitch, A MAP kinase targeted by endotoxin and hyperosmolarity in mammalian cells., *Science*, 1994, **265**, 808–11.

135 P. Moldéus, I. A. Cotgreave and M. Berggren, Lung protection by a thiol-containing antioxidant: N-acetylcysteine., *Respiration.*, 1986, **50 Suppl 1**, 31–42.

Curriculum vitae:

Pablo Bora

ORCID: 0000-0002-8400-5380
ResearcherID: X-2217-2019

Education:

Ph.D.	01/2017 onwards	Jihočeská univerzita v Českých Budějovicích (University of South Bohemia), České Budějovice, Czech Republic
M.Sc.	10/2009 to 06/2011	Bangalore University, Bangalore, India
B.Sc.	08/2006 to 05/2009	Bangalore University, Bangalore, India

Other research positions:

Research Associate	09/2015 to 10/2016	Stempeutics Research Pvt. Ltd., Bangalore, India
Research Assistant	04/2014 to 10/2014	Institute of Molecular Biology (IMB), gGmbH, Mainz, Germany
Junior Research Fellow	03/2013 to 03/2014	Institute for Stem Cell Biology & Regenerative Medicine (inStem), NCBS-TIFR, Bangalore, India
Junior Research Fellow	03/2012 to 12/2012	Institute for Stem Cell Biology & Regenerative Medicine (inStem), NCBS-TIFR, Bangalore, India

Publications & pre-prints:

1. **Pablo Bora**, Lenka Gahurova, Andrea Hauserova, Martina Stiborova, Rebecca Collier, David Potěšil, Zbyněk Zdráhal and Alexander W. Bruce; **DDX21 is a p38-MAPK sensitive nucleolar protein necessary for mouse preimplantation embryo development and cell-fate specification**; *bioRxiv* 2021.04.13.439318; https://doi.org/10.1101/2021.04.13.439318 (accepted at *Open Biology*) — 2021
2. **Pablo Bora**, Lenka Gahurova, Tomáš Mašek, Andrea Hauserova, David Potěšil, Denisa Jansova, Andrej Susor, Zbyněk Zdráhal, Anna Ajduk, Martin Pospíšek and Alexander W. Bruce; **p38-MAPK mediated rRNA processing and translation regulation enables PrE differentiation during mouse blastocyst maturation**; *bioRxiv* 2020.11.30.403931; https://doi.org/10.1101/2020.11.30.403931 (accepted at *Communications Biology*) — 2020
3. Giorgio Virnicchi, **Pablo Bora**, Lenka Gahurová, Andrej Šušor and Alexander W. Bruce; ***Wwc2* Is a Novel Cell Division Regulator During Preimplantation Mouse Embryo Lineage Formation and Oogenesis**; *Frontiers in Cell and Developmental Biology;* September 2020. https://doi.org/10.3389/fcell.2020.00857 — 2020

4. **Pablo Bora**, Vasanth Thamodaran, Andrej Šušor and Alexander W. Bruce; **p38-mitogen activated kinases mediate a developmental regulatory response to amino acid depletion and associated oxidative stress in mouse blastocyst embryos**; *Frontiers in Cell and Developmental Biology*; November 2019, https://doi.org/10.3389/fcell.2019.00276	2019
5. **Pablo Bora** and Anish S Majumdar; **Adipose tissue derived stromal vascular fraction in regenerative medicine: a brief review on biology and translation**; *Stem Cell Research & Therapy*; June 2017, http://dx.doi.org/10.1186/s13287-017-0598-y (Review)	2017
6. Sanjeeb K. Sahu, Alina Fritz, Neha Tiwari, Zsuzsa Kovacs, Alireza Pouya, Verena Wüllner, **Pablo Bora**, Teresa Schacht, Jan Baumgart, Sophie Peron, Benedikt Berninger, Vijay K Tiwari and Axel Methner; **TOX3 plays a role in neuronal progenitor proliferation**; *Biochimica et Biophysica Acta (BBA) - Gene Regulatory Mechanisms*; July 2016, ISSN 1874-9399, http://dx.doi.org/10.1016/j.bbagrm.2016.04.005	2016

Manuscripts in preparation:

1. **mTOR-regulated cap-dependent translation plays a role in first cell-fate decision in mouse preimplantation embryos**. (as a co-author)	2021

Awards & fellowships:

1. Grantová agentura Jihočeská univerzita (funding agency of the University); **2-year Individual research project**.	2019
2. Grantová agentura Jihočeská univerzita (funding agency of the University); **2-year Individual research project**. (Declined)	2018
3. Council of Scientific and Industrial Research (CSIR, Govt. of India) **Junior Research Fellowship**.	2013
4. University Grants Commission (UGC, Govt. of India) **Junior Research Fellowship**.	2011

Conferences:

1. **European Developmental Biology Congress,** Alicante, Spain	Poster	October, 2019
2. **EMBO Workshop**: "**Awakening of the genome: The maternal-to-zygotic transition**"**,** Institute of Molecular Genetics ASCR, Prague, Czech Republic	Poster	May, 2019
3. **Visegrad Group Society for Developmental Biology: Inaugural Meeting,** Masaryk University, Brno, Czech Republic	Poster and flash talk	September, 2018

Training & guiding roles:

Tutorial lecturer for developmental and cell	Training Masters and Bachelors students in mouse oviduct micro-	2018-2019

biology courses at the University of South Bohemia.	dissection, preimplantation embryo isolation and culture.	
Supervision of students at the University of South Bohemia.	Bachelor student (x1)	01/2020 onwards
	Master ERASMUS+ student (x1)	06/2019 to 08/2019

borapa00@prf.jcu.cz

The role of p38-MAPKs in mouse preimplantation embryonic development: Regulating translation towards blastocyst maturation and lineage specification.

Ph.D. Thesis, 2021

University of South Bohemia in České Budějovice
Faculty of Science
Branišovská 1760
CZ-37005 České Budějovice, Czech Republic

Phone: +420 777 6540 76
www.prf.jcu.cz, e-mail: sekret-fpr@prf.jcu.cz